

GATING OF THE SENSORY NEURONAL VOLTAGE-GATED SODIUM
CHANNEL $Na_v1.7$: ANALYSIS OF THE ROLE OF D3 AND D4 / S4-S5
LINKERS IN TRANSITION TO AN INACTIVATED STATE

Brian W. Jarecki

Submitted to the faculty of the University Graduate School
in partial fulfillment of the requirements
for the degree
Doctor of Philosophy
in the Department of Pharmacology and Toxicology
Indiana University

February 2010

Accepted by the Faculty of Indiana University, in partial fulfillment of the requirements for the degree of Doctor of Philosophy

Theodore R. Cummins, Ph.D., Chair

Grant D. Nicol, Ph.D.

Doctoral Committee

Gerry S. Oxford, Ph.D.

Andy Hudmon, Ph.D.

January 14, 2010

John H. Schild, Ph.D.

DEDICATION

This work is dedicated to my thesis mentor, Dr. Theodore R. Cummins, parents, William and Germaine Jarecki, my sister, Sarah, my beautiful wife, Carie and my fantastic children, Aidan and Ayla.

ACKNOWLEDGEMENTS

This dissertation would not have been possible without the inspiration, motivation, and guidance of several individuals whom I have had the great opportunity to either work with or have as a part of my life. I would like to take the time to thank and acknowledge these people.

First and foremost, I would like to thank my family. To my mother, Germaine, and father, William, your hard work, sacrifice, and dedication are the reason I have been able to achieve all that I have done and will do in my lifetime. Sarah, my little sister, your constant drive and motivation to succeed and love for anyone you meet are both humbling and inspirational to me. To my wife, Carie, your endless love for me and unquestionable willingness to stand by my side give me the energy to continue working. To my son and daughter, Aidan and Ayla, you two are the reason I wake up and appreciate everything I have in my life. I look forward to watching you grow into amazing human beings.

Endless showers of praise and gratitude must be given to my brilliant thesis mentor, Dr. Theodore Cummins. Amazed by your patience, ability to reason, and firm grasp on things inside and outside of science, I firmly believe you define what a mentor should be. I cannot thank you enough for taking a chance on me as a student, training me, and mentoring me over the last few years. I sincerely wish you nothing but excellence in all that you do; you deserve it. I have learned more about science and life from you than I could have ever imagined. As I move on, I will continue to use your leadership and drive as an example of how to succeed in science.

I would also like to thank Drs. Nicol, Oxford, Schild, and Hudmon for taking time to be a part of my thesis committee. The ideas generated within this group of outstanding scientists consistently amazed me. Dr. Nicol, I appreciate everything you have done for me and your always encouraging words of advice. Dr. Oxford, the numerous times you were willing to help me out will forever be remembered. I hope to carry this service on as I move through my career. Dr. Schild, your willingness to challenge my thought process has played an important role in the way that I think about electrophysiology. Dr. Hudmon, the multitude of rapid fire ideas that you can generate in a matter of minutes and the way that you think about science amazes and motivates me to always ask questions. Thank you for your mentorship and friendship.

To the faculty of the Pharmacology and Toxicology department and members of the Stark Neurosciences Research Institute (SNRI), thank you for all of your help and guidance. I would especially like to thank Drs. Vasko, Hingtgen, Kamendulis, Khanna, DiMicco, Sullivan, Molosh, and Zhu. Thank you so much for taking a chance on me and guiding me through my graduate career as a student and a friend. I am grateful for having the chance to receive such excellent advice. To everyone in the department and at SNRI; thanks for all of the great wisdom and advice during Friday morning meetings and departmental seminars. Together, you have played an intricate role in developing my scientific mind.

I would also like to thank everyone in the Pharmacology and Toxicology department who has made my life as a graduate student painless. Amy Lawson, Lisa King, Tina Bryant, Miriam Barr, Dan Smith, Cynthia Maverick, Nastassia Belton, Amy Doherty, Lisa Parks-Connell, thank you for all of your hard work and for helping me throughout my graduate career – you are all fantastic!

Special thanks are in order for the members, past and present, of the Cummins lab. James, I am completely humbled by your humility, wisdom, and passion for what you do, no matter what it is. You have been a superb friend and mentor in the many facets of life. I wish you and your family nothing but the best. Patrick, your leadership and success have paved the (uphill) road for graduate students in this department. Your friendship and mentorship are a big reason why I have been able to progress in this field. You and Ted are superb role models and talented scientists. Yucheng, words cannot describe how impressive of an electrophysiologist you are. Your ability to rapidly think and produce data astounds me. Andy, thanks for keeping things lighthearted in the lab and for always asking questions, even if you already know the answers. You have the potential to do whatever you want and I am confident you will do well.

I would also like to thank the students in the Pharmacology and Toxicology department, in particular, Stacy Dixon, Stacy Corthals-Torgerson, Brian Schmutzler, and Weihua Song. You guys have kept me on my toes throughout my time here. Also, to those in the graduate office who have helped with this thesis, particularly Debra Barker, for aiding in fine-tuning of my thesis. Finally, big thanks go to the Indiana Clinical and Translational Sciences Institute for funding my research.

ABSTRACT

Brian W. Jarecki

Gating of the sensory neuronal voltage-gated sodium channel Na_v1.7: Analysis of role of D3 and D4 / S4-S5 linkers in transition to an inactivated state

Voltage-gated sodium channels (VGSCs) are dynamic membrane-spanning proteins crucial for determining the electrical excitability in nerve and muscle. VGSCs transition, or gate, between opened, closed, and inactivated states, in response to changes in transmembrane potential. Altered VGSC gating can affect electrical communication and is implicated in numerous channelopathies. Na_v1.7, a VGSC isoform highly expressed in the peripheral nervous system, plays a unique role in pain perception as evidenced by single point missense mutations causing a spectrum of pain syndromes (inherited erythromelalgia; IEM and paroxysmal extreme pain disorder; PEPD) and nonsense mutations resulting in human insensitivity to pain (CIP). These studies indicate Na_v1.7 is critical in pain transduction and, as such, structural perturbations to Na_v1.7 affecting conformational stability and response to changes in transmembrane potential have the potential to cause pain. Therefore, the aims of this dissertation were to (1) examine the effects of PEPD mutations on the voltage-dependent properties Na_v1.7; (2) investigate the effects Na_v1.7 alternative splicing has on the impact of IEM and PEPD mutations; (3) evaluate the effects channelopathies, resulting from slowed inactivation, have on modulating an unusual type of sodium current that flows during membrane repolarization; and (4) determine the structural components involved in stabilizing

Na_v1.7 inactivation. Standard patch-clamp electrophysiology was used to study changes in channel properties. Results from this dissertation demonstrate that (1) PEPD mutations significantly shift the voltage-dependent properties of Na_v1.7 channels, destabilize an inactivated state in a residue specific manner, and render nociceptive neurons hyperexcitable; (2) alternative splicing can functionally impact PEPD; (3) channelopathies, resulting from slowed inactivation in neuronal and muscle VGSC isoforms, increase an unusual sodium conductance that flows during repolarization; and (4) specific residues located in distinct regions of Na_v1.7 serve as docking sites to stabilize inactivation at different membrane potentials. Overall, this dissertation answers key questions regarding the molecular mechanics required during inactivation and the biophysical consequences of Na_v1.7 mutations implicated in painful disorders. The results of this dissertation are important for a more detailed understanding of pain perception and validate the applicability of studying Na_v1.7 for discovery of therapeutic targets for treatment of pain.

Theodore R. Cummins, Ph.D., Chair

TABLE OF CONTENTS

LIST OF TABLES	xiv
LIST OF FIGURES	xvi
LIST OF ABBREVIATIONS	xxi
I. INTRODUCTION	1
A. Overview	1
B. Brief history and background of voltage-gated sodium channels	3
C. Diversity of VGSC isoforms	9
D. Structural components and gating characteristics of VGSCs	12
1. Abbreviated introduction	12
2. Voltage-gated channel activation and associated gating charge movement	15
3. Ionic current through a channel pore upon opening	18
4. The molecular mechanics of inactivation gating	21
E. VGSCs and peripheral neuropathic pain	32
F. The Na _v 1.7 VGSC isoform and pain	35
G. Understanding components critical to VGSC gating based on Na _v 1.7 channelopathies	41
H. Hypothesis, specific aims, and summary of results	45
II. MATERIALS AND METHODS	49
A. Experimental cDNA constructs	49
B. Mutagenesis of VGSCs	53

C. Transient transfection of hEK ₂₉₃ cells.....	55
D. Harvest and preparation of rat DRG neurons.....	57
E. Biolistic transfection of neurons.....	59
F. Chemicals	61
G. Solutions	62
1. Standard extracellular bathing solution for hEK ₂₉₃ recordings.....	62
2. Standard extracellular bathing solution for rat DRG neurons.....	62
3. Standard CsF dominant electrode solution for hEK ₂₉₃ recordings.....	63
4. Alternative CsCl dominant electrode solution for hEK ₂₉₃ recordings.....	63
5. Standard CsF dominant electrode solution for rat DRG neurons.....	63
H. Whole-cell patch-clamp recordings for hEK ₂₉₃ and rat DRG recordings	64
I. Standard patch-clamp protocol for voltage-clamp recordings	67
J. Data analysis.....	70
III. RESULTS.....	72
A. Paroxysmal extreme pain disorder (PEPD) mutations within the D3 and D4 / S4-S5 linkers of Na _v 1.7 cause moderate destabilization of fast inactivation.....	72

1. PEPD mutations within the D3 / S4-S5 linker have small effects on the voltage dependence of channel conductance but do not alter deactivation time constants.....	72
2. Mutations within the D3 / S4-S5 linker, implicated in PEPD, significantly shift the voltage dependence of the steady-state fast inactivation profile	78
3. PEPD mutant channels reveal an increased persistent component in response to a slow-duration depolarizing ramp stimulus	86
4. PEPD mutations within the D3 / S4-S5 linker differentially affect development of closed-state inactivation (CSI) compared to the I1461T PEPD mutation	87
5. Mutations associated with PEPD increase the recovery rate from CSI	90
6. D3 / S4-S5 and D3-D4 PEPD linker mutations allow Na _v 1.7 channels to recover from open-state inactivation (OSI) faster than wild-type (WT) channels	92
7. An adjacent and identical mutation within the D3 / S4-S5 linker, not implicated in PEPD, displays unique voltage-dependent and kinetic properties compared to neighboring PEPD mutations	94

8. Voltage-dependent slow inactivation properties for PEPD mutant channels are altered in a manner distinct from V1300F mutant channels	99
B. $Na_v1.7$ -PEPD mutant channel M1627K within D4 / S4-S5 alters transition to an inactivated state and renders DRG neurons hyperexcitable	103
1. $Na_v1.7$ -M1627K located in the S4-S5 of D4 and implicated in PEPD, shifts voltage-dependent properties and increases ramp currents similarly to D3 / S4-S5 PEPD mutations	103
2. $Na_v1.7$ -PEPD mutations render DRG neurons hyperexcitable	113
C. Alternative splicing of $Na_v1.7$ exon 5 increases the impact of the painful PEPD mutant channel I1461T	114
1. Abbreviated background regarding $Na_v1.7$ alternative splicing	114
2. Splicing of exon 5 moderately alters WT $Na_v1.7$ channel properties	116
3. Exon 5A PEPD mutant channel affects activation, deactivation, CSI, and ramp current properties	122
4. D1 / S1 IEM mutant channel properties are not affected by exon 5 alternative splicing	126
D. Inherited mutations implicated in neuronal and muscle channelopathies can generate resurgent sodium currents in DRG neurons	134

1. Abbreviated introduction of resurgent currents and a potential role as a disease modifier in inherited voltage-gated sodium channelopathies	134
2. An inherited Na _v 1.7-PEPD disease mutation (I1461T) that destabilizes inactivation produces resurgent current in DRG neurons and increases action potential firing.....	136
3. A cardiac LQT3 / SIDS mutation that slows inactivation increases resurgent Na _v 1.5 currents and broadens action potential waveform in a modeled myocyte.....	144
4. A D4 / S4 PMC mutation that replaces a charged residue and uncouples fast inactivation generates resurgent sodium currents.....	147
5. A homologous inactivation gate mutation engineered into Na _v 1.6 channels dramatically increases resurgent currents and destabilizes transition to an inactivated state.....	149
E. Residues located in the D3 / S4-S5 linker of Na _v 1.7 directly stabilize an inactivated configuration	156
1. Abbreviated introduction for probing intramolecular interaction in ion channels.....	156
2. Cysteine substitution within D3 / S4-S5 and D3-D4 produces functional channels without dramatically altering gating properties.....	162

3. Residues (C1298 and C1299) within the Na _v 1.7 D3 / S4-S5 linker are accessible to MTSET modification and are critical sites for transition to an inactivated state.....	170
4. Proximity for direct interactions between the inactivation gate motif and residues within D3 / S4-S5 can be detected at potentials more negative than those required for Nav1.7 channel opening	178
5. Proposed models for state-dependent D3 / S4-S5 and D3-D4 interactions during transition to an inactivated state based on MTS experiments.....	188
IV. DISCUSSION	192
A. Dissertation research overview	192
B. Paroxysmal extreme pain disorder (PEPD) mutations within the D3 and D4 / S4-S5 linkers of Na _v 1.7 cause moderate destabilization of fast inactivation.....	195
1. Functional consequences of PEPD mutations.....	195
2. Structural role of the Na _v 1.7 D3 / S4-S5 cytosolic linker in channel gating	201
C. Alternative splicing of Na _v 1.7 exon 5 increases the impact of the painful PEPD mutant channel I1461T	204
1. Effects of alternative splicing on Na _v 1.7 disease mutations.....	204
2. Mechanistic implications from amino acid differences between Na _v 1.7 exon 5 splice variants	209

3. Global effects of alternative splicing	211
D. Inherited mutations implicated in neuronal and muscle channelopathies can generate resurgent sodium currents in DRG neurons	212
E. Residues located in the D3 / S4-S5 linker of Na _v 1.7 directly stabilize an inactivated configuration.....	222
F. Summation and future directions.....	230
V. REFERENCES.....	232

CURRICULUM VITAE

LIST OF TABLES

Table 1. Boltzmann parameters of channel activation and steady-state inactivation curves for WT and PEPD mutant Na _v 1.7 channels.....	81
Table 2. Development and recovery inactivation time constant values for WT and PEPD mutant Na _v 1.7 channels	91
Table 3. Comparative Boltzmann parameters of the voltage-dependence of channel activation and steady-state fast-inactivation curves for the respective splice variants of WT, IEM (I136V) and PEPD (I1461T) Na _v 1.7 channels	125
Table 4. Biophysical properties of wild-type and mutant Na _v 1.4, 5, 6 and 7 sodium channels tested for resurgent currents.....	153
Table 5. Boltzmann parameters of channel activation and steady-state inactivation curves for WT and Cys mutant channel constructs	168
Table 6 Recovery inactivation time constant values for WT and Cys mutant channel constructs.....	169

LIST OF FIGURES

Figure 1. Representative traces illustrating voltage-dependent ionic conductance and simplified gating scheme contributing to action potential (AP) generation	7
Figure 2. Representative schematics of voltage-gated sodium channel (VGSC) topology	14
Figure 3. Diagrammatic and sequence schemes of mutated regions within VGSC Na _v 1.7.....	74
Figure 4. Comparison of whole-cell ionic current traces and normalized current-voltage properties in CsF dominant electrode solution.....	76
Figure 5. Effects of PEPD mutations within D3 / S4-S5 and D3-D4 linkers on voltage-dependent gating properties of Na _v 1.7.....	80
Figure 6. Comparison of WT and mutant (I1461T) channels in the presence and absence of auxiliary β-subunits in CsF dominant electrode solution	83

Figure 7. Comparison of whole-cell ionic current traces and normalized current-voltage properties in CsCl/Cs-aspartate dominant electrode solution	85
Figure 8. Effects of D3 / S4-S5 PEPD mutations on inactivation kinetics	89
Figure 9. An adjacent and identical mutation within the D3 / S4-S5 linker of Na _v 1.7, not implicated in PEPD, displays altered voltage-dependent channel properties in a manner distinct from PEPD mutations.....	95
Figure 10. Comparison of kinetic profiles for development and recovery from inactivated (OSI and CSI) states for V1300F mutant and WT channels	98
Figure. 11. Comparison of the derived voltage-dependent slow inactivation properties for WT and mutant channels during transition between distinct states	102
Figure 12. M1627K currents decay slower than WT Na _v 1.7 currents	105
Figure 13. The M1627K mutation alters inactivation properties of Na _v 1.7	108

Figure 14. The M1627K mutation increases the amplitude of currents elicited by slow ramp depolarizations	112
Figure 15. Location of exon 5 splicing region and Na _v 1.7 mutations implicated in IEM and PEPD.....	118
Figure. 16. Effects of exon 5 alternative splicing on WT Na _v 1.7 channels.....	120
Figure 17. Alternative splicing modifies the voltage-dependent properties of the Na _v 1.7-PEPD mutation (I1461T) located in the putative inactivation gate	123
Figure 18. Alternative splicing of exon 5 in Na _v 1.7 does not affect gating properties of the D1 / S1 IEM mutant channels	127
Figure 19. Summary of changes observed in ramp current and potential mechanistic implications for the charge substitution difference between the Na _v 1.7 5N and the 5A splice variants in the D1 / S3-S4 linker	131
Figure 20. State occupancy diagram illustrates increased open-state probability for 5A PEPD mutant channels.....	133

Figure 21. Currents generated by recombinant $\text{Na}_v1.7$ channels expressed in DRG neurons	138
Figure 22. Quantification of resurgent current amplitude	140
Figure 23. Properties of endogenous and biolistically transfected recombinant VGSC currents in the presence and absence of TTX and / or $\text{Na}_v1.8$ -shRNA	141
Figure 24. Resurgent currents are produced by recombinant $\text{Na}_v1.7$ channels expressed in DRG neurons	142
Figure 25. Resurgent currents are produced by $\text{Na}_v1.5$ channels	146
Figure 26. A paramyotonia congenita mutation induces resurgent currents in $\text{Na}_v1.4$	148
Figure 27. $\text{Na}_v1.6$ channels generate large resurgent currents	150
Figure 28. Chemical modification and electrophysiological readout with an accessible engineered cysteine mutation upon internal MTSET application	160

Figure 29. Illustrations of cysteine amino acid modification in the presence and absence of the covalently crosslinking reagent MTS-1-MTS and the predicted effects on the currents assayed using whole-cell voltage-clamp electrophysiology.....	161
Figure 30. Comparison of whole-cell ionic current traces for wild-type (WT) and single / dual cysteine (Cys) modified Na _v 1.7 channels	163
Figure 31. Effects of single Cys substitutions within D3 / S4-S5 and D3-D4 linkers on voltage-dependent gating properties of Na _v 1.7.....	165
Figure 32. Voltage-dependent transitions for WT and Cys mutants can be assayed using specific electrophysiological test protocols	173
Figure 33. WT and single Cys mutant Na _v 1.7 accessibility to MTS modification at varied holding potentials.....	177
Figure 34. Representative current trace comparisons for dual Cys and WT channels in the presence and absence of MTS modification at three different holding potentials.....	180

Figure 35. State-dependent channel conformation locking upon application of an MTS crosslinking reagent	184
Figure 36. Summary of effects on Na _v 1.7 channel gating with MTSET modification	190
Figure 37. Cartoon summary of Na _v 1.7 D3 / S4-S5 crosslinking effects with the putative inactivation gate motif located in D3-D4	191
Figure 38. A D3 / S4-S5 PEPD mutation (V1299F) shifts steady-state inactivation and increases resurgent current amplitude compared to Na _v 1.7 wild-type and I1461T channels in transfected DRG neurons	216
Figure 39. Side chain volume of amino acid substitutions made within the Na _v 1.7 D3 / S4-S5 linker at a location critical for stabilizing inactivation which is mutated in PEPD	218

LIST OF ABBREVIATIONS

5A	“Adult” Exon 5 Splice Variant
5N	“Neonatal” Exon 5 Splice Variant
AP	Action Potential
ANOVA	Analysis of Variance
Arg (R)	Arginine
C	Closed
Ca ⁺⁺	Calcium ion
Ca _v	Voltage-gated Calcium Channel
CIP	Congenital Insensitivity to Pain
CNS	Central Nervous System
CSI	Closed-State Inactivation
Cys (C)	Cysteine
D1-D4	Domains of the Voltage-gated Sodium Channel
DMEM	Dulbecco’s Modified Eagle Medium
DRG	Dorsal Root Ganglion
EGFP	Enhanced Green Fluorescent Protein
G418	Neomycin
GDNF	Glial Cell-Line Derived Neurotrophic Factor
hEK ₂₉₃	Human Embryonic Kidney Cells
I	Inactivated
IEM	Inherited Erythromelalgia
IFMT	Isoleucine, Phenylalanine, Methionine, Threonine; Putative Inactivation Gate Motif
Ile (I)	Isoleucine
IRES	Internal Ribosome Entry Site
K ⁺	Potassium ion
K _v	Voltage-gated Potassium Channel
LA	Local Anesthetic
LQT3	Long-QT Type 3
Lys (K)	Lysine
Met (M)	Methionine
Na ⁺	Sodium ion
Na _v	Voltage-gated Sodium Channel
NGF	Nerve Growth Factor
O	Opened
OSI	Open-State Inactivation
PEPD	Paroxysmal Extreme Pain Disorder
Phe (F)	Phenylalanine
PMC	Paramyotonia Congenita
PNS	Peripheral Nervous System
S1-S6	Interdomain Segments of the Voltage-Gated Sodium Channel
SE	Standard Error

S.E.M.	Standard Error of the Mean
SIDS	Sudden Infant Death Syndrome
TEA	Tetraethylammonium Ion
Thr (T)	Threonine
TTX	Tetrodotoxin
TTX-s	Tetrodotoxin Sensitive
TTX-r	Tetrodotoxin Resistant
Val (V)	Valine
VGCC	Voltage-Gated Calcium Channel
VGKC	Voltage-Gated Potassium Channel
VGSC	Voltage-Gated Sodium Channel
V _m	Membrane Potential or Voltage
WT	Wild-type

“And instead of saying all of your goodbyes, let them know you realize that life goes fast, it's hard to make the good things last, you realize the sun doesn't go down, it's just an illusion caused by the world spinning round.”

Do You Realize??

The Flaming Lips

I. INTRODUCTION

A. Overview

Pain is a widespread medical epidemic. Defined by *The American Academy of Pain Management (AAPM)*, pain is “a complex mélange of emotions, culture, experience, spirit and sensation resulting from an unpleasant sensation and emotional response to that sensation”. Approximately 90 million people live with the devastating neurological disorder of chronic pain (“the disease of pain”) and of these, 45% will seek care at some point during their life, thus, accounting for about 20% of physician’s visits and 10% of drug sales. Unfortunately, treatment for such pain represents a major issue confronting our culture where many of the people suffering from pain are unable to find adequate pain relief. Furthermore, pain therapeutics to date, although initially effective, have the potential to produce addiction, physical dependence, tolerance, as well as unwanted side effects due, in part, to lack of target specificity. With remarkable advances in molecular biology, the scientific community is able to better understand the mechanisms involved in the generation of pain, which will allow for discovery of more unique therapeutic targets and appropriate drug design.

Pain transduction and perception involve complex biological events, utilizing several levels of the nervous system that originate from the periphery. Nociceptors, which are a subpopulation of primary sensory neurons activated by noxious, or painful, stimuli, are the primary afferent neurons where a component of chronic pain arising from pathology in the peripheral nervous system, termed

peripheral neuropathic pain, can be initiated. Compelling evidence suggests that this type of complex pain, is, at least in part, a result of changes in ion channels (transduction proteins) and additional key proteins (Woolf and Salter, 2000; Campbell and Meyer, 2006). In particular, neuronal voltage-gated sodium channels (VGSCs or Na_v) expressed in nociceptive dorsal root ganglia (DRG) neurons have been hypothesized to play a critical role in peripheral sensitization (Amir et al., 2006). VGSCs play a crucial role in generating action potentials (APs), which can transmit and relay information from the periphery to the high order neurons in the central nervous system (CNS) for interpretation.

Because a constellation of VGSCs are expressed in “pain sensing” neurons within the peripheral nervous system (PNS) a substantial amount of pain research has resourcefully exploited this relationship. Changes in neuronal VGSC expression and functional properties can contribute to increased excitability (hyperexcitability) in sensory neurons and increased pain sensation (Matzner and Devor, 1994; Waxman et al., 1994; Akopian et al., 1999). Thus, expression of specific VGSC isoforms in sensory neurons contributes to fine tuning the neuronal firing properties. However, because of the complexity of the VGSC subtype expression in DRG and lingering questions related to how structural changes in these channels affect gating, it has been difficult to determine the precise role of individual isoforms in neuronal hyperexcitability. Additionally, a lack of information regarding the tertiary structure of VGSC subtypes has complicated drug development targeting specific VGSCs. Therefore, a better understanding of the intramolecular interactions during

transitions between gating states will help determine (1) the contribution of specific isoforms during hyperexcitability of sensory neurons leading to peripheral sensitization and (2) potential target sites for therapeutic agents.

The central focus of this dissertation revolves around the structural and biophysical properties of the VGSC isoform $\text{Na}_v1.7$. $\text{Na}_v1.7$ channels, highly expressed peripheral and sympathetic nervous systems, are essential in nociception as evidenced by single point *missense* mutations causing a spectrum of pain syndromes (Drenth et al., 2001; Fertleman et al., 2006; Dib-Hajj et al., 2007), and *nonsense* mutations resulting in human insensitivity to pain (Cox et al., 2006). These studies indicate that $\text{Na}_v1.7$ is a critical component in the pain transduction pathway and, as such, structural perturbations to $\text{Na}_v1.7$ that affect conformational stability and response to changes in transmembrane voltage have the potential to cause extreme pain. Therefore, channelopathies, or inherited diseases caused by defects in ion channel proteins, associated with $\text{Na}_v1.7$ provide useful insight into structural mechanisms involved in channel gating and associated conformations which may aid in a more complete understanding of pain perception and development of novel channel-targeted therapeutic strategies to treat various painful disorders.

B. Brief history and background of voltage-gated sodium channels

Cells are enveloped by a highly lipophilic membrane which serves as a barrier to non-permeable solutes (Singer and Nicolson, 1972). This lipid barrier creates a charge separation across the membrane based on the intracellular and

extracellular charged ionic species composition yielding an electrochemical gradient / transmembrane potential (Cole, 1949a). However, specific modes of transport of these ionic species across the membrane and the importance of this process in communication between nerve and cells were a topic of great debate (Hille, 2001). A series of elegant experiments defining the period of classical biophysics (1935-1952), further established the ionic theory of membrane excitation. It was during this time that Nobel-prize winning (1963) pioneers Sir Alan L. Hodgkin and Sir Andrew F. Huxley published their work detailing the ionic components carrying transmembrane current and the application to conduction and excitation in nerve (Hodgkin and Huxley, 1952). Measuring changes in membrane current across the squid giant axon, Hodgkin and Huxley were able to accurately describe how kinetic changes in ion (Na^+ and K^+) permeability contribute to action potential (AP) generation by clamping the cellular membrane voltage (Cole, 1949b; Marmont, 1949; Hodgkin et al., 1952).

Clamping the membrane voltage enabled Hodgkin and Huxley to measure changes in ionic current, at fixed command membrane potentials, and allowed for a current-voltage relationship to be determined for particular ionic species. This technique differs from current-clamp, which records the variable membrane potential, determined by several ionic species, by injecting current into a cell through a recording electrode. Current-clamp is particularly useful for determining the specific phases of an AP. The voltage-dependent increase in Na^+ or K^+ permeability could be described by the changes in channel conductance for a particular ion species. The direction of the current through a

channel is based on the driving force through an electrochemical gradient according to Ohm's Law. Thus, it was hypothesized that at particular depolarized voltages, relative to the resting potential, Na^+ permeability increased. This was postulated to be based on mobile "activating particles" whose movement through the membrane to occupancy sites is accelerated during depolarization, increasing Na^+ conductance and allowing Na^+ to flow inward down its electrochemical gradient, driving the membrane potential towards the Na^+ reversal potential ($\sim +40$ mV). Because the inward current of Na^+ was transient, Hodgkin and Huxley theorized that separate mobile structures called "inactivating particles" could block the flow of Na^+ , thereby decreasing Na^+ permeability and conductance. The block or "inactivation" of Na^+ current would therefore allow for membrane repolarization and return to a resting potential. Thus, inactivation of Na^+ currents plays an important role during the AP refractory period by decreasing the response probability to an additional stimulus until a large fraction of channels have recovered from inactivation (reprimed or reset). On the other hand, K^+ currents are extremely important in determining resting membrane potential and firing frequency. These K^+ currents are also slowly activated during membrane depolarization, and therefore produce the outward current; flowing down its electrochemical gradient towards K^+ reversal (~ -70 mV), needed to repolarize the membrane potential in addition to Na^+ channel inactivation.

Together, the selective permeability and inward and outward flow of these ions, along with their unique voltage-dependent kinetics, predominantly account for the AP characteristics. However, the currents carried by additional ionic

species such as calcium (Ca^{++}) and chloride (Cl^-) can also alter the shape of the AP. Therefore, the AP represents a change in membrane potential caused by the flow of ions through selective pores in the membrane of excitable cells. Results from these experiments expanded on previous hypotheses (Hodgkin, 1937b, a; Hodgkin and Katz, 1949; Hille, 2001) and verified that changes in the membrane permeability of Na^+ and K^+ are controlled, in part, by changes in membrane voltage (Figure 1A) and that these permeability changes determine the waveform of an AP (Figures 1C and D). An AP waveform can be roughly broken down into three components: (1) a rising phase during membrane depolarization when Na^+ current activation and conductance dominates; (2) falling phase, where K^+ current activation and Na^+ current inactivation take over to repolarize the membrane potential and (3) recovery phase where currents can reprime for rapid regeneration of AP.

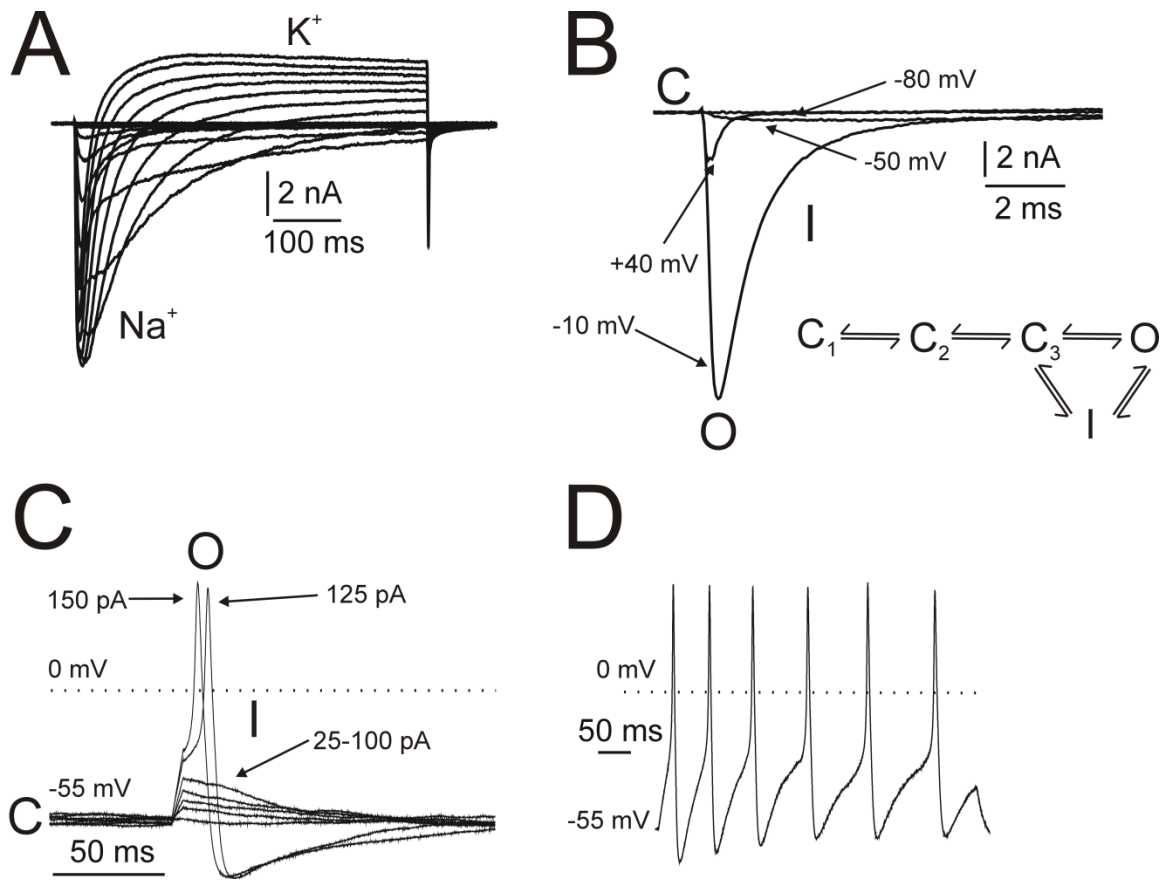


Figure 1. Representative traces illustrating voltage-dependent ionic conductance and simplified gating scheme contributing to action potential (AP) generation. (A) Whole-cell voltage-clamp recording from a small-medium diameter ($< 25 \mu\text{m}$; 16.08 pF) excitable rat dorsal root ganglia (DRG) cell. Inward sodium (Na^+) and outward potassium (K^+) current is noted. The cell was held at -100 mV and stepped from -80 mV to $+60 \text{ mV}$ in $+10 \text{ mV}$ increments. (B) Representative trace from a rat DRG cell transfected with $\text{Na}_v1.7\text{r}$ (see *Methods*). Highlighted traces represent changes in inward Na^+ conductance in response to depolarizing steps ($-80, -50, -10, +40 \text{ mV}$) in membrane potential towards Na^+ reversal potential ($+65 \text{ mV}$) passing through the various populations of voltage-dependent configurations defined as closed (C), open (O), and inactivated (I). Inset shows a simplified state-occupancy gating scheme using the same abbreviations as above. (C) Representative action potential (AP) recording from a rat DRG cell with a resting membrane potential of -55 mV and the response to injected steps ($+25 \text{ pA}$) of current (pA) required to elicit an AP. Dominant state occupancy of the population of VGSCs denoted with C, O, I along the AP shape. (D) Representative train of AP recordings in response to an injected ramp of current over a 500 ms duration.

Based on changes in membrane voltage, Hodgkin and Huxley hypothesized that ion permeability rapidly activates (rises) and inactivates (decays), a process governed, in part, by independent particles (*m* and *h*) or “gates” of conducting pores (Hodgkin and Huxley, 1952). Movement of these activating (*m*) and inactivating (*h*) particles or gates were postulated to act as molecular gatekeepers to allow or restrict Na⁺ flow through the membrane. For example, the rate, based on membrane potential and time, at which the activating (*m*) particle moves determines the rate of Na⁺ current and the rate at which Na⁺ current declines is based on the *h* particle rate of movement. However, further examination and manipulation of these processes required pharmacological intervention.

Toxins isolated from puffer fish and marine dinoflagellates, tetrodotoxin (TTX) and saxitoxin (STX) respectively, revealed that Na⁺ and K⁺ permeation were determined by independent “ion canals / channels” (Narahashi et al., 1964; Nakamura et al., 1965; Narahashi et al., 1967; Hille, 1968). These toxins selectively inhibited Na⁺ conductance, whereas the quaternary ammonium cation tetraethylammonium (TEA) selectively blocked K⁺ conductance (Tasaki and Hagiwar, 1957; Armstrong and Binstock, 1965). Taken together, these seminal experiments added molecular details to the hypothesis that Na⁺ conductance can be modulated by channels that undergo voltage-dependent conformational changes that transition the channel between closed (C), open (O), and inactivated (I) configurations, or states, in response to time, temperature, and membrane voltage (Figure 1). Transition through these states reveals specific

drug-receptor sites for molecules such as TEA. The binding sites for ligands such as TEA, TTX, and STX were useful for shedding light on the intracellular and extracellular topology of these voltage-sensitive channels. Further advancements (Hamill et al., 1981; Sakmann and Neher, 1984) to the voltage clamp technique allowed for increased resolution with recordings from patches of isolated cells expanding the understanding of voltage-dependent gating mechanisms. Experiments outlined throughout this dissertation utilize these electrophysiological techniques to study the voltage-dependent properties of a particular VGSC isoform.

C. Diversity of VGSC isoforms

Voltage-sensitive Na^+ conducting membrane canals, or VGSCs, are dynamic membrane-spanning proteins that play a crucial role in determining the electrical excitability in nerve and muscle (Hodgkin and Huxley, 1952). These channels exist as multi-subunit complexes in the lipid membrane consisting of a highly processed α -subunit that, when expressed alone, can produce functional current, which can also associate with multiple auxiliary β -subunits (Catterall et al., 2005). Nine isoforms of the highly homologous pore-forming α -subunit ($\text{Na}_v1.1-9$, 220-260 kDa) have been identified, each with subtle differences in channel properties likely due to differences in amino acid sequence (Catterall et al., 2005). The α -subunit is important for drug binding, ion selectivity, and pore formation (Catterall, 2000) whereas the auxiliary β -subunits (32-36 kDa) have been suggested to play a key role in channel modulation, adhesion, and

trafficking (Isom et al., 1992; Isom et al., 1995b; Isom et al., 1995a). In addition to the β -subunits, several other proteins interact with VGSCs (Wood et al., 2004) such as calmodulin (Herzog et al., 2003a) and annexin II (Okuse et al., 2002) for example. These interacting proteins have been found to modulate the functional properties of VGSCs.

The sequence conservation and redundancy between each of the various VGSC isoforms likely contributes to their broad similarities (ion selectivity and voltage-dependence), whereas differences in channel coding sequence between isoforms may play a role in evolutionary adaptation, such as pharmacological sensitivities (TTX-sensitive; TTX-s vs. TTX-resistant; TTX-r), kinetic properties (fast vs. slow activating / inactivating channels), or transcriptional editing and tissue specific transcription factors may account for the variety of regional distributions for VGSCs. For example, Na_v1.4 is highly expressed in skeletal muscle (Trimmer et al., 1989), whereas Na_v1.5 is predominantly located in cardiac tissue (Rogart et al., 1989). Interestingly, mRNA and current expression for Na_v1.5 is detectable in dorsal root ganglia (DRG) neurons (Renganathan et al., 2002). Na_v1.1, 1.2, and 1.6 channels are expressed in various combinations in adult CNS neurons (Trimmer and Rhodes, 2004). Adult DRG sensory neurons express a myriad of Na_v1.1, 1.6, 1.7, 1.8, and 1.9 VGSCs (Black et al., 1996; Dib-Hajj et al., 1998; Amaya et al., 2000). It is worth noting that Na_v1.3 is primarily expressed in immature neurons and can be upregulated to levels significantly above native levels under injurious conditions suggesting this

channel may be important in altered pain states (Beckh et al., 1989; Waxman et al., 1994; Boucher et al., 2000).

As mentioned above, the VGSC isoforms can also be pharmacologically separated by their sensitivity to TTX (Baer et al., 1976; Ritchie and Rogart, 1977; Klugbauer et al., 1995; Akopian et al., 1996; Dietrich et al., 1998; Cummins et al., 1999; Meadows et al., 2002), and classified as sensitive (TTX-s = 1-25 nM; Na_v1.1, 1.2, 1.3, 1.4, 1.6, and 1.7) or resistant (TTX-r = 1-60 mM; Na_v1.5, 1.8, and 1.9) to nanomolar (nM) or millimolar (mM) application of TTX. Furthermore, several of the VGSC isoforms can be distinguished by their unique current kinetics and steady-state voltage-dependent properties. For example, VGSC expressed in neurons of the central nervous system (CNS) produce rapidly activating and inactivating currents with a high degree of sensitivity to TTX (Ritchie and Rogart, 1977). Conversely, the population of VGSCs found in dorsal root ganglia (DRG) neurons generates rapid activating and inactivating TTX-s as well as slowly activating / inactivating and persistent TTX-r currents that display more complex kinetics and steady-state properties (Kostyuk et al., 1981). The diverse population of VGSCs and their unique voltage-dependent properties has been proposed to play a critical role in the fine-tuning of electrical communication, via AP generation and propagation in the tissues where they are expressed. With this in mind, alterations to the voltage-sensitivity of these channels and / or their expression patterns can significantly impact the generation and perception of electrical signals in the body.

D. Structural components and gating characteristics of VGSCs

1. *Abbreviated introduction*

As previously mentioned, VGSCs are dynamic Na⁺ conducting proteins with the intrinsic ability to transition between distinct gating configurations based on their capacity to “sense” changes in transmembrane potential. This is in contrast to transmembrane ion-permeable channels, such as nicotinic acetylcholine receptors (nAChR) and ionotropic gamma-aminobutyric acid (GABA_A) receptors that change configuration upon binding their namesake ligand. Several decades of research have shown that many of the characteristic features of VGSCs, such as pharmacological sensitivity and gating kinetics, are due to their unique structural properties, amino acid composition (primary structure) and signature motifs (secondary structure) in regions critical for gating, ion selectivity, and modulation which distinguish them from other ion permeable voltage-sensitive channels (Hille, 2001). The well-conserved topology of the VGSC α -subunit (220-260 kDa) structure (Figure 2A and B) consists of four domains (D1-D4). Biochemical and structural analyses, molecular cloning and hydropathy plots showed that each domain contains six transmembrane α -helical segments (S1-S6) that possess unique properties important for retaining a definitive channel structure (Levinson and Ellory, 1973; Beneski and Catterall, 1980; Noda et al., 1984; Durell and Guy, 1992). For example, evidence indicates the voltage-sensing components in voltage-dependent ion channels (i.e. Na_v, K_v, Ca_v) are the S1-S4 segments in each domain, where the highly positively

charged S4 segments are the mobile charge “voltage sensors” (Armstrong and Bezanilla, 1973; Armstrong, 1981; Stuhmer et al., 1989; Papazian et al., 1991; Chahine et al., 1994; Starace et al., 1997). Conversely, the S5-S6 segments and adjoining P-loops (S5-P-S6) form the aqueous ion-conducting channel pore and ion selectivity filter (Durell and Guy, 1992; Doyle et al., 1998; Yellen, 1998). Specifically, in response to changes in membrane potential, transitions between ion conducting (opened) and non-conducting (closed and inactivated) gating states (Figures 1B, 2B and C) have been linked to particular domains and segments of the channel that cooperatively result in changes to the channel configuration, thus allowing or restricting ion movement through the pore (Catterall, 2000). A description of the molecular components and interactions required for gating are discussed below.

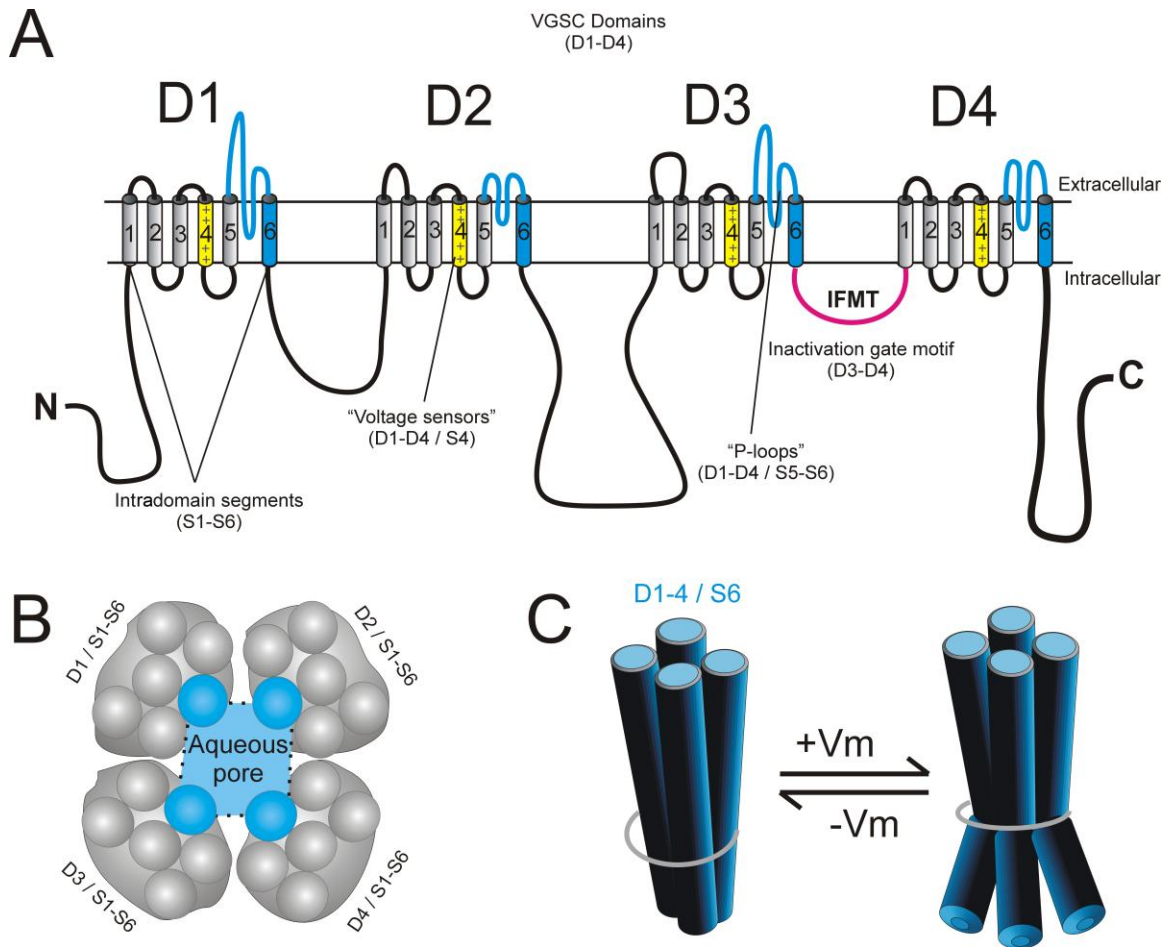


Figure 2. Representative schematics of voltage-gated sodium channel (VGSC) topology. (A) Linear representation of the VGSC topology including the four domains (D1-4) and plasma membrane-spanning intradomain segments (S1-S6). Noted are important mobile motifs for activation (positively-charged S4 "voltage sensors", colored in yellow) and inactivation (D3-D4 inactivation gate motif; colored in pink) gating. Pore forming regions are highlighted in blue. Critical D3-D4 inactivation gate tetrapeptide is labeled with one letter amino acid designations (IFMT) and channel terminal ends are abbreviated at the N and C-termini. (B) Top down extracellular view of the aqueous VGSC pore surrounded by the transmembrane segments. (C) Cartoon image of the structural changes of the pore-surrounding S6 alpha helices in response to changes in membrane potential (V_m). Upon membrane depolarization, residues near the hinge region (grayed half-circle) allow for conformational flexibility and distal S6 splaying conferring an open (ion-conducting) channel conformation. These figures were created using CorelDraw version 9 and were adapted from several models in the literature (Noda et al., 1984; Guy and Seetharamulu, 1986; Stuhmer et al., 1989; Guy and Conti, 1990; Catterall, 2000; Long et al., 2005a).

2. *Voltage-gated channel activation and associated gating charge movements*

Transition between gating states, in part, is determined by a focused electric field based on the ionic charge separation across a lipophilic membrane (capacitor), thus creating an electrical gradient (Asamoah et al., 2003; Sigg and Bezanilla, 2003). The charge gradient supplies voltage-sensitive channels with the potential energy required to surmount conformation-dependent energy barriers (Seoh et al., 1996). Hodgkin and Huxley originally postulated that “changes in ionic permeability depend on the movement of some component of the membrane which behaves as though it had a large charge or dipole moment” (Hodgkin and Huxley, 1952). The structural basis of their theory was validated after the VGSC was cloned. The S4 segments of the cloned VGSC were clustered with basic residues and were hypothesized to act as the voltage sensors (Noda et al., 1984). Indeed, in several electrophysiological experiments the voltage-dependent rise of inward Na^+ conductance described by Hodgkin and Huxley, was due to the mobile charge translocation through the electric field, thus activating the channel (Armstrong and Bezanilla, 1973; Keynes and Rojas, 1973; Armstrong and Bezanilla, 1974; Keynes and Rojas, 1974; Meves, 1974; Stuhmer et al., 1989) which precedes the channels adopting an open (ion-conducting) pore configuration. Upon charge translocation, the channel activation / *m* gates (Hodgkin and Huxley, 1952) were hypothesized to open and allow ion conductance. In contrast, deactivation, or transition from an open to a closed configuration, is thought to involve an integrated return of the S4 voltage-sensors

to a primed state, allowing the activation gates to close, and can, thus, be observed as a tail current of ionic current during membrane repolarization (Oxford, 1981; Kuo and Bean, 1994; Featherstone et al., 1998). The charge movement of the S4 segments through the electric field carried what was defined as gating current from a position buried in the membrane to an accessible extracellular space outside the membrane yielding an outward current (Armstrong and Bezanilla, 1973) distinct from the ionic pore-conducting current (Armstrong and Bezanilla, 1974; Bezanilla and Armstrong, 1974). The voltage-dependent accessibility of these once buried charges was further tested in relation to holding potential using site directed mutagenesis and extracellular pH manipulation or chemical modifying techniques (Yang and Horn, 1995; Larsson et al., 1996; Starace and Bezanilla, 2001; Ruta et al., 2005). These results suggest that the S4 segments donate a specific number of charged residues (per S4 segment) to the extracellular field during channel activation. Recent studies of gating current using fluorescent probes to track the timecourse of gating charge movement demonstrated there are two components (early and late) to VGSC gating charge movement and activation (Chanda and Bezanilla, 2002) determined by a separate gating particle that immobilizes the S4 gating charges (Cha et al., 1999). Thus, sequential S4 activation of all four VGSC S4 segments from membrane depolarization increases the probability, on a millisecond timescale, of channels transitioning to an open configuration. However, several hypotheses with regard to how the S4 segments translocate their charges have been suggested and highly debated.

Theoretical molecular models such as the “stepping ratchet” and “transporter model” involve relatively short distance (2-3 Å) charge movement, whereas the “helical screw” and the “paddle” models involve larger charge movements of 5-13 Å and 15-20 Å, respectively. Several techniques including electrophysiological recordings, scanning mutagenesis, site-directed accessibility studies, cross-linking, fluorometric techniques employing environment-sensitive dyes, and distance measurements using (fluorescence resonance energy transfer) FRET and (luminescence resonance energy transfer) LRET, have been used to track and characterize these movements (Hille, 2001; Tombola et al., 2006). Furthermore, site-directed mutagenesis studies based on inherited channelopathies, or diseases associated with ion channel dysfunction, have demonstrated that several VGSC mutations can alter the voltage-dependent properties of activation and ion conduction (Cannon, 2000; George, 2005; Meisler and Kearney, 2005; Koopmann et al., 2006; Catterall et al., 2008). Studies examining the underlying mechanisms involved in various ion channel disorders implicated in disease have been extremely useful in characterizing several ion channelopathies and the effects inherited mutations have on gating properties. Furthermore, these types of studies have been useful in probing the channels to determine their tertiary structure and topology. Together, these data suggest the movement of the S4 segments is a highly regulated process, determined in part by the primary and secondary structure.

3. Ionic current through a channel pore upon opening

Since ionic (hydrophilic) species will not simply diffuse through a lipophilic barrier, the structural components tethering and translating the voltage-sensing gating charge movement to ion flux through the membrane, and theoretically channel opening, remained somewhat elusive. Based on a model circuit analogy, existence of a conducting medium or pore would allow ion flux through a relatively low energy barrier or pathway. In a series of elegant experiments examining ion permeability, Hodgkin, Huxley, and Keynes, it was hypothesized that the positively charged ionic species pass along several negative charges, as suggested by Hodgkin and Huxley (1952) or in a single file through narrow tubes or channels thus accounting for variations in calculated flux ratios (Hodgkin and Keynes, 1955). Pharmacological experiments utilizing the membrane impermeable TEA⁺, suggested the presence of an aqueous K⁺ permeable pore (Armstrong and Binstock, 1965; Armstrong, 1966, 1969, 1971). It was hypothesized that intracellular application of TEA⁺ could bind to a putative receptor site; distinct from a receptor site from extracellular TEA application, to block K⁺ channels only if a conducting pore was open and available. Furthermore, this theoretical block by TEA⁺ could be overcome by increasing extracellular K⁺ concentration, suggesting a distinct pore block. This open channel block did not affect the inherent pore activation mechanism, however the blocking reaction did progress similarly to what Hodgkin and Huxley called inactivation based on increasing depolarization. Thus, the process of activation in response to depolarization appeared to allow access to an intracellular

receptor site for TEA that could occlude K^+ current (Armstrong, 1974). For the first time, a kinetic scheme detailing a state-dependent blocking event, based on membrane potential, was described suggesting the channel state may allow or deny access to aqueous receptor sites within the channel pore. Additional molecules, such as the local anesthetic lidocaine, exhibited similar voltage-dependent block of ionic current (Strichartz, 1973; Hille, 1977). These models suggested that intracellular application of local anesthetics could reach an ion binding site within the pore if the gating apparatus was open. Alternatively, local anesthetics could reach a binding site through the plasma membrane if one or both of the gates were closed. Taken together, these experiments showed that intracellular application of “blocking” molecules can abolish ionic current in a voltage-dependent manner once a pore-binding site becomes available however; the structural components involved were not resolved.

Structural predictions and analysis of the pore forming components of voltage-gated ion channels have been investigated by using site-directed scanning mutagenesis and cysteine accessibility, toxin binding, ion replacement, and computer modeling. These studies demonstrated that the S5-S6 linker, or P-loop, forms the outer vestibule and selectivity filter of voltage-gated ion channels and the membrane-spanning S6 segments align to form an pore (Hille, 2001). For VGSCs, the inner pore consists of the S6 segments from which the S5-P-S6 “P-loop” extends extracellularly from each of the four domains that contribute residues (DEKA motif; net charge -1) critical for permeant ion selection (selectivity filter) as determined by ion size and radius (Fozzard and Hanck,

1996; Marban et al., 1998). Thus, it was hypothesized that the S6 segments altered their conformation to selectively allow or restrict Na⁺ passage through the aqueous pore in response to changes in transmembrane potential as sensed by the S4 gating charge movement (Yellen, 1998).

Remarkable work from the MacKinnon laboratory finally shed light on the molecular details and components transmitting these gating movements to pore opening and ion selectivity by crystallizing several K⁺ channels in different conducting states (Doyle et al., 1998; Jiang et al., 2002; Jiang et al., 2003; Long et al., 2005b, a; Long et al., 2007). Their results yielded great insight into the molecular details of the aqueous cavity and pore-forming components of ion-selective channels and the way that certain ions are filtered. Further details were noted regarding how the channels open and close. The crystal structure of voltage-sensitive K⁺ channels showed critical motifs, such as (1) a well-conserved glycine residue near the middle of the S6 segments provides flexibility for opening; (2) hydrophobic residues near the intracellular portion of the S6 segments may interact with additional hydrophobic residues during opening; and (3) an S4-S5 linker appeared to come into close proximity of the distal portions of the S6 segments that may be critical for coupling gating charge movement to pore opening, (Long et al., 2005a). Indeed, studies examining the importance of residues in the pore domain (Soler-Llavina et al., 2006), including the putative “glycine hinge” region (Zhao et al., 2004; O'Reilly et al., 2008), and the S4-S5 and C-terminal portion of the S6 segments (Chen et al., 2001; Lu et al., 2001, 2002; Long et al., 2005a; Ferrer et al., 2006; Prole and Yellen, 2006; Labro et al.,

2008) demonstrated these regions of the channel are critical for voltage-sensitive channel opening. However, scanning mutagenesis studies of voltage-gated channels indicate that these regions are important “docking” sites required for the transition to / and stability of an inactivated state (Isacoff et al., 1991; McPhee et al., 1994, 1995; Tang et al., 1996; Lerche et al., 1997; Smith and Goldin, 1997; Filatov et al., 1998; McPhee et al., 1998; Tang et al., 1998; Popa et al., 2004). Because crystal structures capture proteins in only one, static conformation, as opposed to multiple snapshots of several dynamic voltage-dependent transitions, the molecular significance of these regions is still debated and highly studied.

4. The molecular mechanics of inactivation gating

Hodgkin and Huxley originally hypothesized (1952) that the voltage-dependent rate constants, over a millisecond (ms) timescale of the inactivation process did not intimately depend on the state of the rapid channel activation, and therefore were not coupled processes. However, subsequent studies using mathematical modeling (Hoyt, 1963, 1968) suggested the rise and fall of Na^+ conductance during depolarization depends on only one variable controlled by two or more coupled processes. This observation suggested that the voltage-dependence of inactivation (h) gating, proposed by Hodgkin and Huxley (1952), was derived from the more rapid voltage-dependent kinetics of activation gating. Evidence supporting these mathematical implications came from experiments measuring changes in gating currents in response to time and varied conditioning (pre) voltage pulses before a test pulse was implemented in a two-pulse protocol

(Goldman and Schauf, 1972). With a two-pulse protocol the experimenter can determine the fraction of channels accumulating in an inactivated state at specific voltages with respect to time. Results from this study demonstrated that inactivation depends on the Na^+ conductance during a test pulse and the rate of development is a function of the rise of Na^+ conductance during a conditioning pulse. Thus, the inactivation process could modify activation and gating charge movement by charge immobilization, suggesting the gating mechanisms were coupled.

Further studies investigating the mechanics of inactivation suggested a model for the transient, voltage-dependent current block which involved an intramolecular particle acting like a mobile ball tethered to a chain to plug the conducting channel pore (Armstrong and Bezanilla, 1977) and immobilize gating charge movement (Nonner, 1980). This “ball-and-chain” / “foot-in-the-door” inactivation model for channels inactivating from an ion-conducting state, defined as open-state inactivation (OSI), was based on previous studies showing that it was possible to prolong the timecourse of an AP in the presence of proteolytic enzymes, called proteases, or cross-linking reagents (Tasaki and Takenaka, 1964; Rojas and Atwater, 1967; Shrager et al., 1969; Takenaka and Yamagishi, 1969) and voltage-clamp studies internally perfusing pronase (Rojas and Armstrong, 1971; Armstrong et al., 1973), N-bromoacetamide (Oxford et al., 1978), or papain (Quandt, 1987). Notably, VGSCs had also been hypothesized to transition to an inactivated state directly from a resting or closed state, defined as closed-state inactivation (CSI). This idea was based on two key findings: (1)

macroscopic current results demonstrating that steady-state inactivation was accelerated at voltages more hyperpolarized than those required for full activation and Na⁺ conductance (Oxford and Pooler, 1975; Bean, 1981), and (2) single channel studies indicating the probability of inactivation did not depend on that of activation (Horn et al., 1981). Together, these studies suggested an inactivated state (fast inactivation; occurring rapidly on a millisecond timescale) that precedes *m* gate opening, which may also confirm one mode of *h* gate stabilization in the presence of local anesthetics, such as lidocaine, prior to channel activation, from a membrane phase (Hille, 1977).

Hypotheses for an additional inactivation gating mechanism were proposed based on several studies in nerve and muscle demonstrating that ionic conductance decreased during a prolonged depolarization of several seconds (Hille, 2001; Ulbricht, 2005). This type of inactivating mechanism, where development and recovery occur over a second to minute timescale, was defined as slow inactivation. Slow inactivation is distinct from the (fast) inactivation mechanism that rapidly occurs after activation and can be removed by intracellular proteolytic enzyme application (Rudy, 1978). This mechanism of slow inactivation had been postulated to contribute to the repolarization phase of an AP even after removal of fast inactivation aiding in return of the membrane potential to voltages where VGSC activation gates start to close (Armstrong et al., 1973). A more detailed examination of the voltage-dependent kinetics of slow inactivation in the presence of pronase was investigated in the squid giant axon (Rudy, 1978). Results from this study suggest four gating states (*c*; closed,

o; open, *h*; fast-inactivated and *s*; slow-inactivated) for VGSCs where slow inactivation can be accelerated upon destruction of the *h* (fast) inactivation gate. Occupancy of channels from an open state to a slow-inactivated state may therefore explain AP firing adaptation. However, upon removal of fast inactivation with enzymatic treatment that does not directly alter the slow inactivation gate, the development rate of slow inactivation is faster suggesting the fast and slow inactivation mechanisms may be modulated by one another based on the stability of their individual gates and / or channel occupancy in one of the inactivated states. However, the coupled nature of these two gating processes remains controversial because the structural components responsible for transition to a slow inactivated state have not been defined (Ruben et al., 1992; Vedantham and Cannon, 1998).

A suggestion for individual fast and slow inactivation gates came from studies demonstrating that trypsin, which is a serine protease with similar hydrolytic activity to a component in pronase (Rojas and Rudy, 1976), can differentially affect transition to a slow-inactivated state (Starkus and Shrager, 1978). A later kinetic analysis of the steady-state availability of VGSCs and potential interactions between activation and slow inactivation proposed that gating of slow inactivation is controlled by a separate, slow moving voltage sensor that may be electrostatically coupled to the activation voltage sensors (Ruben et al., 1992). Comprehensive state-occupancy models based on cumulative data from single channel, macroscopic and gating current analyses, where forward and reverse rate constants can be calculated at particular

voltages, have been developed to better explain the multi-state paths VGSC can traverse in response to changes in transmembrane voltage with respect to time and temperature (Vandenberg and Bezanilla, 1991). A critical feature that must be noted in the model is that channel recovery from an inactivated state does not traverse through an open state, implying that no ionic current can pass through the channel during recovery from an inactivated state when channels reprime to a closed state. A caveat to this transition, and will be discussed in further detail below, is the probability that ionic currents, in fact, can pass during repriming. These unique types of currents, that “resurge” during membrane repolarization are thought to arise from a competing molecule whose binding affinity is similar to that of the inactivation gate but upon binding only transiently competes with the fast inactivation gate (Raman and Bean, 1997). Thus, upon repolarization, channels that bind this competing particle allow a resurgence of current during a recovery protocol. The components responsible for this current and importance on gating and AP properties will be discussed in more detail in the following sections. Unfortunately, structural implications about the specific gating pathways in the absence of a crystal structure are complicated to validate. However, with the advent of molecular biology and studies utilizing scanning and site-directed mutagenesis, the molecular determinants governing transitions to and from the different inactivation mechanisms were able to be investigated further.

As stated above, upon S4 charge translocation and activation gate / S6 splaying open, Na⁺ conductance through VGSCs is rapidly occluded by a gating

mechanism called fast inactivation which appears to occur via pore blocking by an intracellular component of the channel. Conclusions from studies using blocking agents with specific amino acid side chain moieties (Rojas and Rudy, 1976; Eaton et al., 1978) and amino acid-specific proteolytic enzymes (Oxford et al., 1978) implied certain residues were critical for the binding affinity of the inactivation gate to the receptor site within the channel pore. Several years later, advancements in the field allowed molecular biologists to identify a putative inactivation gate motif within the D3-D4 loop (Stuhmer et al., 1989) critical for fast inactivation utilizing site-directed antibodies (Vassilev et al., 1988; Vassilev et al., 1989; Benz et al., 1997), a molecular scissor approach (Stuhmer et al., 1989), and scanning, deletion, and site-directed mutagenesis (Patton et al., 1992; West et al., 1992; Kellenberger et al., 1997). Collectively, these studies identified an amino acid triad motif (isoleucine, Ile; phenylalanine, Phe; methionine Met), whose one-letter designations are IFM, within the D3-D4 cytosolic linker that serves as a hydrophobic latch for a hinged lid formed by the D3-D4 linker required for complete fast inactivation in VGSCs to occur. Further mutagenic studies suggested that fast and slow inactivation gating mechanisms can be disrupted by mutating the Phe residue within the inactivation motif which was hypothesized to be important for coupling between the two inactivated states (Nuss et al., 1996). However, the extent to which these inactivating mechanisms may be coupled is questionable because longer conditioning pulses (50 sec) used to transition channels to “steady-state” slow inactivation showed no difference in available current from wild-type or Phe mutant Na_v1.4 channels

upon test depolarization (Cummins and Sigworth, 1996). The importance of the residues within the linker was also examined by internal peptide (one-letter amino acid nomenclature, KIFMK) application, bearing a similar triad motif. These studies demonstrated that upon removal of fast inactivation, the peptide mimetic could effectively restore fast inactivation suggesting a putative binding or receptor site for the inactivation gate (Eaholtz et al., 1994; Eaholtz et al., 1998; Eaholtz et al., 1999).

Experiments using substituted cysteine accessibility methods, or SCAM, which allow sulfhydryl chemical modification of engineered cysteine (Cys) residues (Karlin and Akabas, 1998), further validated the structural importance of the inactivation gate motif by demonstrating that (1) the chemical accessibility of the residues in the triad motif changes during depolarization (Kellenberger et al., 1996; Horn et al., 2000), (2) replacement of the aromatic Phe residue with a polar cysteine (Cys) causes incomplete inactivation, whereas modification of the Cys residue to include an aromatic group restored inactivation similar to unmodified channels (Chahine et al., 1997), (3) the hydrophobicity and aromatic side chain moiety Phe along with the location within the gate is critical for stabilizing inactivation (Deschenes et al., 1999), and (4) alterations within the triad motif critical for fast inactivation can disrupt the stability of local anesthetic binding (Vedantham and Cannon, 1999). NMR structural analysis of an isolated inactivation gate also indicates the triad motif faces an aqueous accessible region, with the Phe residue at the apex of the hydrophobic cluster, freely modifiable at hyperpolarized potentials when channel are closed, and may pivot

around hinge regions to bind to a receptor site within the intracellular portion of the channel (Rohl et al., 1999). Because the threonine (Thr) residue, downstream of the IFM motif, has been shown to be important for inactivation gating (Rohl et al., 1999), this dissertation will refer to the putative inactivation motif as a tetrapeptide (IFMT) motif within the D3-D4 linker. Additional scanning and site-directed mutagenesis studies in the D3-D4 linker of several VGSCs also indicate that charged residues and residues available for phosphorylation, adjacent to the triad motif, serve unique functions during gating charge immobilization, inactivation gate stabilization, and channel modulation (Hille, 2001; Ulbricht, 2005). It is worthwhile to note that the inactivation gate motif (IFMT) is highly conserved in all isoforms of VGSCs (Catterall, 2000), which may suggest unique importance for gating. An interesting study examining the importance of this hydrophobic motif during inactivation has shown that the motif can bind to a functional receptor site within *Shaker* K⁺ channels and block K⁺ flux (Patton et al., 1993). Several lines of evidence support the importance of these residues for gating based on single-point mutations within the inactivation gate motif that are implicated in numerous channelopathies associated with a wide range of inherited neuronal and muscle disorders (Cannon, 2000; George, 2005; Meisler and Kearney, 2005; Koopmann et al., 2006; Catterall et al., 2008).

An additional and somewhat controversial mechanism proposed to compete with inactivation gating has been postulated to underlie generation of a unique type of conductance defined as resurgent currents. In contrast to typical inactivation gating that transitions the channels into a refractory state, an

endogenous particle that transiently binds and competes with the inactivation gate, readily unbinds during repolarization and allows a resurgence of current to flow before channels would otherwise reprime (Raman and Bean, 1997, 2001). Structurally, the putative open-blocking particle, hypothesized to be the C-terminal tail of the auxiliary $\beta 4$ -subunit, has lower affinity for an overlapping inactivation “docking” motif compared to the inactivation gate motif (Grieco et al., 2005). Evidence supporting this competing mechanism came from studies that artificially slowed inactivation, upon toxin application, and increased the resurgence of Na^+ currents upon membrane repolarization (Grieco and Raman, 2004). Thus, it was suggested that by slowing transition to a fast-inactivated state, the opportunity for the open-blocking particle to bind was increased. Additional mechanisms, suggesting production of these currents can be tuned via post-translational modification (Grieco et al., 2002) and the unique cellular background of neuronal cells (Chen et al., 2008), have also been proposed. The TTX-s $\text{Na}_v1.6$ channels appear to predominantly generate resurgent currents (Raman et al., 1997; Cummins et al., 2005); these currents may be physiologically relevant in that they allow production of subthreshold Na^+ current relevant to repetitive AP firing which may be required for high-frequency firing in cerebellar Purkinje neurons (Raman and Bean, 1997). However, despite the critical importance of inactivation gating the putative receptor or “docking” sites for the inactivation motif are still not well defined and the molecular details regarding the stabilizing interactions during inactivation are still debated. Additionally, since inactivation of VGSCs is critical for repolarization of the

membrane potential during AP propagation, understanding the molecular details involved in channel inactivation can provide valuable insight into (1) the complexity of inactivation gating and AP propagation, (2) how the process is regulated and can become deregulated, thus, leading to disorders, and (3) strategies for pharmacological intervention because several therapeutic agents target this gating state.

From a structural standpoint, open-channel fast inactivation is thought to be tightly regulated by the D3 / S4 and (late) D4 / S4 translocation, coupling the voltage-dependent activation mechanisms to inactivation (Chahine et al., 1994; Chen et al., 1996; Kontis and Goldin, 1997; Kontis et al., 1997; Cha et al., 1999; Groome et al., 1999; Horn et al., 2000). However, very little is known about the definitive sites required to bind or stabilize the inactivation gate. Therefore, based on the aforementioned crystal structure of a voltage-sensitive K^+ channel and gating charge immobilization studies, one would predict that the C-terminal segments linking S4 charge translocators to the pore may be involved in “docking” of, or interactions with, the putative inactivation gate. The crystal structure of $K_v1.2$ (Long et al., 2005a) predicts the α -helical S4-S5 segments to be good candidates near the intracellular mouth of the channel pore where, based on the models for fast inactivation, the inactivation gate binds. Indeed, interaction or “docking” sites for the mobile inactivation gate have been proposed to be localized to the D3 and D4 / S4-S5 linkers and the distal portions of the S6 segments C-terminal to a flexible glycine hinge region within the aqueous pore (McPhee et al., 1994, 1995; Tang et al., 1996; Lerche et al., 1997; Smith and

Goldin, 1997; Filatov et al., 1998; McPhee et al., 1998; Tang et al., 1998; Popa et al., 2004). However, these data are variable and inconsistent and, moreover, contradict the early models suggesting the inactivation gate must bind to residues within the channel pore to occlude Na⁺ movement. Conclusions reached from these studies raise the following questions: (1) If the inactivation gate must bind within the channel pore why would mutations within the S4-S5 intracellular loops of D3 and D4 impair channel inactivation, (2) Is it possible that these intracellular loops of D3 and D4 sit within the proposed pore of the channel formed by the S6-segments, (3) Is it possible there are multiple binding sites for the inactivation gate that involve the S6-segments and intracellular loops of D3 and D4 working in a coordinated fashion to transition through a series of inactivated steps, and (4) Are structural differences in these regions key determinants in the variability of inactivation properties between VGSC subtypes? These intriguing questions inspired me to further investigate the role of D3 and D4 / S4-S5 linkers in stabilizing the putative inactivation gate and how these interactions relate to the structural changes of the channel during inactivation. Studies in this dissertation focus on residues in these regions of Na_v1.7, highly expressed in the PNS, because several single-point mutations located in these cytosolic linkers have been implicated in unique disorders resulting in extreme pain.

E. VGSCs and peripheral neuropathic pain

Neuropathic pain is pain that originates from pathology in the nervous system, both central (CNS) and peripheral (PNS), although a substantial amount of research has focused on neuropathic pain arising from peripheral regions. In particular, peripheral neuropathic pain is associated with sensitization of the nociceptive, “pain-sensing” neurons as a result of changes in ion channels (transduction proteins) and additional key proteins (Campbell and Meyer, 2006). These proteins determine the excitability of the nociceptive neurons (Matzner and Devor, 1994; Scholz and Woolf, 2007; Costigan et al., 2009). For example, expression and activity of several voltage-gated potassium channels (VGKCs) are important for setting resting membrane potential (RMP), repolarizing the membrane, and balancing AP firing frequency in excitable cells (Coetzee et al., 1999). Notably, manipulating the expression or gating of particular VGKC isoforms such as $K_v1.1$ (Clark and Tempel, 1998) and $K_v4.2$ (Hu et al., 2006) can increase sensitivity to mechanical and thermal nociceptive stimuli. Altered function of these two isoforms can influence neuronal excitability (Rogawski, 1985; Chi and Nicol, 2007) and would be expected to contribute to the population of potassium channels whose amplitudes are decreased under inflammatory conditions (Stewart et al., 2003). Additionally, neuronal VGSCs, expressed in dorsal root ganglia (DRG) neurons, are hypothesized to play a critical role in peripheral sensitization (Devor, 2006). Changes in neuronal DRG VGSC expression, which include a variety of pharmacologically and kinetically distinct populations (Kostyuk et al., 1981; Caffrey et al., 1992; Roy and Narahashi, 1992;

Elliott and Elliott, 1993; Ogata and Tatebayashi, 1993; Rizzo et al., 1994; Rush et al., 1998; Cummins et al., 1999), and functional properties can contribute to hyperexcitability in sensory neurons and to increased pain sensations. For example, the slow inactivating TTX-r currents may prolong action potential (AP) duration, thus modulating changes in neurotransmitter release (Amir et al., 2006), whereas TTX-s currents, including some persistent (or non-inactivating) currents in CNS and PNS neurons, significantly influence AP threshold (Baker et al., 1987; Crill, 1996; Cummins and Waxman, 1997). With several breakthroughs in molecular biology, including the molecular cloning of rat VGSCs (Beneski and Catterall, 1980; Hartshorne and Catterall, 1981), a more detailed picture of the role of particular VGSCs in determining cellular excitability has taken shape.

Na⁺ permeability was shown to play an important role in AP generation and propagation (Hodgkin and Huxley, 1952). Therefore, it was hypothesized that alterations in the voltage-sensitive channels controlling Na⁺ conductance would impact AP properties. However, this process was more intricate than originally postulated. The pharmacologically and kinetically distinct populations of VGSC currents were shown to be comprised of nine VGSC isoforms (Catterall et al., 2005). The evolutionary conservation of VGSCs has been thought to contribute to fine tuning mechanisms in excitable cells such as the DRG. Adult DRG neurons express a complex array of TTX-s (Na_v1.1, 1.3, 1.6, and 1.7) and TTX-r (Na_v1.8 and 1.9) sodium channels which play important roles in AP firing properties (Rush et al., 2007) suggesting these isoforms would be ideal targets for developing therapeutic strategies aimed at alleviating pain perception. For

example, the slow onset of closed-state inactivation and slow repriming properties of the TTX-s $\text{Na}_v1.7$ are thought to lend to ramp current generation and amplification of subthreshold stimuli which determine AP threshold parameters. TTX-s $\text{Na}_v1.6$ channels, which rapidly recover from inactivation (reprime), contribute to high frequency firing. Conversely, the relatively depolarized activation and inactivation characteristics of TTX-r $\text{Na}_v1.8$ channels are major current contributors to AP upstroke. Despite these distinctive gating features and relative contributions to AP firing, useful pharmacological intervention targeting specific VGSC isoforms, especially the TTX-s populations which contribute to nociception, remains extremely limited.

Compelling evidence suggests that under peripheral neuropathic pain conditions ectopic activity in primary (nociceptive) sensory neurons increases, of which, VGSCs can contribute. Changes in peripheral VGSC expression or gating kinetics, for example, during injury or with inherited channelopathies, respectively, have been proposed as modes to increase cellular excitability, thus contributing to nociception in primary afferent sensory neurons. Clinical studies have shown that administration of VGSC blockers such as lidocaine are efficacious and relieve symptoms of neuropathic pain in patients with painful peripheral neuropathies (Kastrup et al., 1987; Arner et al., 1990; Ferrante et al., 1996; Sindrup and Jensen, 1999). Experimental evidence suggests expression of several peripheral VGSC isoforms are altered in animal-modeled injury conditions (Amir et al., 2006). For example, $\text{Na}_v1.1$ and 1.2 are down-regulated following axotomy (Kim et al., 2001); however expression of the $\text{Na}_v1.3$ channel,

normally not found in adult DRG, is significantly up-regulated following complete and partial nerve injury and after induction of diabetes (Waxman et al., 1994; Black et al., 1999; Dib-Hajj et al., 1999; Kim et al., 2001; Craner et al., 2002). Of interest, axotomy-increased $\text{Na}_v1.3$ expression can be partially reversed (Leffler et al., 2002) by neurotrophic factors (glial cell-line derived neurotrophic factor; GDNF and nerve growth factor; NGF) which can experimentally rescue axotomized conditions (Fjell et al., 1999). Additionally, expression of $\text{Na}_v1.6$, 8, 9 have all been shown to be differentially regulated under modeled neuropathic pain conditions (Amir et al., 2006). Despite several mechanistic and behavioral studies indicating VGSC expression changes during modeled neuropathic pain conditions, few studies have genetically linked structural mutations that alter gating properties in “nociceptive VGSCs” to peripheral neuropathic pain. However, convincing evidence has accumulated in the past few years demonstrating that $\text{Na}_v1.7$ channelopathies that alter activation and inactivation characteristics are implicated in painful neuropathic disorders.

F. The $\text{Na}_v1.7$ VGSC isoform and pain

Research from this dissertation focuses primarily on the gating properties of the TTX-s VGSC isoform $\text{Na}_v1.7$, originally referred to as hNE(9) or PN1, which was initially cloned from neuroendocrine cells (Klugbauer et al., 1995). Transcripts from this isoform were not identified in pituitary gland, heart, brain, liver or kidney suggesting $\text{Na}_v1.7$ may be an evolutionary link between brain and muscle VGSCs (Klugbauer et al., 1995). The protein structure of $\text{Na}_v1.7$,

encoded by the *SCN9A* gene, is composed of 1977 amino acids and displays high homology to other isoforms in the VGSC superfamily (Catterall et al., 2005) with notable differences in the D1 / S5 extracellular loop and pore region, the D1-D2 intracellular loop and the carboxy (COOH) terminus (Figure 1). This isoform is predominantly expressed in neurons of the DRG and sympathetic ganglion within the PNS (Black et al., 1996; Sangameswaran et al., 1997; Toledo-Aral et al., 1997) compared to other isoforms previously mentioned. Additional studies have shown that Na_v1.7 immuno-staining is highly localized to the unmyelinated polymodal C-fibers of nociceptive neurons, suggesting Na_v1.7 channels may play a role in regulating the highly afferent “second pain” carried by the slowly conducting C-fibers (Djoughri et al., 2003).

The macroscopic kinetic features of Na_v1.7 currents indicate these channels rapidly activate and inactivate (Klugbauer et al., 1995) in response to strong membrane depolarization in a similar manner to other TTX-s VGSCs, however these currents develop (Cummins et al., 1998) and recover (Cummins et al., 1998; Herzog et al., 2003b) from inactivation in a more distinct fashion. The modest development of inactivation at intermediate potentials (i.e., at -60 mV before the population of channels have reached an open or conducting state), indicates Na_v1.7 channels slowly transition to closed-inactivated states, where a fraction of the S4 segments have activated, but channels are not in an open configuration (Oxford and Pooler, 1975; Armstrong, 2006). The relatively slow transitions of Na_v1.7 to and from closed-inactivated states are thought to contribute to production of physiologically relevant subthreshold currents in

response to slow depolarizing ramp stimuli at hyperpolarized potentials near resting membrane potential (RMP) for nociceptive DRG neurons (Rush et al., 2006; Rush et al., 2007). These $\text{Na}_v1.7$ ramp currents have been proposed to play roles in amplifying subthreshold currents at relatively hyperpolarized voltages nearing AP firing threshold (Cummins et al., 1998; Herzog et al., 2003b). Thus, the ramp current generated by $\text{Na}_v1.7$ channels is implicated as a critical component in determining AP firing threshold (Blair and Bean, 2002). The gating properties of $\text{Na}_v1.7$ channels are consistent with the firing rates of C-fibers where these channels were localized based on the aforementioned immuno-staining results. Taken together, $\text{Na}_v1.7$ channels are thought to be critical determinants in setting threshold for APs in small-diameter nociceptive neurons.

Indeed, peripheral tissue inflammation increases the amplitude of TTX-s currents in DRG neurons, which is paralleled by increased $\text{Na}_v1.7$ transcript and protein levels (Black et al., 2004). Additionally, the inflammatory cytokine, nerve growth factor (NGF), may contribute to the increased levels of $\text{Na}_v1.7$ during inflammation because NGF can upregulate $\text{Na}_v1.7$ (Toledo-Aral et al., 1995; Toledo-Aral et al., 1997; Gould et al., 2000). The increase of $\text{Na}_v1.7$ could increase neuronal excitability and modulate pain perception. However, additional studies have shown that mice with the $\text{Na}_v1.7$ gene selectively knocked out in nociceptive DRG neurons do not differ from wild-type counterparts in development of pain associated with a non-noxious mechanical stimulus or mechanoallodynia (Nassar et al., 2004). Furthermore, because expression of

specific VGSCs can contribute to determining neuronal excitability (Rush et al., 2006), mice with deleted $\text{Na}_v1.7$, critical for amplifying subthreshold currents, and 1.8, important for generating AP upstroke, channels were developed. In these mice mechanoallodynia develops normally compared to wild-type mice (Nassar et al., 2005). Additional studies have shown that $\text{Na}_v1.7$ expression is increased in rat DRG under induced conditions of diabetic neuropathy using streptozotocin as a trigger (Hong et al., 2004). Taken together, these results indicate $\text{Na}_v1.7$ plays an important role in inflammatory pain, but may not be a key regulator of neuropathic pain. However, the possibility for compensatory mechanisms that may work to counterbalance channel knockouts cannot be ruled out in these animal models. It should also be noted that, as discussed below, $\text{Na}_v1.7$ is critical in diseases associated with extreme pain in humans.

Interestingly, more than 20 single-point *missense* (gain-of-function) mutations, in the *SCN9A* gene encoding $\text{Na}_v1.7$ have been identified to date, and convincingly linked to two separate peripheral neuropathic pain syndromes: Inherited erythromelalgia (IEM) and paroxysmal extreme pain disorder (PEPD). These are inherited autosomal dominant disorders with remarkably distinct phenotypes (Fertleman et al., 2006; Dib-Hajj et al., 2007; Estacion et al., 2008; Choi et al., 2009; Fischer et al., 2009; Han et al., 2009). Although many cases described have been from an inherited origin, it should be noted that *de novo* mutations have been found (Yang et al., 2004; Fertleman et al., 2006; Han et al., 2006; Harty et al., 2006). IEM is characterized by intermittent attacks of extreme burning pain sensations associated with red, warm, and swollen hands, feet,

arms and torso that, when provoked, can lead to multiple flares a day (Drenth and Michiels, 1992; Orstavik et al., 2004; Drenth et al., 2005). These attacks initially occur within the first and second decades of life and can be triggered by mild warmth or exercise along with erythema and mild swelling in the areas of localized pain and are partially relieved by cooling these areas. Although treatment with sodium channel blockers is usually ineffective, some patients with IEM have reported relief from local anesthetics such as lidocaine and mexiletine (Kuhnert et al., 1999; Davis and Sandroni, 2002; Legroux-Crespel et al., 2003; Nathan et al., 2005).

Patients with PEPD, which was previously referred to as familiar rectal pain, report severe bouts of intense burning pain in the rectum, eye, and jaw (Hayden and Grossman, 1959; Fertleman et al., 2006; Fertleman et al., 2007). Initially, the pain can be localized to one or more of these areas during the attacks and then spreads towards the periphery. The sharp burning pain in these patients is usually accompanied by tonic posturing and flushing of the lower limbs which can start as early as birth (or *in utero*) and an itch component. Attacks associated with PEPD can be triggered by cold or visual irritants. These individuals, in contrast to IEM patients, appear to respond well to the use-dependent sodium channel inhibitor, carbamazepine, which preferentially binds to inactivated sodium channels.

It is interesting to note that Na_v1.7, along with other VGSC isoforms, can have alternative splice patterns yielding spliced variants of particular isoforms (Raymond et al., 2004). Alternative VGSC splicing can alter channel kinetics,

pharmacological sensitivity and tissue distribution under pathological conditions, and can also be developmentally regulated (Sarao et al., 1991; Dietrich et al., 1998; Alessandri-Haber et al., 2002; Tan et al., 2002; Zimmer et al., 2002; Copley, 2004; Fraser et al., 2005; Haufe et al., 2005; Onkal et al., 2008; Lossin, 2009). In particular, splicing within the exon 5 and 11 regions of the *SCN9A* gene result in long (L), short (S), adult (A) and neonatal (N) variants with differential biophysical properties and regulation (Chatelier et al., 2008) and expression patterns (Raymond et al., 2004). Further evidence suggests that $\text{Na}_v1.7$ splice variants are found in DRG neurons and that the splicing patterns of this isoform can change in response to spinal nerve ligation (Raymond et al., 2004), common model for neuropathic pain (Kim and Chung, 1992). Therefore, as discussed in more detail, I chose to examine the potential impact of splice variants on disease mutations.

In addition to pain-producing channelopathies that result from single-point missense mutations in $\text{Na}_v1.7$, there have been reports of individuals with a congenital inability to perceive any form of pain (CIP), but otherwise function normally except for deficits in olfaction (Goldberg et al., 2007) and changes in gait (Cox et al., 2006). These people have distinct homozygous *nonsense* mutations in the *SCN9A* gene that result in a loss-of-function of $\text{Na}_v1.7$ (Cox et al., 2006). The mutations are hypothesized to yield prematurely truncated proteins or nonsense mediated mRNA decay and loss of function of $\text{Na}_v1.7$ channels (Cox et al., 2006; Goldberg et al., 2007). Thus, mutations in $\text{Na}_v1.7$ channels resulting in a gain or loss-of-function suggest this channel may act as a

threshold sensor or gauge when interpreting stimuli as pain at critical interfaces between the periphery and central brain center in humans. Taken together, these results indicate the interpretation of pain is complex, multifaceted process that may intricately involve Na_v1.7 channels during signal transmission. These observations further suggest channel dysfunction associated with IEM and PEPD may offer additional insight into the pathophysiology of pain.

G. Understanding components critical to VGSC gating based on Na_v1.7 channelopathies

In absence of a fully solved VGSC crystal structure, channel mutations have provided significant insight into the molecular mechanics of voltage-dependent gating (Hille, 2001). Furthermore, the myriad of perturbations in channel structure implicated in inherited disorders have greatly enhanced the knowledge of how VGSCs are involved in the physiology of pain and offer the potential to link functional consequences, at a molecular level, to clinical phenotypes (Cannon, 2000; George, 2005; Meisler and Kearney, 2005; Koopmann et al., 2006; Catterall et al., 2008). Expression of recombinant channels in heterologous systems, such as hEK₂₉₃ cells (refer to *Methods*), has provided great detail on the effects of mutations on functional properties of the channel and as such, has been useful in determining how changes in channel function likely result in distinct channelopathies. Channelopathies, or inherited diseases caused by disturbances (such as mutations) in ion channel function, have been somewhat useful in practical translation of bench science to clinical

applications. As described above, missense (gain-of-function) mutations in the *SCN9A* gene encoding Na_v1.7 have been linked to the peripheral neuropathic pain syndromes: IEM and PEPD, inherited autosomal dominant disorders with distinct phenotypes hypothesized to arise from the specific alterations to Na_v1.7 gating based on the location of the mutation. For example, specific mutations in clustered regions of the channel known to alter activation and inactivation have been identified in IEM and PEPD. Many of the mutations overlap with additional inherited mutations in muscle and neuronal VGSCs suggesting these regions may be “hotspots” for mutation (Cannon, 2000; George, 2005; Meisler and Kearney, 2005; Koopmann et al., 2006; Catterall et al., 2008).

IEM mutations are generally located within the voltage-sensing segments and the pore forming regions of the channel responsible for channel activation and opening. Whole-cell voltage-clamp electrophysiological studies have demonstrated that IEM mutations predominantly affect activation and deactivation properties of the channel, resulting in a lowered threshold for activation response and increases in subthreshold currents in response to a depolarizing ramp stimulus (Dib-Hajj et al., 2007). The hyperpolarizing shifts in activation threshold therefore, increase the Na_v1.7 steady-state “window” of flowing current. Together, the alterations in voltage-dependence associated with IEM mutations produces a depolarization of RMP in DRG neurons which reduces current threshold for the all-or-none AP firing and increases repetitive firing to a given stimulus compared to WT channels (Dib-Hajj et al., 2005; Rush et al., 2006). Because the majority of IEM mutations are in regions involved in

activation and opening, one can hypothesize that IEM mutations alter the structural characteristics such that one of four potential conclusions can be reached. First, the mutations may alter the tight packing interactions and stability of a closed or default state at equilibrium potentials such that mutant channels now favor an open state and activate / open to subthreshold stimuli. Second, the mutations within the voltage-sensing components of the channel destabilize the buried position of the S4 segments within the plasma membrane such that, they move more freely in response to a smaller depolarizing stimulus, or that they are partially activated at a resting or closed state thus requiring less activation energy to open. Third, the mutations may uncouple the finely tuned mechanics of voltage-sensing and regulated channel opening. Fourth, mutations within the pore domain may alter the energetics of Na⁺ flux through the pore in response to small depolarizations. Unfortunately, these issues remain unresolved. But the location of the IEM mutations and the phenotype associated with this disorder are quite intriguing when compared to a second set of mutations in Na_v1.7 implicated in PEPD.

Mutations located in cytosolic linkers that lie within regions critical for inactivation, such as the D3-D4 inactivation gate motif and D3 / D4 S4-S5 linkers, have been genetically identified and implicated in PEPD. Voltage-dependent characterization of some of the PEPD mutations within the inactivation gate demonstrates that these mutations shift the steady-state properties to more depolarized potentials, causing a persistent component to the decay phase of the inward ionic currents that appears to be reduced upon carbamazepine

application (Fertleman et al., 2006). These results suggest PEPD mutations may increase window current by allowing channels to open at potentials that would normally inactivate channels. Thus, these changes would be predicted to have effects on the refractory period of an AP. However, the effects of several mutations outside of the putative inactivation gate on voltage-dependence and kinetic properties of Na_v1.7 channels were not characterized. Additionally, the effects of PEPD mutations on AP properties had not been evaluated. Together, the origins of these disorders is intriguing because they suggest single-point mutations within the same VGSC isoform can predominantly alter specific modes of gating which, along with cellular background (Rush et al., 2006), may contribute to the location of pain perception and response to therapeutic agents.

The spectral dichotomy of the effects of Na_v1.7 mutations, on gating and perceived pain are of great interest, in particular those implicated in PEPD, because there is still debate regarding the mechanics of channel inactivation and the role of specific regions during transition to this state and the resulting conformational change. Additionally, studies on sensory neuronal VGSCs, such as Na_v1.7 or Na_v1.8 are lacking and their role in nociception is still not completely understood. These observations are also fascinating in that single-point missense mutations in the same VGSC isoform can produce two distinct disorders and may provide information regarding how alterations in gating activity lead to specific types of chronic pain. Taken together, the PEPD mutations provide an excellent opportunity to better understand the intramolecular interactions of Na_v1.7 that play an important role in transition to the inactivated

state and may be a useful tool in understanding the etiology of pain and development of more selective therapeutic agents.

H. Hypothesis, specific aims, and summary of results

The following studies in this dissertation focus on residues in these regions of Na_v1.7 because several single-point mutations located in these cytosolic linkers have been implicated in PEPD and should yield insight into the complexities of stability of and transition to an inactivated state. The overall hypothesis of this dissertation is that PEPD mutations differentially alter the voltage-dependent properties of inactivation and that understanding the biophysical consequences of specific PEPD mutations will provide mechanistic insight into how sodium channel alterations can contribute to chronic pain and other disorders of excitability. Studies designed to test this hypothesis involved site-directed mutagenesis, whole-cell voltage and current-clamp electrophysiology, SCAM analysis and intramolecular cross-linking. To this extent, I first asked if PEPD mutations in the D3 and D4 S4-S5 linkers alter voltage-dependent inactivation properties and channel kinetics in a manner similar to PEPD mutations within the inactivation gate motif. Second, I asked if PEPD mutations in these cytosolic linkers destabilize inactivation, are the effects location and residue specific. Finally, I inquired if the PEPD mutations affect transition to an inactivated state, and if the mutations alter AP characteristics and propagation. Results from these studies demonstrate that (1) mutations within the S4-S5 linkers of D3 and D4 affect inactivation of Na_v1.7 in a residue-specific

manner, (2) PEPD mutations within S4-S5 differentially alter transition to a closed-inactivated state compared to those in the putative inactivation gate, and (3) PEPD mutations increase neuronal excitability. However, because the age-onset, response to therapeutic agents, “pain-inducing” triggers, and location of the perceived pain between IEM and PEPD patients differ, questions pertaining to the contributing factors for these differences remained unanswered.

Recent evidence suggested that alternative splice variants of Na_v1.7 are found in DRG neurons and that spinal nerve ligation in rats, can alter the splicing patterns of this isoform (Raymond et al., 2004). Therefore, the next question I asked was: Can alternative splicing of Na_v1.7 differentially affect the voltage-dependent properties of mutations implicated in IEM and / or PEPD and could this begin to explain some of the differences in sites of pain perception between the two disorders? The second aim of this dissertation was then, to examine the voltage-dependent effects alternative splicing of Na_v1.7 has on the impact of mutations implicated in IEM and PEPD. Results from these experiments (1) suggest an additive effect of Na_v1.7 exon 5 alternative splicing and the PEPD mutation (I1461T) which could further impact the disease phenotype and (2) offered insight into how alternative splicing within exon 5 affects specific intramolecular interactions critical for voltage-dependent gating.

We also considered the possibility that other contributing factors such as post-translational modifications and protein trafficking, cellular background, lipid environment, signaling mechanisms, and cellular reduction-oxidation balance may contribute to the differences noted between IEM and PEPD. Based on work

from this dissertation and the location of Na_v1.7 channels, an intriguing hypothesis we discussed was the potential for mutations implicated in PEPD to increase unique inward currents that flow through a channel population re-opening during membrane repolarization, termed resurgent currents. We hypothesized that inherited Na_v1.7-PEPD mutations could produce resurgent Na⁺ currents. Although Na_v1.6 channels appear to be the predominant generator of resurgent currents under normal conditions, we postulated that mutations that slow the rate of inactivation would increase resurgent currents because binding of the putative open-blocking particle to a theoretical receptor site may be enhanced. The initial aim of this study was to determine if PEPD mutations that slow the rate of inactivation increase resurgent currents in DRG neurons. Thus, we first evaluated the effects PEPD mutations had on the potential for Na_v1.7 channels, transfected into DRG neurons, to induce resurgent sodium currents. Exciting results from these studies demonstrated, for the first time that inherited mutations disrupting inactivation, associated with a variety of channelopathies (Na_v1.4-PMC; Na_v1.5-LQT3 / SIDS; Na_v1.7-PEPD) increased resurgent sodium currents. Additionally, because these currents flow at potentials near neuronal RMP, we showed that they could contribute to changes in neuronal and cardiac AP properties under computer-modeled conditions.

Finally, lingering questions regarding the molecular mechanics of inactivation and the contribution inherited mutations have on the stability of the channel structure and the potential these mutations have to induce unique sodium currents were examined using voltage-dependent conformational

probing. Thus, I asked if residues within the inactivation gate could directly interact with residues within the D3 / S4-S5 linker within a calibrated distance in a range of potentials. Results from studies utilizing site-directed mutagenesis, based on the location of PEPD mutations, SCAM, and cross-linking demonstrate that at potentials sufficient to induce closed-state inactivation key “docking” residues, outside the aqueous channel pore, within D3 / S4-S5 can interact with the inactivation gate motif within a calibrated distance. Therefore, mutations in these “hotspot” regions are appropriate to disrupt the stability of an inactivated state and contribute to increased resurgent currents, which together, can increase neuronal excitability.

Overall, this dissertation addresses important questions regarding the molecular mechanics required during transition to an inactivated state and the biophysical consequences of mutations in “hotspot” regions of Na_v1.7. Recent evidence demonstrating Na_v1.7 channels, highly expressed in DRG neurons, are essential in nociception (Dib-Hajj et al., 2007), as evidenced by the critical role these channels have in fine-tuning pain perception, validate the applicability of studying Na_v1.7 for discovery of isoform-specific therapeutic targets for treatment of painful disorders.

II. MATERIALS AND METHODS

A. Experimental cDNA constructs

Functional properties of VGSCs were studied by expressing recombinant channels in hEK₂₉₃ (human embryonic kidney) cells and dorsal root ganglia (DRG) neurons. Constructs encoding the open reading frame for the voltage-gated sodium channel (VGSC) α -subunit isoforms Na_v1.4, 1.5, 1.6, and 1.7, auxiliary VGSC β -subunits (β 1 and β 2) and an shRNA plasmid targeting the rat Na_v1.8 (rNa_v1.8) channels were used throughout the experiments in this dissertation. The human Na_v1.4 (hNa_v1.4) subtype was previously cloned (George et al., 1992). The sub-cloned hNa_v1.4pRc / CMV (Chahine et al., 1998) channel insert was then sub-cloned into the RBG4 vector containing the rat Na_v1.4 (rNa_v1.4) channel (Ukomadu et al., 1992) yielding a final hNa_v1.4pRBG4 construct to facilitate linker swapping between human and rat channels and to use the same promoter to control expression of the two inserts (Cummins et al., 2002). The hNa_v1.5 channel insert, originally located in a pSP64T vector (Gellens et al., 1992), was further sub-cloned into a pcDNA 3.1 vector in the lab of Dr. Theodore R. Cummins to aid in expression. The mouse Na_v1.6 (mNa_v1.6) channel insert was sub-cloned from the pLCT_{1-A} vector (Smith et al., 1998), which was modified from the pLCT₁ oocyte expression vector (Smith and Goldin, 1998), and inserted into a modified pcDNA3.1 vector (Klugbauer et al., 1995) yielding an mNa_v1.6pcDNA3.1 construct (Herzog et al., 2003a). The modified pcDNA 3.1 (-) vector allows for a low copy plasmid to be generated which aids in growing up

channel constructs. The hNa_v1.7 channel was previously cloned and constructed into the modified pcDNA 3.1 (-) vector (Klugbauer et al., 1995). Subsequent mutations inserted into the constructs listed above for all of the experiments discussed were all designed and performed within the lab of Dr. Theodore R. Cummins.

For select experiments recombinant VGSCs were expressed in DRG neurons. Since a population of TTX-s and TTX-r Na⁺ currents are functionally expressed in DRG neurons, we isolated our currents of interest pharmacologically and using RNA silencing methods. Recombinant channels used for rat DRG transfections were either naturally (Na_v1.5), or mutated to be (Na_v1.4, Na_v1.6, Na_v1.7), resistant to TTX. Thus, to aid in isolation and characterization of sodium currents generated in DRG neurons by recombinant VGSCs, cDNA constructs for Na_v1.4, Na_v1.6, and Na_v1.7 were modified with single point mutation to confer high resistance to TTX (K_i ~100 μM (Leffler et al., 2005); referred to as Na_v1.4r, 1.6r and 1.7r). These mutations were engineered using the QuikChange XL (Stratagene, La Jolla, CA, U.S.A.) mutagenesis kit as previously described (Herzog et al., 2003b; Herzog et al., 2003a). Na_v1.5 channels are natively resistant to TTX (K_i ~2 μM), therefore their sensitivity to TTX was not modified. Additional channelopathy constructs (Na_v1.4r-R1448P, Na_v1.5-F1486L, Na_v1.6r-I1477T and Na_v1.7r-I1461T) were made by inserting the respective mutation into the TTX-r cDNA constructs using the QuikChange XL (Stratagene, La Jolla, CA, U.S.A.) mutagenesis kit following manufacturer instructions. Mutations were confirmed by sequencing the entire insert region.

Experiments using hEK₂₉₃ cells as an expression system for transfected VGSCs were co-transfected with auxiliary human $\beta 1$ (h $\beta 1$) and $\beta 2$ (h $\beta 2$) subunits. Channel α -subunits were co-transfected with auxiliary β -subunits because studies have suggested the β -subunits play a role in trafficking and modulation of several VGSC isoforms and may be important for appropriate insertion and conformational stability in the membrane (Isom et al., 1992; Isom et al., 1995b; Isom et al., 1995a). The auxiliary h $\beta 1$ -subunit was sub-cloned into the pCD8-IRES (CD8: cluster of differentiation 8, IRES: internal ribosome entry site) vector yielding a pCD8-IRES-h $\beta 1$ construct. The h $\beta 2$ -subunit is located in the pEGFP-IRES vector yielding a pEGFP-IRES-h $\beta 2$ construct. Plasmids for the h $\beta 1$ and h $\beta 2$ auxiliary VGSC subunits were used for transient transfection of hEK₂₉₃ cells in their respective plasmid constructs (Lossin et al., 2002; Lossin et al., 2003). For example, upon transfection with the h $\beta 1$ construct hEK₂₉₃ cells will efficiently express both h $\beta 1$ and CD8, whereas the h $\beta 2$ construct will allow expression of h $\beta 2$ and EGFP. Since CD8 and EGFP are useful biological markers we can determine transfection efficiency. In particular, experiments in this dissertation utilizing transfected cell systems relied on expression of EGFP (Prasher et al., 1992; Chalfie et al., 1994) as a molecular determinant for patching cells because expression of the marker was assumed to correlate with channel and auxiliary subunit expression. It is worthwhile to note that experiments performed by Andrew D. Piekarcz from the lab of Dr. Theodore R. Cummins demonstrate that greater than 89% of hEK₂₉₃ cells expressing an

extracellular CD8 marker also express the h β 2 auxiliary subunit using Dynabeads (Dynai®, Brown Deer, WI, and U.S.A.).

A short hairpin RNA-mediated (shRNA) construct targeting the rat Na_v1.8 channel was also used in experiments with DRG neurons (Mikami and Yang, 2005). In short, this construct allowed the experimenter to knock down / silence the rat Na_v1.8 mRNA and abolish endogenous rat Na_v1.8 currents which could contaminate interpretation of results for the resurgent current studies. Na_v1.8 currents are TTX-r and can interfere with characterization of recombinant channel properties. Design of this construct (Mikami and Yang, 2005) was performed by identifying nineteen base pair targets for short interfering RNA within the coding sequence for rat Na_v1.8. A sense and antisense target sequence, linked by an 11 base pair loop (short hairpin construct) was then incorporated into an oligonucleotide reverse primer and PCR products were then sub-cloned into a Topo 2.1 vector (Invitrogen, Carlsbad, CA, U.S.A.). The vector was sequenced and the U6-shRNA cassette was digested and sub-cloned into the pLL3.7 lentivirus shuttle vector. Experiments utilizing this construct in rat DRG neurons were validated by knockdown of Na_v1.8 ionic current, which has distinct activation and inactivation kinetics compared to other endogenous VGSCs. Additionally, the rat Na_v1.8-shRNA was in an IRES-EGFP vector, allowing transfected cells to be selected visually based on the ability to express the green fluorescent protein EGFP (Prasher et al., 1992; Chalfie et al., 1994).

B. Mutagenesis of voltage-gated sodium channels

Site-directed mutagenesis of VGSCs were performed to characterize voltage-dependent effects of single-point missense mutations on several ($\text{Na}_v1.4$, 5, 6, 7) constructs. Studies using a substituted cysteine accessibility method (SCAM) (Karlin and Akabas, 1998) involved engineering dual cysteine (Cys) mutations into the $\text{Na}_v1.7$ constructs in order to perform chemical cross-linking of Cys residues. Additional studies required engineering a second chimeric point mutation in disease mutant constructs to endow them with resistance to TTX. The properties of the channels were examined using voltage and current-clamp electrophysiology in the appropriate expression system. Site-directed mutagenesis of VGSC constructs was performed using the channel constructs listed in the cDNA vectors section (above). Mutagenic primers were designed (Vector NTI Advance 10, Invitrogen, Carlsbad, CA, U.S.A.) to introduce the correct base pair change and anneal to the same sequence on opposite strands of the plasmid(s). Sequencing primers were ordered to verify mutated regions. QuikChange® II XL Site-Directed Mutagenesis Kits (Stratagene, La Jolla, CA, U.S.A.) were used according to the manufacturer's protocol. Mutant colonies were grown up following the QuikChange® protocol. After antibiotic-resistant colonies had grown on antibiotic / LB agar plates, individual colonies were selected using a 100 μL pipette tip and transferred to a 14 mL round bottom Falcon tube (Becton Dickinson Labware, Franklin Lakes, NJ, U.S.A.) containing 5 mL of LB broth and the appropriate antibiotic for mini culture initiation. The mini cultures were then placed in a 37°C shaking incubator (I2400 Incubator Shaker,

New Brunswick Scientific, Edison, NJ, U.S.A.) according to the plasmid miniprep kit (GeneJET™ Plasmid Miniprep Kit, Fermentas Life Sciences Inc., Glen Burnie, MD, U.S.A.).

Mini culture plasmid purification was performed according to manufacturer's protocol. Once the plasmid was purified and isolated, potential mutant constructs were screened using restriction enzyme digestion and confirmed by DNA sequencing using the corresponding sequence primers. DNA sequencing was performed at the DNA Sequencing Core Facility in the Biochemistry Biotechnology Facility of Indiana University School of Medicine (Indianapolis, IN, U.S.A.). After the sequence of the constructs was verified, maxi cultures were grown according to manufacturer's protocol (NucleoBond® Xtra Maxi Plus, Macherey-Nagel, Easton, PA, U.S.A.) in 1000 mL culture flasks in a 37°C shaking incubator.

When maxi cultures had grown, plasmid purification for downstream applications was followed according to manufacturer's protocol. After the maxi plasmid purification was complete, cDNA constructs were checked for purity (Nanodrop ND-1000 Spectrophotometer, Thermo Fisher Scientific Inc., Wilmington, DE, U.S.A.) and the concentration was brought to approximately 1 µg / µL with double distilled water. Purified constructs were then used for transfection and testing in an expression system.

C. Transient transfection of hEK₂₉₃ cells

Experiments utilizing human embryonic kidney (hEK₂₉₃; American Type Culture Collection, Manassas, VA, U.S.A.) cells for expression of various VGSC constructs were done using a calcium-phosphate transient transfection method, unless otherwise noted (such as the stable hNa_v1.7r_M1627K hEK₂₉₃ cell line which was selected based on neomycin / G418 resistance and cultured according to Dib-Hajj (2008) and used for voltage-clamp experiments with D4 / S4-S5 PEPD mutations). In brief, hEK₂₉₃ cells were grown under standard tissue culture conditions (37°C, 5% CO₂) in serum-complete (10% fetal bovine serum (FBS; Cellgro, Herndon, VA, U.S.A.) / 1% Penicillin-Streptomycin (Invitrogen, Grand Island, NY, U.S.A.)) Dulbecco's modified Eagle's medium (DMEM; Invitrogen, Grand Island, NY, U.S.A.) until a confluent density of 70-80% was obtained for a 35 mm culture dish (Corning Inc.®, Corning, NY, U.S.A.). At this point, the 10% serum-complete cell medium was exchanged out for a 5% reduced serum-complete cell medium and allowed to incubate under standard tissue culture conditions for approximately 30 minutes before the calcium-phosphate precipitation.

Next, transfection solutions (2M CaCl₂, double-distilled water, and 2X HBS = 1.6 g NaCl, 0.021 g Na₂HPO₄, 1.3 g Na-HEPES / 100 mL; adjusted to pH 7.0) and cDNA were allowed to equilibrate to room temperature. Various sets (i.e., 4 X 1.5 mL for one transfection condition) of tubes were labeled. The contents of the tubes were as follows:

Tube set 1

50 μ L 2X HBS

Tube set 2

2.8 μ g total cDNA (2 μ g α -subunit /
channel, 0.4 μ g β 1-subunit, 0.4 μ g β 2-
subunit)

5 μ L 2M CaCl_2

QS to 50 μ L with double distilled water

The contents of the tubes were allowed to sit for approximately 10 minutes before combination. Tube 2 was then added to Tube 1 drop-wise with vigorous stirring using the 100 μ L pipette tip. Four to five bubbles were then slowly generated, from the bottom of the tube, using the pipette tip. The calcium phosphate-DNA mixture was then incubated at room temperature for about 20-30 minutes after which it was then added, drop-wise, to the hEK₂₉₃ cells incubated in 5% reduced serum-complete medium and slowly rocked until the mixture dissolved.

The transfected cells were then left in the sterile Laminar tissue culture flow hood at room temperature for 15 minutes to allow the fine precipitate grains to settle onto the cells. After 15 minutes, the culture dishes were checked for a fine, dusting of precipitate grains sprinkled throughout the cells before return to the incubator for 2.5-3 hrs. Following this incubation, the 5% reduced serum-complete cell medium was exchanged twice for 10% serum-complete cell medium to remove precipitate before returning the transfected cells, in 10% serum-complete cell medium, to the incubator overnight.

Transfected cells were allowed to incubate for 24 hrs before re-plating onto 12 mm laminin-coated glass coverslips. To re-plate the cells, a fire polished glass Pasteur pipette was used to break up the cells and split them at a

moderate density (1-2 drops per coverslip) into single wells of a 24 well plate (Costar 3524, Corning Inc.®, Corning, NY, U.S.A.) containing 500 μ L of 10% serum-complete medium. Transfected hEK₂₉₃ cells were used for electrophysiological whole-cell patch clamp recordings 24-72 hrs post-transfection. Cells were selected based on the ability to express EGFP and used for data collection if whole-cell ionic current was obtained at greater than or equal to 1 nA to minimize signal to noise ratios during analysis.

D. Harvest and preparation of rat DRG neurons

Two to three month old male Sprague-Dawley rats (100-120 grams; Harlan Laboratories, Indianapolis, IN, U.S.A.) were used for DRG harvests under the Indiana University School of Medicine Laboratory Animal Resource Center Guidelines. The animal room was artificially illuminated from 7:00 A.M. to 7:00 P.M. Animal care was in accordance with the Guide for the Care and Use of Laboratory Animals (National Institutes of Health publication 85-23, Bethesda, MD, U.S.A.) and approved by the Institutional Animal Care and Use Committee of the Indiana University School of Medicine. Rat DRG neurons were studied after long-term culture (2-5 days).

The rat DRG harvest was performed as previously described using lumbar L4-L5 DRGs (Caffrey et al., 1992; Herzog et al., 2003b; Dib-Hajj et al., 2009). Briefly, rats are, first, rendered unconscious by exposure to CO₂ and decapitated to ensure sacrifice complying with the ethical guidelines described by the Indiana University School of Medicine. Skin surrounding the spinal column was cut away

with sterile tools and the spinal column was removed by making two lateral incisions, one through the upper (rostral) axis, and one through the lower (caudal) axis. The spinal column (~3-4 inches) was removed and excess muscle was trimmed away before cutting through vertebral column from the rostral to the caudal axis yielding two parts. The vertebral column was then placed in a 10 mL Petri dish (Corning Inc. ®, Corning, NY, U.S.A.) with cold bicarbonate-free DMEM (bfDMEM). DRG were manually isolated from the column using forceps and then placed in a clean Petri dish containing cold bfDMEM. Once the L4 and L5 ganglia were isolated, forceps and fine scissors were used to trim nerve roots from ganglia. Cells were then added to a cocktail of dissociation enzyme (2 mg/mL collagenase A, D and 5 mg/mL protease) and bfDMEM and incubated at 37°C with moderate shaking for approximately 40 minutes.

Enzyme treated cells were then placed into a 15 mL conical tube with bfDMEM at a final volume of 7 mL using a sterile glass pipette. Cells were broken apart using sterile fire polished pipettes in approximately 2-3 mL of 10% FBS / DMEM complete culture medium. Cell aliquots of about 100 µL were then plated onto 12 mm glass coverslips coated with poly-D-lysine and laminin within the wells of a 24-well plate. After 10-15 minutes wells were flooded with 500 µL of the complete culture medium and placed in an incubator. Cultures were maintained at 37°C in a 5% CO₂ incubator and the media was changed every two days until used for electrophysiological recordings.

E. Biolistic transfection of neurons

The biolistic transfection method utilized the Helios Gene Gun System from BioRad Laboratories (Hercules, CA, U.S.A.). Tubing, gold, polyvinylpyrrolidone (PVP), Tubing Prep Station, Helios Gene Gun, Gene Gun Barrels and Cartridge holders were ordered from BioRad Laboratories (Hercules, CA, U.S.A.). Protocols for this transfection method were optimized according to the experimenter's desired parameters to increase expression efficiency and health of transfected cells. Optimized protocols were designed and modified based on the manufacturer's instructions (Bio-Rad Laboratories Helios Gene Gun System) and a collaborating laboratory (Dib-Hajj et al., 2009). Briefly, a 24 inch piece of tubing was cut to fit the saddle of the Tubing Prep Station and ultrapure grade nitrogen (Praxair Inc., Indianapolis, IN, U.S.A.) was allowed to flow (0.3-0.4 LPM) through the plastic tubing for approximately 20 minutes to purge ambient oxygen contents and completely dry tubing. A 15 mg (1:1 ratio of mg gold to μg cDNA) aliquot of gold microcarriers (1 μm size) was weighed. Fresh aliquots were made from stock solutions of PVP (20 mg/mL) and spermidine (1 M) using fresh, high grade (dehydrated) ethanol (EtOH; Spectrum Chemical MGF. CORP., Gardena, CA. U.S.A.). Stock solutions were stored at -20°C. Final concentrations of PVP and spermidine aliquots are 0.05 mg/mL and 0.05 M, respectively.

Total volume of solutions was determined based on total cDNA volume. For experiments where rat DRG neurons were transfected, 10 μg of the rat

Na_v1.8-shRNA and 5 µg of channel plasmid were used. The calculated volumes of spermidine and 1 M CaCl₂ added were at a 1:1 ratio based on the total volume of the cDNA. Spermidine was added to the gold microcarriers and the complex was vigorously mixed by vortex and sonicated to break up large particles. Calculated amounts of cDNA were then added and mixed before adding 1 M CaCl₂ drop-wise while on the vortex. The complex was allowed to sit for 10 min before pelleting the complex and removing the liquid volume.

The gold-DNA pellet was then washed and reconstituted three times with the fresh dehydrated EtOH. After removal of the last EtOH wash, the gold-DNA complex was then washed out and reconstituted using the entire volume of the PVP aliquot and transferred to a 15 mL conical tube. The contents of the conical tube were drawn into the nitrogen purged tubing using a syringe and were carefully placed back into the Tubing Prep Station saddle. The complex rested in the tubing, undisturbed, for approximately 3-5 minutes before slowly removing the liquid (EtOH) contents with a syringe at a rate of 0.5-1.0 in/sec, after which the automatic rotation of the plastic tubing was started. After this time, the nitrogen was turned back on at a flow of 0.3-0.4 LPM for approximately 20 min. Cartridges were cut and placed into the Helios Gene Gun cartridge holder and contents were shot using the helium pressure within the gene gun onto 24 well plates containing 12 mm glass coverslips of recently harvested (~24 hrs) rat DRG neurons. Unused cartridges were placed in storage tubes with a dessicator pellet and stored in a dessicator at 4°C. Transfected neurons expressed EGFP

and green fluorescence was visible within 24 hrs post-transfection. Cells were patched 24-72 hrs post-transfection.

F. Chemicals

Experiments studying cysteine accessibility and cross-linking interactions made use of several methanethiosulfonate (MTS) reagents (Toronto Research Chemicals Inc., North York, ON, Canada). A 10 mM stock solution of the reagents [2-(Trimethylammonium)ethyl] methane thiosulfonate bromide (MTSET; F.W. 278.24 g/amu), Sodium (2-sulfonatoethyl) methanethiosulfonate / Methanesulfonothioic acid, sodium salt (MTSES; F.W. 242.28 g/amu), and Benzyl methanethiosulfonate (MTSBn; F.W. 340.30 g/amu) were prepared fresh using sterile double distilled water. Since the MTS reagents exhibit high reactivity in salt (nucleophile) solutions and rapidly undergo oxidation via hydrolysis the aliquots were prepared fresh before each individual recording by adding 65 μ L of the 10 mM MTSET stock into 585 μ L of the standard intracellular recording solution diluent to yield a 1 mM aliquot, unless otherwise noted. Fresh stock solutions (10 mM) of the non-water soluble cysteine cross-linking compound 1, 1-Methanediyl bismethanethiosulfonate (MTS-1-MTS; F.W. 236.35 g/amu) were prepared by dissolving the reagent with 3-5% DMSO/water diluents. Fresh aliquot solutions of MTS-1-MTS were prepared right before recording as outlined above to yield a final intracellular electrode concentration of 1 mM.

G. Solutions

1. Standard extracellular bathing solution for hEK₂₉₃ recordings

The standard hEK₂₉₃ extracellular bathing solution was used to bathe hEK₂₉₃ cells during all whole-cell voltage-clamp electrophysiology experiments utilizing transfected and non-transfected hEK₂₉₃ cells. The chemical components used for this recording solution (at ~304 mOsm) consisted of (in mM): 140 NaCl, 1 MgCl₂, 3 KCl, 1 CaCl₂, and 10 HEPES, pH 7.3 (adjusted with 1.0 N NaOH). Cells on glass coverslips were transferred to a recording chamber containing 250 μ L of bathing solution. Whole-cell electrophysiology experiments using hEK₂₉₃ cells were performed in the presence and absence of 500 nM (25 μ L of 5 μ M TTX stock into 225 μ L of extracellular bathing solution) TTX, depending on the experimental design.

2. Standard extracellular bathing solution for rat DRG neurons

The standard rat DRG extracellular bathing solution was used to bathe rat DRG neurons during all whole-cell voltage-clamp electrophysiology recordings utilizing transfected and non-transfected rat DRG neurons. The composition for this solution (at ~300 mOsm) consisted of (in mM): 130 NaCl, 30 TEA Chloride, 1 MgCl₂, 3 KCl, 1 CaCl₂, 0.05 CdCl₂, 10 HEPES, 10 D-Glucose. Recording solutions were adjusted using 1.0 N NaOH and D-Glucose to maintain physiological pH and osmolarity values. Cells on glass coverslips were

transferred to a recording chamber containing 250 μ L of bathing solution. Whole-cell electrophysiology experiments using DRG neurons were performed in the presence and absence of 500 nM (25 μ L of 5 μ M TTX stock into 225 μ L of extracellular bathing solution) TTX, depending on the experimental design.

3. *Standard CsF dominant electrode solution for hEK₂₉₃ recordings*

The standard CsF dominant electrode solution (at \sim 293 mOsm) used for all hEK₂₉₃ cellular recordings, unless otherwise noted, consisted of (in mM) 140 CsF, 10 NaCl, 1.1 EGTA, and 10 HEPES, pH 7.3 (adjusted with 1.0 N NaOH).

4. *Alternative CsCl electrode solution for hEK₂₉₃ recordings*

The alternative CsCl/Cs-aspartate dominant electrode solution (at \sim 293 mOsm) used for hEK₂₉₃ electrophysiological recordings, primarily for the D3 / S4-S5 Na_v1.7-PEPD characterization experiments, consisted of (in mM) 50 CsCl, 70 Cs-aspartate, 10 NaCl, 10 HEPES, 11 EGTA, 1 CaCl₂, and 2 Mg-ATP, pH 7.3. The standard bathing solution consisted of (in mM) 140 NaCl, 1 MgCl₂, 3 KCl, 1 CaCl₂, and 10 HEPES, pH 7.3 (adjusted with 1.0 N NaOH).

5. *Standard CsF dominant electrode solution for DRG neurons*

The standard CsF dominant electrode solution (at \sim 290 mOsm) used for all rat DRG recording experiments consisted of (in mM): 140 CsF, 10 NaCl, 1.1

EGTA, and 10 HEPES. Recording solutions were adjusted using 1.0 N NaOH and D-Glucose to maintain physiological pH and osmolarity values.

H. Whole-cell patch-clamp recordings for hEK₂₉₃ and rat DRG recordings

Fire-polished electrodes were fabricated from 1.7 mm VMR Scientific (West Chester, PA, U.S.A.) capillary glass using a Sutter P-97 puller (Novato, CA, U.S.A.). For rat DRG recording experiments, the tip exterior contact surface of the fire polished electrodes was coated in sticky wax (KerrLab, Orange, CA) to minimize capacitive artifacts and increase series resistance compensation. Cells on laminin-coated glass coverslips (12 mm) were transferred to a recording chamber containing 250 μ L of bathing solution in the presence or absence of 500 nM TTX to pharmacologically distinguish between TTX-s and resistant sodium currents. The recording chamber was designed from a 35 mm cell culture dish (Corning Inc.®, Corning, NY, U.S.A.) filled with silicone elastomer base (Sylgard®, World Precision Instruments Inc., Sarasota, FL, U.S.A.) mixed with curing agent, and allowed to solidify. After the solidification, a single 12 mm coverslip was placed in the center of the silicone and a razor blade scalpel was used to cut around the circular coverslip, and the loose inner portion was discarded. The center portion of the recording chamber was large enough to house, without solution leak, a coverslip and approximately 250-300 μ L of solution.

Recording chambers containing transfected cells were set onto an Nikon Eclipse TE2000-U inverted microscope stage (Nikon Instruments Inc., Melville,

NY, U.S.A.) equipped with a white (Nikon TE2-PS100W) and fluorescent halogen light source (X-Cite® 120, Photonic Solutions Inc., Mississauga, ON, Canada), Nikon contrast objectives (10X and 40X), and dual Nikon ocular lenses. The microscope was on an isolation nitrogen infused air table (50-60 psi maintained air pressure) with a 2 inch stainless steel laminate (63-500 Series, Technical Manufacturing Company, Peabody, MA, U.S.A.) to counter effects of vibration on the microscope stage. All electrophysiological experiments were performed on an air-table housed with a Faraday cage with multiple wires used to ground all metal surfaces to alleviate any aberrant electrical noise. The wires were run together at a single point on the air-table allowing a single wire to be connected to the ground input of the amplifier.

Detailed protocol for whole-cell voltage-clamp electrophysiology recordings can be found via online resources such as the Axon Guide to Patch Clamp (Axon Instruments, Foster City, CA, U.S.A.). In brief, whole-cell patch-clamp recordings were conducted using a HEKA EPC-10 amplifier (HEKA Instruments Inc., Bellmore, NY, U.S.A.) under voltage-clamp mode. Recordings were obtained at room temperature (~22.0°C; monitored using a temperature gauge; Fisher Scientific, U.S.A.) after obtaining a Giga-ohm seal (glass pipette tip to cell lipid membrane; 1-20 GΩ) Cells were selected based on their, morphology, and ability to express EGFP. However, for control experiments with rat DRG neurons, cells not expressing EGFP (non-transfected) were also utilized during recording experiments as controls. A fresh polished pipette electrode (pipette resistance ~1.0-5.0 MΩ) back-filled with the appropriate intracellular

solution was used for each recording. Offset potential was zeroed before patching the cell of interest. A silver chloride (AgCl) coated silver wire was used as a reference electrode with one end connected to the ground input of the amplifier headstage and the AgCl coated end directly inserted into the bathing solution. Capacitive artifacts were cancelled using the computer-controlled circuitry of the patch clamp amplifier. Liquid junction potential for all solutions was not corrected for during experiments and data analysis. Because for this dissertation, comparisons were always made between two groups of channel constructs or before and after drug application the relative shift would be within a predictable range for comparable groups and could be viewed as negligible. Series resistance errors, due to potential drop across the pipette and resistors in series with the pipette, were always compensated, typically between 70-90%, to be less than 3 mV during voltage-clamp recordings. Leak currents were linearly cancelled by digital P/-N subtraction (Bezanilla and Armstrong, 1977).

Membrane currents were sampled at 20 kHz and filtered at 5 kHz and tail currents were filtered at 10 kHz and sampled at 40 kHz. For the majority of hEK₂₉₃ and rat DRG experiments, data were collected only after five minutes of attaining the whole-cell configuration, this allowed adequate time for the electrode solution to equilibrate with the cytosol. However, for the cysteine accessibility and cross-linking experiments investigating potential intracellular interactions, recordings started approximately one minute after whole-cell configuration was established. Whole-cell patch recordings did not last more than 45 min and cells were not held in the standard bathing solution for more

than one hour. Inward Na^+ currents had a reversal potential of $\sim +65$ mV, corresponding closely to the calculated Nernst potential, observed during the standard I/V protocol. Data were acquired on a Windows-based Pentium IV computer (Dell Computers, Round Rock, TX, U.S.A.) using the Pulse program (v 8.65, HEKA Elektronik, Germany).

I. Standard patch-clamp protocol for voltage-clamp recordings

Holding potential for all hEK₂₉₃ recordings was set to -120 or -100 mV, unless otherwise noted as in the cysteine cross-linking experimental results section. Holding potential for all rat DRG recordings was set to -100 mV. Current-voltage (I/V) relationships were determined by an incremental depolarizing step protocol, testing every + 5 mV for 50 or 100 ms, from at least -80 to +60 mV. To determine the fraction of channels transitioning to a fast-inactivated state a double-pulse protocol (h_{∞}/V) was employed which incrementally conditioned the channels from -150 to -10 mV for 100 or 500 ms before testing for the fraction of channels available at 0 mV. Voltage-dependent deactivation kinetics were assessed by eliciting tail currents at a range of potentials after briefly activating the channels (0 mV, 0.5 ms). The averaged voltage-plot for deactivation was compiled using time constants (τ_d) obtained from tail current recordings which were determined by fitting each decay component with a single-exponential equation. Time course for the development of closed-state inactivation (CSI) was obtained using a time-varied conditioning pulse at various hyperpolarized potentials (mV) for 500 ms before testing for the

available fraction of channels at 0 mV for 20 ms. Time constants (τ) were determined using a single-exponential fit. Time course for the recovery from CSI was tested using a two-step protocol where the channels were conditioned at various potentials (mV) for 500 ms, then hyperpolarized to the holding potential for various times before testing for the fraction of channels available during a depolarizing step to 0 mV for 20 ms. Recovery from open-state inactivation (OSI) was tested by pre-pulsing to a relatively depolarized potential (0 mV, 20 ms) then hyperpolarized to various potentials between -120 to -60 mV for increasing time increments and were then tested for current available using a strong depolarizing stimulus to 0 mV for 20 ms. Plotted values were fitted with a single exponential function to determine time constant (τ) values. Generation of ramp current was assayed using a slow depolarizing ramp (0.27 mV/ms) stimulus from -120 mV to +40 mV at a holding potential of -120 mV. Inward ramp current displayed is a result of dividing the individual traces by the peak transient Na⁺ current obtained during the I/V protocol, thus yielding the percentage of peak current for each recording.

Channels capable of generating resurgent Na⁺ currents were tested using a two step protocol. Cells were assayed for the ability to produce resurgent sodium currents using a step protocol that initially conditioned the cells to +30 mV for 20 ms, from a holding potential of -100 mV, before repolarizing the membrane potential from 0 to -80 mV (in -5 mV increments) to test for resurgent current, then cells were returned to their holding potential. Resurgent sodium currents display distinct features (Raman and Bean, 1997) and these were used

to determine if a cell generated resurgent currents. For example, resurgent currents display a unique voltage-dependence where the peak resurgent currents are elicited by moderately hyperpolarized potentials relative to the holding potentials during the repolarizing steps. For all cells identified with resurgent current in the current study, maximal peak currents during the repolarizing pulses were produced within a window of potentials from -35 to -50 mV and were first observed around -10 mV. Additionally, these currents displayed unique gating kinetics within the window of potentials with a noticeably slower onset and decay phase. This is in contrast with classic VGSC tail currents, which are observed instantaneously following hyperpolarizing steps and decay within a few milliseconds. Currents were analyzed with leak subtraction on in PulseFit and were filtered at 1000 Hz to reduce noise but maintain the current waveform. The resurgent current amplitude was measured relative to the leak-subtracted baseline. The relative amplitude of the resurgent current was calculated as a percentage of the peak transient current by multiplying the peak resurgent current by 100 and then dividing by the peak transient current generated during a test pulse to -10 mV from a holding potential of -100 mV. The average resurgent current amplitude for each VGSC construct was only calculated using data from those cells where resurgent current was detected. Recordings contaminated with endogenous TTX-resistant currents, determined from steady-state inactivation plots were not used for further analysis. Cells that expressed recombinant currents with peak transient sodium current amplitudes that were less than 5 nA were also excluded from the overall analysis because of

uncertainties associated with measuring resurgent current amplitude in cells that had small peak current amplitudes.

J. Data analysis

Voltage-clamp experimental data were analyzed using the Pulsefit (v 8.65, HEKA Elektronik, Germany), Origin (v 7.0, OriginLab Corp., Northhampton, MA, U.S.A.), Prism (Prism v 4.0, GraphPad Software, La Jolla, CA, U.S.A.) and Microsoft Excel software programs. Normalized conductance-voltage (G-V) relationships were derived using Eq. 1:

$$(1) \quad G_{\text{Na}} = I_{\text{max}} / (V_{\text{m}} - E_{\text{Na}})$$

Where G_{Na} is macroscopic sodium conductance, I_{max} is calculated as peak current in response to the test pulse, V_{m} is the test pulse voltage, and E_{Na} is the measured Na^+ equilibrium potential. Normalized availability curves were fit using a standard single-phase Boltzmann distribution for G/V, during the m_{∞}/V protocol and steady-state fast-inactivation (h_{∞}/V) data. Midpoint ($V_{1/2}$) and slope factors (Z) of (activation) conductance-voltage (G/V) and voltage-dependent steady-state fast inactivation curves were calculated using a standard single-phase Boltzmann distribution fit according to Eq. 2:

$$(2) \quad I(V) = \text{Offset} + \left[\frac{\text{Amplitude}}{1 + \exp(-(V - V_{1/2}) / Z)} \right]$$

All data are shown as means \pm S.E.M. Comparison of frequency was determined using χ^2 test. Statistical significance was assessed with Microsoft

Excel using the 2-tailed Student's unpaired t -tests. Statistical significance of difference was accepted at P value less than 0.05.

III. RESULTS

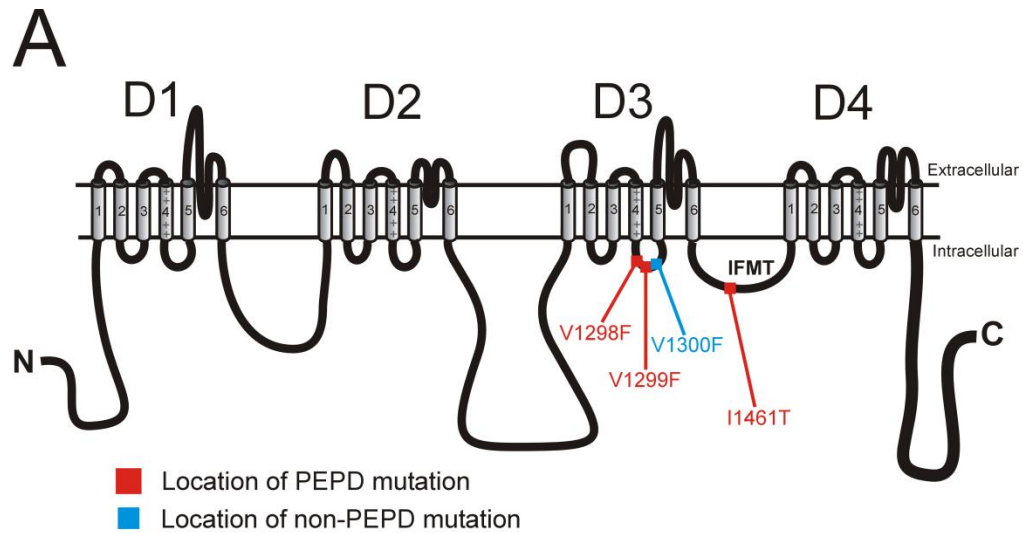
A. Paroxysmal extreme pain disorder (PEPD) mutations within the D3 / S4-S5 linker of Na_v1.7 cause moderate destabilization of fast inactivation

Based on the evidence presented in the *Introduction* section of this dissertation, the initial hypothesis for this series of experiments was that Na_v1.7 mutations identified in different families with PEPD would destabilize sodium channel inactivation, but the biophysical consequences of this destabilization would depend on the location of the mutation. Results from these studies were hypothesized to yield information about the putative “docking” sites critical for transition to an inactivated state.

1. PEPD mutations within the D3 / S4-S5 linker have small effects on the voltage dependence of channel conductance but do not alter deactivation time constants

The S4-S5 cytosolic linkers of several ion channels have been hypothesized to be a critical interface for inactivation gate “docking” interactions (Tang et al., 1996; Lerche et al., 1997; Smith and Goldin, 1997; Filatov et al., 1998; McPhee et al., 1998; Tang et al., 1998; Popa et al., 2004) and the packing of a closed / resting configuration and stability of a splayed-open channel configuration (Chen et al., 2001; Lu et al., 2002; Long et al., 2005a; Ferrer et al., 2006; Prole and Yellen, 2006; Soler-Llavina et al., 2006; Labro et al., 2008).

However, the structural role of residues within these cytosolic linkers during voltage-sensing / pore opening and stabilizing inactivation is not well understood. Thus, questions remain regarding the specific role of the S4-S5 linker during VGSC gating. Intriguingly, several mutations implicated in PEPD lie within these regions of Na_v1.7 (Figure 3). Several mutations are highly localized to cytosolic linkers, D3 and D4 / S4-S5 and D3-D4, of Na_v1.7 predicted to be critical components for inactivation gating. While some of the PEPD mutations were characterized and shown to alter transition to an inactivated state, several residues within the D3 / S4-S5 linker mutated in PEPD had not been functionally characterized. Therefore, our goal was to functionally characterize these D3 / S4-S5 PEPD mutations.



B

	<u> D3 S4 **S4-S5 linker* D3 S5 </u>
hNav1.7	KSLRTLRLRPLRALS RFEGMR V VNALIGAI PSIMNVLLVCLIFWLIFSIMGVNLFA
hNav1.1	KSLRTLRLRPLRALS RFEGMRVVNALLGAI PSIMNVLLVCLIFWLIFSIMGVNLFA
hNav1.2	KSLRTLRLRPLRALS RFEGMRVVNALLGAI PSIMNVLLVCLIFWLIFSIMGVNLFA
hNav1.3	KSLRTLRLRPLRALS RFEGMRVVNALLGAI PSIMNVLLVCLIFWLIFSIMGVNLFA
hNav1.4	KSLRTLRLRPLRALS RFEGMRVVNALLGAI PSIMNVLLVCLIFWLIFSIMGVNLFA
hNav1.5	KSLRTLRLRPLRALS RFEGMRVVNALLGAI PSIMNVLLVCLIFWLIFSIMGVNLFA
hNav1.6	KSLRTLRLRPLRALS RFEGMRVVNALLGAI PSIMNVLLVCLIFWLIFSIMGVNLFA
hNav1.8	KALRTLRLRPLRALS RFEGMRVVVDALVGAIP SIMNVLLVCLIFWLIFSIMGVNLFA
hNav1.9	KSFRTLRLRPLRALS SQFEGMKVVNALIGAIPAILNVLLVCLIFWLIVFCILGVYFFS

	<u> D3-D4 linker </u>
hNav1.7	QD I FMTEEQKKYYNAMKKLGS
hNav1.1	QDIFMTEEQKKYYNAMKKLGS
hNav1.2	QDIFMTEEQKKYYNAMKKLGS
hNav1.3	QDIFMTEEQKKYYNAMKKLGS
hNav1.4	KDIFMTEEQKKYYNAMKKLGS
hNav1.5	QDIFMTEEQKKYYNAMKKLGS
hNav1.6	QDIFMTEEQKKYYNAMKKLGS
hNav1.8	QDIFMTEEQKKYYNAMKKLGS
hNav1.9	QDIFMTEEQKKYYNAMKKLGS

Figure 3. Diagrammatic and sequence schemes of mutated regions within VGSC Na_v1.7. (A) Linear representation of VGSC α-subunit structure with putative inactivation motif labeled with amino acid residues IFMT. Mutations within the D3 / S4-S5 and D3-D4 linker implicated in PEPD are indicated with filled red square symbols. An adjacent and identical mutation (V1300F), not implicated in PEPD, is indicated with a filled blue square. (B) Sequence alignment of human voltage-gated sodium channels. Mutated residues implicated in PEPD are emphasized with bold lettering. Underlined are regions of Na_v1.7 mutated in this study which include adjacent hydrophobic valine residues (V1298, V1299, and V1300) within the D3 / S4-S5 cytosolic linker and the isoleucine within the putative inactivation motif (I1461) within the D3-D4 cytosolic linker.

To determine the effects of previously uncharacterized PEPD mutations in D3 / S4-S5, hEK₂₉₃ cells were transfected PEPD mutant and wild-type (WT) channel cDNA in order to establish the consequences of channel mutations on the voltage-dependent properties. Rapidly activating and inactivating TTX-sodium currents were observed in hEK₂₉₃ cells transiently co-transfected with cDNA for either WT or PEPD mutant Na_v1.7 channels and auxiliary hβ1 and hβ2-subunits (Figures 3 and 4). The Na_v1.7-PEPD mutant construct design was based on the location and residue substitution of three inherited mutations identified in three different families (Fertleman et al., 2006). Surprisingly, initial comparison of the current traces did not suggest any major differences in channel kinetics (Figure 4A) or current-voltage (I/V) properties (Figure 4B). However, expression levels of channels with the V1298F mutation (-144.4 ± 32.3 pA/pF, n = 7) were significantly lower than WT (-332.6 ± 59.4 pA/pF, n = 11), V1299F (-213.3 ± 63.6 pA/pF, n = 9), and I1461T (-321.3 ± 63.8 pA/pF, n = 14) channels as determined by current density.

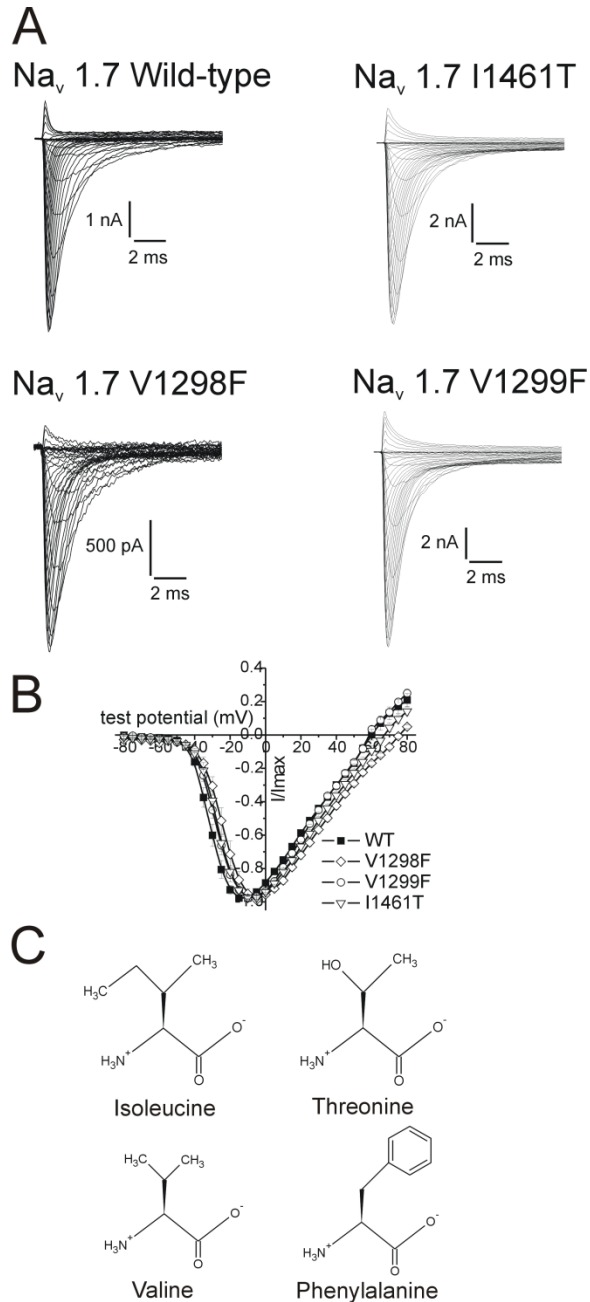


Figure 4. Comparison of whole-cell ionic current traces and normalized current-voltage properties in CsF dominant electrode solution. (A) Representative traces from WT and PEPD mutant Na_v1.7 channels co-expressed with β 1 and β 2-subunits in hEK₂₉₃ cells. (B) Normalized current-voltage (I - V) properties were assessed using depolarizing step pulses. Cells were held at -120 mV. The currents were elicited by 100 ms test pulses to various potentials from -80 to +90 mV stepped in increments of +5 mV. The peak current evoked by each pulse, normalized to the maximum peak current, is plotted versus the pulse voltage. (C) Two-dimensional representation of native amino acid residues and mutated side chain moieties implicated in PEPD.

Voltage-dependent gating properties were investigated to determine the effects of D3 / S4-S5 PEPD mutations on transitions between conducting and non-conducting channel states. The V1298F and V1299F mutations caused small, but significant (Table 1), depolarizing shifts in the voltage-dependence of channel conductance (G/V) and an increase in conductance slope factor for $Na_v1.7$ channels. These shifts were parameterized by fitting data to a single-phase Boltzmann function and comparing the voltage at which 50% of the channel population ($V_{1/2}$) was conducting Na^+ and the fitted slope factor (Z) at this voltage (Figure 5A). A significant shift in the $V_{1/2}$ of channel conductance or the slope factor for the PEPD mutation (I1461T) in the D3-D4 linker located in the putative inactivation gate was not observed, which suggests the I1461T mutation does not affect gating charge movement. The effects of the PEPD mutations on deactivation, which involves rapid, voltage-dependent transitions from open to closed states via an integrated return of the S4 voltage sensors to a primed position, were also evaluated (Oxford, 1981; Kuo and Bean, 1994; Featherstone et al., 1998). The voltage-dependent deactivation time constants (τ_d), examined by eliciting tail currents at a range of potentials after briefly activating the channels for the mutant PEPD channels, were not significantly affected when compared to WT (Figure 5B). Taken together, these data suggest that PEPD mutations within the D3 / S4-S5 segments can have some impact on transmission of voltage-sensing, from the S4 segments, to pore conductance of Na^+ . Although this does not appear to alter the coupling of S4 translocation to pore opening, it may affect the rate of S4 charge movement. Conversely, the

I1461T mutation which is within the inactivation gate motif, did not affect activation or pore conductance suggesting this region may not be critical for the initial activation gating process.

2. Mutations within the D3 / S4-S5 linker, implicated in PEPD, significantly shift the voltage dependence of the steady-state fast inactivation profile

The voltage-dependence of fast inactivation for WT and PEPD mutant channels was tested using a two-step protocol (Figure 5C) to determine the fraction of channels transitioning to an inactivated (non-conducting) state in response to changes in membrane potential. To ensure steady-state conditions (h_{∞}) over the full range of potentials tested, 500 ms conditioning pulses were used. The PEPD mutations (V1298F, V1299F, and I1461T) caused a significant depolarizing shift in the $V_{1/2}$ of fast inactivation with no significant change in slope factor. The $V_{1/2}$ of inactivation (defined as the voltage at which 50% of the channel population has transitioned to a non-conducting state) was depolarized by ~20 mV for each mutant channel (Table 1) compared to WT, thus, resulting in an increased fraction of mutant channels available to conduct Na^+ at more depolarized potentials. The increased availability is likely due to decreased stabilization of the inactivated states. To evaluate the contribution of decreased stabilization on the kinetics of the Na^+ current decay phase, the time constants for inactivation (τ_h) during depolarization to various potentials using a Hodgkin-Huxley (m^3h) model to estimate open-state inactivation were calculated (Figure

5D). At positive potentials (beyond -10 mV) the inactivation time constants for the PEPD mutant channels were significantly larger compared to WT channels (Table 2). Therefore, the decay phase of raw current traces for the PEPD mutants at +10 mV, a potential where the mutant channel time constants seemed to plateau in response to further depolarizing steps in voltage, was compared (Figure 5E). The decay phase of the current elicited for PEPD mutant traces was broader compared to WT (Figure 5E) and revealed a small persistent component (~6% normalized current remaining at 8 ms). Thus, it is possible PEPD mutations disrupt the molecular interactions required to stabilize the fast-inactivated state. However, this effect may be due to either (1) destabilization of a putative “docking” site, outside of the channel pore, for the inactivation gate motif directly affecting stabilizing interactions or (2) indirect modifications of C-terminal portions of the S6 segments which are required to be stabilized for the inactivation gate to bind within the intracellular mouth of the channel pore. Because the effects the PEPD mutations have on gating is measured based on changes in ion conductance through the pore, which is not a direct determinant of binding interactions, direct or indirect destabilization of transition to an inactivated state cannot be clearly defined. Nevertheless, because the voltage-dependent transition and the persistent current are affected with the PEPD mutations, one would postulate both direct and indirect changes may account for the destabilization.

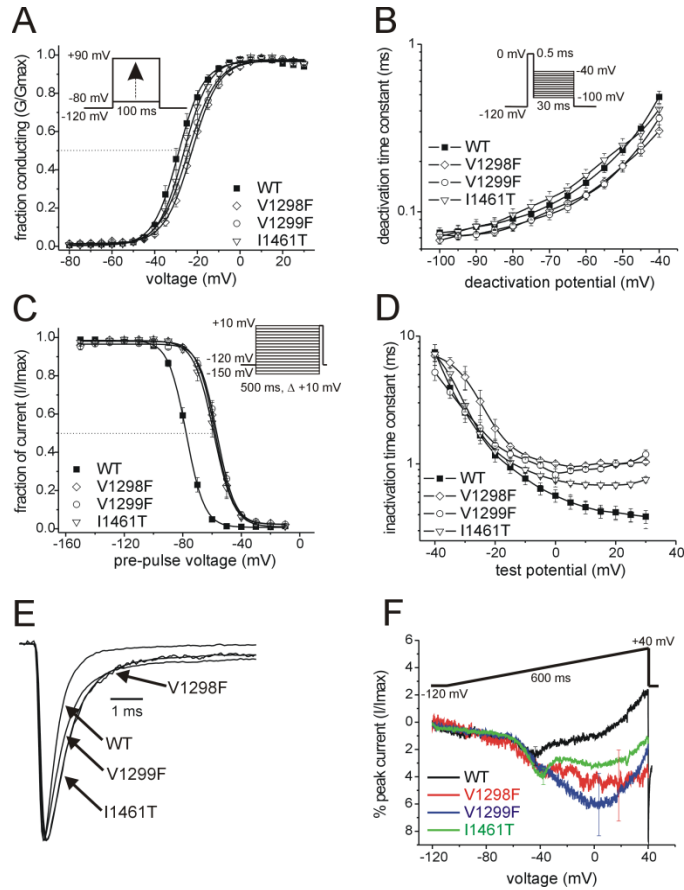


Figure 5. Effects of PEPD mutations within D3 / S4-S5 and D3-D4 linkers on voltage-dependent gating properties of Na_v1.7. (A) Comparison of the whole-cell conductance-voltage properties (G/V), calculated from current-voltage (I/V) relationship. (B) Voltage-dependent time constants for tail current deactivation (τ_d) at repolarization potentials ranging from -40 to -100 mV. (C) Comparison of steady-state inactivation for WT and mutant channels from a holding potential of -120 mV. (D) Time-constants for open-state fast-inactivation as a function of voltage for WT and mutant channels. The decay phases of currents elicited during channel activation protocol were fitted with a Hodgkin-Huxley type m^3h model to estimate open-state inactivation time constants (τ_h). (E) Representative normalized currents from whole-cell recordings of cells expressing either WT or PEPD mutant channels at +10 mV. (F) Averaged inward ramp current (I_{ramp}) traces ($n = 6-14$) elicited with a slow depolarizing (0.27 mV/ms) stimulus from a holding potential of -120 mV to +40 mV for PEPD mutant and WT channels. Ramp current amplitude is expressed as a percentage of the peak transient current elicited with a standard I/V protocol. Plotted values for (A) and (C) were normalized and fit with a single-phase Boltzmann distribution for WT and PEPD mutant channels. Voltage protocols are displayed within the insets.

Table 1. Boltzmann parameters of channel activation and steady-state inactivation curves for WT and PEPD mutant Na_v1.7 channels.

Channel	Voltage-dependence of activation			Voltage-dependence of steady-state fast-inactivation		
	V _{1/2} (mV)	Slope (mV/e-fold)	<i>n</i>	V _{1/2} (mV)	Slope (mV/e-fold)	<i>n</i>
WT	-28.9 ± 0.2	5.9 ± 0.2	11	-77.6 ± 0.1	6.1 ± 0.1	11
V1298F	-22.6 ± 0.2	6.4 ± 0.2	7	-57.8 ± 0.2	6.2 ± 0.2	7
V1299F	-24.4 ± 0.2	6.7 ± 0.2	9	-56.6 ± 0.2	6.1 ± 0.2	9
I1461T	-26.4 ± 0.2	6.0 ± 0.2	14	-58.8 ± 0.2	6.8 ± 0.2	14

Values derived for V_{1/2}, the voltage of half maximal activation and inactivation, and the slopes were derived from Boltzmann distribution fits to the averaged and normalized (± S.E.M.) voltage-dependence of activation and steady-state inactivation curves.

Although impaired fast inactivation was observed with the PEPD mutations, the severity of the impairment produced by the I1461T mutation was much less than that previously reported for this mutation (Fertleman et al., 2007). Fertleman and colleagues observed a similar depolarizing shift in voltage-dependence of inactivation; however a 40% non-inactivating component was reported. One possible reason for the differences observed was that we co-transfect the Na_v1.7 cDNAs with auxiliary β 1 and β 2-subunits and they did not. This raises the question as to the role β -subunits play in modulating gating transitions. Therefore, hEK₂₉₃ cells were co-transfected with WT or I1461T constructs with and without β -subunits (using EGFP as our transfection control), to determine if this might influence the size of the non-inactivating component (Figure 6). The inclusion or exclusion of β -subunits during hEK₂₉₃ transfection did not increase the non-inactivating component of WT or I1461T currents. Thus, these results suggest that the differences noted in the non-inactivating component between Fertleman et al. and our lab are not accounted for by the presence or absence of the auxiliary β 1 and β 2-subunits.

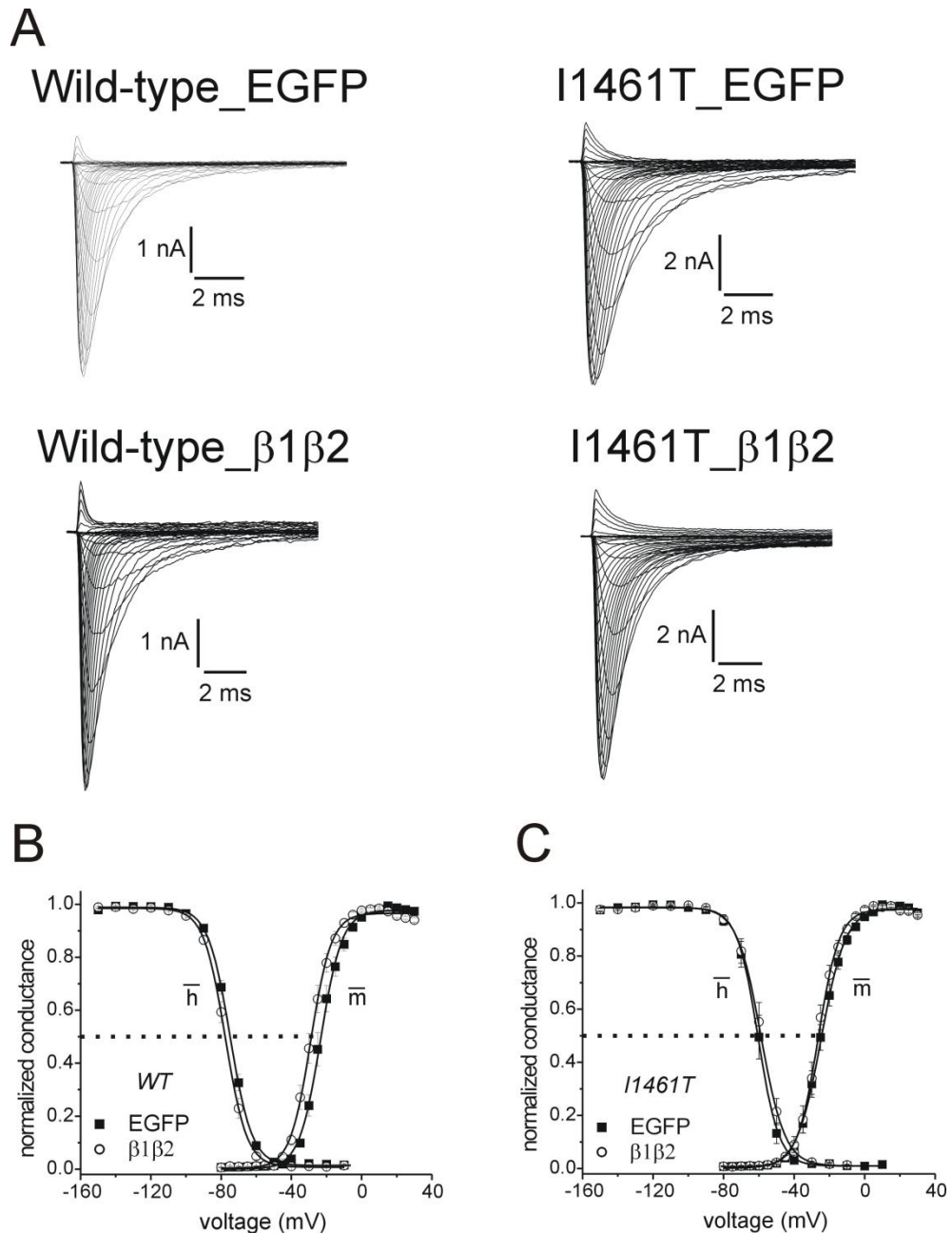


Figure 6. Comparison of WT and mutant (I1461T) channels in the presence and absence of auxiliary β -subunits in CsF dominant electrode solution. (A) Representative traces for WT and mutant (I1461T) channels co-transfected with EGFP or β -subunits. (B) Normalized fraction of available WT channels in response to changes in membrane potential co-transfected with EGFP or β -subunits. (C) Normalized fraction of mutant (I1461T) channels available over a range of tested potentials co-transfected with EGFP or β -subunits. Data for (B) and (C) were fit using a standard single-phase Boltzmann distribution.

Another possible factor for the discrepancy between observations was that we used 140 mM CsF in our electrode solution and Fertleman et al. used 13 mM CsF. Fluoride has been reported to alter persistent sodium currents in Na_v1.3 channels (Chen et al., 2000; Meadows et al., 2002). Therefore, additional recordings of V1299F, I1461T and WT channels using a CsCl/Cs-aspartate dominant electrode solution that did not contain fluoride were performed (Figure 7). The voltage-dependence of channel conductance and steady-state fast inactivation obtained with this solution were depolarized compared to those obtained with fluoride as has been observed with other VGSC experiments, but we did not see evidence of incomplete steady-state inactivation. However, the amount of persistent current observed at the end of 25 ms depolarizing pulses was slightly greater in the absence of fluoride for I1461T (~8% of peak) and V1299F (~15% of peak). This data was consistent with observations suggesting VGSCs can mediate more pronounced persistent currents when recorded from an hEK₂₉₃ expression system in the absence of intracellular fluoride ions (Chen et al., 2000; Meadows et al., 2002). However, differences between the components of the electrode solutions between these experiments and those of Fertleman et al. do not completely explain the observation of a non-inactivating component (Fertleman et al., 2006). Thus, one may reach the conclusion that Fertleman and colleagues did not use an appropriate duration for a conditioning pulse to examine transition to a fast-inactivated state for Na_v1.7 channels which could lead to an exaggeration of the effects of mutations implicated in PEPD that affect inactivation.

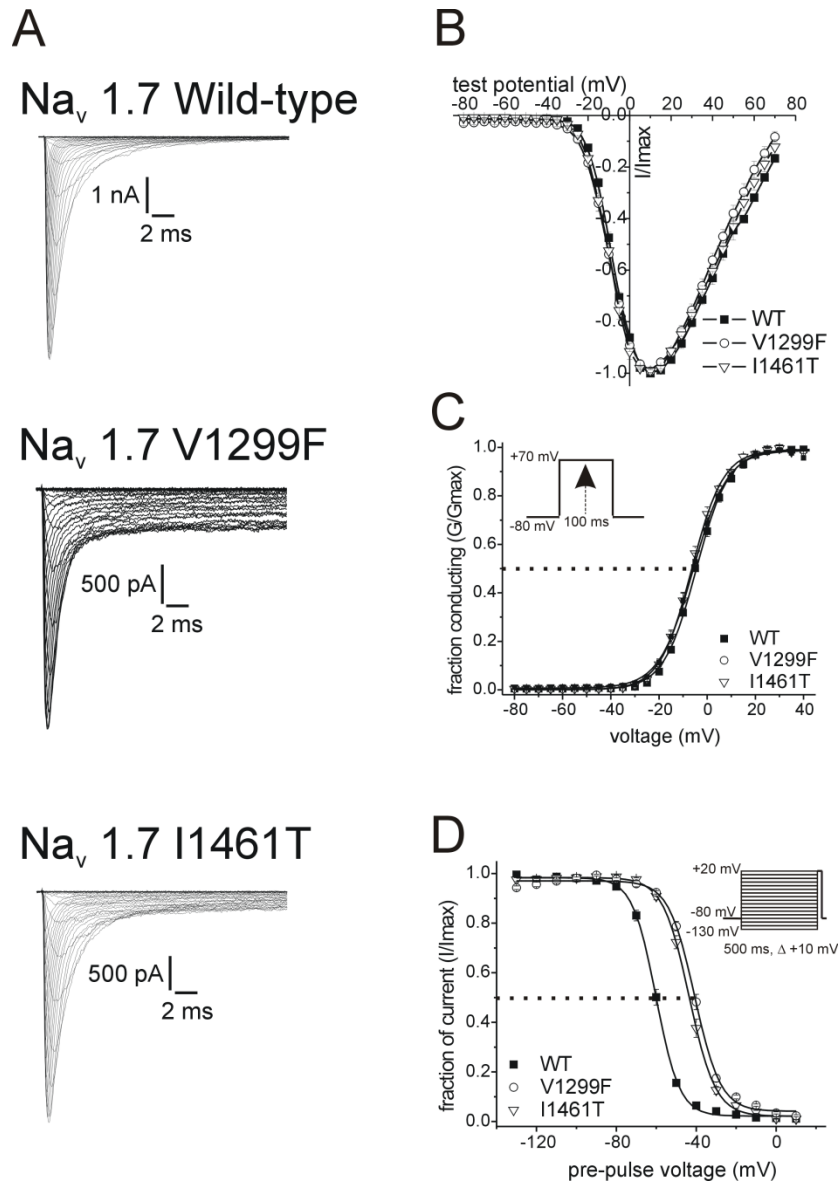


Figure 7. Comparison of whole-cell ionic current traces and normalized current-voltage properties in CsCl/Cs-aspartate dominant electrode solution. (A) Representative traces from WT and PEPD mutant Na_v1.7 channels (V1299F and I1461T) co-expressed with hβ1 and hβ2-subunits in hEK₂₉₃ cells. (B) Normalized current-voltage (I/V) properties were assessed using depolarizing step pulses. Cells were held at -80 mV. The currents were elicited by 100 ms test pulses to various potentials from -80 to +70 mV stepped in increments of 5 mV. (C) Voltage-dependence of activation was derived from the I/V data points to determine fraction of channels conducting in response to changes in voltage. (D) Steady-state inactivation for WT and mutant channels determined using the protocol displayed within the inset from a holding potential of -80 mV.

3. *PEPD mutant channels reveal an increased persistent component in response to a slow-duration depolarizing ramp stimulus*

Destabilization of the inactivated state can affect the region where steady-state channel activation and inactivation overlap, resulting in an increased probability of channel re-opening before inactivating near resting membrane potential (RMP), and the development of persistent “window” currents (Hodgkin and Huxley, 1952). Furthermore, it has been proposed that because persistent neuronal currents, or ramp currents (I_{ramp}), are activated near RMP, these currents may influence AP threshold and cellular excitability (Crill, 1996). Therefore, in order to better quantify the persistent component observed above in the PEPD mutant channel traces, WT and PEPD mutant $\text{Na}_v1.7$ currents evoked by a slow depolarizing ramp (0.27 mV/ms) stimulus, from a holding potential of -120 mV, were examined. A significant increase in the amplitude of the ramp currents elicited especially at more depolarized potentials for the mutations implicated in PEPD within the D3 / S4-S5 and D3-D4 intracellular linkers compared to WT channels in response to a slow depolarizing ramp stimulus was observed (Figure 5F). Interestingly, the I_{ramp} characteristics for the PEPD mutations revealed an impaired transition to a non-conducting state, confirming a destabilized channel configuration at more depolarized potentials. As mentioned previously, $\text{Na}_v1.7$ channels are thought to contribute to setting the threshold for AP firing. Therefore, an increase in the peak ramp current elicited and the persistent component revealed at more depolarized voltages suggests the PEPD mutations may (1) alter threshold of AP at potentials when channels would

normally transitioning to closed-state inactivation (CSI), thus, reducing AP threshold and (2) prolong the AP duration, when channels are transitioning to open-state inactivation (OSI) during the falling phase of an AP where the membrane is repolarizing to RMP. These voltage-dependent changes may be relevant in patients whose sensitivity for non-noxious stimuli, originating the rectal, ocular and mandibular regions, is heightened. However, the location for the pain perception cannot be fully explained by the voltage-dependent gating changes alone because these patients do not experience pain throughout the body as would be expected based on the expression patterns of Na_v1.7 channels.

4. *PEPD mutations within the D3 / S4-S5 linker differentially affect development of closed-state inactivation (CSI) compared to the I1461T PEPD mutation*

Before reaching an open (ion conducting) state, VGSCs can transition to an inactivated state during small depolarizing steps, to relatively negative potentials, thereby reducing the population of channels available for activation by stronger depolarizing steps (Oxford and Pooler, 1975; Bean, 1981). Furthermore, transition to the closed-inactivated state (CSI) can play an important role in Na⁺ channel response during sub-threshold depolarizations (Cummins et al., 1998). Therefore, the effects the PEPD mutations have on development of CSI were tested. A time varied conditioning pulse to -60 mV was implemented, from a holding potential of -120 mV, followed by a test pulse to 0

mV for 20 ms, to determine the fraction of channels available. A conditioning voltage of -60 mV was utilized because this potential is near RMP for nociceptive sensory neurons, thus, changes in VGSC gating properties near this potential may have a large impact on AP threshold (Herzog et al., 2001; Renganathan et al., 2001; Rush et al., 2006; Rush et al., 2007). Consistent with our steady-state inactivation data, a decrease in the fraction of mutant channels transitioning to a closed-inactivated state at this potential was observed compared to WT (Figure 8A). Additionally, a significant difference in the time constants (τ_{-60}) for CSI between PEPD mutations in the D3 / S4-S5 and D3-D4 (inactivation gate) linker was noticed (Table 2). Surprisingly, the PEPD mutations within the D3 / S4-S5 linker (V1298F and V1299F) displayed time constants smaller than those for both the WT channels and channels with the mutation within the putative inactivation gate (I1461T), indicating a faster transition to closed-inactivated states for the D3 / S4-S5 PEPD mutants. These results together, suggest the transition rate and binding sites for inactivation are altered with the PEPD mutations at potentials critical for transition to closed-inactivated states.

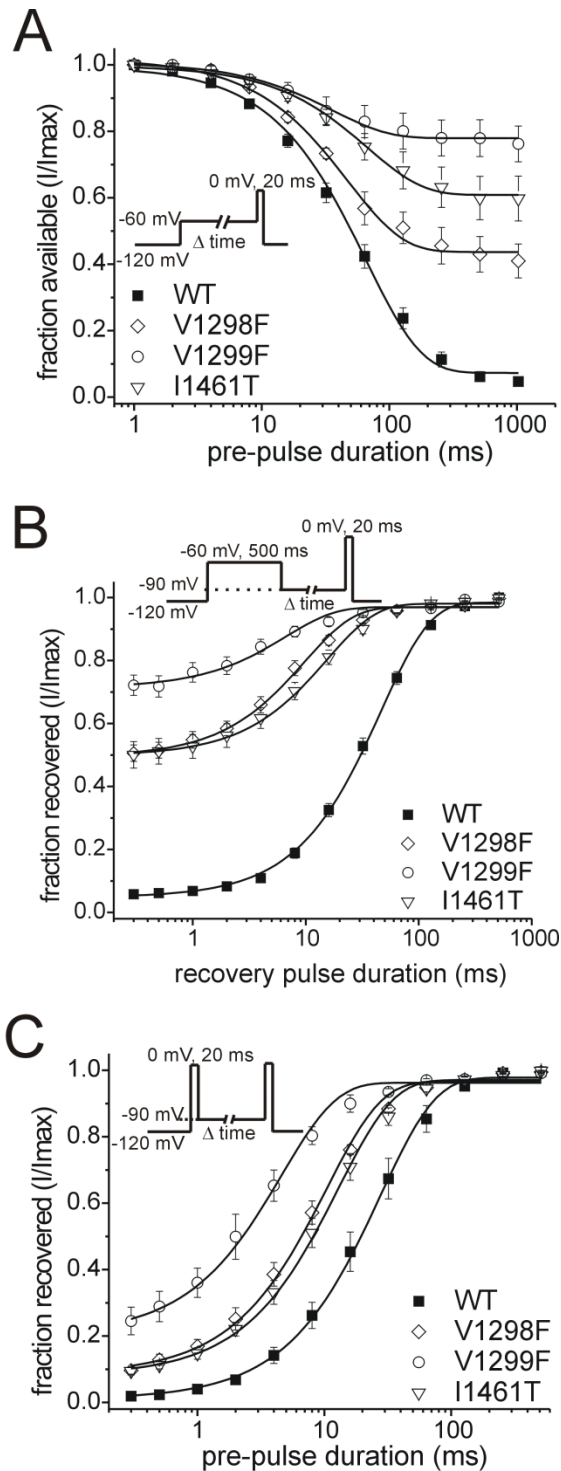


Figure 8. Effects of D3 / S4-S5 PEPD mutations on inactivation kinetics. (A) Development of CSI near RMP ($n = 5-16$). (B) Time course for recovery from CSI near resting membrane potential ($n = 7-10$). (C) Recovery from OSI to a primed channel state ($n = 4-6$). Plotted values were fit with a single exponential function to determine time constant values (τ). Development and recovery protocols are displayed within the insets.

5. Mutations associated with PEPD disrupt the stability of inactivation and increase the recovery rate from CSI

The decrease in the inactivation time constant (τ_{-60}) and incomplete development of CSI for the PEPD mutations within the D3 / S4-S5 linker are intriguing because they suggest that these residues may play a direct role in stabilizing the closed-inactivated state of Na_v1.7. Therefore, the inactivation kinetics were next examined by evaluating the effects the PEPD mutations had on recovery from CSI by pulsing cells to -60 mV for 500 ms and then allowing channels to recover at -90 mV for varied time increments before testing for available current (Figure 8B). All of the PEPD mutant channels tested (V1298F, V1299F, and I1461T) recovered from CSI faster than WT. The recovery time constants (τ_{-90}) for the PEPD mutant channels were significantly faster (3-8 fold) than those for WT channels (Table 2). Thus, these faster recovery rates likely contribute to the incomplete development of CSI for the PEPD mutant channels at this potential.

Table 2. Development and recovery inactivation time constant values for WT and PEPD mutant Na_v1.7 channels.

Channel	Development time constant (τ) (ms)	<i>n</i>	Recovery time constant (τ) (ms)	<i>n</i>
<i>Closed-state inactivation</i>				
WT	74.2 ± 8.2	16	46.9 ± 3.3	6
V1298F	49.3 ± 2.7	4	9.7 ± 0.9	7
V1299F	31.7 ± 3.5	8	7.3 ± 1.1	8
I1461T	68.8 ± 3.2	5	15.6 ± 1.2	10
<i>Open-state inactivation</i>				
WT	0.6 ± 0.1	11	30.6 ± 5.6	6
V1298F	1.0 ± 0.03	7	9.6 ± 0.7	4
V1299F	0.8 ± 0.1	9	4.2 ± 0.7	5
I1461T	0.8 ± 0.03	14	13.0 ± 2.1	5

Time constant values for development (τ_{-60}) of and recovery (τ_{-90}) from CSI. Additionally, we obtained time constant values for development (τ_0) of and recovery (τ_{-90}) OSI. Voltage-derived time constant values for development of OSI at 0 mV were determined by fitting the decay phases of currents elicited for WT and mutant channels using a Hodgkin-Huxley m^3h function. Development of CSI and recovery from OSI and CSI data were fit using a single-exponential function and time constant values were calculated and averaged from individual cell recordings.

6. *D3 / S4-S5 and D3-D4 PEPD linker mutations allow Na_v1.7 channels to recover from open-state inactivation (OSI) faster than wild-type (WT) channels*

Because we observed a depolarizing shift in the $V_{1/2}$ of steady-state inactivation (h_{∞}) and changes in the kinetics of CSI for PEPD mutant channels compared to WT we also examined channel recovery from open-state inactivation (OSI). VGSCs quickly transition to an open-inactivated state after reaching an ion-conducting (open) state (Hodgkin and Huxley, 1952; Hoyt, 1971; Goldman and Schauf, 1972; Armstrong et al., 1973; Armstrong and Bezanilla, 1977; Bezanilla and Armstrong, 1977). To examine recovery from OSI cells a two-step protocol was implemented. Cells were conditioned at depolarized potentials (0 mV, 20 ms) before hyperpolarizing the membrane potential (-90 mV) for varied times and then testing for available current (0 mV, 20 ms). We chose a recovery potential of -90 mV based on our steady-state inactivation (h_{∞}) data which shows that a large population (~90%) of WT channels are available for ion conductance at this potential. All PEPD mutant channels recovered from OSI faster than WT channels with significant decreases in recovery time constants (τ_{90}) (Figure 6C). This is consistent with a decreased fraction of mutant channels transitioning to the fast open inactivated states at 0 mV.

Notably, upon inspection of the development and recovery rates for all of the mutant constructs, the development of CSI is incomplete at 1000 ms indicating that the interactions required to stabilize the inactivated state are

disrupted. However, the rate of development for the inactivation gate mutation (I1461T) is not affected suggesting the rate at which the inactivation gate motif binds to a putative “docking” site is not altered, however the stability, presumably from the amino acid substitution, is significantly reduced such that the inactivation gate does not bind with high affinity to the putative “docking” site. These results are confirmed upon observation of the recovery rates for all PEPD mutant channels including the I1461T. The recovery kinetics for all PEPD mutant channels is accelerated compared to WT channels, most notably within the initial phase of the protocol. Taken together, these results indicate that the mutations (V1298F and V1299F) located in the D3 / S4-S5 linker, a proposed interface for voltage-sensing and inactivation stability, alter both development and recovery from -60 mV along with the stability of inactivation, whereas a mutation located solely in the inactivation gate component primarily affects recovery rate and affinity of the inactivation reaction. Thus, the development and recovery for all PEPD mutant constructs contribute to the changes noted in the ramp current properties at potentials negative to the activation threshold (Figure 5F). Using a pharmacologic analogy and imagining the inactivation gate acts as a “ligand” binding to a theoretical “receptor” site, the mutations in these regions have the ability to alter both affinity and potency of this stabilizing reaction and suggest these regions are part of a critical interaction unit required for proper inactivation gating.

7. *An adjacent and identical mutation within the D3 / S4-S5 linker, not implicated in PEPD, displays unique voltage-dependent and kinetic properties compared to neighboring PEPD mutations*

Based on amino acid sequence analysis and helical wheel projections, it has been proposed that the D1-D4 / S4-S5 linkers of VGSCs adopt a highly conserved α -helical secondary structure (Lerche et al., 1997; Filatov et al., 1998). The secondary structure of the linkers would indicate that residues may interact based on their orientation around the α -helix. To test this possibility, an adjacent and identical residue (V1300F), not implicated in PEPD, was mutated within the S4-S5 linker of D3 to examine the location-specific effects of the valine to phenylalanine substitutions within the S4-S5 linker. This mutant channel produced currents with rapid conductance and inactivation characteristics (Figure 9A). The I/V properties of the V1300F mutant in comparison to WT channels were further examined (Figure 9B). The V1300F mutation resulted in a decreased probability of the channel population opening at voltages near activation threshold (-40 mV), which were sufficient to allow sodium flux through WT channels. This suggests the V1300F mutation decreases the initial voltage-sensitivity required for D3 activation and thus, impairs the fraction of channels available to open. As such, the voltage-dependent properties and kinetics of gating for the V1300F mutant channel were evaluated in a similar manner as described for the PEPD mutations.

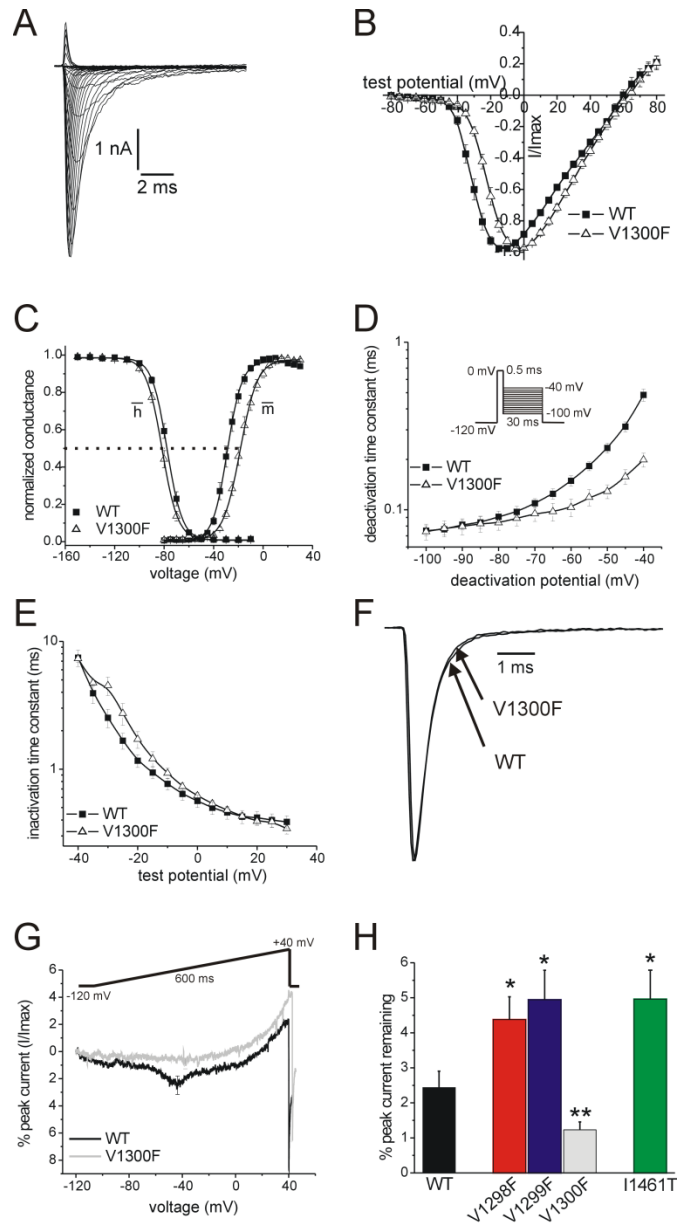


Figure 9. An adjacent and identical mutation within the D3 / S4-S5 linker of Na_v1.7, not implicated in PEPD, displays altered voltage-dependent channel properties in a manner distinct from PEPD mutations. (A) Representative current trace for the V1300F mutant channels co-expressed with β 1 and β 2 obtained from a holding potential of -120 mV to elicit inward Na⁺ current in a CsF dominant electrode solution. (B) Normalized current-voltage (I/V) plot comparison of WT and V1300F mutant channels. (C) Steady-state gating characteristics of WT and V1300F mutant channels determined from separate activation and inactivation pulse protocols. Voltage-dependent conductance properties were derived from I/V data and the steady-state inactivation profiles were determined using stepwise conditioning pulses (D) Voltage-dependent deactivation characteristics were examined for WT and V1300F channels using

the protocol displayed within the inset. **(E)** Open-state fast-inactivation (OSI) time constants (τ_h) were determined using a Hodgkin-Huxley (m^3h) type fit to the decay phase of individual current traces in a similar manner as described for Figure 5D. **(F)** Representative current trace for WT and mutant channels at +10 mV emphasizing the decay phase for each trace. **(G)** Averaged inward ramp current (I_{ramp}) elicited in response to slow depolarizing stimulus (0.27 mV/ms) for WT and V1300F channels utilizing the same protocol that was used to examine PEPD mutant channels. Ramp current amplitude is expressed as a percentage of the peak transient current elicited with a standard I/V protocol. **(H)** Bar graph interpretation of percent peak inward current during the slow depolarizing ramp stimulus for all channels examined in this study (n = 6-14). A significant increase in percent peak current is denoted with a single asterisk (*), whereas a significant decrease in percent peak current is symbolized with a double asterisk (**).

When comparing WT and mutant G/V characteristics, a significant depolarizing shift in the $V_{1/2}$ of conductance (-18.50 ± 0.20 mV) and increase in the activation slope factor (6.92 ± 0.18 mV/e-fold) was observed for the V1300F mutant channel, and a small, but significant, hyperpolarizing shift in $V_{1/2}$ of steady-state inactivation (-81.96 ± 0.15 mV) with no significant change in inactivation slope factor (6.39 ± 0.13 mV/e-fold) (Figure 9C). Additionally, in contrast to the adjacent PEPD mutations, the V1300F mutation significantly increased the voltage-dependent deactivation time constants (τ_d) at -60 and -40 mV (Figure 9D) and had little effect on OSI at potentials near +10 mV (Figures 9E and F). We also compared I_{ramp} elicited using a slow depolarizing stimulus (0.27 mV/ms) for WT and mutant channels (Figure 9G) and noticed a significant decrease in the percent peak current remaining for the V1300F mutant channels compared to WT (Figure 9H). This was in contrast to the adjacent PEPD mutations that significantly increased ramp current elicited. Consistent with this, an enhanced transition to CSI for the V1300F mutant channels, and a significant decrease in the time constant (τ_{-60}) for CSI compared to WT were observed (Figure 10A). However, this mutation did not significantly alter the time constants for recovery from CSI or OSI compared to WT (Figures 10B and C).

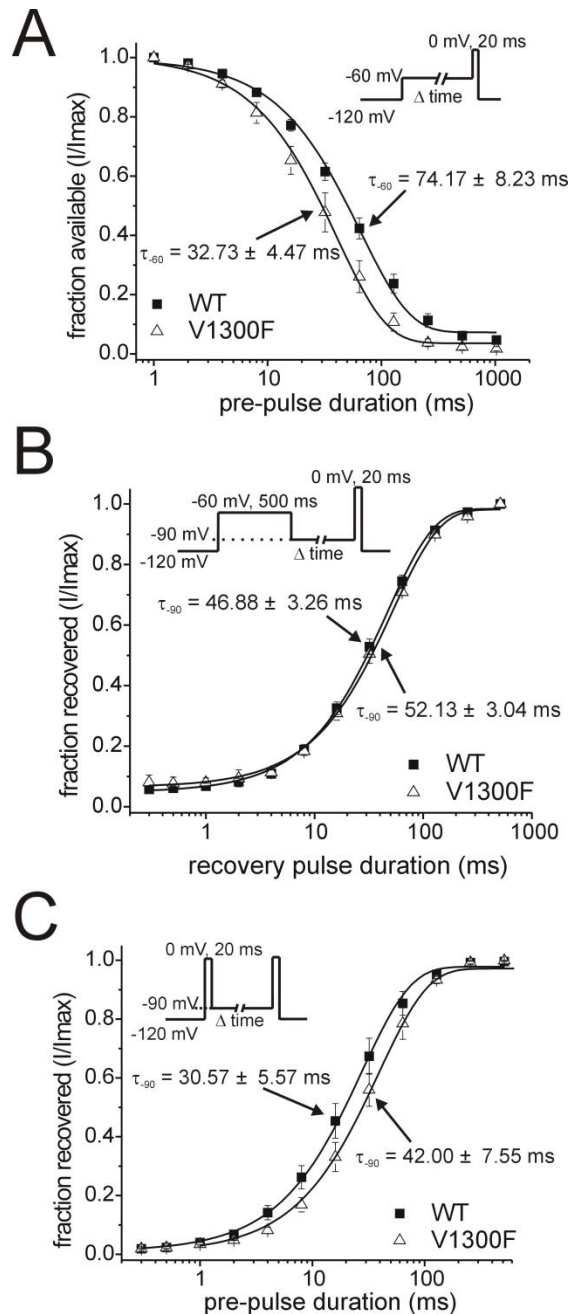


Figure 10. Comparison of kinetic profiles for development and recovery from inactivated (OSI and CSI) states for V1300F mutant and WT channels.

(A) Development of CSI at -60 mV for V1300F and WT channels was examined using a two-step pulse protocol shown within the inset. (B) Recovery from CSI was tested experimentally using a two-step pulse protocol shown within the inset to determine the fraction of WT and mutant channels that recover at -90 mV. (C) Recovery from OSI was evaluated using a two-step protocol with a strong conditioning pre-pulse to 0 mV followed by a time-varied hyperpolarizing pulse (-90 mV) and a test pulse (0 mV) to determine the fraction of channels recovering from OSI.

8. *Voltage-dependent slow inactivation properties for PEPD mutant channels are altered in a manner distinct from V1300F mutant channels*

In addition to transitioning to a fast-inactivated state, VGSCs can transition to an additional inactivated state called slow-inactivation, that occurs over seconds or even minutes, and slowly recovers (Vilin and Ruben, 2001). As evidence of the physiological importance of slow inactivation, mutations that decrease the fraction of channels accumulating in a slow-inactivated state in response to changes in voltage may play an important role in determining cellular excitability in skeletal muscle (Cummins and Sigworth, 1996; Bendahhou et al., 2002) and computer-modeled DRG neurons (Sheets et al., 2007). The effects of the Na_v1.7 PEPD mutations on transition to a slow-inactivated state have not been determined. Therefore, the voltage-dependent properties of slow inactivation for WT and each of the mutant channels were examined using an extended (10 sec) conditioning pulse followed by a brief hyperpolarizing pulse that allowed for recovery of fast-inactivated channels, before testing for the available population of channels (Figure 11). Interestingly, all of the PEPD mutant channels decreased the voltage-dependent transition to a slow-inactivated state when compared to WT. Results for the PEPD mutant channels were in contrast to the non-PEPD mutant channel (V1300F) which did not decrease transition to the slow-inactivated state compared to WT. Both WT and V1300F channel availability were fit well ($r^2 = 0.99$) with a double-phase Boltzmann distribution, suggesting that the population of channels transitioned

between two slow-inactivated states. However, the PEPD mutant channel transition to slow inactivation was fit well with a single-phase Boltzmann distribution. Therefore, it is possible that in addition to their role in impairing fast inactivation, the D3 / S4-S5 mutations implicated in PEPD also affect the voltage-dependent transition to a slow-inactivated state.

These results are intriguing based on the controversy regarding the coupled nature of the fast and slow inactivation mechanisms (Featherstone et al., 1996; Vedantham and Cannon, 1998; Hilber et al., 2002) and the proposal for separate independent voltage-sensing components for each process (Ruben et al., 1992; Casini et al., 2007). Results from experiments in this section of the dissertation are consistent with the two gating states when compared to WT, in that, the PEPD mutations appear to (1) destabilize fast inactivation and shift the voltage-dependence rightward and (2) shift the voltage-dependent transition to a slow-inactivated state rightward and modify the occupancy in a particular component of slow inactivation such that the majority of PEPD mutant channels can be fit into one population.

These results demonstrate that the PEPD mutant channels can increase the window current primarily by shifting transition to an inactivated state. This is in contrast to an adjacent non-PEPD mutation within the D3 / S4-S5 linker that reduces the size of window current and overlap between activation and inactivation gating. This effect may be due to a constrained voltage-sensitivity for activation and a moderate voltage-dependent uncoupling between activation and inactivation. Taken together, these results demonstrate that mutations along the

D3 / S4-S5 linker can differentially affect voltage-dependent channel gating and the stability of pore conductance and inactivation.

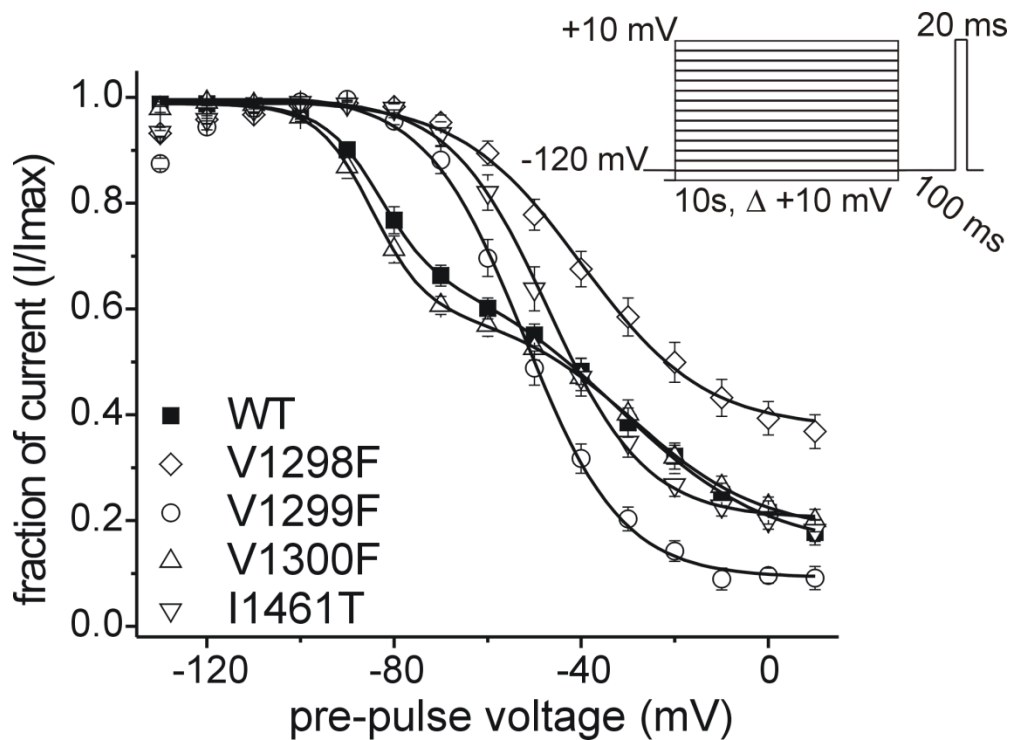


Figure 11. Comparison of the derived voltage-dependent slow inactivation properties for WT and mutant channels during transition between distinct states. All D3 / S4-S5 (V1298F, V1299F, and V1300F) and D3-D4 (I1461T) linker mutant channels were tested experimentally to determine the fraction of channels transitioning to slow-inactivated states in response to changes in voltage. To examine this transition we used a pulse protocol that included a +10 mV stepwise conditioning pulse from -130 mV to +10 mV for 10 seconds, and then quickly hyperpolarized cells to -120 mV to allow rapid recovery of fast-inactivated channels before testing for available channels for 20 ms at +10 mV. WT and V1300F channels were fit using a double-phase Boltzmann distribution whereas PEPD mutant channels were fit using a single-phase Boltzmann distribution.

B. *Na_v1.7-PEPD mutant channel M1627K within D4 / S4-S5 alters transition to an inactivated state and renders DRG neurons hyperexcitable*

1. *Na_v1.7-M1627K located in the S4-S5 of D4 and implicated in PEPD, shifts voltage-dependent properties and increases ramp currents similarly to D3 / S4-S5 PEPD mutations*

The voltage-sensing S4 segment of D4 in VGSCs is crucial for coupling voltage-dependent channel activation to inactivation (Chahine et al., 1994; Chen et al., 1996; Cha et al., 1999). Residues within the adjacent D4 / S4-S5 linker of VGSCs play a unique role in stabilizing a fast-inactivated configuration (Tang et al., 1996; Filatov et al., 1998; McPhee et al., 1998). Of interest, an inherited PEPD mutation (M1627K), within this cytosolic region of Na_v1.7 which replaces a highly conserved methionine (Met, M) for a positively charged lysine (Lys, K), had originally been identified in a patient from France (Fertleman et al., 2006). Charge-substituted mutations in the S4-S5 segments of D3 and D4 slow transition to an inactivated state using engineered scanning mutagenesis (Smith and Goldin, 1997; Filatov et al., 1998) and site-directed mutagenesis based on locations of inherited channelopathies (Cannon, 2000; Meisler and Kearney, 2005; Koopmann et al., 2006; Catterall et al., 2008). This mutation occurs within a highly conserved Met doublet in the S4-S5 of D4 of VGSCs that plays an important role in stabilizing transition to an inactivated state (Filatov et al., 1998) and may tune gating properties in response to oxidative modifications

(Kassmann et al., 2008) suggesting this Met doublet may lie within a “hotspot” region of VGSCs prone to mutation which cause gating defects. Therefore, we investigated the effects of a novel M1627K mutation on voltage-dependent channel properties and action potential (AP) firing. This mutation was identified in the *SCN9A* coding exons from an English patient diagnosed with PEPD.

Human embryonic kidney (hEK₂₉₃) cell lines, stably expressing TTX-r forms of the WT (Na_v1.7r) and mutant (Na_v1.7r-M1627K) VGSCs were used to determine changes in channel properties. The M1627K mutation slowed decay rates of current traces (Figure 12) elicited during an I/V protocol, but did not statistically alter the voltage-dependent activation and deactivation channel properties compared to WT (Figure 13A and B). These results are in agreement with those demonstrating the VGSC S4 segment of D4 is a critical component for coupling activation to inactivation (Chahine et al., 1994; Chen et al., 1996; Cha et al., 1999; Chanda and Bezanilla, 2002) and could suggest the tethered S4-S5 interface for voltage-sensing transmission may be more important during inactivation and gating charge immobilization compared to activation. However, evidence indicating that the D4 / S4 gating charge movement during membrane repolarization is not limited by inactivation gate binding or immobilizing the return, argues against a potential role for the S4-S5 interface during inactivation. Notably, these discrepancies are hard to resolve in the absence of a crystal structure snapshot at several voltage-dependent states or chemically modifiable direct interactions at a range of voltages.

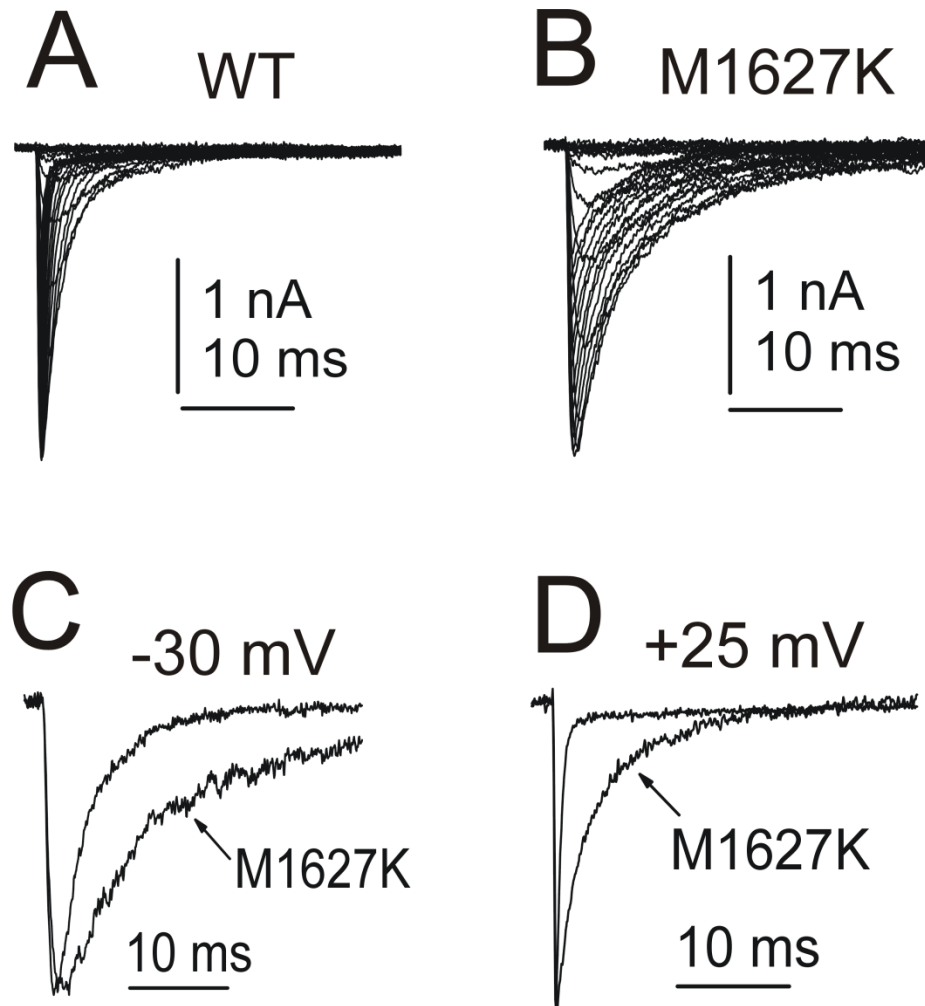


Figure 12. M1627K currents decay slower than WT $\text{Na}_v1.7$ currents. Representative WT (A) and M1627K (B) $\text{Na}_v1.7$ currents are shown. Cells were held at -100 mV and currents were elicited with 50 ms test pulses to potentials ranging from -80 to +40 mV. For better comparison, WT and M1627K currents elicited with -30 mV (C) and +25 mV (D) depolarizations are shown superimposed. Although the rate of activation is not apparently altered, the decay phase is substantially faster for WT currents.

Similar to other PEPD mutations, the charge-substituting M1627K mutation significantly depolarized the midpoint of steady-state fast inactivation (approximately +20 mV) and decreased the slope factor (Figure 13C). However, the fraction of current remaining available after the -10 mV inactivation prepulse was not significantly different between WT ($1.3 \pm 0.3\%$) and M1627K ($1.9 \pm 0.5\%$) channels. By contrast, the voltage-dependence of slow inactivation of $\text{Na}_v1.7r$ currents was moderately altered by the M1627K mutation (Figure 13D). Ten second pre-pulses, followed by 100 ms recovery pulses to -120 mV to allow recovery from fast-inactivation, preceded the test pulse (to 0 mV for 20 ms) to determine the fraction of current available. The M1627K mutation reduced the fraction of slow-inactivated channels that occurred at -80, -70 and -60 mV, which might contribute to increased channel availability at normal resting membrane potentials.

As noted above, PEPD mutant channels exhibited slower current decay characteristics (Figure 12) compared to WT channels. Therefore, we investigated the rates of inactivation for WT and M1627K mutant channels. Upon inspection of gating kinetics, we observed significant differences in the time constants for current inactivation between WT and M1627K channels. The rate of OSI was quantified by fitting the decay phase of the macroscopic current with a single exponential function. The time constants estimated from these fits are plotted as a function of the test potentials (Figure 13E). The time constants were much larger for M1627K currents than for WT currents over voltages range from -30 to +40 mV. At -30 mV, for example, WT currents inactivated with a time

constant of 5.8 ± 0.8 ms ($n = 6$) whereas M1627K currents inactivated with a time constant of 9.9 ± 1.3 ms ($n = 6$). At +25 mV WT currents inactivated with a time constant of 0.44 ± 0.01 ms ($n = 6$) and M1627K currents inactivated with a time constant ten times larger (4.9 ± 0.4 ms, $n = 6$). These differences were statistically significant. We also examined the development of CSI at voltages ranging from -90 to -50 mV (Figure 13E, triangular symbols). Cells were stepped to the inactivation potential (from a holding potential of -100 mV) for increasing durations, and then stepped to the test potential (0 mV) to measure the fraction of the remaining available channels. The data from these cells were fitted with a single exponential function. Interestingly, the time course for the development of inactivation from the closed state was not significantly altered by the M1627K mutation, indicating that the M1627K mutation has a greater effect on OSI than CSI.

The time course for recovery from fast inactivation (repriming) of WT and M1627K channels was measured at recovery voltages ranging from -140 to -60 mV. Fast inactivation was induced with 20 ms inactivating pre-pulses to -20 mV. The time course for recovery from inactivation for both WT and M1627K currents could be fitted with single exponential functions. Recovery from inactivation was significantly faster for M1627K channels than for WT channels (Figure 13F). For example, the time constant for recovery of WT channels ($\tau = 92 \pm 11$ ms, $n = 7$) was almost 4-fold larger at -70 mV than the corresponding time constant for M1627K channels ($\tau = 26 \pm 3$ ms, $n = 7$).

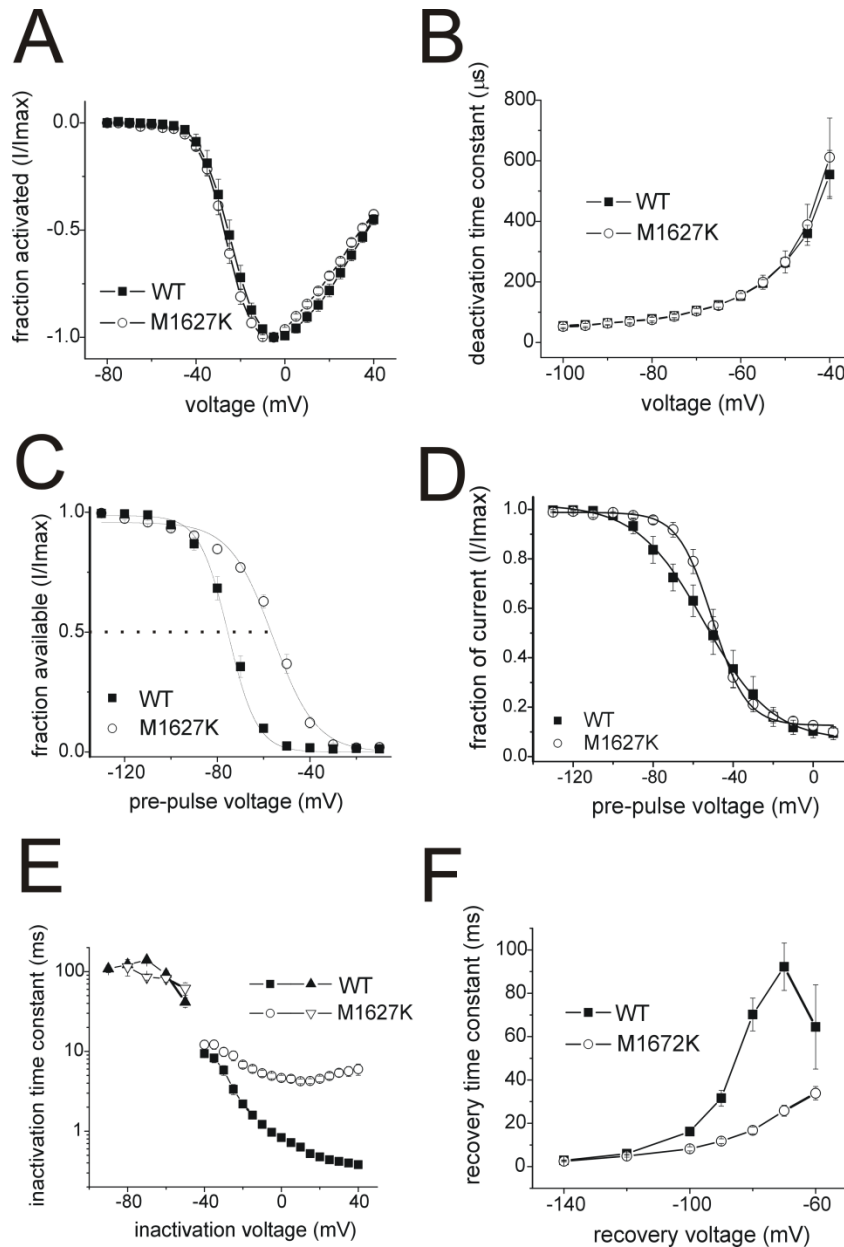


Figure 13. The M1627K mutation alters inactivation properties of Na_v1.7. (A) Normalized peak current-voltage relationship for WT (filled squares, n = 11) and M1627K (open circles, n = 15) channels. Cells were held at -100 mV and currents were elicited with 50 ms test pulses to potentials ranging from -80 to +40 mV. (B) Time constants for tail current deactivation at repolarization potentials ranging from -40 to -100 mV for WT (filled squares, n = 8) and M1627K (open circles, n = 9) Na_v1.7 channels. Time constants were obtained with single exponential fits to the deactivation phase of the currents. (C) Comparison of steady-state fast inactivation for WT (filled squares, n = 11) and M1627K (open circles, n = 15) Na_v1.7 channels. Currents were elicited with test pulses to 0 mV following 500 ms inactivating pre-pulses. (D) Comparison of slow inactivation for WT (filled squares, n = 3) and M1627K (open circles, n = 4) Na_v1.7 channels.

Slow inactivation was induced with 10 s pre-pulses, followed by 100 ms pulses to -120 mV to allow recovery from fast inactivation. A test pulse to 0 mV for 20 ms was used to determine the fraction of current available. **(E)** Time constants for development of fast inactivation as a function of voltage for WT (filled symbols, $n = 6$) and M1627K (open symbols, $n = 6$) $\text{Na}_v1.7$ channels are shown. Open-channel inactivation time constants were measured at voltages ranging from -45 to +40 mV by fitting the decay phase of currents elicited with depolarizing pulses with single exponentials. The time constants for development of closed-state inactivation were estimated from single exponential fits to time courses measured at inactivation potentials ranging from -90 to -50 mV for WT (filled triangles, $n = 6$) and with M1627K (open triangles, $n = 6$) $\text{Na}_v1.7$ channels. **(F)** Recovery from inactivation kinetics are faster for M1627K mutant channels (open circles, $n = 7$) than for WT $\text{Na}_v1.7$ channels (filled squares, $n = 7$). Time constants were estimated from single exponential fits to time courses measured at recovery potentials ranging from -140 to -60 mV. The recovery from inactivation voltage protocol involved prepulsing the cell to -20 mV for 20 ms to inactivate all of the current, then stepping the membrane potential back to the recovery potential for increasing recovery durations prior to the test pulse to 0 mV. The maximum pulse rate was 0.5 Hz.

We also examined the currents induced in WT and M1627K channels by small, slow depolarizations (ramp stimulus). Figure 14A shows the ramp current recorded from a M1627K cell producing a current with peak amplitude of 2.8 nA, compared to the ramp current recorded from a WT cell producing a comparable current with a peak amplitude of 3.4 nA. The ramp currents elicited with slow ramp (0.27 mV/ms) depolarizations from -100 to +20 mV were expressed as a percentage of peak current (Figure 14B) and the relative amplitude of the ramp currents were significantly larger for M1627K channels ($7.0 \pm 1.0\%$; $n = 9$) than for WT channels ($1.0 \pm 0.2\%$; $n = 7$). We compared the relative amplitude of the ramp currents with the extent of overlap between the voltage-dependence of activation and steady-state fast inactivation (Figure 14C). As shown, the relative amplitude of the WT and M1627K ramp currents, and the voltage-dependence of these currents, correlates reasonably well with the respective overlap between the voltage-dependence of activation and steady-state fast inactivation. Taken together, the voltage-dependent shifts in inactivation for the M1627K mutation share common features with the other PEPD mutations identified in the D3 / S4-S5 and D3-D4 inactivation gate that have been characterized in experiments outlined in this dissertation. It is interesting to note that although some of the IEM mutations characterized, for example A863P (Dib-Hajj et al., 2005; Han et al., 2006; Harty et al., 2006), can shift steady-state inactivation by +10 mV, symptoms described do not overlap with those for PEPD, suggesting genetic factors, cellular background, or modulating factors may contribute to the distinct clinical manifestation of these disorders and responsiveness to therapeutic

agents. The M1627K mutation, similar to the other PEPD mutations characterized in the experiments above, increased ramp current elicited during a slow depolarizing ramp stimulus for Na_v1.7 channels. Since the ramp currents generated by Na_v1.7 channels have been shown to be important for AP threshold properties (Cummins et al., 1998; Rush et al., 2007), depending on cellular background (Rush et al., 2006), we anticipated the M1627K mutation would increase AP response to subthreshold stimuli. Thus, we hypothesized that the M1627K mutation would alter excitability in the nociceptive neuronal background in which they are present.

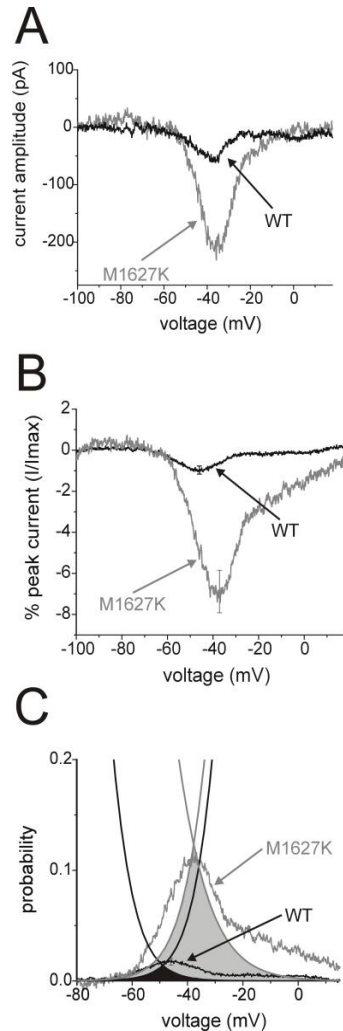


Figure 14. The M1627K mutation increases the amplitude of currents elicited by slow ramp depolarizations. (A) Representative ramp currents elicited by 600 ms long ramp depolarizations from -100 to +20 mV are shown recorded from a hEK₂₉₃ cell expressing WT channels (black trace) and from one expressing M1627K channels (gray trace). The peak transient current amplitude elicited in the WT cell was larger (3.4 nA) than that of the M1627K cell (2.8 nA). (B) The average relative ramp current (ramp current divided by peak transient current amplitude) is larger for M1627K cells (gray trace, n = 9) than for WT cells (black trace, n = 7). (C) The properties of the averaged ramp currents are compared to the overlap between the voltage-dependence of activation (derived from the current-voltage relationship) and steady-state fast inactivation. The inverted amplitude of the WT ramp current was scaled so that it corresponded to the peak overlap between WT activation and steady-state fast inactivation (black shaded area). As can be seen, voltage-dependence of the WT ramp current corresponds to the region of overlap. Furthermore, the relative amplitude and voltage-dependence of the M1627K ramp currents corresponds to the overlap between M1627K activation and steady-state fast inactivation (gray shaded area).

2. *Na_v1.7-PEPD mutations render DRG neurons hyperexcitable*

In addition to examining channel properties in response to changes in membrane potential, a collaborative effort was put forth between the Cummins and Waxman laboratories to investigate the effects of Na_v1.7r-M1627K mutant channels on AP firing activity (performed by Dr. Mark Estacion; Waxman laboratory) because previous studies had not looked at these parameters. Recordings were obtained from transfected rat DRG neurons of similar size (Dib-Hajj et al., 2008) and were chosen based on EGFP expression. Expression of M1627K mutant channels caused a significant reduction in the threshold to generate APs without altering input resistance, resting membrane potential (RMP), or AP amplitude between the two groups. Of note, neurons expressing M1627K channels fired more APs in response to a supra-threshold graded stimuli (1 sec long depolarizing current injection) and to stimuli 3X, and above, threshold calibrated to individual experimental (WT and M1627K) groups (Dib-Hajj et al., 2008).

Taken together, these results demonstrate that single-point PEPD mutations, within the S4-S5 linkers of D3 and D4, increase neuronal excitability in rat DRG, in part, because of altered inactivation properties of Na_v1.7 channels. It is worthwhile to note that although single-point missense mutations implicated in the painful disorders IEM and PEPD alter distinct gating properties of Na_v1.7 channels; both increase neuronal excitability in nociceptive DRG neurons. Therefore, additional modulating factors must contribute to the perceived

locations, temperature-dependent and environmental triggering mechanisms, and age-onset of pain in addition to response to different therapeutic agents.

C. Alternative splicing of Na_v1.7 exon 5 increases the impact of the painful PEPD mutant channel I1461T

1. Abbreviated background regarding Na_v1.7 alternative splicing

The sequence conservation between each of the segments in various VGSC isoforms is likely to contribute to their broad similarities (ion selectivity and voltage-dependence), whereas differences in the coding sequence between isoforms may play a role in evolutionary adaptation, such as pharmacological sensitivities (TTX-s vs. TTX-r), kinetic properties (fast vs. slow activating / inactivating channels), or transcriptional processes important for regional distributions and channel trafficking. As such, single-point missense mutations in “hotspot” regions of the channel, critical for precise gating, can disrupt the ability of the channel to transition between states and alter the configuration required to stabilize the channels at a particular membrane potential.

As previously mentioned there are notable differences between patients with IEM and PEPD, even though the disorders have been implicated to distinct single-point missense mutations in the Na_v1.7 channel highly expressed in the peripheral and sympathetic nervous system. Although the mutations differentially alter gating of Na_v1.7, one would not predict this would be the sole cause for such wide variation between the two groups. For example, patients with different

IEM or PEPD mutations report differential age onsets (Drenth et al., 2005; Fertleman et al., 2006; Dib-Hajj et al., 2007) The contributing factors to these differences are not clear. However, post-translational modification, alternative splicing, and expression of auxiliary β -subunits have been reported to modulate sodium current properties (Catterall et al., 2005). For instance, as stated in the background of this dissertation, alternative splicing of $\text{Na}_v1.7$ has been shown to alter channel kinetics, pharmacological sensitivities, and tissue distribution under pathological conditions, and can also be developmentally regulated. Additional evidence suggests that alternative splice variants of $\text{Na}_v1.7$ are found in dorsal root ganglia (DRG) neurons and that under modeled neuropathic pain conditions in rats splicing patterns of this isoform can change (Raymond et al., 2004). Furthermore, a recent study (Chatelier et al., 2008) has reported that alternative splice variants of $\text{Na}_v1.7$ exon 5 “*neonatal*” and “*adult*” (5N and 5A), which differ by two amino acids (L201V, N206D) in the D1 / S3-S4 linker, differentially affect the amplitude of currents generated in response to a slow depolarizing ramp stimulus. The gating characteristics of an additional set of $\text{Na}_v1.7$ splice variants occurring from alterations to exon 11 “*long*” and “*short*” (11L and 11S) were also studied. Alternative splicing in this region, which differs by an 11 amino acid stretch included or excluded from the D1-D2 loop between the 11L and 11S variants, impacted current properties which was shown to be differentially modified by PKA regulation (Chatelier et al., 2008).

We explored the option as to whether alternative splicing of $\text{Na}_v1.7$ could contribute to the discrepancies between IEM and PEPD. Thus, we hypothesized

that alternative splicing of Na_v1.7 may functionally impact IEM and PEPD, acting as a disease modifier, based on the expression patterns of the particular splice variants of this isoform. We hypothesized that, in addition to the gating changes in Na_v1.7 due to IEM or PEPD mutations which are sufficient to cause extreme pain, alternative splicing could contribute to the regional differences in perceived location of pain and age-onset between IEM and PEPD. Indeed, alternative VGSC splicing has been shown to increase ramp currents in Na_v1.7 channels. Additionally, IEM and PEPD mutations also alter Na_v1.7 ramp current properties. Together, alternative splicing may, in an additive manner, contribute to the chronic pain induced by these mutations. Therefore, we investigated whether alternative splicing of exon 5 might impact the functional consequences of IEM (I136V) and PEPD (I1461T) mutations. Results from these experiments (1) suggest an additive effect of the Na_v1.7 exon 5 alternative splicing and the PEPD mutation (I1461T) which could further impact the disease phenotype and (2) offer insight into how alternative splicing within exon 5 affects specific intramolecular interactions critical for voltage-dependent gating.

2. Splicing of exon 5 moderately alters WT Na_v1.7 channel properties

Wild-type (WT) Na_v1.7 exon 5 (Figure 15) splice variants (5N and 5A) produced rapid activating and inactivating inward sodium current upon membrane depolarization (Figure 16A). Initial comparison of the current traces did not suggest noticeable differences in channel kinetics or expression levels of

the 5N (-374.3 ± 65 pA/pF, $n = 13$) compared to the 5A (-320.7 ± 44 pA/pF, $n = 11$) form.

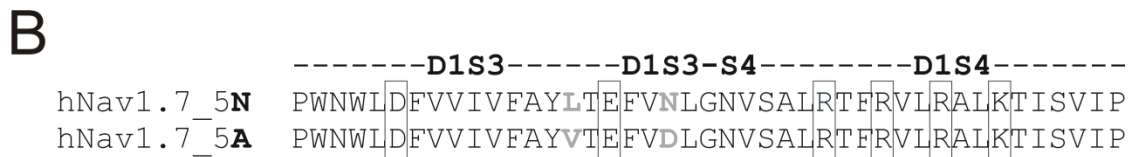
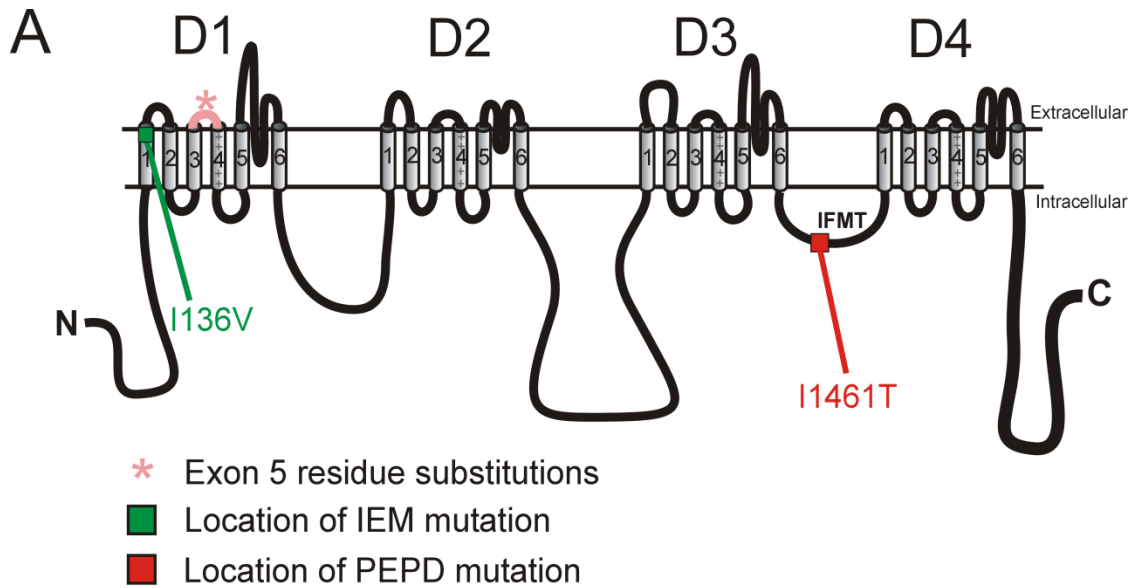


Figure 15. Location of exon 5 splicing region and $\text{Na}_v1.7$ mutations implicated in IEM and PEPD. (A) Depicted above is a linear representation of the VGSC α -subunit and the corresponding D1 / S3-S4 region for exon 5. The coding region of $\text{Na}_v1.7$ exon 5, located in the D1 / S3-S4 region, is noted with a pink star (*). Numerical position, amino acid mutation, and locations of the tested mutant channels in this study are designated with a green filled (IEM) or red filled (PEPD) square. Tested IEM mutant construct was D1 / S1 I136V and the tested PEPD mutant construct was D3-D4 I1461T located within the putative inactivation gate of $\text{Na}_v1.7$. (B) Sequence alignment of $\text{Na}_v1.7$ D1 / S3 through the region D1 / S4. Exon 5 amino acid differences, located within the D1 / S3-S4 linker, between the 5N versus the 5A splice forms are highlighted with grayed letters. Conserved *native* charged residues are illustrated with an encompassing rectangle in the sequence alignment. A substituted charged residue in the D1 / S3-S4 of the $\text{Na}_v1.7$ 5A form is emphasized with a star and a dashed line leading to the amino acid structural differences at physiological pH. In the 5N form there is an uncharged asparagine (N) residue characterized by the grayed amide moiety, whereas the 5A residue is a charged aspartic acid (D), with the charged moiety also noted in gray.

Changes in activation (m_{∞}/V), determined by whole-cell ionic conductance, and inactivation (h_{∞}/V), determined by the fraction of channels available after a 500 ms conditioning prepulse, were examined for the WT splice variants by comparing their respective midpoints ($V_{1/2}$) and slope factors (Z) in response to changes in command voltage (Figure 16B). Additionally, the rapid, integrated transition from channels activating and opening to closing, or deactivation, was evaluated (Figure 16C). In agreement with Chatelier et al. (2008) a small hyperpolarizing (~ 2 mV) shift in the $V_{1/2}$ of activation for the WT 5A variant was observed, whereas changes in steady-state inactivation and deactivation kinetics (τ_d), at potentials from -100 to -40 mV, were not observed (Table 3). These results suggest the D1 / S3-S4 splicing differences between the two $\text{Na}_v1.7$ splice variants do not significantly alter steady-state activation, deactivation, or inactivation properties in response to changes in membrane potential.

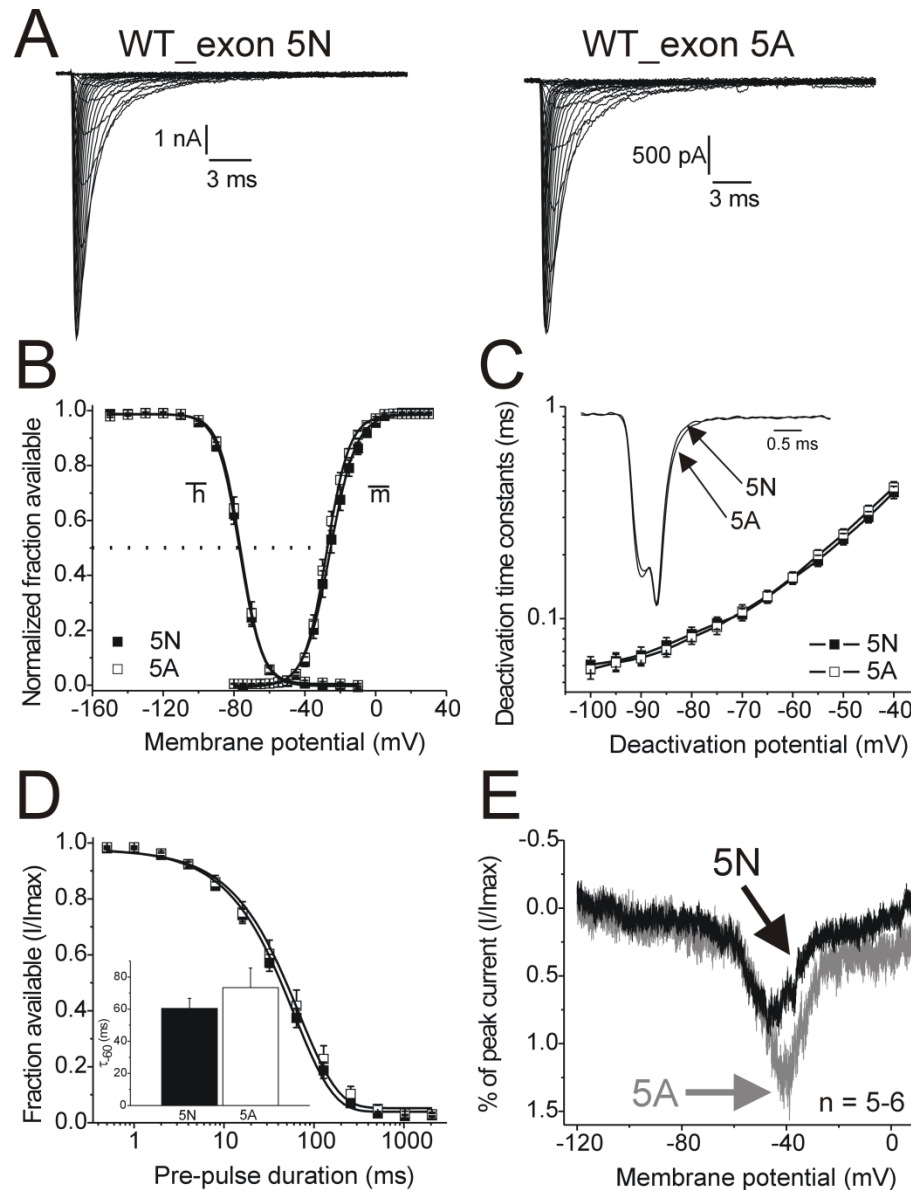


Figure 16. Effects of exon 5 alternative splicing on WT $\text{Na}_v1.7$ channels. (A) Representative sodium current traces for WT exon 5N versus 5A channels elicited using an incremental depolarizing step protocol. (B) Normalized fraction of channels available (G/V) during steady-state activating (m_∞/V) and fast-inactivating (h_∞/V) protocols. (C) Deactivation kinetics were compared using single-exponential fits to tail currents. (D) Time course for the development of closed-state inactivation (CSI) at -60 mV. The bar graph inset represents the averaged time constant (τ_{-60}) values for the recordings \pm S.E.M. (E) Channel ramp current generation was assayed using a slow depolarizing ramp (0.27 mV/ms) stimulus from -120 mV to $+40$ mV at a holding potential of -120 mV. Illustrated are the averaged ($n = 5-6$) ramp current traces for each splice variant. Averaged data for the WT 5N variant is colored in black and the 5A splice variant is colored in gray.

The relatively slow transitions of Na_v1.7 to and from closed-inactivated states are thought to contribute to production of physiologically relevant ramp current in response to slow depolarizing stimuli at hyperpolarized potentials near resting membrane potential for nociceptive DRG neurons (Rush et al., 2006; Rush et al., 2007). These Na_v1.7 ramp currents have been proposed to play roles in amplifying subthreshold generator potentials at relatively hyperpolarized voltages (Cummins et al., 1998; Herzog et al., 2003b). Thus, the ramp current generated by Na_v1.7 channels is implicated as a critical component in determining AP firing threshold (Blair and Bean, 2002). For these reasons, as well as recent reports suggesting differences in ramp current between Na_v1.7 splice variants (Chatelier et al., 2008), we examined development of and recovery from a closed-inactivated state (CSI) at -60 mV and changes in the ramp currents. Development of CSI (τ_{-60}) for the WT 5N (60.4 ± 6.3 ms, $n = 11$) compared to the 5A (73.4 ± 12.2 ms, $n = 11$) form was not significantly different (Figure 16D). Comparison of the recovery from -60 mV did not reveal a significant difference between the time constants for WT 5N (10.4 ± 1.1 ms, $n = 8$) and 5A (9.5 ± 0.7 ms, $n = 10$). The ramp current generated in response to a slow depolarizing ramp stimulus (0.27 mV/ms) by the 5A variant was increased by approximately 40% compared to the 5N form (Figure 16E). Although this increase was not significantly different between the two WT splice variants, it is consistent with results from Chatelier et al. (2008). This relatively small increase in ramp current could, in part, be due to the moderate shift in activation and the

trend towards a slowed development of CSI that was observed compared to the WT 5A splice variant.

3. *Exon 5A PEPD mutant channel affects activation, deactivation, CSI, and ramp current properties*

We next examined the effects alternative splicing has on a PEPD mutation (I1461T) located within the putative D3-D4 intracellular inactivation gate (Figure 15). The I1461T mutation, and other PEPD mutations that have been previously characterized in the 5N splice variant, shift the voltage-dependence of steady-state inactivation in the positive direction, slow the rate of open-state fast-inactivation and increase the amplitude of ramp currents at positive potentials compared to WT 5N channels (Fertleman et al., 2006; Dib-Hajj et al., 2008; Jarecki et al., 2008). The whole-cell inward sodium currents generated by the I1461T 5N and 5A splice variants were similar (Figure 17A) and current expression was not statistically different between the 5N (-171.2 ± 26 pA/pF, $n = 12$) and the 5A (-179.2 ± 27 pA/pF, $n = 12$) variants. Steady-state inactivation properties (h_{∞}/V) were not significantly different, however the ~ 5 mV hyperpolarizing shift in the midpoint of activation (m_{∞}/V) for I1461T 5A was significantly different compared to the 5N form (Figure 17B, Table 3). Furthermore, the deactivation time constants (τ_d) for the I1461T 5A form were slowed compared to the 5N. For example, deactivation at -60 mV, a potential near RMP for nociceptive neurons, was significantly slowed for the 5A splice variant (Figure 17C).

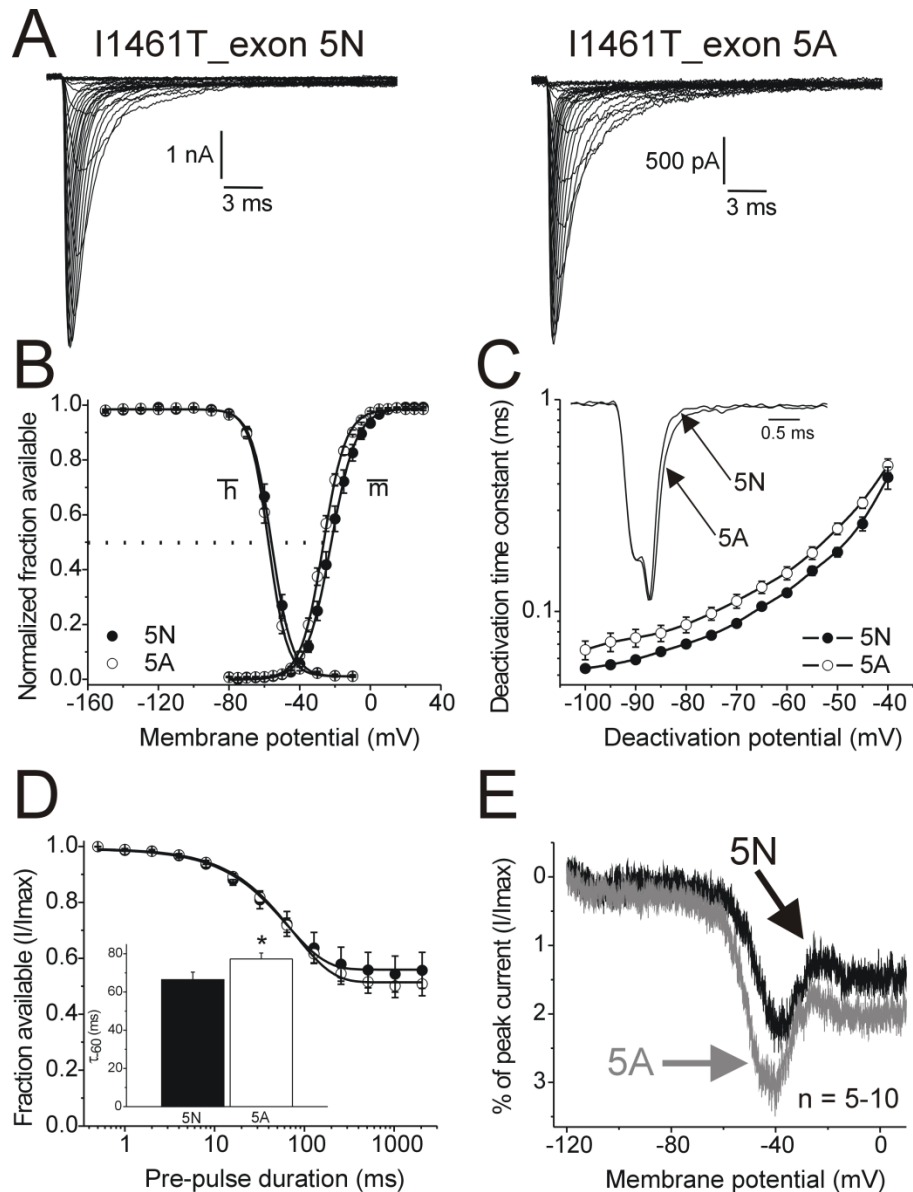


Figure 17. Alternative splicing modifies the voltage-dependent properties of the Na_v1.7-PEPD mutation (I1461T) located in the putative inactivation gate. (A) Shown above are representative whole-cell sodium current traces for the exon 5N and 5A forms of the I1461T mutant channel. (B) Comparison of conductance voltage (G/V) properties and steady-state fast inactivation in response to changes in membrane potential. (C) Changes in channel deactivation for the PEPD mutant were determined at a range of membrane potentials by observing tail current properties. Inset figure shows representative traces elicited during a deactivating protocol. (D) Development plot for the I1461T splice variants during transition to a closed-inactivated state at -60 mV. (E) Averaged ramp current elicited in response to a slow depolarizing stimulus for I1461T mutant channels. Traces were compiled from 5-10 individual recordings and then plotted versus membrane potential.

Examination of CSI at -60 mV also revealed the I1461T 5A channels transition to a close-inactivated state with a significantly slower time constant (τ_{60}) than the 5N channels (Figure 17D). However, recovery from CSI was not significantly different between the 5N (4.7 ± 0.3 ms, $n = 11$) and the 5A (4.9 ± 0.2 ms, $n = 11$) variants. Taken together, these data indicate that, at -60 mV, the 5A variant of the I1461T channels has a higher probability of remaining in an activated state, and may be more likely to transition to an ion-conducting state at more hyperpolarized voltages compared to the I1461T 5N variant. When the 5A PEPD mutant ramp current was compared to the 5N channels an increase in peak ramp current elicited was observed at all potentials tested. Furthermore, the 5A PEPD mutant channels displayed a more hyperpolarized onset of ramp current activation (Figure 17E). These results demonstrate that the I1461T 5A splice variant significantly increases ramp current amplitude at negative and positive potentials compared to the 5N variant (Figure 19A).

Table 3. Comparative Boltzmann parameters of the voltage-dependence of channel activation and steady-state fast-inactivation curves for the respective splice variants of WT, IEM (I136V) and PEPD (I1461T) Na_v1.7 channels.

Splice form	Channel	Voltage-dependence of activation			Voltage-dependence of steady-state fast-inactivation		
		V _{1/2} (mV)	Slope (mV/e-fold)	<i>n</i>	V _{1/2} (mV)	Slope (mV/e-fold)	<i>n</i>
5N	WT	-25.7 ± 1.3	6.2 ± 0.3	13	-76.8 ± 1.0	5.09 ± 0.2	12
	I1461T	-22.4 ± 1.4	6.2 ± 0.2	12	-55.9 ± 1.2	5.2 ± 0.1	12
	I136V	-37.5 ± 1.7	5.1 ± 0.3	5	-78.1 ± 2.0	5.7 ± 0.2	5
5A	WT	-27.7 ± 0.9	5.8 ± 0.3	11	-76.2 ± 1.1	5.5 ± 0.1	12
	I1461T	-26.8 ± 0.8	5.9 ± 0.2	12	-57.6 ± 0.9	5.0 ± 0.1	12
	I136V	-36.9 ± 1.8	6.0 ± 0.4	7	-79.3 ± 2.1	5.8 ± 0.2	7

Values for V_{1/2}, the voltage of half-maximal activation and inactivation, and the slope factors were derived from Boltzmann distribution fits to the individual recordings and averaged to determine the mean and standard error of the mean (± S.E.M) displayed above.

4. *D1 / S1 IEM mutant channel properties are not affected by exon 5 alternative splicing*

Mutations associated with IEM are commonly located in D1 and D2 and predominantly shift the voltage-dependence of activation to more hyperpolarized potentials without disturbing steady-state inactivation (Dib-Hajj et al., 2007). We examined the effects of alternative splicing on a nearby D1 / S1 (Figure 15) IEM mutation (I136V), which exhibits a delayed age of onset for pain sensations compared to other IEM mutations (Cheng et al., 2008). The currents generated by the 5N and 5A splice variants of the I136V mutant were similar (Figure 18A) with no statistical difference in current expression between the 5N (-339.1 ± 85 pA/pF, $n = 6$) and the 5A (-214.9 ± 31 pA/pF, $n = 9$) variants. Further inspection of the voltage-dependent channel characteristics did not yield significant differences between the I136V splice variants for the ability to activate during the m_{∞}/V protocol, inactivate during the h_{∞}/V protocol, or deactivate (τ_d) at the range of transmembrane potentials measured (Figures 16B-C). Additionally, no changes in the ability of the I136V-IEM splice variants to transition to a closed-inactivated state were observed at -60 mV (Figure 18D). Recovery from CSI between the 5N (10.5 ± 1.0 ms, $n = 3$) and the 5A (10.5 ± 2 ms, $n = 3$) IEM variants also did not differ.

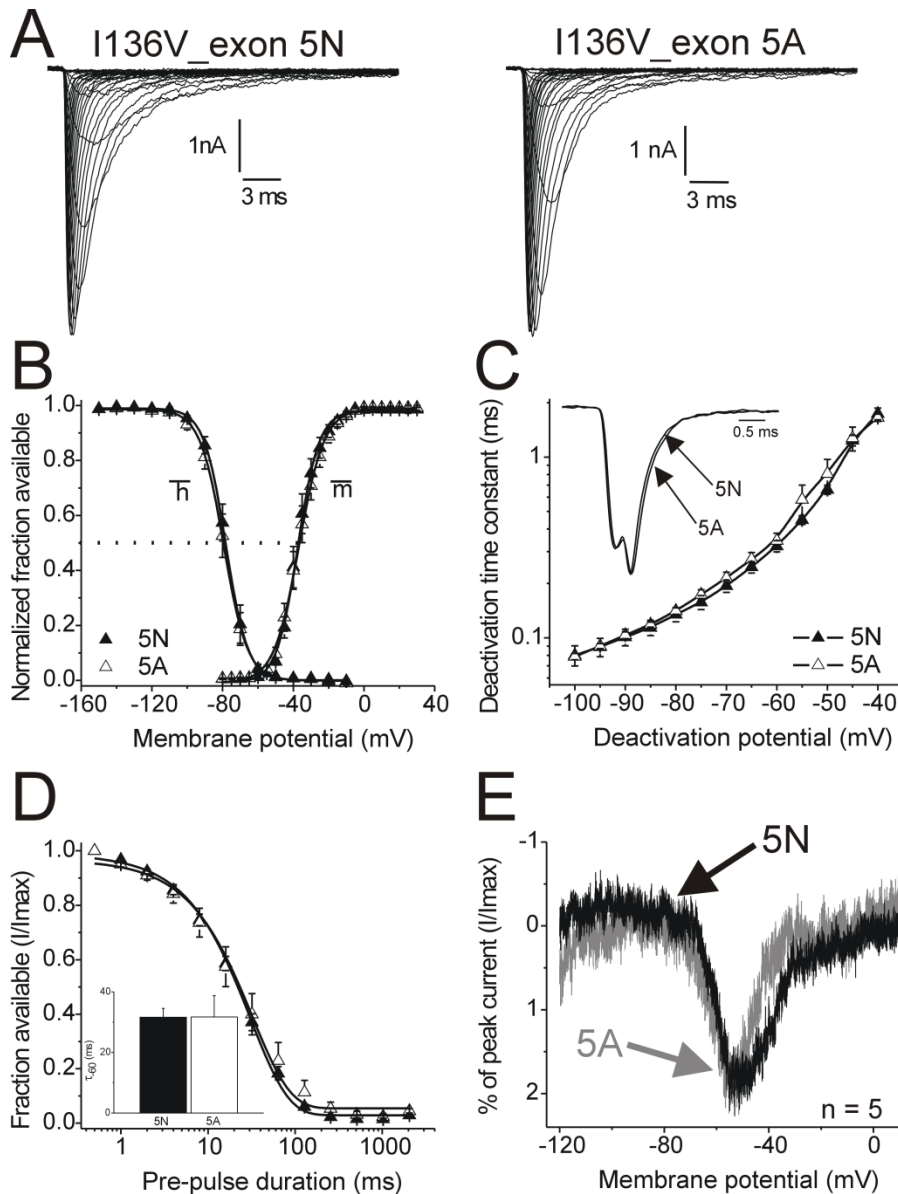


Figure 18. Alternative splicing of exon 5 in $\text{Na}_v1.7$ does not affect gating properties of the D1 / S1 IEM mutant channels. (A) Characteristic inward sodium traces for the I136V-IEM splice forms. (B) Steady-state activating and inactivating properties of I136V are displayed and plotted with respect to membrane potential to determine the fraction available at the range potentials depicted. (C) Voltage-dependent deactivation properties of I136V 5N and 5A splice variants are illustrated in the graph and representative traces are shown within the inset. (D) Development of closed-state inactivation at -60 mV is unchanged when comparing the I136V splice forms. No significant difference in the time constants was observed at -60 mV. (E) Changes in ramp current elicited during a slow-depolarizing stimulus for the I136V splice variants were not observed.

The ramp current elicited for the D1 / S1 IEM mutant was not statistically different when comparing the percentage of peak current between the splice variants (Figure 18E). It is interesting to note that, in contrast to WT and I1461T channels, there was not even a hint of an increase in ramp current amplitude. These results indicate that differences in the splice variants do not affect the I136V mutant channel properties.

Since a majority of the IEM mutations have been shown to primarily alter the voltage-dependent activation and deactivation properties (Dib-Hajj et al., 2007) the relatively small shifts induced by the 5A splice variant on voltage-dependent activation may be masked. The I136V mutation alone shifted the midpoint of activation by approximately -8 mV compared to WT, which is much larger than the shift observed for the WT-5A compared to WT-5N splice variants. Our results suggest that IEM mutations are not additively affected by the 5A splicing. However, our results for the PEPD (I1461T) splice variants are intriguing because they indicate that the impact of PEPD mutations and exon 5 changes are additive. Our results also demonstrate that the 5A splice variant of WT channels moderately hyperpolarizes the midpoint of activation and increases ramp current, which are in agreement with Chatelier et al. (2008). Since the stability of the inactivated conformation is decreased by the I1461T mutation, the effects of the 5A alternative splicing for the I1461T channels would be predicted to amplify the overlap between channels opening versus inactivating (window current) and increase the probability of channel opening in an additive manner (Figure 20). Interestingly, upon inspection of ramp current properties for the

I1461T-5A splice variant there appears to be three components when compared to the 5N variant. The 5A variant results in an increased ramp current threshold, responding at more negative potentials, an increase in peak ramp current, and a persistent element along the range of positive potentials compared to the 5N splice variant. This indicates that the activation profile for the 5A variant, in addition to the inherent defects in inactivation, contribute to the triple-phase characteristics of the ramp currents generated and would therefore affect transition from closed to open states. The effects of the I1461T-5A splice variant would therefore alter the rate and voltage-dependence of transition to open and inactivated gating states (Figure 20).

Structural implications suggest the charge replacement between the variants could contribute to the shift in the activation properties of the 5A variant. The coding region for Na_v1.7 exon 5 includes a portion of the D1 / S3 segment through the C-terminal end of the positively charged D1 / S4 (Raymond et al., 2004). The residue differences between the 5N and the 5A variants are localized to the extracellular portion of the D1 / S3 and the D1 / S3-S4 cytosolic linker (Figure 19B). Interestingly, the residue difference in the cytosolic linker of the 5A variant contains a polar, negatively charged (acidic) residue (Asp206) compared to the 5N variant which retains a polar, non-charged Asn at the 206 position at a physiological pH (Figure 19B). This acidic residue substitution could contribute an additional negative charge to the electrostatic field surrounding the D1 / S4 (Asamoah et al., 2003; Sigg and Bezanilla, 2003). Additionally, the Asp206 may form electrostatic interactions with N-terminal residues in the mobile D1 / S4

charge translocator, which is laden with positive residues (Cha and Bezanilla, 1998; Sorensen et al., 2000).

Together, based on our data with the I1461T PEPD mutation (Figures 17 and 20), we predict that the changes induced by splicing are likely have a functional impact on other disease mutations that alter inactivation and this could be useful in understanding the underlying molecular mechanisms. It is likely that expression patterns of splice variants in human populations are altered during painful conditions (Raymond et al., 2004; Fraser et al., 2005; Altier et al., 2007) and may result in unique differences in response to pharmacological agents (Tan et al., 2002). However, one cannot exclude the possibility of additional factors such as cellular background or post-translational modifications that regulate expression patterns or gating properties of specific VGSCs during pain transduction in response to a perceived painful stimulus, shifting pain threshold and altering interpretation of a given stimulus.

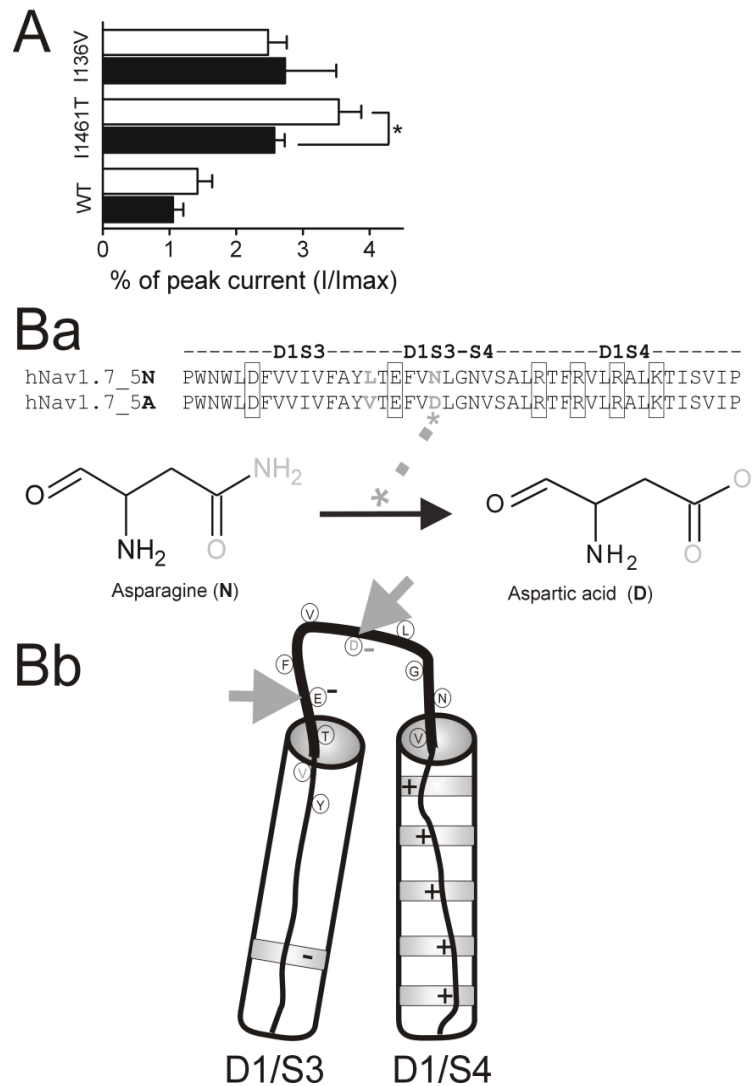


Figure 19. Summary of changes observed in ramp current and potential mechanistic implications for the charge substitution difference between the Na_v1.7 5N and the 5A splice variants in the D1 / S3-S4 linker. (A) Summary bar graph of the percent of peak current determined for each channel. Denoted on the y-axis are the channel types (WT and numbered IEM or PEPD mutants). The x-axis represents the percentage of peak ramp current elicited for the splice variants in each group, where the 5N forms are highlighted in blackened or filled horizontal bars, and the 5A forms are highlighted with unfilled bars. Raw numerical data were determined by selecting the peak ramp current elicited from each trace, filtered at 250 Hz to reduce stochastic noise, and then divided by the peak transient sodium current elicited during an activating protocol, then multiplied by 100 to yield the percent of peak current for individual recordings. Raw data was then compiled and averaged to determine group mean and standard error. Statistical significance was set at $p < 0.05$ and noted with a star

(*). **(Ba)** Sequence alignment of Na_v1.7 D1 / S3 through the region D1 / S4. Exon 5 amino acid differences, located within the D1 / S3-S4 linker, between the 5N versus the 5A splice forms are highlighted with grayed letters. Conserved *native* charged residues are illustrated with an encompassing rectangle in the sequence alignment. A substituted charged residue in the D1 / S3-S4 of the Na_v1.7 5A form is emphasized with a star and a dashed line leading to the amino acid structural differences at physiological pH. In the 5N form there is an uncharged asparagine (N) residue characterized by the grayed amide moiety, whereas the 5A residue is a charged aspartic acid (D), with the charged moiety also noted in gray. **(Bb)** Structural diagram of the Na_v1.7 D1 / S3-S4 transmembrane segments and the adjoining extracellular linker predicted for the 5A splice variant. Single-letter residues from the above sequence alignment are inserted along predicted exon 5 coding region chain from the upper portions of the segments and the linker region. Native charged residues conserved between the splicing forms are highlighted with the corresponding charge (+ or -) within the segments and linker regions. Residue substitutions between the 5N and the 5A variants are grayed and highlighted with an arrow. Note that the charge substitution within the linker between the splice variants occurs near the highly charged S4 segment of D1.

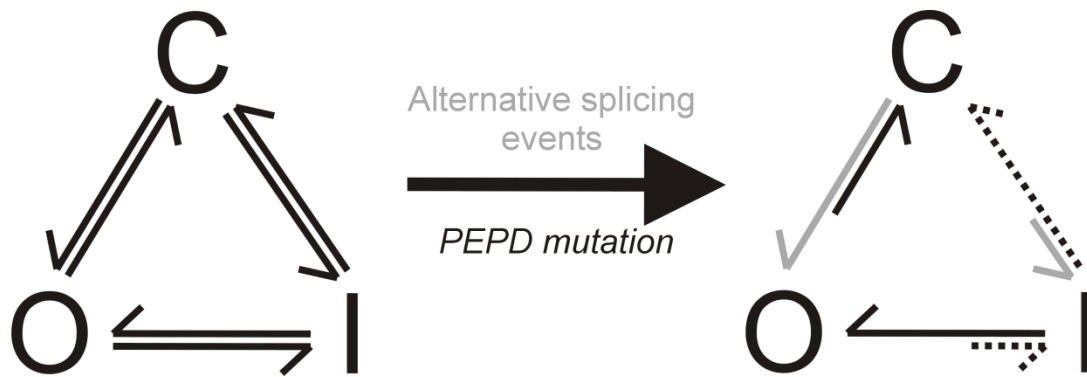


Figure 20. State-occupancy diagram illustrates increased open-state probability for 5A PEPD mutant channels. Simplified three-state diagram of transitions between closed (C), open (O), and inactivated (I) where movement between the states is dependent on membrane potential and time. Illustrated in the model on the left of the reaction arrow are theoretical transitions between each state for a WT 5N splice form. To the right of the reaction arrow are the effects the PEPD mutation (I1461T) has on transition between the simplified states, primarily on the stability of the inactivated configuration highlighted with dotted lines. Also noted to the right of the reaction arrow are the effects the 5A alternative splicing substitutions have (highlighted by the grayed arrow) on the simplified transitions.

D. Inherited mutations implicated in neuronal and muscle channelopathies
can generate resurgent sodium currents in DRG neurons

1. *Abbreviated introduction of resurgent currents and a potential role
as a disease modifier in voltage-gated sodium channelopathies*

Over two hundred different missense mutations in seven VGSCs have been identified as causing disorders of excitability, or channelopathies, in humans (Cannon, 2000; George, 2005; Meisler and Kearney, 2005; Koopmann et al., 2006; Catterall et al., 2008). Although these channelopathies are relatively rare, understanding the functional consequences of the disease mutations provides invaluable insight into the roles that VGSCs play in normal and abnormal excitability. Mutant channels have been extensively studied in non-excitable heterologous expression systems, providing substantial knowledge; however a major concern is that the functional properties of VGSCs in neurons and muscle cells are not always accurately reproduced in non-excitable cells. A prime example of this phenomenon is VGSC resurgent currents. The properties of the coined term, resurgent currents, originally described in cerebellar Purkinje neurons, involved a “resurgence” of inward sodium currents during membrane repolarization (Raman and Bean, 1997). As described earlier (refer to *Background* section of dissertation) the “resurgence” of sodium currents, whose predominant generator is Na_v1.6 channels (Raman et al., 1997; Raman and Bean, 1999b; Cummins et al., 2005), flowed when the channels should be

inactivated and thus reducing to the AP refractory period and high frequency firing (Raman and Bean, 1997, 1999a, b, 2001). Artificial slowing of VGSC inactivation via toxin application can induce resurgent currents in Purkinje neurons isolated from Na_v1.6 knock-out mice (Grieco and Raman, 2004), indicating that other VGSCs, besides Na_v1.6, may have the capacity to generate resurgent sodium currents. While resurgent VGSC currents have been recorded from neurons, it has not been possible to record resurgent currents in non-excitabile heterologous expression systems (Raman et al., 1997; Cummins et al., 2005; Chen et al., 2008) and it is not known if VGSC mutations that cause channelopathies alter resurgent currents.

Na_v1.7 channels, highly expressed in DRG neurons, are essential in nociception as evidenced by single point *missense* mutations causing a spectrum of pain syndromes, including PEPD, and *nonsense* mutations resulting in human insensitivity to pain (Dib-Hajj et al., 2007). However, the means by which these channels are regulated (or deregulated) during cellular hyperexcitability and their overall contributions to increased pain perception are still debated (Amir et al., 2006; Cummins et al., 2007). As shown earlier in this dissertation, the potential contribution alternative splicing has on impact of painful mutations in Na_v1.7 was explored (Jarecki et al., 2009). Additional factors that may modulate excitability, and thus pain perception, include changes in, for example, post-translational modifications and protein trafficking, cellular background, lipid environment, signaling mechanisms, and cellular oxidation-reduction balance (Scholz and Woolf, 2002; Woolf and Ma, 2007; Costigan et al., 2009). One intriguing

hypothesis from our laboratory suggested that post-translational modifications and cellular background which may increase resurgent sodium currents could play a unique role in the spectrum of disorders associated with Na_v1.7 point mutations. Although Na_v1.7 channels were previously shown to not produce resurgent currents (Raman and Bean, 1997; Cummins et al., 2005), the possibility that Na_v1.7-PEPD mutations, which, as we have shown, slow and destabilize inactivation, increase cellular excitability, and contribute to increases in pain perception, allow for generation of resurgent currents had not been explored. Therefore, in a collaborative effort with fellow graduate student Andrew D. Piekarz and Theodore R. Cummins, we asked if the inherited Na_v1.7-PEPD mutation (I1461T) would enable Na_v1.7 channels with the ability to produce resurgent currents.

2. An inherited Na_v1.7-PEPD disease mutation (I1461T) that destabilizes inactivation produces resurgent current in DRG neurons and increases action potential firing

We first asked if a mutation in Na_v1.7 that slows inactivation and causes paroxysmal extreme pain disorder (PEPD) (Jarecki et al., 2008) could generate resurgent sodium currents. Na_v1.7 channels, highly expressed in DRG neurons, are essential in nociception as evidenced by single-point *missense* mutations causing a spectrum of pain syndromes, including PEPD, and *nonsense* mutations resulting in human insensitivity to pain (Dib-Hajj et al., 2007). Although Na_v1.7 channels have been shown to not produce resurgent currents, PEPD

mutations destabilize inactivation, shifting the voltage-dependence and decreasing the rate of inactivation (Dib-Hajj et al., 2008; Jarecki et al., 2008). Therefore, we hypothesized that PEPD mutations might induce resurgent currents. We studied the Na_v1.7-PEPD mutation I1461T, which is located within the highly conserved D3-D4 inactivation particle (IFMT) critical for VGSC inactivation (Stuhmer et al., 1989; Patton et al., 1992; West et al., 1992). Modified WT Na_v1.7 (Na_v1.7r) and Na_v1.7-I1461T (Na_v1.7r-I1461T) channels that generate currents that can be pharmacologically isolated were expressed in adult rat DRG neurons as described in the *Methods*. In DRG neurons, robust transfected current was observed for wild-type (WT) and mutant Na_v1.7 channels (Figure 21A and B). In addition to the recombinant channel of interest, neurons were also co-transfected with a second plasmid encoding for both EGFP, to help identify transfected neurons, and a specific Na_v1.8-shRNA, to minimize endogenous Na_v1.8 currents as described in detail in the *Methods* section (refer to Figure 23 for an example). In DRG neurons, the I1461T PEPD mutation impaired inactivation (Figure 21C and D; Table 4) but did not alter activation of Na_v1.7r channels. The persistent component (*I*_{per}), measured at the end of a 50 ms pulse to -10 mV, was also significantly larger for the I1461T channels than for wild-type Na_v1.7r channels (*I*_{per} = 0.2 ± 0.2% of peak transient current for wild-type, n = 13 and 1.0 ± 0.3% for Na_v1.7r-I1461T, n = 22). These changes were identical to those observed for wild-type and I1461T Na_v1.7 channels expressed in human embryonic kidney 293 (hEK₂₉₃) cells (Jarecki et al., 2008).

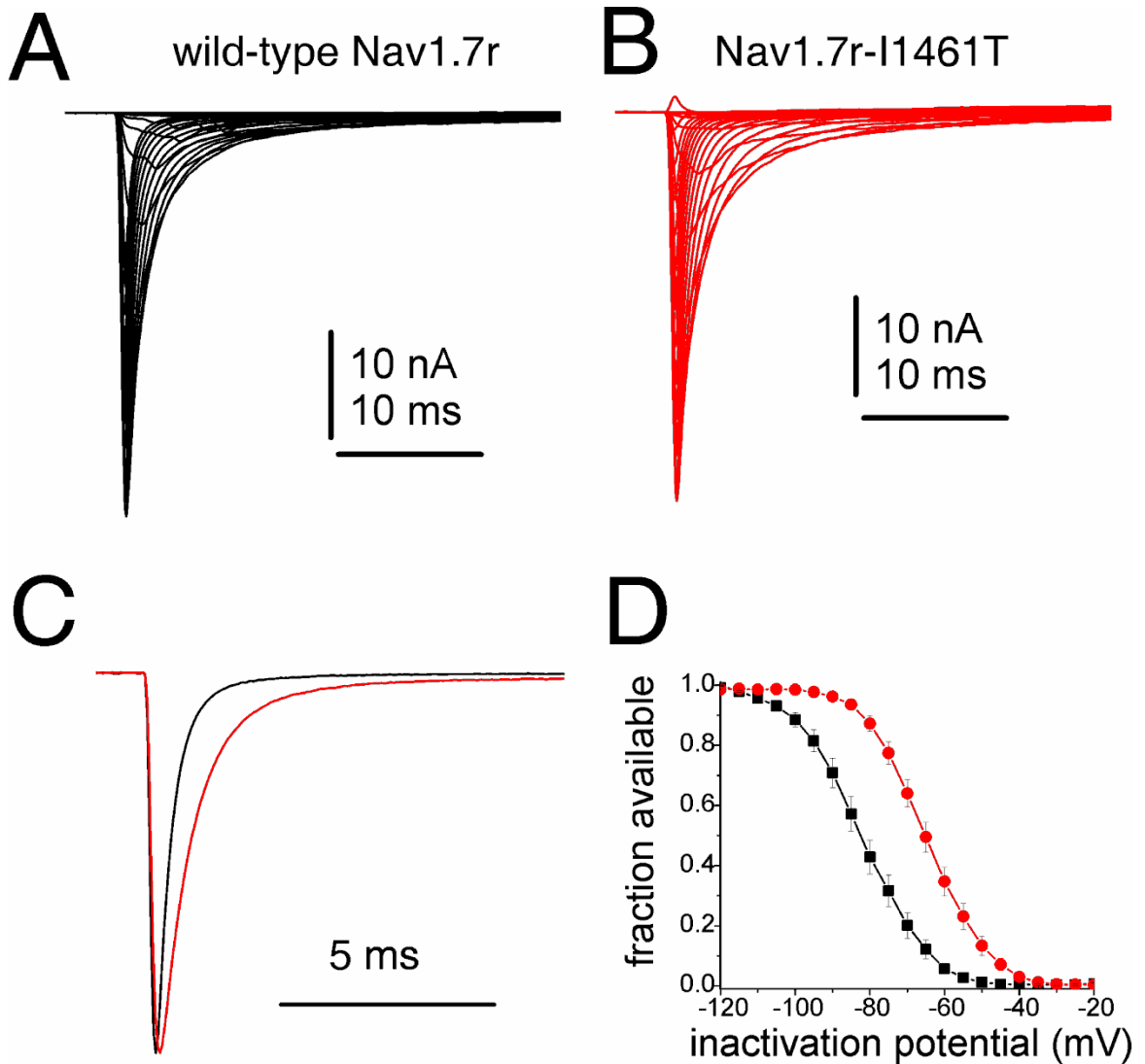


Figure 21. Currents generated by recombinant Nav_v1.7 channels expressed in DRG neurons. (A) Representative Nav_v1.7r current traces recorded from a transfected DRG neuron. (B) Representative Nav_v1.7r-I1461T current traces recorded from a transfected DRG neuron. Currents were elicited with step depolarizations to voltages ranging from -80 to +40 mV from a holding potential of -100 mV. (C) The painful mutation I1461T slows the rate of inactivation of Nav_v1.7r. The black trace is wild-type Nav_v1.7r and the red trace is Nav_v1.7r-I1461T. Currents were elicited with a step depolarization to +10 mV. (D) Steady-state inactivation curves for Nav_v1.7r (black data) and Nav_v1.7r-I1461T (red data) channels expressed in DRG neurons. Cultured adult rat DRG neurons were transfected with the recombinant VGSC construct and Nav_v1.8-shRNA and recordings were done in the presence of 500 nM TTX.

Surprisingly, in DRG neurons both wild-type $\text{Na}_v1.7r$ and $\text{Na}_v1.7r\text{-I1461T}$ channels also generated resurgent sodium currents (Figure 24). The characteristic properties of resurgent sodium currents differed from those observed for tail currents, assayed during a deactivation protocol, and transient currents, elicited during an I/V protocol (Figure 22). Resurgent sodium currents were observed in 5 of 21 neurons transfected with wild-type $\text{Na}_v1.7r$ (Figure 24A and B), with an average amplitude, expressed as a percentage of the peak transient sodium current elicited with a test pulse to -10 mV, of $1.0 \pm 0.5\%$ for these five neurons. By contrast, 20 of 30 neurons expressing $\text{Na}_v1.7r\text{-I1461T}$ channels produced resurgent sodium current (Figure 22C and D). The frequency of observing resurgent with $\text{Na}_v1.7r\text{-I1461T}$ channels was significantly increased (Chi squared < 0.05) compared to wild-type $\text{Na}_v1.7r$ channels. Moreover, the relative amplitude of the resurgent current ($2.0 \pm 0.1\%$) was also significantly greater for $\text{Na}_v1.7r\text{-I1461T}$ than for wild-type $\text{Na}_v1.7r$ channels. Because all PEPD mutations characterized, to date, result in slower inactivation of $\text{Na}_v1.7$ (Dib-Hajj et al., 2008; Jarecki et al., 2008) we predict all PEPD mutations are likely to increase resurgent current generation.

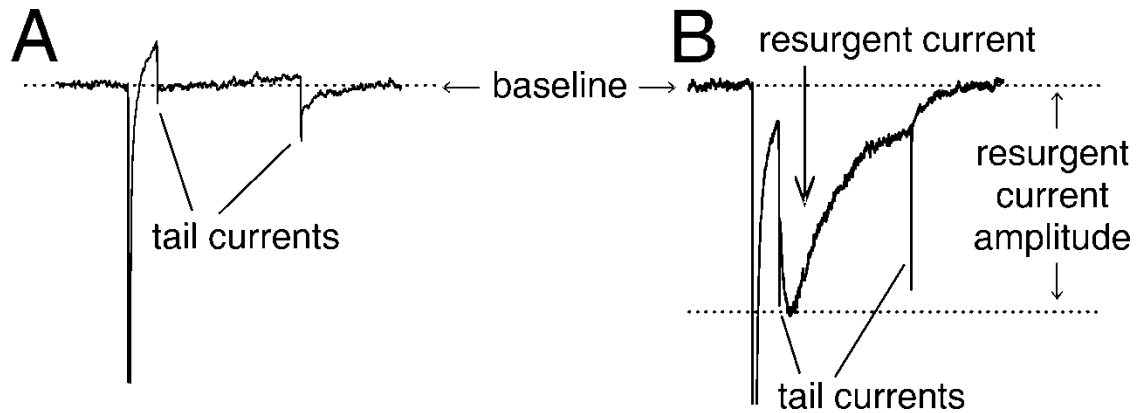


Figure 22. Quantification of resurgent current amplitude. Sodium currents recorded from two different neurons expressing $Na_v1.6r$ currents are shown. Currents were elicited with a 20 ms pulse to +30 mV followed by a 100 ms pulse to -40 mV from a holding potential of -100 mV. Rapid tail currents can be seen in the recordings from both neurons (**A** and **B**). In addition, robust resurgent current, with slower onset and decay than the tail currents, can be seen in the recording shown in (**B**). The amplitude of the resurgent current is measured relative to the baseline obtained at the holding potential. Tail currents are not included in the measurement of resurgent current amplitudes through judicious use of the measurement cursors in the analysis program.

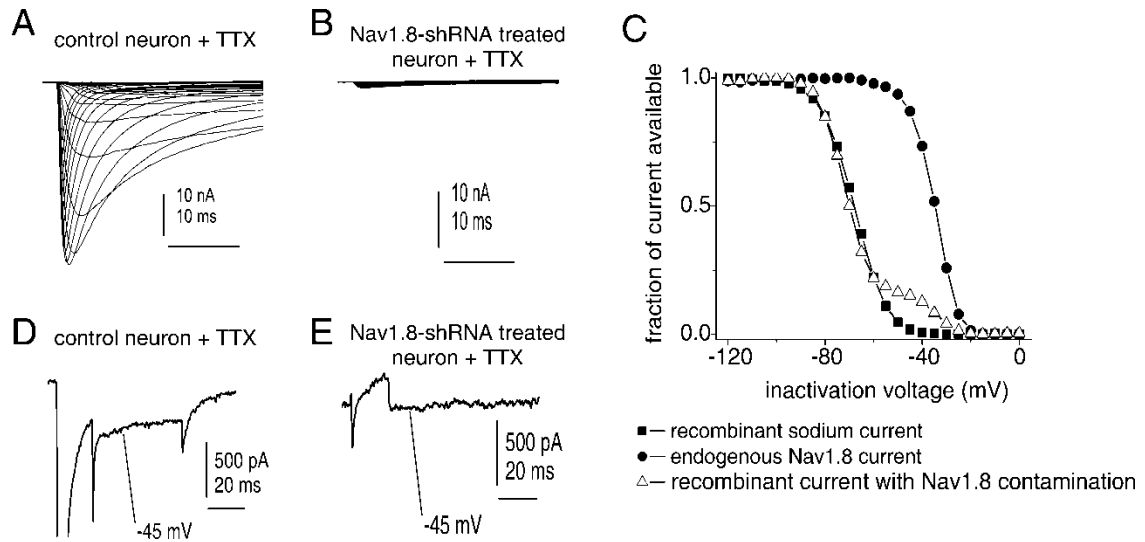


Figure 23. Properties of endogenous and biolistically transfected recombinant VGSC currents in the presence and absence of TTX and / or $Na_v1.8$ -shRNA. (A) Representative TTX-resistant currents recorded from a cultured adult rat DRG neuron in the presence of 500 nM TTX. Currents were elicited with voltage steps ranging from -80 to +40 mV in 10 mV increments. These currents show the kinetic properties typical of $Na_v1.8$ currents. (B) Representative currents recorded from a cultured adult rat DRG neuron transfected with $Na_v1.8$ -shRNA but no recombinant VGSC construct. Scale is the same as in (A) for comparison. In the presence of TTX, very little sodium current is elicited. This demonstrates the $Na_v1.8$ -shRNA transfection combined with application of 500 nM TTX effectively blocks the majority of endogenous voltage-gated sodium currents in cultured DRG neurons. (C) Steady-state inactivation curves for endogenous $Na_v1.8$ currents (filled circles) recorded from the same neuron used in (A), a transfected neuron expressing recombinant $Na_v1.5r$ current without evidence of $Na_v1.8$ contamination (closed squares) and a transfected neuron expressing recombinant $Na_v1.5r$ current with ~20% contamination by endogenous $Na_v1.8$ currents (open triangles). $Na_v1.8$ contamination is evidenced by the biphasic voltage-dependence of steady-state inactivation. Recordings were done in the presence of 500 nM TTX and recombinant $Na_v1.5r$ was co-transfected with $Na_v1.8$ -shRNA. (D) Resurgent currents are not detected in control neurons in the presence of 500 nM TTX. Currents are recorded from the same neuron used in (A) and are magnified 30x relative to the peak current elicited with a test pulse to -10 mV. (E) Resurgent currents are not detected in neurons transfected with $Na_v1.8$ -shRNA but no recombinant VGSC construct in the presence of 500 nM TTX. Currents are recorded from the same neuron used in (B) and are shown on the same scale as in (D) for comparison.

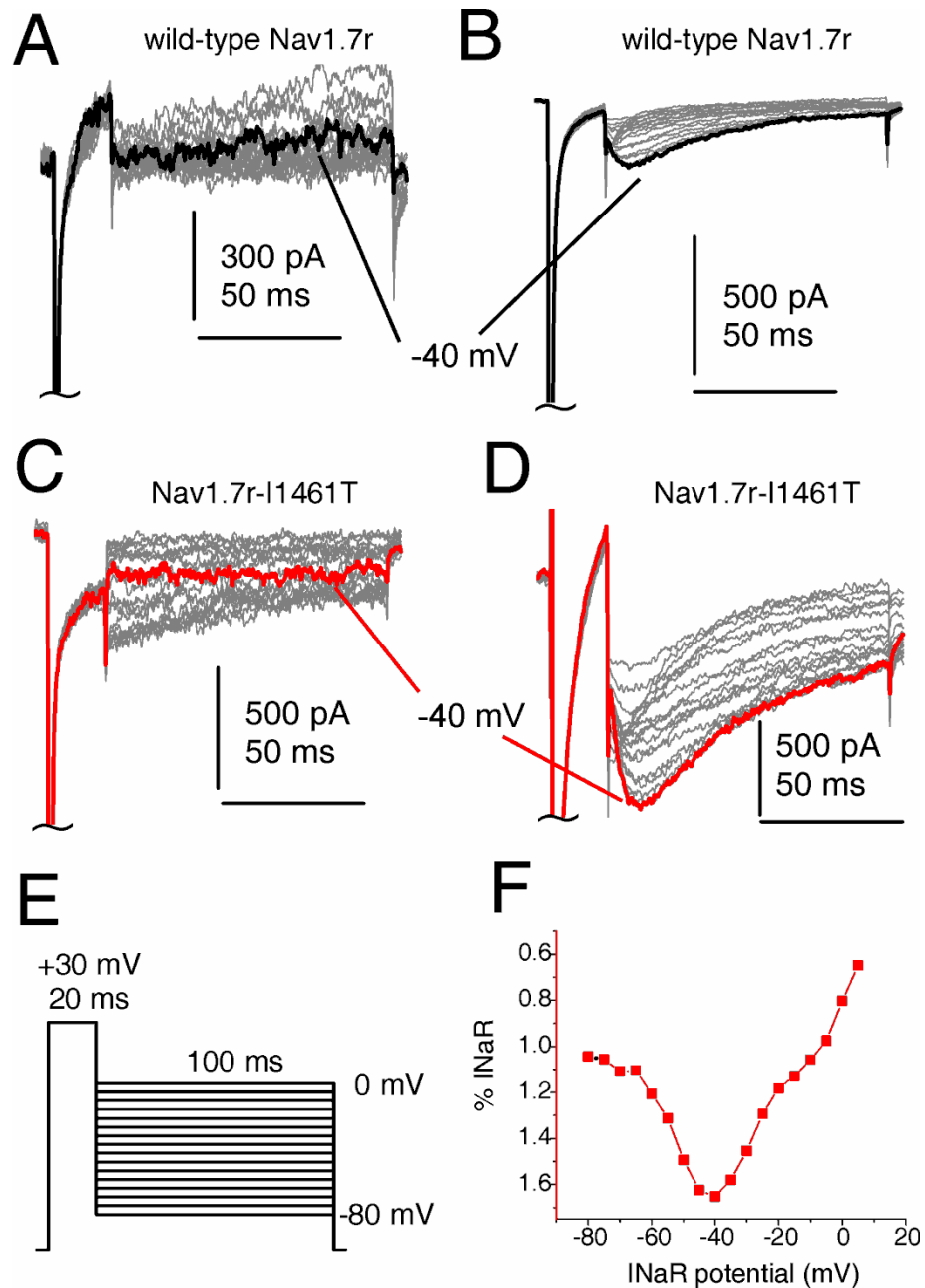


Figure 24. Resurgent currents are produced by recombinant $Na_v1.7$ channels expressed in DRG neurons. Representative current traces recorded from DRG neurons expressing wild-type $Na_v1.7r$ that did not (A) and that did (B) generate resurgent currents. Representative current traces recorded from DRG neurons expressing $Na_v1.7r-I1461T$ channels that did not (C) and that did (D) generate resurgent currents. Resurgent currents were larger on average for $Na_v1.7r-I1461T$ than for wild-type $Na_v1.7$ channels. Currents are magnified 30x relative to the peak transient current (elicited with a pulse to -10 mV) to emphasize the resurgent current components. (E) Resurgent current voltage protocol. (F) Voltage-dependence of resurgent current shown in (D).

Based on work done in cerebellar Purkinje neurons (Raman et al., 1997), we anticipated that increased resurgent sodium currents generated by PEPD mutations may result in spontaneous and / or repetitive APs in DRG neurons. To test this, we performed computer simulations of DRG neuron excitability. We used an established model of DRG neuron excitability (Sheets et al., 2007), with modifications only to the appropriate sodium channel formulation, simulated and evaluated the impact of the I1461T mutation and resurgent currents on AP firing. The resurgent current blocking factor was implemented using a previously described strategy without modifications (Khaliq et al., 2003). In our model, developed and simulated by Dr. Theodore R. Cummins, the blocking factor induced resurgent current was 1.0% of the peak transient current in the modeled wild-type $\text{Na}_v1.7$ conductance and 2.0% of the peak transient current in the modeled $\text{Na}_v1.7$ -I1461T conductance. The computer simulations of AP firing in DRG neurons indicate that while the destabilization of inactivation caused by the I1461T mutation is sufficient to decrease the threshold for eliciting an AP, inclusion of the resurgent current blocking factor leads to high-frequency trains of APs. It is important to note that even when the transition rate expressions for the blocking factor were adjusted so that the wild-type resurgent current was doubled (2% of peak), a 70 pA stimulus still only elicited a single action potential in the model neuron. These results indicate the resurgent current blocking factor and the I1461T mutations act synergistically to increase neuronal excitability and that resurgent currents probably contribute to the extreme pain sensations associated with PEPD mutations (Jarecki et al., 2010).

3. *A cardiac LQT3 / SIDS mutation that slows inactivation increases resurgent $Na_v1.5$ current and broadens action potential waveform in a modeled myocyte*

Disease mutations that impair inactivation have also been identified in several other VGSCs, including $Na_v1.1$ and $Na_v1.3$ mutations associated with epilepsies, $Na_v1.4$ mutations associated with skeletal muscle myotonias, and $Na_v1.5$ mutations associated with cardiac arrhythmias (Cannon, 2000; George, 2005; Meisler and Kearney, 2005; Cannon, 2006; Koopmann et al., 2006). Over 50 different disease mutations that impair inactivation have been characterized. However, these mutations have all been characterized in heterologous expression systems that do not support the generation of resurgent sodium currents. Therefore, we next used the DRG expression system to determine if the $Na_v1.5$ long-QT type 3 / sudden infant death syndrome (LQT3 / SIDS) associated mutation F1486L (Wang et al., 2007) could generate increased resurgent currents. As has been previously shown in hEK₂₉₃ cells (Wang et al., 2007), the F1486L mutation, which is also located in the IFMT inactivation particle, slowed the rate of inactivation, increased the fraction of persistent currents and shifted the voltage-dependence of activation in the depolarizing direction (Table 4). However, 9 of 18 transfected DRG neurons expressing wild-type $Na_v1.5$ generated resurgent currents (Figure 25A and B; Table 4). In our expression system the $Na_v1.5$ -F1486L LQT3 / SIDS mutation significantly increased the relative amplitude of the resurgent currents (Table 4). Eight out of seventeen neurons expressing $Na_v1.5$ -F1486L channels generated resurgent

currents with average relative amplitude of $2.0 \pm 0.4\%$ (Figure 25C and D; Table 4).

As resurgent sodium currents are activated during repolarization, increased resurgent currents in $\text{Na}_v1.5$ would be expected to broaden the AP, increase the QT interval and thus contribute to the potentially lethal cardiac arrhythmias associated with LQT3 / SIDS mutations. Mathematical modeling was performed by Dr. Theodore R. Cummins using a modified mathematical model of cardiac AP firing (Luo and Rudy, 1994; Courtemanche et al., 1998) to simulate the impact of the F1486L LQT3 / SIDS mutation and resurgent currents. The cardiac myocyte model was previously implemented by Ingemar Jacobson in the NEURON simulation environment (Hines and Carnevale, 1997). Simulated models of resurgent sodium currents and computer simulations of a cardiac myocyte (Courtemanche et al., 1998) indicate that an increase in resurgent currents in $\text{Na}_v1.5$ broaden the cardiac AP and increase the QT interval (Jarecki et al., 2010).

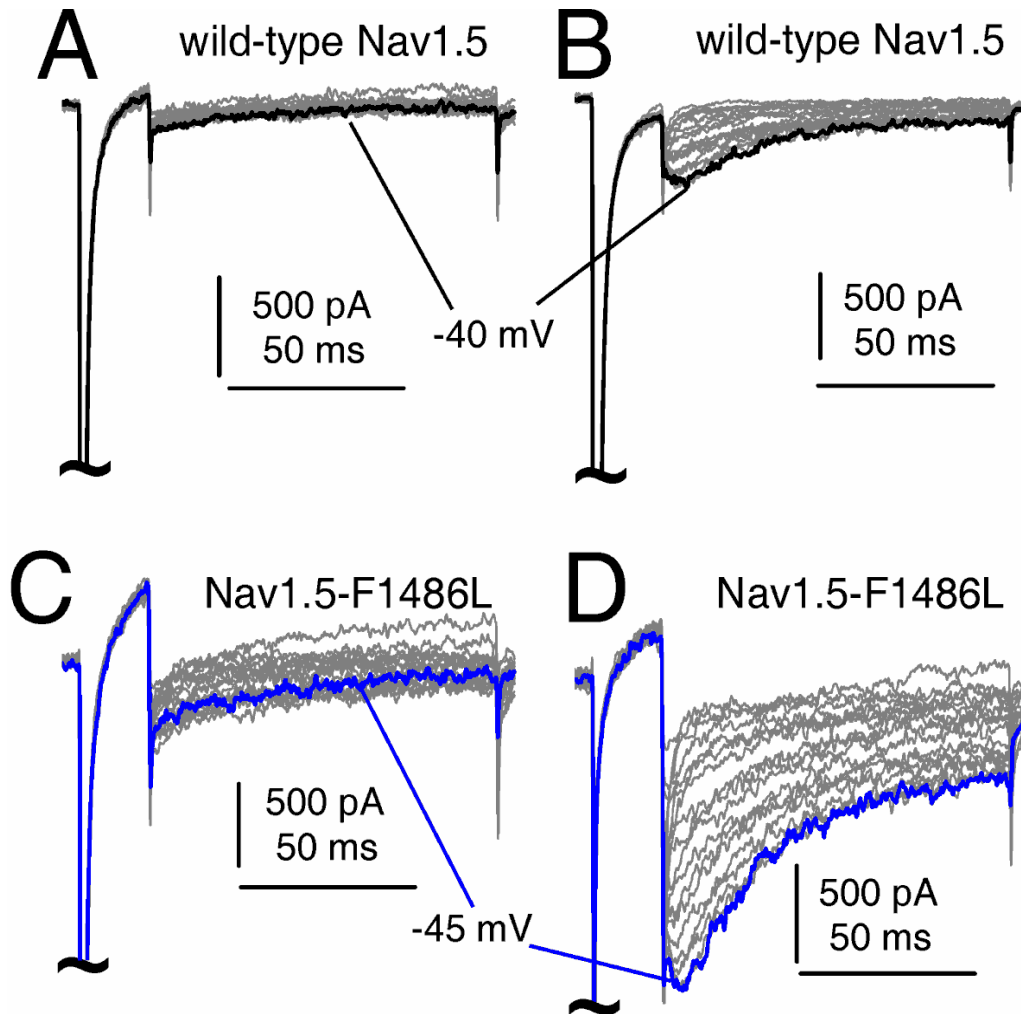


Figure 25. Resurgent currents are produced by $Na_v1.5$ channels. Representative current traces recorded from DRG neurons expressing wild-type $Na_v1.5$ that did not (A) and that did (B) generate resurgent currents. Representative current traces recorded from DRG neurons expressing LQT3 / SIDS $Na_v1.5$ -F1486L channels, emphasized in blue, that did not (C) and that did (D) generate resurgent currents. Resurgent currents were larger on average for $Na_v1.5$ -F1486L than for wild-type $Na_v1.5$ channels. Currents were elicited with the standard resurgent current protocol shown in Figure 24E and are magnified 30x relative to the peak current amplitude.

4. A D4 / S4 PMC mutation in Na_v1.4 that replaces a charged residue and uncouples fast inactivation generates resurgent sodium currents

We next asked if a mutation that slows inactivation of Na_v1.4 and causes paramyotonia congenita (PMC) could induce resurgent sodium currents. We studied the R1448P mutation (Featherstone et al., 1998) which alters the outermost extracellular charged residue in the sodium channel voltage sensor that couples channel activation and inactivation (Chahine et al., 1994). Interestingly, while this mutation slows the inactivation of Na_v1.4 currents by ~10-fold (Figure 26A) it causes a hyperpolarizing shift in the voltage-dependence of inactivation (Table 4). In a previous study, resurgent sodium currents were not detected in any of 41 DRG neurons transfected with wild-type skeletal muscle sodium channel Na_v1.4r (Cummins et al., 2005). While we, again, did not detect resurgent currents in any of 11 neurons expressing wild-type Na_v1.4r (Figure 26B), 13 of 20 neurons expressing Na_v1.4r-R1448P channels generated resurgent currents (Figure 26C), with an average relative amplitude of $4.8 \pm 0.7\%$ of peak. Thus, at least for Na_v1.4, slowing the rate of inactivation seems to be crucial to the production of resurgent sodium currents and the impact of the mutation on the voltage-dependence of inactivation may be less important. It should be noted that while the R1448P mutation does not alter the voltage-dependence of activation, it slows deactivation (the rate at which open channels transit to the closed state) (Oxford, 1981; Featherstone et al., 1998), and slower

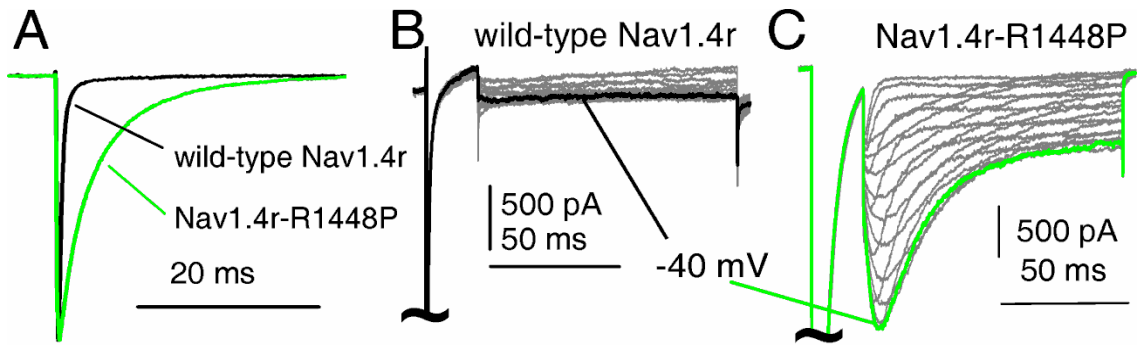


Figure 26. A paramyotonia congenita mutation induces resurgent currents in $\text{Na}_v1.4$. (A) The paramyotonia congenita R1448P mutation, highlighted in green, causes a pronounced slowing of the rate of $\text{Na}_v1.4r$ inactivation. Currents were elicited with a step depolarization to +10 mV. Resurgent currents were not detectable in any of the neurons expressing wild-type $\text{Na}_v1.4r$ channels (B). By contrast, the majority of neurons expressing $\text{Na}_v1.4r$ -R1448P channels generated robust resurgent currents (C). Resurgent currents were elicited with the protocol shown in Figure 24E and are magnified 20x relative to the peak current amplitude.

deactivation might also contribute to enhanced resurgent currents, especially in combination with slower inactivation.

Resurgent currents generated by $\text{Na}_v1.4$ are likely to increase repetitive AP firing in skeletal muscle, which is one of the hallmarks of PMC. However, it should be noted that patients with PMC can also experience episodes of muscle weakness or paralysis in addition to myotonia (Heatwole and Moxley, 2007). Although resurgent currents could clearly contribute to myotonic activity associated with PMC, incomplete inactivation observed with mutant PMC channels is likely to be an important factor in muscle weakness associated with PMC (Cannon, 2006).

5. A homologous inactivation gate mutation engineered into $\text{Na}_v1.6$ channels dramatically increases resurgent currents and destabilizes transition to an inactivated state

Since $\text{Na}_v1.6$ appears to be the predominant generator of resurgent currents in cerebellar Purkinje neurons and DRG neurons (Raman et al., 1997; Cummins et al., 2005), we next compared the amplitude of resurgent currents generated by $\text{Na}_v1.6$ channels with those produced by the $\text{Na}_v1.4$, $\text{Na}_v1.5$ and $\text{Na}_v1.7$ disease mutations. Resurgent currents were detected in 8 of 14 DRG neurons expressing wild-type $\text{Na}_v1.6r$ channels, with an average relative amplitude of $2.4 \pm 0.3\%$ of the peak current (Figure 27A). This relative amplitude is similar to that produced by the $\text{Na}_v1.7r$ -I1461T PEPD mutant and the $\text{Na}_v1.5$ -F1486L LQT3 / SIDS mutant, but slightly smaller than that produced by the

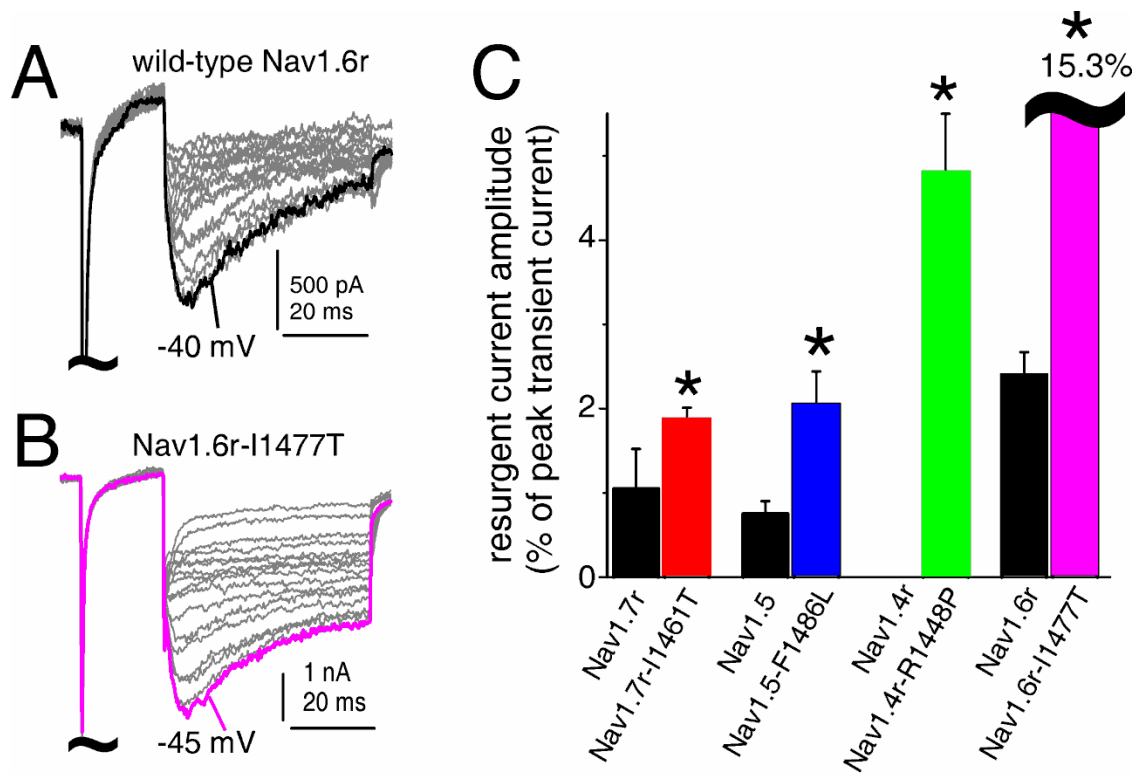


Figure 27. $Na_v1.6$ channels generate large resurgent currents. Representative resurgent currents recorded from a neuron expressing wild-type $Na_v1.6r$ (**A**) and $Na_v1.6r$ -I1477T (**B**) channels. The current traces are magnified 20x (**A**) and 5x (**B**) relative to the peak current. (**C**) Comparison of the relative resurgent current amplitude, expressed as a percentage of peak transient current, for wild-type and mutant voltage-gated sodium channels. * indicates significant difference ($p < 0.05$) between wild-type and mutant channels for a given isoform. Color-coding is conserved throughout figures in this section.

Na_v1.4r-R1448P PMC mutant (Figure 27C). This indicates that the resurgent currents produced by the disease mutants are indeed likely to have important impact on cellular excitability.

Remarkably, gain-of-function disease mutations, to date, have not been identified in Na_v1.6 channels. To determine the potential impact of mutations in Na_v1.6 that impair inactivation, we asked if a mutation in Na_v1.6 (I1477T) corresponding to the I1461T mutation in Na_v1.7 could increase resurgent sodium currents generated by Na_v1.6. The Na_v1.6r-I1477T mutation shifted the voltage-dependence of inactivation in the depolarizing direction, slowed the rate of inactivation and significantly increased the persistent sodium current (Table 4). Resurgent currents were observed in 7 of 14 neurons expressing Na_v1.6r-I1477T channels. Notably, these currents were approximately 8-fold larger than those produced by either wild-type Na_v1.6r or Na_v1.7r-I1461T PEPD channels, with an average relative amplitude of $15.3 \pm 3.4\%$ (Figure 27C). These data suggest that mutations impairing inactivation of Na_v1.6 may be lethal due to the proclivity of Na_v1.6 to generate resurgent currents. Upon sequence alignment of the D3-D4 residues of Na_v1.6 and 1.7, I noticed a non-conserved residue, five amino acids upstream from the Na_v1.7-I1461 location. The residue at the 1456 position in Na_v1.7 is a Leu, with an aliphatic side chain, and is a Phe, with a bulky side chain in Na_v1.6. It is intriguing to hypothesize that this non-conserved residue difference between Na_v1.6 and 1.7 may contribute to the proclivity of Na_v1.6 channels to generate resurgent currents compared to Na_v1.7. Future studies,

performed by me, using point-chimeras will be performed to further investigate these differences.

Table 4. Biophysical properties of wild-type and mutant Na_v1.4, 5, 6 and 7 sodium channels tested for resurgent currents.

Construct	V _{1/2} inactivation ¹ (mV)	Tau-h ² (ms)	Persistent current ³ (%)	Resurgent current ⁴ (%)
Na _v 1.7r	-80.1 ± 1.6 n = 25	0.85 ± 0.06 n = 23	0.19 ± 0.16 n = 13	1.0 ± 0.5 n = 5 (of 21)
Na _v 1.7r-I1461T	-61.8 ± 1.3 * n = 37	1.07 ± 0.07 * n = 35	1.04 ± 0.25 * n = 13	2.0 ± 0.1 * n = 20 (of 30)
Na _v 1.5	-88.1 ± 1.7 n = 20	0.9 ± 0.07 n = 20	0.2 ± 0.08 n = 15	0.6 ± 0.1 n = 9 (of 18)
Na _v 1.5-F1486L	-80.1 ± 1.6 n = 18	1.31 ± 0.14 * n = 15	0.64 ± 0.15 * n = 10	2.0 ± 0.4 * n = 8 (of 17)
Na _v 1.4r	-77.3 ± 2.1 n = 11	0.34 ± 0.03 n = 11	0.17 ± 0.13 n = 10	None detected (out of 11)
Na _v 1.4r-R1448P	-91.1 ± 2.4 * n = 20	3.92 ± 0.25 * n = 21	0.95 ± 0.28 * n = 20	4.2 ± 0.6 * n = 13 (of 20)
Na _v 1.6r	-71.3 ± 1.9 n=17	1.02 ± 0.1 n = 17	0.69 ± 0.16 n = 11	2.4 ± 0.3 n = 8 (of 14)
Na _v 1.6r-I1477T	-58.6 ± 1.2 * n = 18	1.25 ± 0.09 n = 18	7.4 ± 0.68 * n = 14	15.3 ± 3.4 * n = 7 (of 14)

¹V_{1/2} inactivation is the mid-point voltage of the steady-state inactivation curve as determined with a standard Boltzmann distribution fit. ²Tau-h: time constant for current decay during +10 mV step depolarization. ³Persistent current measured at 50 ms during step depolarization to +10 mV and reported as a percentage of peak current amplitude elicited by the step depolarization. ⁴Resurgent sodium current measured with protocol shown in Figure 24E and reported as a percentage of the peak current amplitude elicited by a step depolarization to -10 mV. The average resurgent current amplitude is only calculated from those cells where resurgent current was detected. * indicates significant difference for mutant channels compared to respective wild-type channel (p < 0.05).

Together, results from this study provide the first evidence that inherited channelopathies resulting from mutations that slow VGSC inactivation can increase resurgent sodium currents. We have also shown with simulated models how the increase in resurgent current along with inherited mutations that slow inactivation can impact AP properties. Thus, an increase in resurgent currents, with mutations implicated in several inherited channelopathies, provides evidence for a novel mechanism by which AP firing may be affected.

From a structural standpoint, it is intriguing to note that (1) these effects are not only observed with inherited mutations within the putative D3-D4 inactivation gate motif (IFMT), but also with mutations in a voltage-sensing component (D4 / S4) critical for coupling activation to inactivation and (2) the effects can be observed in several VGSC isoforms upon transfection into a cellular background appropriate to produce resurgent currents. This suggests that although $Na_v1.6$ channels appear to be the predominant generator of resurgent currents, other VGSC isoforms have the ability to produce resurgent currents under certain conditions, indicating additional factors such as cellular background, post-translational mechanisms, tissue expression, presence of auxiliary subunits, or protein chemistry must also play an important role. This could broadly be explained by assuming mutations that affect inactivation properties may be sufficient to shift the balance of resurgent current production into a window of resolution and potentially of physiological importance, but may not be the only component necessary. However, as we have demonstrated, altered gating and channel stability is one mechanism that allows several VGSC

isoforms to generate resurgent sodium currents to flow during membrane repolarization. Additionally, since VGSC isoforms have been suggested to derive their unique voltage-dependent gating characteristics and pharmacological sensitivities from residue differences in well-conserved regions of the channel, it is interesting to hypothesize the role non-conserved amino acid residues may play in tuning the threshold for susceptibility of the VGSC isoforms to production of resurgent currents.

However, in light of the structural perturbations caused by these single-point mutations implicated in the channelopathies outlined above, the intramolecular interactions required to stabilize an inactivated state are still unclear. We have shown that Na_v1.7 channel stability during transition to an inactivated state is crucial for proper voltage-dependent gating (Dib-Hajj et al., 2008; Jarecki et al., 2008) and orchestration of AP firing (Dib-Hajj et al., 2008). The importance of this transition is confirmed by the numerous therapeutic agents targeted to stabilize inactivation or an “inactivated-like state” (Butterworth and Strichartz, 1990; Fozzard et al., 2005). Additionally, unpublished work from our laboratory has shown that perturbations that alter transition to an inactivated state can affect the binding affinity of therapeutic agents targeted to stabilize inactivation. We have also described a novel mechanism by which inherited mutations that alter inactivation gating can increase resurgent currents (Jarecki et al., 2010) hypothesized to be via an increased probability of an open-blocking particle to bind within the putative “docking” sites for the inactivation gate (Raman and Bean, 2001; Grieco and Raman, 2004; Grieco et al., 2005). Thus, a central

question to understanding the dysfunction in gating and the consequences this has on the physiological system is: where does the inactivation gate “dock” and how do specific interactions stabilize the channel during depolarization such that Na^+ flux is occluded after the activation gates open?

E. Residues located in the D3 / S4-S5 linkers of $\text{Na}_v1.7$ directly stabilize a fast-inactivated configuration

1. *Abbreviated introduction for probing intramolecular interactions in ion channels*

I next investigated the intramolecular interactions involved in inactivation using site-directed mutagenesis, whole-cell electrophysiology, and protein chemistry. In addition to scanning and site-directed mutagenesis, ion channel topology and the regions critical for gating and ion flux have been explored using a wide variety of chemical tools and manipulations. Ion channel biologists have innovatively used tools such as synthesized ligands, tethered blockers, unnatural amino acid incorporation (Morin and Kobertz, 2008; Ahern and Kobertz, 2009), residue crosslinking and modification (Karlin and Akabas, 1998; Horn et al., 2000) as well as several fluorometric approaches (Blunck et al., 2005; Gorostiza and Isacoff, 2008) to probe the architecture of voltage-sensitive ion channels, thus expanding on previous hypotheses and shedding new light on the dynamic nature of ion channel gating hypothesized by Hodgkin and Huxley in their series of seminal electrophysiology experiments (1952). One such approach, defined

as the substituted cysteine accessibility method, or SCAM (Karlin and Akabas, 1998), has been coupled with voltage-clamp electrophysiology and extensively used to elucidate information about the intramolecular confines of channel proteins such as the ligand-gated nicotinic acetylcholine receptor α -subunit (nAChR), gamma aminobutyric acid (type A) receptors (GABA_AR), as well as voltage-gated channels such as potassium (K_v) and sodium (Na_v) channels (Hille, 2001). Briefly, SCAM allows for the chemical modification of substituted cysteine (Cys) residues in the presence of a variety of modifying reagents. These modifying reagents have the ability to add charged, hydrophobic, or photoreactive moieties to the sulfhydryl group on available Cys residues, used as a labeling reporter, via a nucleophilic attack reaction which occurs within seconds. An additional set of compounds have been designed and synthesized to covalently crosslink available Cys residues within a calculated distance based on the alkyl chain spacer in between the bi-functional reactive groups. The advantage to using this type of method to probe ion channel structure allows the Cys modifying reagents to provide a measurable change in the function of the channel which can then be monitored using electrophysiological techniques to dissect information concerning the timecourse, state-dependence and membrane-sidedness of the accessibility of the introduced Cys (Akabas et al., 1992).

Because the coupling of SCAM with electrophysiology has yielded significant insight into state-dependent structural interactions, this inspired me to probe the D3 / S4-S5 of Na_v1.7 for interactions with the putative inactivation gate

at a range of potentials that allow the channels to transit between closed, opened, and inactivated states. Residues (D3 / S4-S5, V1298, V1299, V1300; D3-D4, I1461) for modification were determined based on the location of mutations described in the first section of the *Results* within this dissertation (Jarecki et al., 2008) which differentially affected inactivation properties. The first hypothesis for this study was that single Cys residues substituted at the 1298 and 1299 position, but not the 1300 position, within the D3 / S4-S5 and 1461 position within the D3-D4 inactivation gate would disrupt the stability of inactivation and increase the persistent inward “leak” of Na⁺ at depolarized potentials (Figure 28). These studies would take advantage of chemical modifying reagents that add a positively charged group to available Cys residues within the intracellular portion of the channel. Therefore, if inactivation is destabilized upon modification one explanation could be disruption of a putative “docking” site for the inactivation gate. Thus, the second hypothesis of this study was that the V1298 and V1299 residues within the D3 / S4-S5 linker, mutated in PEPD, can directly interact with the inactivation gate (probed using an engineered Cys at the 1461 position within D3-D4) at potentials more negative than those required to fully activate and open the Na_v1.7 channel using dual Cys substitutions. These studies would utilize the crosslinking reagents that covalently modify, and essentially “lock” two nearby substituted Cys residues within a calculated distance (Figure 29). Together, results from these studies should yield insight into the probability of residues within the D3 / S4-S5 linker of

Na_v1.7 serving as a putative “docking” site during transition to an inactivated state.

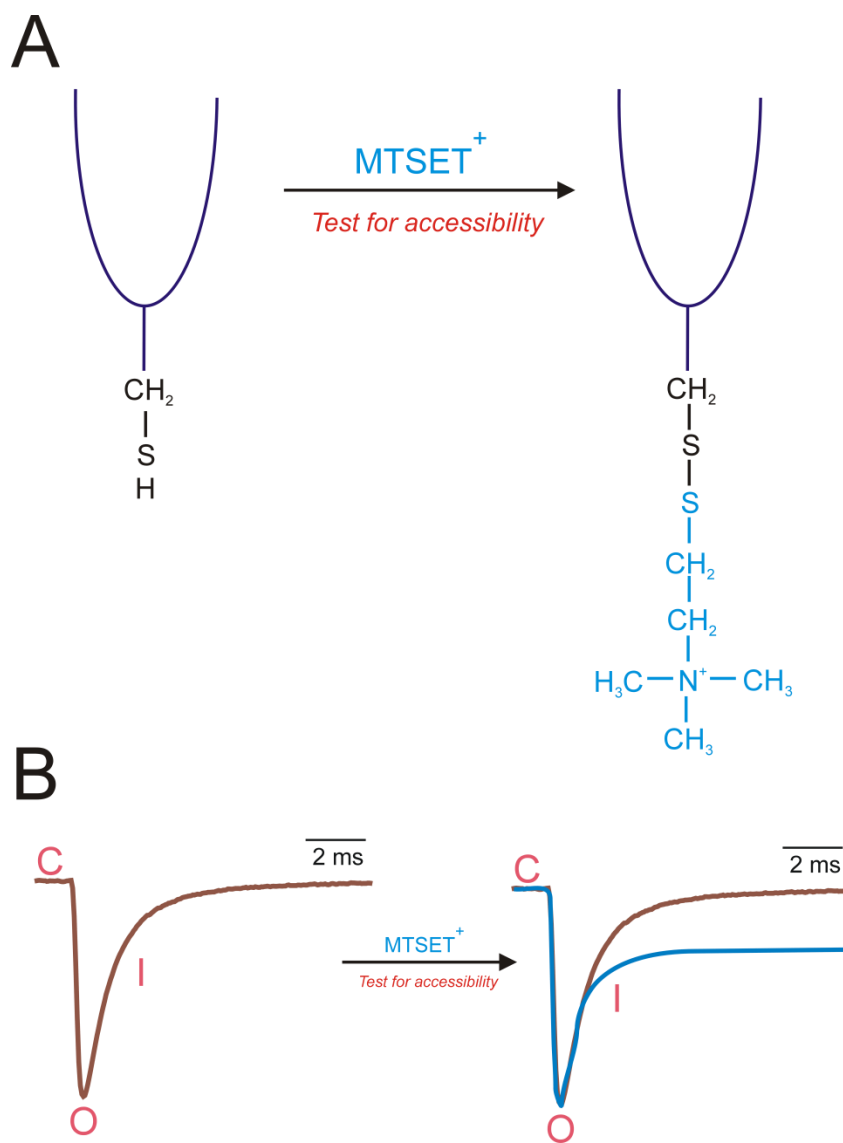


Figure 28. Chemical modification and electrophysiological readout with an accessible engineered cysteine mutation upon internal MTSET application. (A) Cartoon of an engineered cysteine (Cys) residue depicting the sulfhydryl modifying reaction in the absence (left) and presence (right) of MTSET and the added charged moiety donated by MTSET. The modification is emphasized with blue highlight. (B) Anticipated electrophysiological readout of current properties in response to a depolarizing step to -10 mV from -120 mV. To the left is a current trace recording with a step described above following transitions from closed (C), opened (O) and inactivated (I) in the absence of MTSET. To the right is the same trace from the left with an additional, hypothetical current trace in the presence of MTSET emphasized in blue highlight with altered stability of an inactivated state.

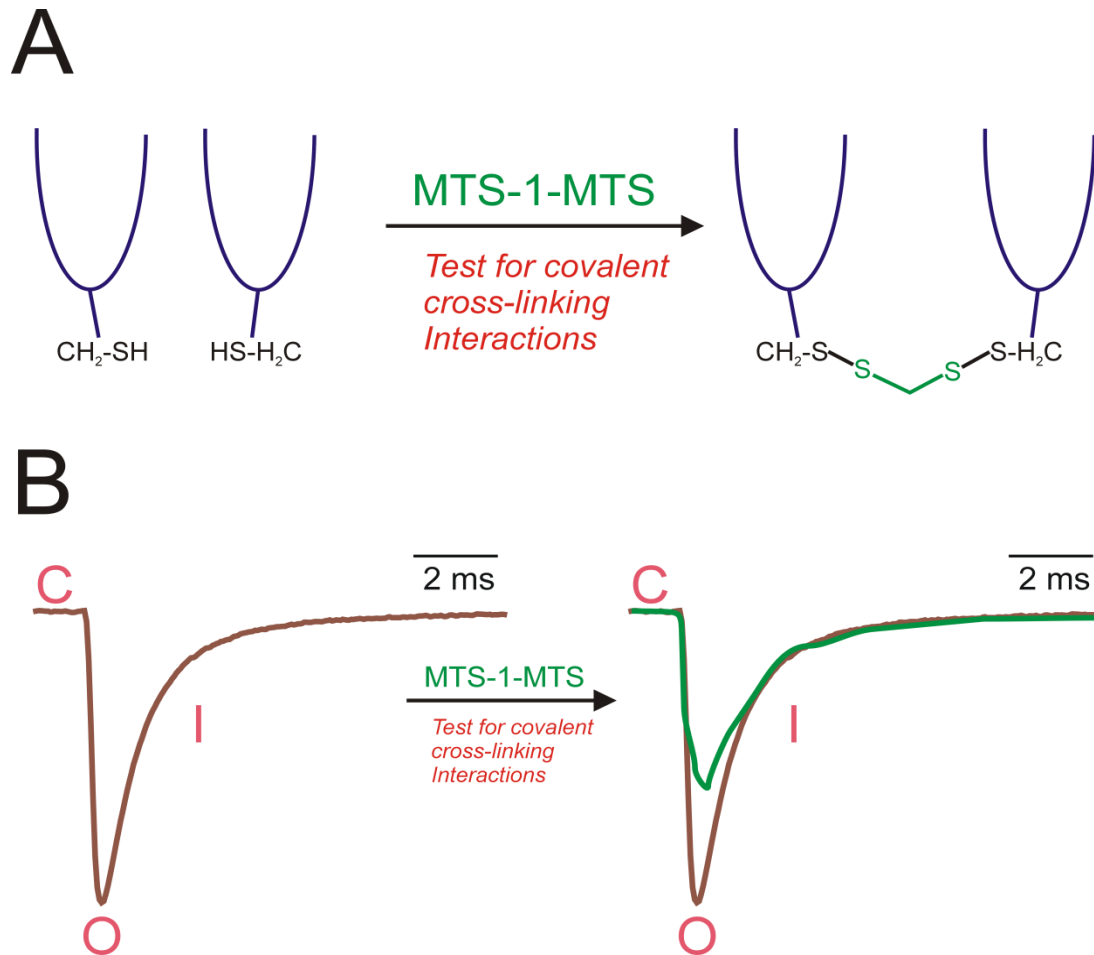


Figure 29. Illustrations of cysteine amino acid modification in the presence and absence of the covalently crosslinking reagent MTS-1-MTS and the predicted effects on the currents assayed using whole-cell voltage-clamp electrophysiology. (A) Cartoon of an unmodified cysteine (Cys) residue in the absence (left) and presence (right) of MTS-1-MTS and the ensuing covalent modification of nearby sulfhydryl groups within a specified distance. The donated moiety is highlighted in green. (B) Electrophysiological output in the absence and presence of the covalent crosslinker (MTS-1-MTS) using a similar protocol described in Figure 28. The hypothetical modification of the current trace upon crosslinking is highlighted in green coloring.

2. Cysteine substitution within D3 / S4-S5 and D3-D4 inactivation gate produces functional channels without dramatically altering gating properties

Native residues within the D3 / S4-S5 (V1298, V1299, V1300) and D3-D4 (I1461) linkers of Na_v1.7 were each individually substituted to a cysteine (Cys) which has a reactive sulfhydryl group in the side chain. This yielded a single Cys replacement in four separate constructs (V1298C, V1299C, V1300C, and I1461C). An additional Cys substitution, adding a Cys at the 1461 position into each of the D3 / S4-S5 single Cys constructs yielded dual Cys constructs (V1298C_I1461C, V1299C_I1461C, and V1300C_I1461C). The dual Cys constructs were critical for testing direct interactions using the covalent MTS crosslinking reagent. The Cys substitution, for all constructs, replaces an alkyl side chain with a sulfhydryl group and would not be predicted to increase the rigidity or steric hindrance of the secondary structure as in the case of replacements with tryptophan (Trp), tyrosine (Tyr), phenylalanine (Phe), or proline (Pro) (Voet and Voet, 1990). The functionality of the constructs was tested using whole-cell voltage-clamp electrophysiology. Robust rapidly activating and inactivating sodium currents were observed in hEK₂₉₃ cells transiently transfected with wild-type (WT) and Cys mutant Na_v1.7 channels (Figure 30).

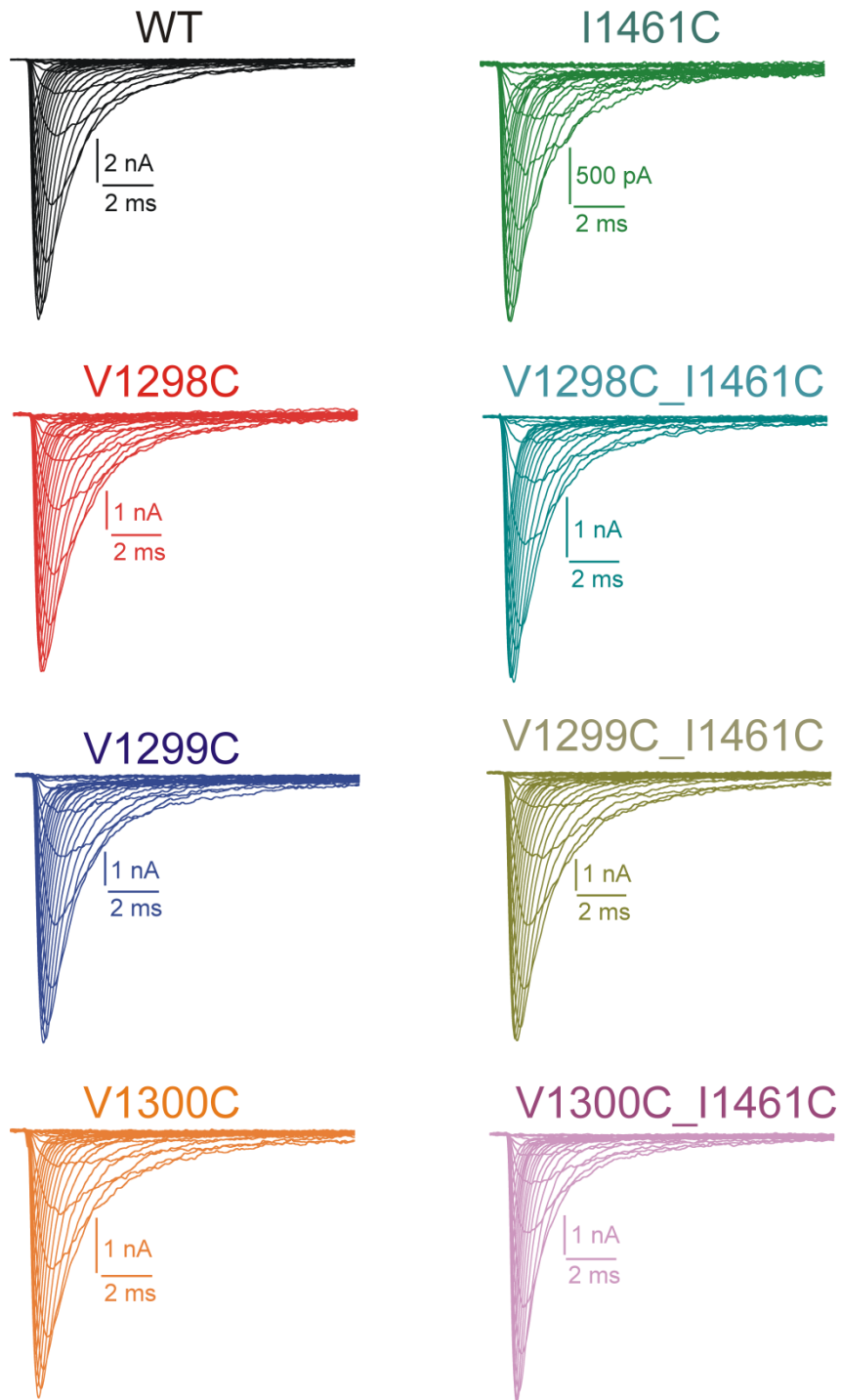


Figure 30. Comparison of whole-cell ionic current traces for wild-type (WT) and single / dual cysteine (Cys) modified $\text{Na}_v1.7$ channels. Currents were elicited during incrementally depolarizing steps of +5 mV, from -80 mV to +60 mV, from a holding potential of -120 mV. Construct nomenclature is denoted above the family of current traces for each group. Color-coding is conserved throughout this section of the dissertation.

Initial comparison of the current traces did not suggest any major differences in channel kinetics and generation of functional constructs indicated the Cys substitutions were well-tolerated and did not disrupt the ability of Na_v1.7 channels to open and inactivate in response to depolarizing steps (Figure 30). Since all of the Cys substitutions within Na_v1.7 are novel and therefore have not been characterized, the next step was to characterize the voltage-dependent gating properties in order to better develop protocol to probe interactions with the MTS reagents. Voltage-dependence of activation and inactivation was investigated to determine the effects of the single Cys substitutions on transitions between conducting and non-conducting states. A majority of the Cys substitutions did not significantly alter activation (Table 5) and deactivation properties compared to WT, suggesting the Cys substitution did not affect S4 gating charge movement or pore stability during opening (Figure 31A-C). However, the V1300C mutation significantly shifted the activation threshold (Figure 31A) and $V_{1/2}$ by approximately +6 mV (Figure 31C, Table 5) and appeared to accelerate deactivation kinetics (Figure 31B) compared to WT. Upon comparison of the inactivation properties, neither the V1298C nor V1299C significantly altered the steady-state inactivation $V_{1/2}$, whereas the $V_{1/2}$ for both the V1300C and I1461C was depolarized by +6 and +13 mV, respectively (Figure 31C, Table 5). It is worth noting that these shifts in steady-state gating properties may be via different mechanisms. For example, as has been shown by work in this dissertation and other labs, the primary effect of mutations within the D3-D4 inactivation gate is on the stability of inactivation. This effect is observed with the

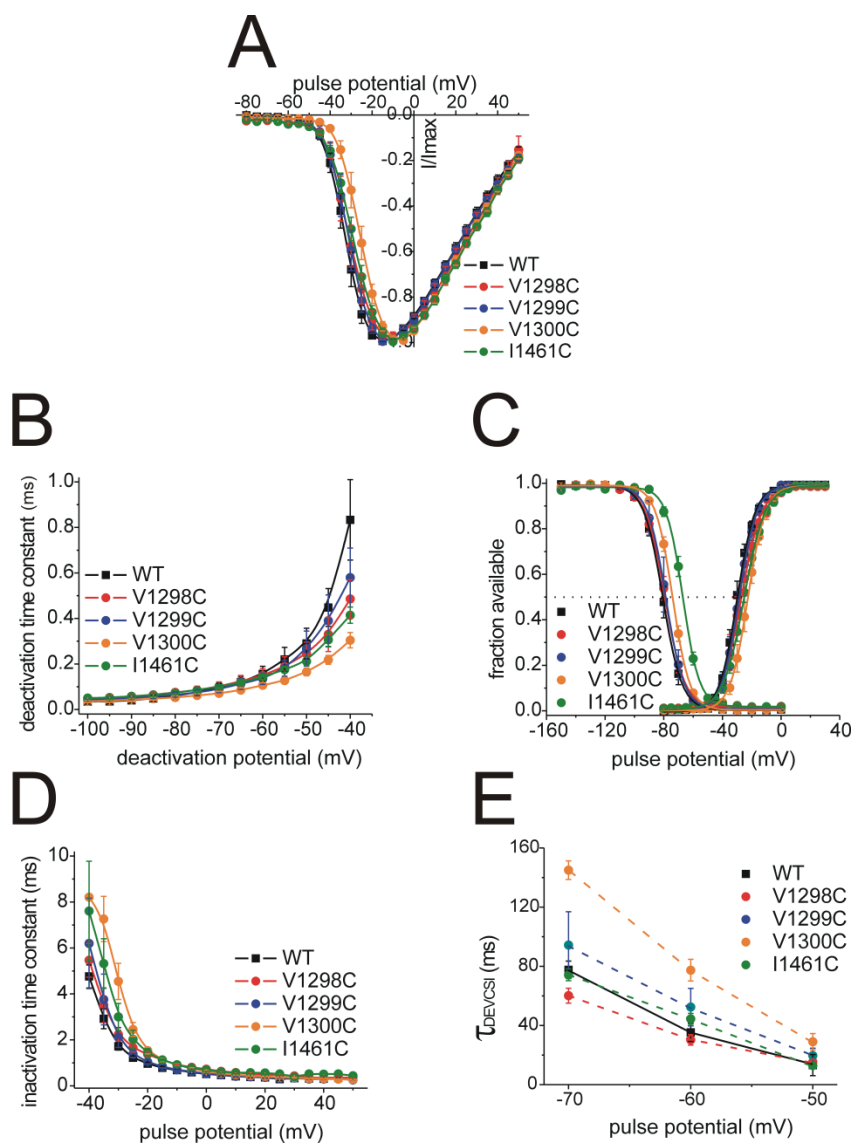


Figure 31. Effects of single Cys substitutions within D3 / S4-S5 and D3-D4 linkers on voltage-dependent gating properties of Na_v1.7. (A) Normalized current-voltage (I/V) properties for each construct. (B) Voltage-dependent time constants for deactivation (τ_d) surveyed at several potentials along the x-axis and fit with a single-exponential. (C) Normalized voltage-dependence of steady-state activation and inactivation fit with a single-phase Boltzmann function. (D) Time constants for development of open-state fast inactivation (OSI) as a function of voltage for WT and mutant channels. The decay phases of currents elicited during channel activation protocol were fitted with a Hodgkin-Huxley type m^3h model to estimate open-state inactivation time constants (τ_h). (E) Time constants for development of closed-state inactivation (CSI) assayed at -50, -60, and -70 mV. Time constants for each construct at the potentials mentioned were obtained for single current traces elicited during a CSI development protocol and then averaged for graph plotting. Protocol for each graph is described within the *Methods* section.

I1461C substitution. However, the depolarizing shifts in activation and inactivation, observed with the V1300C substitution, may be due to a decreased sensitivity to changes in voltage and D3 / S4 gating charge movement, thus shifting both the activation and inactivation properties in a depolarizing direction by approximately the same displacement voltage (+6 mV). It is also worthwhile to note that when the I1461C mutation was engineered in the background of the other constructs, yielding dual Cys constructs, activation properties were not significantly (Table 5) affected, however there was a trend towards shifting the inactivation $V_{1/2}$ to more depolarized potentials which reached statistical significance with the V1300C_I1461C construct.

Comparison of development of OSI (Figure 31D) did not indicate any significant differences between the constructs at potentials positive to -20 mV when the open probability is approaching maximum based on the G/V plot (Figure 31A). Additionally, examination of development of CSI (Figure 31E) did not suggest statistical difference between the single Cys constructs, compared to WT, at -60 and -50 mV which are potentials where VGSC D3 gating charge displacement can occur prior to channel opening (Chanda and Bezanilla, 2002) and the channels can transit to a closed-inactivated state (Vandenberg and Bezanilla, 1991; Armstrong, 2006). However, the V1300C substitution appeared to moderately slow development of CSI at the range of potentials listed which would be expected based on the depolarizing shift in the steady-state activation and inactivation responses. Further investigation of the recovery time constants from CSI, determined with a -60 mV conditioning pulse, and OSI, determined

with a conditioning pulse to 0 mV, did not yield significant changes to the recovery time constants from CSI or OSI for any of the modified constructs compared to WT (Table 6). However, again, a tendency for accelerated recovery was observed for the dual Cys constructs. Taken together, although there appeared to be small shifts in the steady-state activation and inactivation properties for some of the constructs, the general trend of gating within potentials used to assay for transitions to and from open and inactivated states is within a predictable voltage range.

Table 5. Boltzmann parameters of channel activation and steady-state inactivation curves for WT and Cys mutant channel constructs.

Channel	Voltage-dependence of activation			Voltage-dependence of steady-state fast-inactivation		
	$V_{1/2}$ (mV)	Slope (mV/e-fold)	n	$V_{1/2}$ (mV)	Slope (mV/e-fold)	n
WT	-29.0 ± 1.1	5.6 ± 0.3	6	-80.5 ± 1.7	6.0 ± 0.2	6
V1298C	-27.4 ± 2.2	6.0 ± 0.5	5	-79.4 ± 1.5	6.4 ± 0.4	5
V1298C_I1461C	-32.5 ± 3.3	6.0 ± 0.3	4	-79.0 ± 2.8	6.3 ± 0.2	5
V1299C	-29.0 ± 1.7	5.5 ± 0.2	4	-78.7 ± 3.1	5.3 ± 0.2	4
V1299C_I1461C	-28.1 ± 2.0	5.9 ± 0.5	7	-75.0 ± 1.8	6.4 ± 0.2	7
V1300C	-22.9 ± 1.5	5.6 ± 0.2	4	-74.0 ± 1.0	5.7 ± 0.1	5
V1300C_I1461C	-28.7 ± 1.9	5.6 ± 0.3	5	-67.5 ± 1.0	5.7 ± 0.2	5
I1461C	-25.6 ± 1.2	6.0 ± 0.2	5	-67.1 ± 1.0	5.5 ± 0.2	5

Values derived for $V_{1/2}$, the voltage of half-maximal activation and inactivation, and the slopes were derived from Boltzmann distribution fits to the averaged and normalized (\pm S.E.M.) voltage-dependence of activation and steady-state inactivation curves.

Table 6. Recovery inactivation time constant values for WT and Cys mutant channel constructs.

Channel	Recovery time constant (τ) (ms)	<i>n</i>
<i>Closed-state inactivation (CSI)</i>		
WT	13.4 ± 3.1	5
V1298C	8.6 ± 0.9	4
V1298C_I1461C	7.6 ± 0.7	4
V1299C	16.4 ± 5.8	4
V1299C_I1461C	12.8 ± 1.8	7
V1300C	10.2 ± 0.9	5
V1300C_I1461C	6.3 ± 0.2	5
I1461C	6.5 ± 0.5	5
<i>Open-state inactivation (OSI)</i>		
WT	13.3 ± 4.4	4
V1298C	7.8 ± 0.8	4
V1298C_I1461C	7.1 ± 1.1	4
V1299C	16.3 ± 5.6	4
V1299C_I1461C	8.6 ± 1.0	6
V1300C	10.6 ± 0.9	5
V1300C_I1461C	5.8 ± 0.2	5
I1461C	5.5 ± 0.5	5

Time constant values for recovery from closed (CSI) and open-state (OSI) inactivation. Recovery from CSI was determined by conditioning the cells to -60 mV and obtaining time constant values for recovery to -120 mV. Recovery from OSI was determined by conditioning the cells to 0 mV and obtaining time constants for recovery to -120 mV. Detailed protocol can be found in the *Methods* section. Data for recovery from OSI and CSI was fitted using a single-exponential function and time constant values were calculated and averaged from individual cell recordings.

3. *Residues (C1298 and C1299) within the Na_v1.7 D3 / S4-S5 linker are accessible to MTSET modification and are critical sites for transition to an inactivated state*

Previous work described within this dissertation has demonstrated that specific residues within the D3 / S4-S5 of Na_v1.7 are critical for the stability of inactivation utilizing site-directed mutagenesis. The previous studies were motivated by an inherited Na_v1.7 channelopathy, implicated in PEPD, caused by single-point missense mutations within cytosolic regions important for inactivation gating. Our results showed that mutation of two highly-conserved Val residues (V1298 and V1299) to the bulky side-chain Phe residue (V1298F and V1299F) destabilized transition to an inactivated state, whereas mutation of an adjacent and identical residue (V1300F), not implicated in PEPD, did not (Jarecki et al., 2008). Based on those results, two alternative hypotheses were formulated for the mechanism of the apparent destabilized inactivation. First, I hypothesized that the V1298F and V1299F PEPD mutations altered direct “docking” sites for the inactivation gate upon depolarization. Second, I postulated that the mutations may be indirectly affecting the inactivation gate binding within the pore by disrupting critical interactions with residues in the C-terminal portions of the D3 / S6 segment. To determine if direct interactions with the inactivation gate were disrupted, these Val (V1298 and V1299) residues, along with the adjacent V1300 residue, were mutated to Cys residues, which have the ability to be chemically modified, and were exposed to the membrane-impermeable Cys

modifying reagent MTSET (via the pipette) at various potentials. Since the Cys substitutions did not result in an increased persistent component or dramatically alter the transition to an inactivated state, it was assumed that the substitutions were mild and well-tolerated and thus did not dramatically alter potential intramolecular interactions. However, I hypothesized that upon application of MTSET accessible Cys residues will be modified and if they are critical for stabilizing inactivation will result in an increased persistent current component at potentials that should yield complete inactivation (Figure 28). The changes in current properties should resemble those observed for a Cys mutation within the D3-D4 inactivation gate in the presence of MTSET, as the native residue is on the accessible face (Rohl et al., 1999) of the inactivation gate motif (West et al., 1992), critical for inactivation. Three specific holding potentials were chosen based on the characterization data for the Cys mutant constructs compared to WT and a protocol was developed to minimize occupancy in additional transition states (Figure 32). A holding potential of -120 mV allows a large fraction of channels to reside in a closed (primed) state and transition from this initial state to open and inactivated states upon depolarization. An intermediate holding potential of -60 mV, theoretically allows a fraction of channels to populate a closed-inactivated state, where the S4 voltage sensors are predicted to start to translocate charge (Chanda et al., 2004; Armstrong, 2006). A depolarized holding potential of -20 mV allows for a fraction of the channels to populate open and open-inactivated states. Using these holding potentials, I can probe for intramolecular interactions that occur to stabilize different states of the channel

upon depolarization. I hypothesized that at hyperpolarized potentials, when a large population of channels are in a closed state and the inactivation gate accessible, MTSET would modify the V1299C, and the I1461C, but not the V1300C channels. However, upon depolarization, when the inactivation gate starts to interact with “docking” sites to occlude sodium flux, the V1299C, and I1461C channels would no longer undergo modification. Because the effects observed in the characterization studies, as well as those for the PEPD mutant studies listed in a previous section, for the V1298 and V1299 mutant channels are similar, only the V1299C channel was used for further comparison with the MTS reagents.

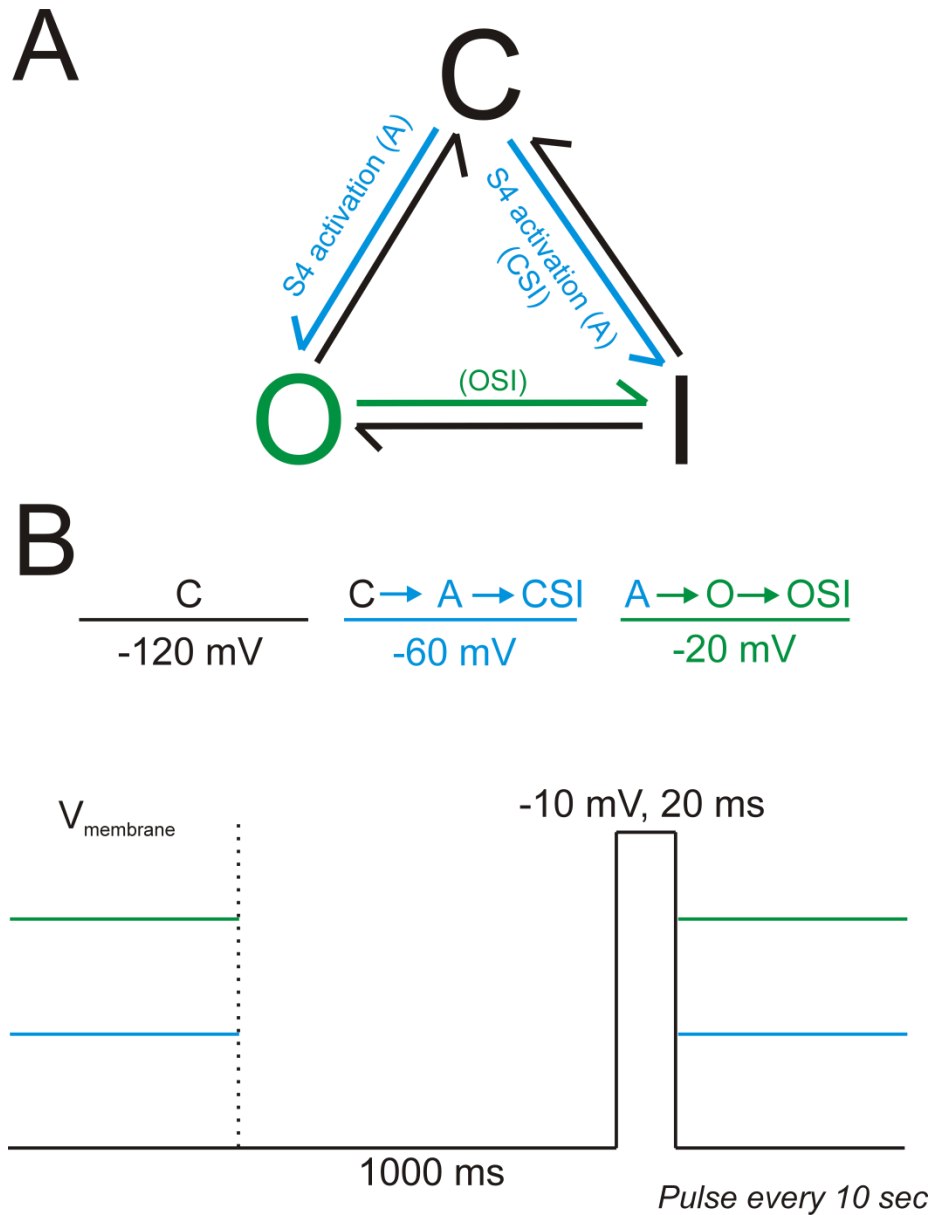


Figure 32. Voltage-dependent transitions for WT and Cys mutants can be assayed using specific electrophysiological test protocols. (A) Simplified state-occupancy diagram outlining transitions of interest between closed (C), opened (O), and inactivated (I) states. (B) Hypothetical transition scheme tested using a step protocol pulsing every 10 sec to test for available sodium current. Color scheme used throughout the figure to outline state transitions is conserved in the voltage-step protocol.

This hypothesis was tested using transiently transfected cells in the presence and absence of intracellular MTSET application. Recordings were started within one minute after establishing whole-cell configuration because the reaction occurs rapidly upon exposure to modifying reagents (Kellenberger et al., 1996; Karlin and Akabas, 1998) and electrode solution equilibration with the cytosol. Since residue accessibility is the rate-limiting step in modification, the electrophysiological readout of changes in current properties should be observed within minutes after application if substituted Cys residues are accessible. As shown in Figure 33A, in the absence of MTSET, hereafter referred to as controls, none of the WT or Cys mutant channels were modified by the holding potentials (-120, -60, and -20 mV) used. These results indicate that the Cys mutations did not affect the properties of rapid activation or inactivation during the test protocols. However, upon intracellular application of MTSET, accessible residues were modified at -120 mV leading to a reduction in the population of channels stabilized in an inactivated state, thus increasing the persistent inward sodium current during the decay phase of the current trace for the V1299C, and I1461C channels. The rapid onset of the inward component, reflecting activating and ion-conducting transitions was not altered. This change in current properties was not observed for WT channels. This effect was not surprising because upon alignment of the predicted intracellular regions of Na_v1.7 there are no native Cys residues, and therefore one would not expect WT Na_v1.7 channels to be modified with MTSET. The highly reactive sidechain of Cys residues, which readily forms covalent disulfide bonds important for several biological functions, are primarily

found on the extracellular portions of VGSCs since most intracellular compartments have a reducing environment which significantly reduces the stability of disulfide bonds (Voet and Voet, 1990). Additionally, even though the V1300C was accessible and modifiable at -120 mV, the effect on the decay phase of the current was not nearly as large for the other single Cys modified channels. This suggests the V1300 residue, although accessible, may not be important for stability of an inactivated configuration. Still, it is hard to completely rule out the possibility that the V1300 residue may be located on an inner turn, facing the intracellular portion of the lipid membrane, of the predicted α -helical secondary structure of D3 / S4-S5 linker which houses approximately 3.6 residues / turn (Filatov et al., 1998), and may not be as accessible as the neighboring Val residues. Computer-based homology modeling studies that I carried out suggests this could be the case. However, the current snapshots compared at 10 min after MTSET application allows for a majority of the modification to take place at the concentrations used in this study (Kellenberger et al., 1996; Karlin and Akabas, 1998), and therefore may argue against the complete lack of accessibility for V1300C.

Intriguingly, the single Cys mutant channels did not appear to be modified at more depolarized holding potentials compared to WT (Figure 33, middle and right panels). Based on my hypothesis, this effect may be due to structural rearrangements along a gradient of depolarization that alter intramolecular interactions during transition to and from CSI and OSI, such that putative D3 / S4-S5 “docking” sites may no longer be available for modification. As stated

above, this could be caused by direct interaction with the inactivation gate motif. However, the inactivation gate motif has also been hypothesized to “dock” to sites within the intracellular mouth of the aqueous channel pore (Armstrong and Bezanilla, 1977), formed by the S6 segments of voltage-sensitive channels (Doyle et al., 1998). If this is indeed the case, I should be able to test for direct stabilizing interactions of the D3 / S4-S5 and the inactivation gate motif at a range of potentials before and after the channel activation gates open and the channel adopts an open / ion-conducting configuration. Therefore, I should be able to determine if it is possible for the inactivation gate motif to interact directly with residues outside of the pore at potentials more negative than those required to open the channel. These types of interactions during depolarization may begin to shed light into distinct roles of the inactivation gate “docking” sites during intersegment gating current immobilization between D3 and D4 (Cha et al., 1999; Sheets and Hanck, 2005).

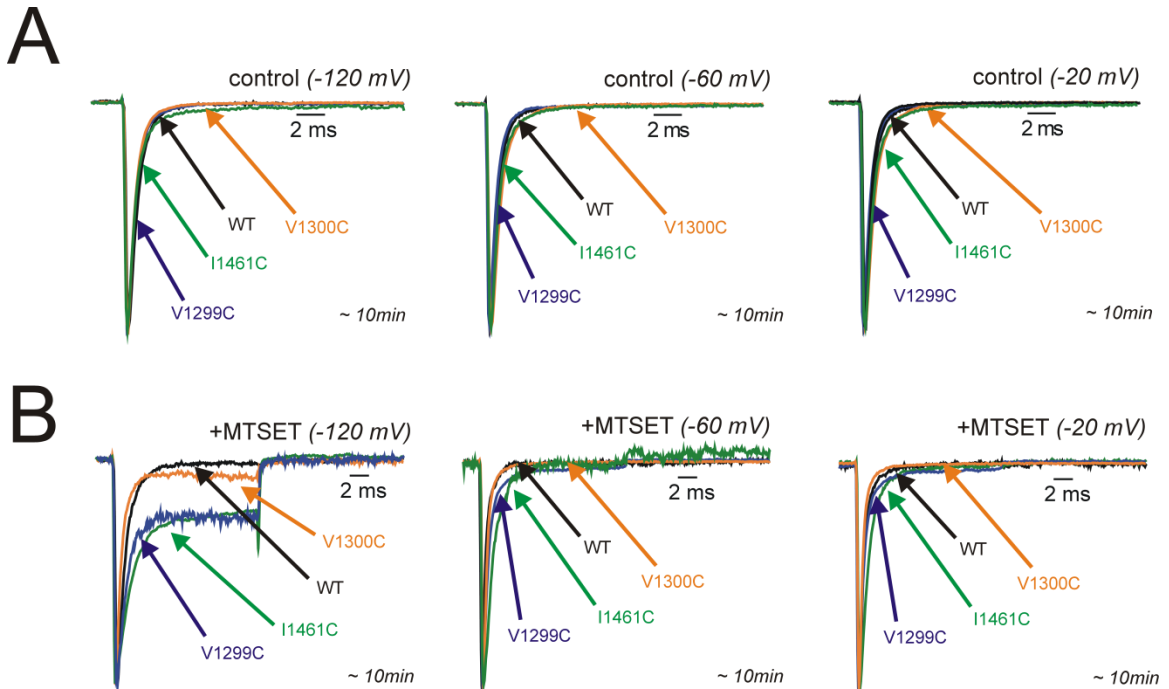


Figure 33. WT and single Cys mutant $\text{Na}_v1.7$ accessibility to MTS modification at varied holding potentials. Normalized snapshots at 10 min of representative current traces in the absence (**A**) and presence (**B**) of 500 μM MTSET performed for all constructs (WT, V1299C, V1300C, and I1461C) at holding pulses of -120, -60, and -20 mV to test for available sodium current using the protocol outlined in Figure 32. Preparation of MTSET is described in detail within the *Methods* section of this dissertation. Color-coding is conserved throughout this experimental section of the dissertation.

4. Proximity for direct interactions between the inactivation gate motif and residues within D3 / S4-S5 can be detected at potentials more negative than those required for Na_v1.7 channel opening

In order to probe the proximity for direct intramolecular interactions over a range of holding potentials (Figure 32) at which the mobile inactivation gate may “dock” to intracellular regions of the Na_v1.7 channel upon depolarization, mutant channels, with two Cys residues engineered into potential interacting sites within the cytosolic D3 / S4-S5 linker and the D3-D4 inactivation gate motif were utilized. Because these dual Cys channels are functional and conduct sodium currents in response to depolarization, it is unlikely that the engineered Cys within the intracellular linkers spontaneously form covalent disulfide bonds with one another or with any other amino acid side chain within the reducing environment of the cytosol. First, the reactivity of the dual Cys channels was tested with MTSET modification to current properties. Because MTSET attaches a charged moiety to accessible Cys residues, as shown above, I hypothesized that the addition of the I1461C mutation to the background of the other D3 / S4-S5 single Cys constructs would affect the inactivation decay component of the current traces. This was hypothesized because the C1461 substitution enabled Na_v1.7 channels to be modified by MTSET resulting in a destabilized transition to an inactivated state. Indeed, upon inspection of the control (Figure 34A) and MTSET treated (Figure 34B) groups the C1461 substitution enhanced response in the dual Cys channel V300C_I1461C to MTSET at all holding potentials

tested. This indicates that the I1461C mutation engineered into this construct is dominant residue site contributing to current modification (compare Figures 33B and 34B). Comparison of the dual Cys current traces at -60 and -20 mV holding potentials did not suggest any additional modification in the presence of MTSET compared to the single Cys traces (compare Figures 33B and 34B). These results demonstrate that upon depolarization, to either -60 or -20 mV, the intramolecular rearrangement of the cytosolic regions of the channel are packed in a new configuration where the (D3 / S4-S5) C1299 and (D3-D4) inactivation gate C1461 residues are not accessible to MTSET modification upon intracellular exposure. One hypothesis is that the two residues may occlude MTSET modification via direct and stabilizing interactions with one another. Since these regions of the channel have been proposed to be dynamic and flexible a direct interaction between the two residues was tested using a bifunctional crosslinking reagent that forms a covalent bond between two nearby Cys residues within a calculated distance, thus acting like a molecular caliper to approximate distances upon depolarization.

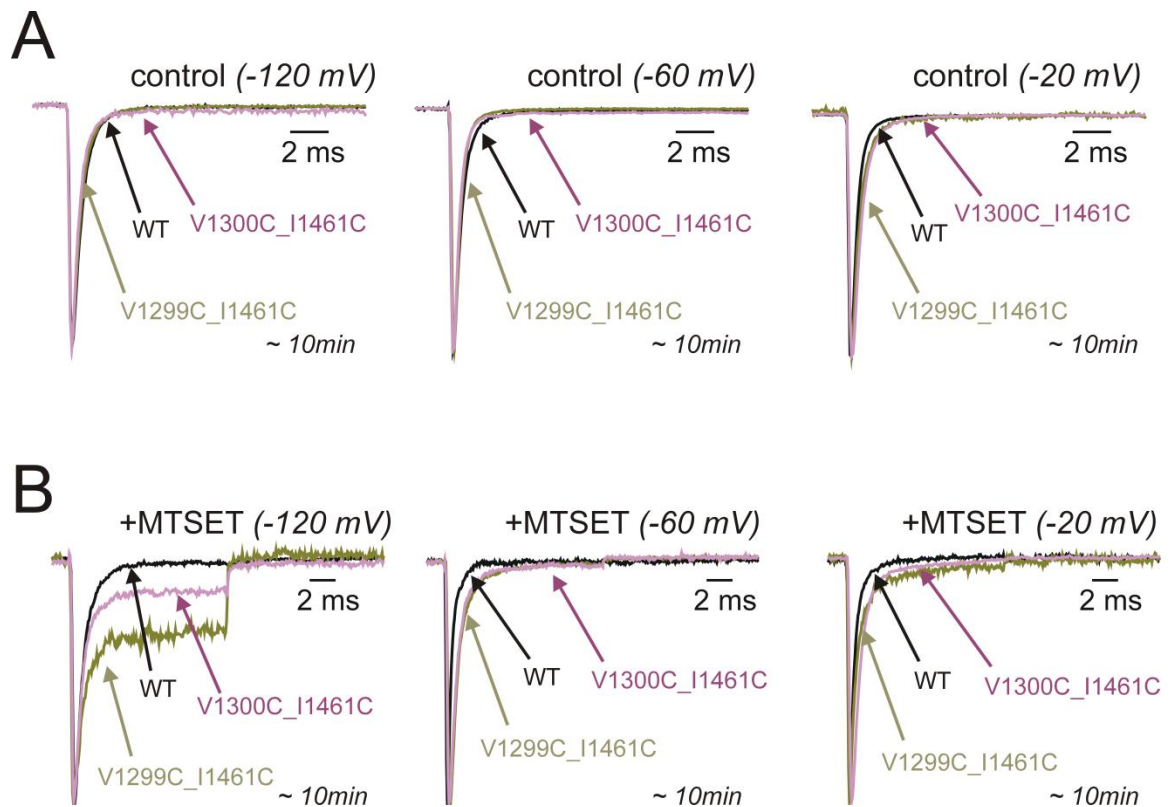


Figure 34. Representative current trace comparisons for dual Cys and WT channels in the presence and absence of MTS modification at three different holding potentials. Transfected cells expressing WT or dual Cys channels were tested under control conditions (**A**) at three different potentials (-120, -60, and -20 mV) or in the presence of intracellular application of 500 μ M MTSET (**B**) at the same holding potentials for controls. All current traces were normalized and shown at 10 min after whole-cell configuration was established.

Several crosslinking reagents have found application in mapping the interactions of mobile regions in ion channels during electrophysiological experimentation (Horn et al., 2000; Popa et al., 2004; Prole and Yellen, 2006; Bell et al., 2008; DeCaen et al., 2008). For studies in this dissertation, a bifunctional MTS crosslinking reagent (MTS-1-MTS) was used to probe for potential “docking” interactions between the D3 / S4-S5 linker and the D3-D4 inactivation gate motif. The MTS-1-MTS reagent should crosslink nearby Cys residues within a ~ 5 Å distance based on the spacer size in between the functional groups (Green et al., 2001; Loo and Clarke, 2001). Upon crosslinking of nearby Cys residues, based on the state-dependent accessibility of the engineered Cys residues I predict that the channels would be “locked” in a particular voltage-dependent conformation (Figure 29). However, because the Cys residues were modifiable with the MTSET reagent at a holding potential of -120 mV, I would not anticipate covalent crosslinking to occur at this potential. I would hypothesize that the inactivation gate has not been triggered to move towards a “docking” site at this hyperpolarized potential when gating charges have not been displaced, however upon depolarization and channel rearrangement, during S4 voltage-sensing, the coupled movement of activation to inactivation would favor transition to an inactivated configuration stabilized by theoretical “docking” or interacting sites.

These theoretical interactions were probed at different holding potentials, as before, in the presence of intracellular MTS-1-MTS application. Examination of WT channels with MTS-1-MTS at all potentials tested did not reveal any

changes in current amplitude over the timecourse (~20 min) of recording (Figure 35A). These results indicate that the MTS-1-MTS reagent is not covalently modifying any native residues within WT channels at the range of potentials tested. Additionally, these results suggest the MTS-1-MTS reagent is not significantly altering the ability of WT channels to respond to changes in voltage and to open and close during the duration of the experiment. However, the D3 / S4-S5 and D3-D4 dual Cys mutant construct (V1299C_I1461C) yielded quantitative insight into a potential interaction between the inactivation gate and a proposed “docking” site outside of the mouth of the aqueous pore. As hypothesized, at a holding potential of -120 mV when a large population of the channels are in a closed state, the ability to covalently crosslink the two Cys residues was unlikely as depicted in Figure 35B (black squares). Conversely, upon holding the membrane potential at -60 mV (Figure 35B; red squares), when the probability of channels transitioning to a closed-inactivated state is increased (Figure 32), apparent crosslinking was observed between the two Cys residues engineered at the 1299 and 1461 positions. These results indicate that the two Cys residues at these locations can come into contact with one another within a distance of ~5 Å or less allowing the MTS-1-MTS to covalently crosslink the two Cys residues. This interaction supports the hypothesis that the mobile inactivation gate can “dock” to sites outside of the channel pore at potentials more negative than those required to open the activation gate and transition the channel to an ion-conducting configuration. The MTS-1-MTS crosslinker likely decreases current amplitude because it locks the channels in the inactivated

state. Thus, I next probed for interactions at a holding potential of -20 mV, which allows for a majority of the channels to open and inactivate from an open

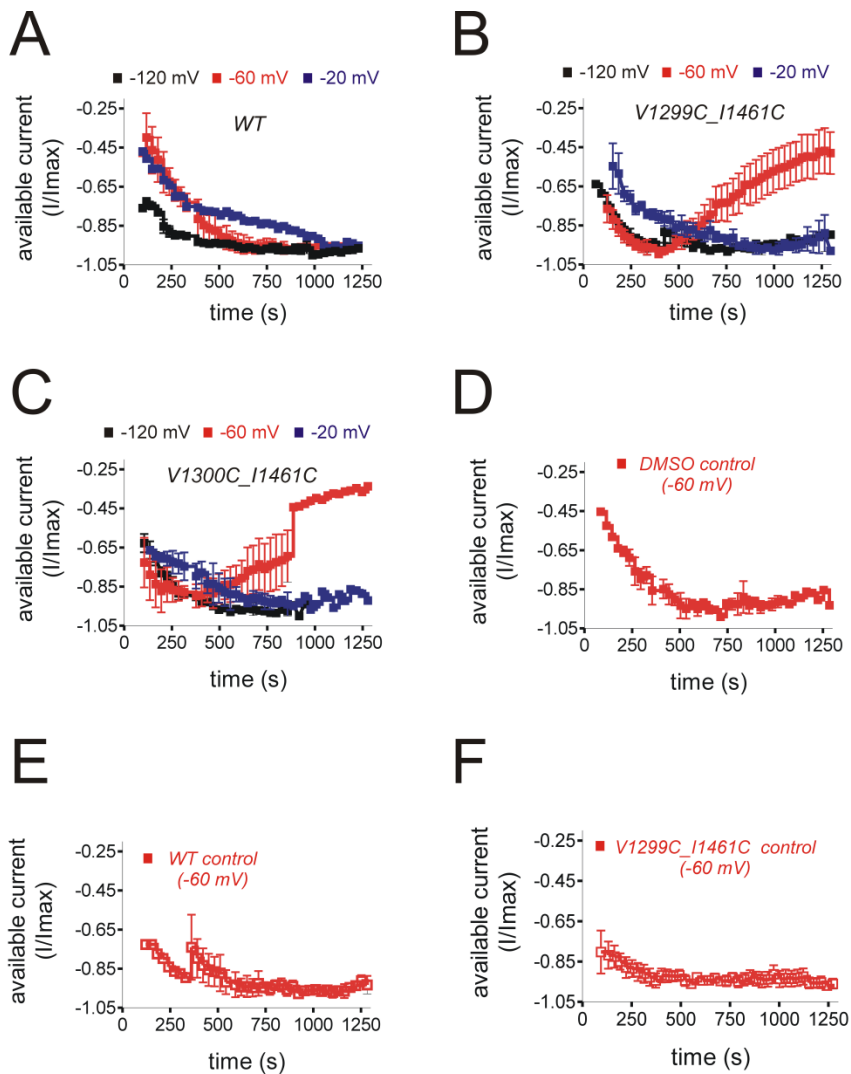


Figure 35. State-dependent channel conformation locking upon application of an MTS crosslinking reagent. (A-C) WT and dual Cys mutant constructs (V1299C_I1461C and V1300C_I1461C) were exposed to intracellular application of 500 μ M MTS-1-MTS at different holding potentials (-120, -60, and -20 mV) and currents were recorded soon after whole-cell configuration was established. Preparation of MTS-1-MTS is described in detail in the *Methods* section of this dissertation. Currents were normalized to the peak current recorded over the approximately 20 min timecourse. (D-F) Control recordings at a holding potential of -60 mV for channels upon intracellular application of vehicle control (DMSO) or in the absence of any reagent added to the electrode solution. Timecourse for changes in whole-cell currents were determined in a similar manner as those for the MTS-1-MTS experimental studies above. Initial increase in current before 500 sec is due to the components of the electrode solution, notably CsF, which has been shown to increase sodium current amplitude over time. Color-coding is conserved in all images within this particular figure.

configuration (OSI), based on the voltage-dependent properties displayed in Figure 31. Interestingly, a decrease in the current at a holding potential of -20 mV was not observed (Figure 35B; blue squares). These results have three explanations. First, the mobile inactivation gate may “dock” at a second site within the channel pore at this holding potential of -20 mV, compared to -60 mV, upon opening of the channel activation gates. This interpretation is hard to validate with the current model and available Cys residues. To confirm this type of interaction, an additional construct with a Cys residue located at the intracellular mouth of the pore would need to be tested along with the Cys substitution in the inactivation gate. Second, it is also possible that the accessibility of the Cys substituted at the 1461 or 1299 position is hindered by the side chains of residues within the C-terminal portions of the S6 segments that are predicted to splay outward upon depolarization (Lu et al., 2002; Long et al., 2005a; Soler-Llavina et al., 2006; Long et al., 2007; Labro et al., 2008; Muroi et al., 2010). Third, an additional reason for the differences in crosslinking may be due to the movement of the S4 voltage-sensing segments at the two holding potentials. Because the C1299 substitution is near the N-terminal portion of the D3 / S4-S5, the proximity (within ~ 5 Å) to the inactivation gate may be outside of the distance window for covalent modification with the MTS-1-MTS spacer upon strong depolarizations required for full channel activation and opening. Evidence supporting this theory comes from gating charge and site-directed mutagenesis experiments investigating the contribution of charged residues within the voltage-sensing (S4) segments to gating charge and channel activation and their

“outward” displacement from a buried to an exposed position at different potentials, thus increasing probability of channel opening (Hodgkin and Huxley, 1952; Hirschberg et al., 1995; Bezanilla, 2000). To further evaluate this possibility, an additional set of experiments using an MTS crosslinking reagent with a larger alkyl spacer to calibrate the distance could be tested. Such exploratory experiments and hypotheses will be discussed in more detail in the *Discussion* section of this dissertation.

When the V1300C_I1461C channels were probed for interaction at -120 mV, there was no decrease in the current over the recording duration (Figure 35C; black squares). However, covalent crosslinking was observed using a -60 mV holding potential (Figure 35C; red squares), but not at a -20 mV holding potential (Figure 35C; blue squares). These results were interesting, in that, the Cys substitution at the 1300 position was not detectably modified in the presence of the MTSET reagent suggesting that the residue was either inaccessible or not critical for stabilizing an inactivated state. But, upon closer inspection of the data the results are in line with interaction between the C1299 and C1461 substituted residues. Since the limiting factor of the MTS-1-MTS reagent is the spacer, which determines the crosslinking distance, interaction with Cys residues within the ~5 Å or less distance, would be expected to crosslink. Therefore, because the C1300 substitution is one position downstream of the C1299, predicted to be within the same turn of the α -helix a crosslinking reaction is not surprising. Thus, the accessibility of the C1300 substitution would not be predicted to be the limiting factor for the results observed in Figures 33 and 34. However, the

contribution of this residue to the overall stability of transition to an inactivated state appears to be minor, as shown in Figures 33 and 34 for the Cys substitution and Figure 9 for the Phe substitution. To support these findings, previous experiments have also demonstrated unique roles for the amino acids based residue location and the respective side chain in terms of gating and pore stabilization (Lu et al., 2002; Long et al., 2005a; Soler-Llavina et al., 2006; Long et al., 2007; Labro et al., 2008; Muroi et al., 2010).

Control experiments at a holding potential of -60 mV were also performed to test the changes in current in response to the diluents (DMSO vehicle control) for the MTS-1-MTS compound (Figure 35D) and in the absence of any added reagent, for the WT and V1299C_I1461C channels, to the electrode solution over the same timecourse (Figures 35E and F). The experiments primarily focused on the -60 mV holding potential because intramolecular interactions in the presence of the MTS crosslinking reagent at this holding potential were predominant compared to -120 and -20 mV. In all of the control experiments no reduction in current amplitude was observed suggesting that the changes in current with the MTS-1-MTS reagent were due to the ability to crosslink engineered Cys residues within a distance of ~ 5 Å or less.

5. *Proposed models for state-dependent D3 / S4-S5 and D3-D4 interactions during transition to an inactivated state based on MTS experiments*

The accessibility and crosslinking studies described in this section begin to shed light on the role of the D3 / S4-S5 linker during inactivation. Electrophysiological studies examining the role of this linker in VGSC gating have suggested this cytosolic linker is important for inactivation (Smith and Goldin, 1997; Popa et al., 2004; Jarecki et al., 2008), acting as a putative “docking” site for the inactivation gate motif, and pore stabilization / electromechanical coupling (Muroi et al., 2010) during transition to an ion-conducting state. However, based on the predicted α -helical structure of this linker, different residues comprising the D3 / S4-S5 may be involved in distinct features of gating based on their accessibility during depolarization, side-chain properties, and location within the linker. Studies described within this dissertation indicate that the two Val residues mutated in PEPD at the 1298 and 1299 positions in Na_v1.7 are, in a similar manner to the Ile at the 1461 position within the putative inactivation gate motif, important for stabilizing transition to an inactivated state (Figure 5). Furthermore, residues, when substituted to a Cys at the same position, are accessible at holding potentials where a large population of channels reside in a closed state (-120 mV) but not at depolarized potentials (-60 and -20 mV) when the channels are starting to transition to an inactivated state (Figure 36). Additionally, the adjacent Cys substituted residue at the 1300 position, did not appear to destabilize inactivation when compared to WT and the other Cys

substituted channels (Figure 36). Interestingly, upon examination of the ability for the Cys substituted channel to crosslink during depolarization, Cys substituted residues within the D3 / S4-S5 and the D3-D4 inactivation gate motif appeared to covalently link (Figure 37). This covalent linking was not observed at hyperpolarized holding potentials (-120 mV) when a large population of the channels are closed, or at more depolarized holding potentials (-20 mV) when channels have opened and are inactivated from the open state. Together, these results strongly suggest that specific residues (V1298 and V1299) within the D3 / S4-S5 linker can interact with the putative inactivation gate motif during depolarization required to inactivate Na_v1.7 channels, within ~5 Å, and may represent a “hotspot” region within the linker that upon mutation can have significant effects on the stability of the channel configuration and gating.

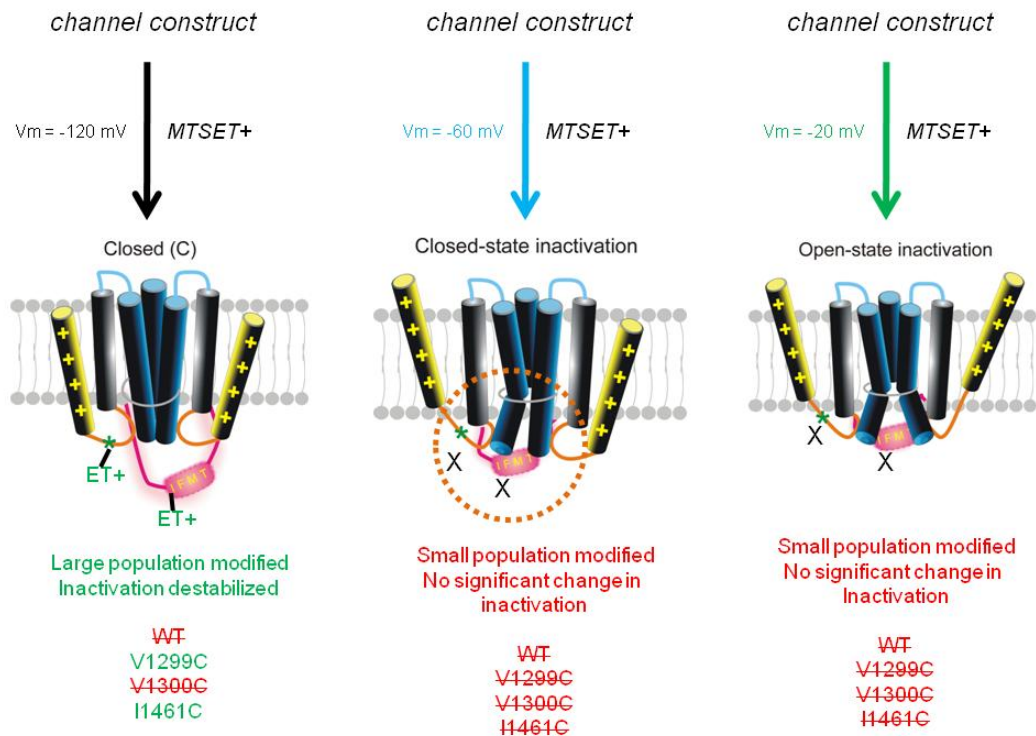


Figure 36. Summary of effects on $Na_v1.7$ channel gating with MTSET modification. Depicted above are cartoon images of the D3 and D4 S4-S6 segments. The S4 segments, highlighted in yellow, are laden with positive (+) charges that are predicted to translocate upon depolarization. The S6 pore forming segments, highlighted in blue, are predicted to splay outward upon depolarization and S4 gating charge displacement. The putative inactivation gate motif (IFMT) highlighted in a pink oval, within the D3-D4 linker, is a mobile entity that can interact with intracellular “docking” sites upon depolarization to occlude Na^+ flux. The D3 and D4 / S4-S5 are colored in orange and the location of Cys substitutions within the D3 / S4-S5 is denoted with a green asterisk (*). Summarizing results denoted in pictorial format indicate that at hyperpolarized holding potentials (-120 mV) only the Cys substitutions at the 1299 and 1461 positions, in the presence of MTSET, altered the stability of transition to an inactivated state indicating that modification of these residues (ET^+) resulted in destabilized inactivation. This was observed as an increase in the persistent Na^+ current during the decay phase of a current trace. Depolarized holding potentials (-60 and -20 mV) did not dramatically affect the population of channels transitioning to an inactivated state.

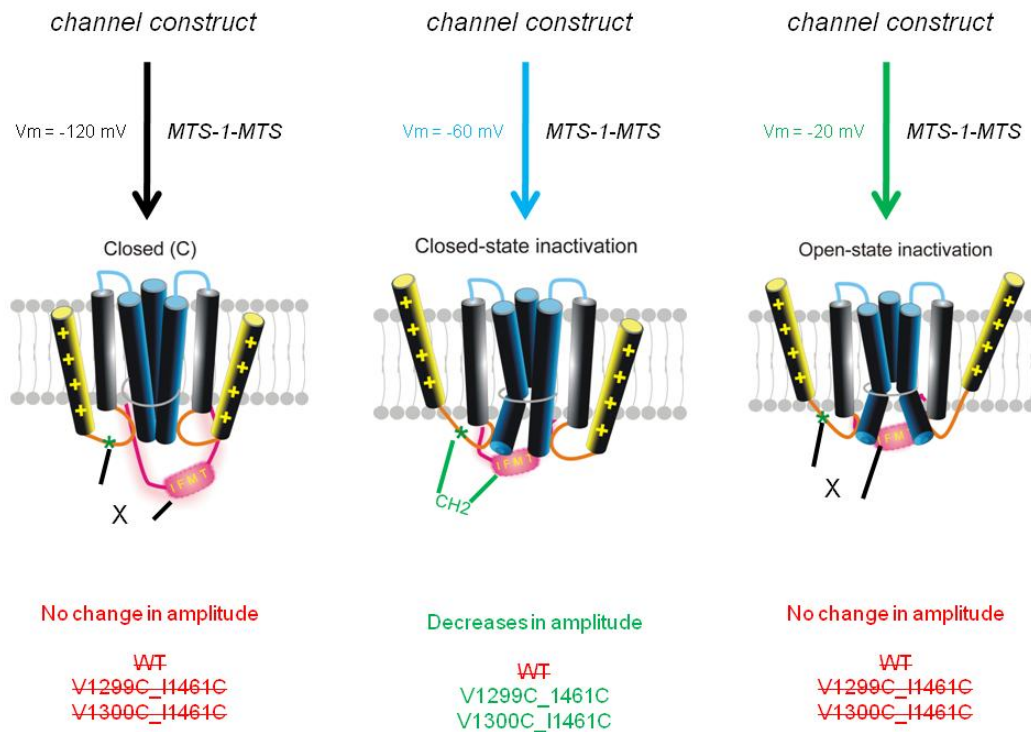


Figure 37. Cartoon summary of $Na_v1.7$ D3 / S4-S5 crosslinking effects with the putative inactivation gate motif located in D3-D4. Structural and color scheme is the same as described for Figure 36 above. Cys substituted residues within the D3 / S4-S5 and putative inactivation gate motif were not covalently crosslinked at a holding potential of -120 mV, however upon depolarizing the holding potential to -60 mV, covalent crosslinking was observed for the Cys substituted constructs in the presence of MTS-1-MTS noted by a decrease in current amplitude over the recording timecourse. There was no change in current amplitude observed at a holding potential of -20 mV.

IV. DISCUSSION

A. Dissertation research overview

This dissertation primarily focused on the structural and functional roles of the neuronal VGSC isoform $\text{Na}_v1.7$ during transition to an inactivated state. Using whole-cell voltage-clamp electrophysiology I was able to examine the functional impact of structural alteration to regions critical for inactivation to determine (1) the significance that inherited point mutations, implicated in a painful disorder, have on stability of inactivation, (2) how alternative splicing can affect gating properties of painful mutant channels, (3) the modulating role resurgent sodium currents have in inherited channelopathies, and (4) the interactions that may be important in transition to an inactivated state within a theoretical “hotspot” region of $\text{Na}_v1.7$. To evaluate the significance single-point missense mutations have on gating, the effects of several $\text{Na}_v1.7$ -PEPD mutations on voltage-dependent properties were characterized. Results demonstrated that two PEPD mutations within the D3 / S4-S5 linker significantly altered transition to an inactivated state in a similar manner to a mutation within the D3-D4 putative inactivation gate (Jarecki et al., 2008). These effects were residue and location specific suggesting a spatial orientation within the D3 / S4-S5 that may allow for interactions critical for stabilizing an inactivated state resulting in a normal AP response to a given stimulus. Indeed, additional experiments indicated an importance for the S4-S5 PEPD mutations in AP firing properties, in that, PEPD mutations can render neurons hyperexcitable, thus

yielding an abnormal response to a given stimulus (Dib-Hajj et al., 2008). Because the location of pain, response to therapeutics, and age-onset is distinct for PEPD compared to an additional disorder (IEM), caused by $\text{Na}_v1.7$ mutations, the effects of alternative $\text{Na}_v1.7$ splicing on the impact of PEPD and IEM was investigated. Results from these experiments indicated that the functional impact of PEPD was affected by alternative splicing, whereas IEM was not (Jarecki et al., 2009). This effect was predicted to be caused by a unique charge substitution difference between the splice variants that would shift the activation window and additively increase the probability for PEPD mutant channels to reside in an open state. We further examined the potential modulatory role of resurgent sodium currents in voltage-gated sodium channelopathies that result from slowing of inactivation, as this may be another factor for the distinct age-onset and location of pain perceived in PEPD. Our results demonstrate that inherited mutations in several channelopathies can increase resurgent sodium currents which are predicted to impact neuronal and muscle AP firing properties (Jarecki et al., 2010). Finally, because the structural interactions required for stabilizing transition to an inactivated state appear to be highly regulated, as evidenced from all of the previous experiments described above, direct interactions during inactivation were surveyed. Results from these studies, guided by the locations of PEPD mutations within $\text{Na}_v1.7$, indicate that specific residues within the D3 / S4-S5 are critical for stability of transition to an inactivated state and may serve as a putative “docking” site for the inactivation

gate motif. Below is the detailed discussion of these results and how they impact our knowledge of $\text{Na}_v1.7$ electrophysiology.

B. Paroxysmal extreme pain disorder (PEPD) mutations within the D3 and D4 / S4-S5 linkers of Na_v1.7 cause moderate destabilization of fast inactivation

1. *Functional consequences of PEPD mutations*

Two molecular neuropathic pain syndromes, inherited erythromelalgia (IEM) and paroxysmal extreme pain disorder (PEPD) are caused by mutations in *SCN9A* gene encoding for Na_v1.7, and the consequences of these mutations are distinct. Patients with PEPD have paroxysmal episodes of intense burning pain localized in (but not limited to) the rectal, ocular, and jaw areas accompanied by autonomic changes such as skin flushing near the perceived site of pain (Fertleman et al., 2007). IEM is characterized by episodes of burning pain triggered by warmth or exercise, along with erythema and mild swelling in the extremities, ears, and face (Drenth and Michiels, 1992; Drenth et al., 2001; Drenth et al., 2005; Novella et al., 2007). A majority of the *SCN9A* mutations implicated in IEM are found within transmembrane segments and cytoplasmic linkers of D1 and D2 in Na_v1.7. D1 and D2 IEM mutant channels, expressed in hEK₂₉₃ cells, cause a lowering of VGSC activation threshold, slowing of deactivation, and increased ramp current amplitudes between -60 and -40 mV (Dib-Hajj et al., 2007). DRG neurons transfected with Na_v1.7 channels containing IEM mutations increase neuronal excitability (Dib-Hajj et al., 2005; Rush et al., 2006) and computer simulations indicate the hyperpolarizing shift in activation is a major determinant of this hyperexcitability (Sheets et al., 2007).

In the first part of this dissertation, it was investigated whether single-point missense mutations in Na_v1.7 D3 / S4-S5, implicated in paroxysmal extreme pain disorder (PEPD), alter voltage-dependent gating properties similar to PEPD mutations within the D3-D4 putative inactivation gate motif (IFMT). Although it was originally proposed that all PEPD mutations might selectively cause marked deficits in fast inactivation (Fertleman et al., 2006), only three of the eight known PEPD mutations, identified in 11 families, had been functionally characterized. Furthermore, the initial functional characterization, while intriguing, was not comprehensive. For example, PEPD mutations that overlap with a putative “docking” site for the VGSC inactivation gate (Smith and Goldin, 1997; Popa et al., 2004) within the D3 / S4-S5 linker were not evaluated. Therefore, we examined the consequences of three PEPD mutations; the I1461T mutation studied by Fertleman et al. (2006) and two uncharacterized mutations identified within the cytosolic S4-S5 linker of D3, C-terminal to D3 / S4. The initial hypothesis of this study was that PEPD mutations located in the D3 / S4-S5 linker would differentially affect transition to an inactivated state compared with those found in the inactivation gate motif.

We investigated whether two of the D3 / S4-S5 PEPD mutations (Figure 3) had similar effects on voltage-dependent gating properties of Na_v1.7 channels utilizing whole-cell voltage-clamp electrophysiological techniques. Both D3 / S4-S5 PEPD mutations (V1298F and V1299F) significantly shifted the $V_{1/2}$ of steady-state inactivation by ~20 mV in the depolarizing direction compared to WT (Figure 5). This was nearly identical to the effect of the I1461T mutation on

steady-state fast inactivation we observed (Figure 5). However, our data differs from that of Fertleman et al. (2006), which indicated the I1461T mutation impaired fast inactivation to a much greater extent than we observed. In Fertleman et al., it was shown that ~40% of the I1461T current failed to inactivate during a “steady-state inactivation protocol”. Conversely, we observed nearly complete steady-state inactivation with the PEPD mutants (Figure 5C). One reason for the differences observed in “steady-state inactivation” is that the protocol used in Fertleman et al. employed 60 ms inactivating pre-pulses, which, as can be seen in Figure 4A, is inadequate to obtain steady-state conditions. Na_v1.7 channels exhibit slow kinetics for the development of closed-state inactivation (Cummins et al., 1998) and therefore 500 ms conditioning pulses are needed to ensure steady-state conditions over the full-range of potentials tested. Our data is consistent with Fertleman et al., in that mutations implicated in PEPD disrupt the voltage-sensitivity of the fast-inactivated state, resulting in a decreased fraction of channels transitioning to a non-conducting state at potentials between -90 and -20 mV. However, because our data shows that PEPD mutations do not substantially increase the non-inactivating component under true steady-state inactivating conditions (with both fluoride containing and non-fluoride containing electrode solutions), this indicates the impairment of fast inactivation by PEPD mutations can be more moderate than previously suggested.

Our data also show that the D3 / S4-S5 PEPD mutations, as well as the I1461T mutation, increase the inactivation time constants (τ_h) compared to WT at

potentials positive to -10 mV. This indicates rate transitions for inactivation of mutant channels become less voltage-dependent at potentials positive to -10 mV thus, providing further evidence the PEPD mutations destabilize the inactivated configuration. Upon inspection of the mutant I/V traces at -10 mV, we observed a small persistent component (6% of peak) with the three PEPD mutant traces compared to WT (Figure 5E) By contrast, Fertleman et al. reported that short depolarizing pulses elicited relatively large persistent components (~40% of peak) for I1461T currents. A mutation that induces non-inactivating components that are 40% of the total current would be expected to have major consequences on the neuronal excitability of every cell exhibiting that mutation and would, therefore, be predicted to cause more widespread pain than is typically observed in many individuals with PEPD, as Na_v1.7 channels are highly expressed throughout the PNS. Our data, demonstrating the impairment of inactivation caused by the V1298F, V1299F, and I1461T PEPD mutations can be more moderate than previously indicated for the I1461T mutation, help explain why PEPD mutations do not cause pain throughout the body.

We further evaluated the effects the PEPD mutations had on the stability of the inactivated state by testing channel development and recovery from open-state inactivation (OSI) and closed-state inactivation (CSI). All three PEPD mutations increased the recovery rates for CSI and OSI. Surprisingly, the V1298F and V1299F mutations within the D3 / S4-S5 linker increased the rate of development of CSI, whereas the I1461T mutation within the putative inactivation gate did not. Although the rate for development of CSI at -60 mV was increased,

the fraction of channels undergoing CSI at -60 mV was greatly reduced for the three PEPD mutant channels, compared to WT channels, which likely reflects disruption of strong binding of the inactivation gate by the PEPD mutations.

Since it has been demonstrated that variability of CSI kinetics between different VGSC subtypes can influence I_{ramp} amplitudes (Cummins et al., 1998) we examined currents elicited by a slow (0.27 mV/ms) depolarizing ramp stimulus. We observed a significant increase in the I_{ramp} for all three PEPD mutant channels at potentials positive to -20 mV when compared to WT, which is likely due to the decreased rate of OSI at these potentials. While both IEM and PEPD mutations are likely to increase ramp current amplitudes, the voltage-dependence of the ramp currents observed with the PEPD mutant channels are distinct from the ramp currents observed with several of the $\text{Na}_v1.7$ IEM mutant channels, which exhibit increased ramp current amplitudes at negative potentials but not at potentials near -10 mV compared to WT channels (Cummins et al., 2004). Voltage ramp protocols are useful to assay subthreshold currents near RMP. Thus, ramp current properties may yield insight into changes that may significantly influence excitability. As such, the PEPD mutations may differentially alter action potential (AP) properties when compared to the IEM mutations because PEPD mutations primarily slow transition to an inactivated state. The PEPD mutations are likely to contribute to broadening of the AP duration, enhanced repetitive or burst firing and decreased AP threshold, but probably do not depolarize the resting membrane potential (RMP) in the same manner as IEM mutations (Dib-Hajj et al., 2005; Rush et al., 2006). We also

show that PEPD mutations can alter the voltage-dependence of slow inactivation of $\text{Na}_v1.7$. The impairment of slow inactivation that we observe at potentials between -90 and -60 mV with all three of the PEPD mutations examined in this study is also likely to increase $\text{Na}_v1.7$ channel availability near resting potential and therefore contribute to enhanced excitability of sensory neurons. In a parallel study, determining the effects of a novel mutation (M1627K) from a previously unreported family with PEPD, we showed that this mutation, located in the D4 / S4-S5 linker of $\text{Na}_v1.7$ displays similar voltage-dependent gating characteristics to those we reported for the S4-S5 of D3. Additionally, using current clamp, we show that M1627K PEPD mutant channels lower threshold for single APs and increase number of APs in response to graded stimuli in small DRG neurons, most of which are nociceptors. The lowered AP threshold and increased repetitive firing are two hallmarks of nociceptor hyperexcitability and are likely to contribute to neuropathic pain in PEPD. It is interesting to note that several of the PEPD mutations identified, to date, are primarily found in the D3 and D4 / S4-S5 linkers and within the putative inactivation gate (Dib-Hajj et al., 2007). These regions have been hypothesized to be critical for stabilizing the transition to an inactivated state, however, direct evidence supporting this statement is lacking.

2. Structural role of the Na_v1.7 D3 / S4-S5 cytosolic linker in channel gating

Specific regions within each of the four domains (D1-D4) of VGSCs are thought to have distinct, but integrated roles in channel gating and conformational stability in response to changes in membrane potential (Noda et al., 1984; Stuhmer et al., 1989; West et al., 1992; Cha et al., 1999; Hille, 2001; Chanda and Bezanilla, 2002; Chanda et al., 2004). Significant advances in understanding the structural interactions involved in voltage-sensitive channel gating have been demonstrated through the determination of the structure of potassium channels using X-ray crystallography (Doyle et al., 1998; Long et al., 2005b, a; Long et al., 2007) and computer-based homology modeling using the potassium channel template (Lipkind and Fozzard, 2000). The modeled crystal structure of the K_v1.2 channel shows the α -helical S4-S5 segments crossing over hydrophobic regions of the S6-segments. It has been proposed that the distal portion of the S6-segments need to pivot or splay during the activating transition to the ion-conducting state and that the voltage-dependent outward displacement of the S4 segments is coupled to channel opening via hydrophobic interactions of the S4-S5 and S6-segments. A crystal structure has not been obtained for mammalian VGSCs. While homology modeling of VGSCs based on potassium channel structures provides some insight, study of disease-associated and laboratory-designed mutations has significantly enhanced our knowledge of the secondary structure and critical features involved in gating of VGSCs (Hille, 2001). Studies have indicated that residues within the D3 / S4-S5 linker can (1)

act as a part of the unique “docking” site for the VGSC putative inactivation gate via direct interactions and / or (2) indirectly stabilize the fast-inactivated configuration via cooperative interactions with specific residues located in the D4 / S4-S5 cytosolic linker as the inactivation gate (IFMT) docks at a site within the channel pore (Smith and Goldin, 1997; Popa et al., 2004). Our data demonstrate that V1298 and V1299 are important to help stabilize the fast-inactivated states of Na_v1.7. Our data on the adjacent and identical mutation V1300F within D3 / S4-S5 of Na_v1.7 indicate that orientation and / or position-specific interactions are also important. In contrast to V1298F and V1299F, the V1300F mutation had very small effects on inactivation, shifting the $V_{1/2}$ of steady-state inactivation by 4 mV in the hyperpolarizing direction and decreased the percentage of peak current elicited during a slow ramp depolarization compared to WT channels. The V1300F mutation had a more pronounced effect on activation, shifting the $V_{1/2}$ of channel conductance by ~10 mV in the depolarizing direction and decreasing the voltage-dependent time constants for deactivation. The distinct effects of adjacent, identical mutations are consistent with the hypothesis that the D3 and D4 / S4-S5 linkers of VGSCs retain an alpha-helical secondary structure (Filatov et al., 1998). These studies are important because they suggest that mutation within the D3 and D4 / S4-S5 linkers may, in an isoform-specific manner, predictably disrupt critical stabilizing interactions that decrease the overall affinity of gating reactions, which may offer insight on structural requirements for gating. Thus, our studies confirm an important structural and functional role for D3 / S4-S5 of Na_v1.7 during stabilization of the inactivated

states, such that mutation of residues critical during transition decreases the voltage-dependent probability of channels residing in this configuration and indicate the extreme precision with which the interactions critical for gating orchestrate opening and closing of these channels in response to changes in membrane potential.

Overall, these experiments show that D3 / S4-S5 mutations identified in patients with the inherited molecular neuropathy PEPD result in destabilization of the fast and slow-inactivated states of Na_v1.7, thus, contributing to depolarizing shifts in the steady-state inactivation profiles and enhancing ramp currents. It is worthwhile to note that at least 11 additional D3 / S4-S5 VGSC mutations have been associated with inherited disorders of excitability, including epilepsy (Heron et al., 2002; Berkovic et al., 2004; Meisler and Kearney, 2005), ataxia (Kohrman et al., 1996), long QT syndrome type 3 (LQT3) (Wang et al., 1996; Smits et al., 2005), Brugada syndrome (Casini et al., 2007), myotonia (Yang et al., 1994; Richmond et al., 1997; Bouhours et al., 2005), and hypokalemic paralysis (Sugiura et al., 2003), indicating this region may be a “hotspot” for disruptive mutation. These disorders are a result of single-point mutations occurring in a highly conserved region of various VGSC isoforms. Interestingly, some of these disease-related mutations predominately alter the voltage-dependence of channel conductance. Although many of these mutations slow the rate of inactivation, none substantially increase the percentage of non-inactivating current. Here, our studies show that, contrary to prior reports, PEPD mutations do not necessarily cause marked loss of fast inactivation. The moderate

decrease in the stability of the fast-inactivated configuration we observe might help explain why the pain associated with PEPD mutations in Na_v1.7 is typically not associated with all nociceptive neurons expressing Na_v1.7. However, several issues regarding the age-onset, therapeutic efficacy, pain triggers, and location of pain perception still remain unresolved for patients with PEPD and IEM, both of which result from single-point missense mutations in Na_v1.7. It is interesting to note that modulating factors that affect VGSC gating properties such as cellular redox balance (Kassmann et al., 2008) and temperature (Bouhours et al., 2004; Foulkes and Wood, 2007; Han et al., 2007; Zimmermann et al., 2007), along with cellular background (Leffler et al., 2002; Rush et al., 2006; Yiangou et al., 2007) and alternative splicing (Raymond et al., 2004) could affect some of the noted differential factors for patients with IEM versus PEPD. It remains to be seen if there is one answer for the differences or if it involves a myriad of molecular components, however, further investigation into these mechanisms could provide valuable insight into developing more specific pain therapeutics.

C. Alternative splicing of Na_v1.7 exon 5A increases the impact of the painful PEPD mutant channel I1461T

1. Effects of alternative splicing on Na_v1.7 disease mutations

The potential reasons for the differences noted between IEM and PEPD inspired the design of the second part of this dissertation. As mentioned above, notable differences such as age-onset, therapeutic efficacy, triggers of painful

episodes, and location of perceived pain have been documented for patients with IEM and PEPD. One of the intriguing possibilities for these differences is alternative splicing of Na_v1.7. Indeed, alternative splicing within exons 5 and 11 of Na_v1.7 has been shown to occur resulting in two separate pairs of splice variants (Raymond et al., 2004). Variants within exon 5 have been termed 5A (“adult”) and 5N (“neonatal”), although the logic is not clear because the expression patterns are not well-correlated with age. Residue differences are noted within the exon 5 coding region, which is located within an area of D1 / S3-S4. Variants from exon 11 splicing are defined as 11S (“short”) and 11L (“long”), where the short form lacks an 11 amino acid stretch excluded from the D1-D2 loop. In particular, a recent study has shown that alternative splicing of Na_v1.7 channels can affect the biophysical properties (Chatelier et al., 2008). Interestingly, the exon 5 variants, which differ by two amino acids (L201V, N206D) in the D1 / S3-S4 linker, differentially affect the amplitude of currents generated in response to a slow depolarizing ramp stimulus. IEM and PEPD mutations also alter Na_v1.7 ramp current properties and this is thought to contribute to the chronic pain induced by these mutations. Therefore, it was hypothesized that alternative splicing of Na_v1.7 could impact the functional consequences of IEM (I136V) and PEPD (I1461T) mutations.

The second overall goal of this dissertation was to determine if exon 5 splicing impacts the biophysical properties of IEM and / or PEPD using a single-point missense mutation associated with each painful disorder. We present evidence that the 5A alternative splice variant of Na_v1.7 alters the biophysical

properties of a disease mutation implicated in PEPD (I1461T) but not IEM (I136V). Since a majority of the IEM mutations primarily alter the voltage-dependent activation and deactivation properties (Dib-Hajj et al., 2007) the relatively small shifts induced by the 5A splice variant on voltage-dependent activation may be masked. The I136V mutation alone shifted the midpoint of activation by approximately -8 mV compared to WT, which is much larger than the shift observed for the WT-5A compared to WT-5N splice variants. Our results suggest that IEM mutations are not additively affected by the 5A splicing. These results are in agreement with those from Han et al. (2009) showing that the voltage-dependent properties of another “late-onset” IEM mutation (Q10R) are also not affected by alternative splicing. However, our results for the PEPD (I1461T) splice variants are intriguing because they indicate that the impact of PEPD mutations and exon 5 changes are additive. Mutations associated with PEPD generally affect the voltage-dependent transition to an inactivated state and thus, destabilize an inactivated channel configuration allowing an increasing fraction of channels to remain available for activation and opening (Fertleman et al., 2006; Dib-Hajj et al., 2008; Jarecki et al., 2008). Many of the characterized PEPD mutations shift the voltage-dependent inactivation properties to more depolarized potentials and yield incomplete development of closed-inactivation and accelerated recovery from inactivation compared to wild-type (Jarecki et al., 2008). Conversely, our results demonstrate that the 5A splice variant of WT channels moderately hyperpolarizes the midpoint of activation and increases ramp current, which are in agreement with Chatelier et al. (2008). Since the

stability of the inactivated conformation is decreased by the I1461T mutation, the effects of the 5A alternative splicing for the I1461T channels would be predicted to amplify the overlap between channels opening versus inactivating (window current) and increase the probability of channel opening in an additive manner. Indeed, when the ability of channels to generate subthreshold ramp currents was assayed the I1461T 5A variant significantly increased the peak current and shifted the ramp current threshold to more hyperpolarized potentials compared to the 5N variant. The changes observed in ramp current for the I1461T 5A variant could be caused by a lowered energy barrier for the channels to activate relative to deactivation, and a slowed and incomplete development of a closed-inactivated state thus favoring ion flux. It is worthwhile to note that the voltage-dependent properties of the ramp current for the I1461T 5A variant, even when compared to the wild-type 5A variant, resemble a melding of those observed for IEM mutations (Cummins et al., 2004; Dib-Hajj et al., 2005; Cheng et al., 2008) and PEPD mutations (Dib-Hajj et al., 2008; Jarecki et al., 2008) in Na_v1.7 channels. These effects were similar to those observed for a novel mutation that caused patient symptoms associated with both disorders (Estacion et al., 2008). The overlapping functional effects for these separate painful mutations are particularly interesting because patients diagnosed with PEPD have reported differential age-onset of pain compared to IEM patients (Fertleman et al., 2007). Therefore, it is appealing to consider that temporal and tissue specific increases in relative expression of the 5A variant could result in a transition to a state where

patients with disease mutations in Na_v1.7 experience more frequent and diverse attacks.

2. *Mechanistic implications from amino acid differences between Na_v1.7 exon 5 splice variants*

The coding region of exon 5 includes a portion of the Na_v1.7 gene that extends from the D1 / S3 segment to the C-terminal end of the positively charged D1 / S4 (Raymond et al., 2004). The residue differences between the 5N and the 5A variants are localized to the extracellular portion of the D1 / S3 and the D1 / S3-S4 cytosolic linker. Interestingly, the residue difference in the cytosolic linker of the 5A variant contains a polar, negatively charged (acidic) residue (Asp206) compared to the 5N variant which retains a polar, non-charged Asn at the 206 position at physiological pH. This acidic residue substitution could contribute an additional negative charge to the electrostatic field surrounding the D1 / S4 (Asamoah et al., 2003; Sigg and Bezanilla, 2003). Additionally, the Asp206 may form electrostatic interactions with N-terminal residues in the mobile D1 / S4 charge translocator, which is laden with positive residues (Cha and Bezanilla, 1998; Sorensen et al., 2000). In fact, alternative splicing in this region of Na_v1.5 has been explored (Onkal et al., 2008), wherein a positively charged residue (Lys) has been substituted for a negative residue (Asp) between variants. Results from Onkal and colleagues suggest that this reversal of residue charge impacts the voltage-sensitivity and kinetics of channel activation, such that the positively charged splicing substitution within D1 / S3-S4 depolarized the activation midpoint and slope factor, and slowed the time to peak, all of which were reversed upon switching the charged residue substitution. Since movement

of the D1 / S4 is critical during the early fast component of gating charge translocation and channel activation (Cha et al., 1999; Chanda and Bezanilla, 2002), a negative charge on an extracellular linker within proximity to accessible positively charged D1 / S4 residues could accelerate the movement of this segment during depolarization. Indeed, several studies have shown that the upper portion of charged residues within the S4 is accessible in the extracellular space during depolarization (Yang and Horn, 1995; Larsson et al., 1996; Starace and Bezanilla, 2001; Ruta et al., 2005). Thus, small changes such as increased electrostatic interactions that may lower the energy barrier for activation for the S4 segments would be predicted to enhance their gating movement, reduce deactivation, and increase the probability to generate subthreshold currents at more hyperpolarized potentials. The other amino acid change that results from the alternative splicing involves a more conserved substitution (Leu to Val at position 201), but as conserved substitutions can have important consequences (i.e., I136V causes chronic pain); we cannot rule out a role for this amino acid change in altered channel gating. Furthermore, we cannot overlook the possibility that the combination of the two substituted residues that differ in the 5N versus the 5A variants decreases the stability of the channel population in the closed state relative to the open state. And finally, it is worthwhile to consider the possibility that particular VGSC auxiliary subunits, expressed in nociceptive neurons, may differentially augment channel properties in response to regulation of alternative splicing events.

3. *Global effects of alternative splicing*

Alternative splicing affects the properties of a variety of sodium channels (Sarao et al., 1991; Dietrich et al., 1998; Tan et al., 2002; Raymond et al., 2004; Fraser et al., 2005; Liu et al., 2008; Onkal et al., 2008), calcium channels (Liao et al., 2004; Shen et al., 2006; Altier et al., 2007; Liao et al., 2007; Shcheglovitov et al., 2008; Tang et al., 2008; Adams et al., 2009), and potassium channels (Bassi et al., 2005; Aydar and Palmer, 2006; Xu et al., 2007). In particular, $Na_v1.1$ -3, 5 and 6, in addition to $Na_v1.7$, have alternative splicing within exon 5 that involves a change in the charge of one residue (Raymond et al., 2004). Interestingly, of the Na_v isoforms with exon 5 splicing, disease-associated (gain-of-function) mutations have also been identified in $Na_v1.1$ and 1.2 (epilepsy) (Catterall et al., 2008; Lossin, 2009) and 1.5 (LQTS) (Koopmann et al., 2006) and, as with the PEPD mutations, some of these mutations primarily impair inactivation. Therefore, based on our data with the I1461T PEPD mutation, we predict that the changes induced by splicing likely have a functional impact on other disease mutations and this could be useful in understanding the underlying molecular mechanisms inactivation gating. It is likely that expression patterns of splice variants in human populations are altered under pathological conditions (Raymond et al., 2004; Fraser et al., 2005; Altier et al., 2007) and may result in unique differences in response to pharmacological agents (Tan et al., 2002). Although the interactions and effects may be complex, physiological regulation of the splice variants may prove useful in better understanding disparities in

pathophysiology related to patient age or genetic background. Understanding how alternative splicing alters intramolecular interactions during channel gating could lead to the development of novel pharmacological strategies. However, alternative splicing of Na_v1.7 may be just one piece of the puzzle which may account for differences in symptoms between patients with IEM and PEPD. Unraveling further structural and molecular details that account for differences in localization of pain and therapeutic efficacy may further enhance our knowledge of pain signaling and understanding of how dysfunction in one component of the process lower the threshold and / or response to non-noxious stimuli.

D. Inherited mutations implicated in neuronal and muscle channelopathies can increase resurgent sodium currents in DRG neurons

We also hypothesized that an increased contribution of inward current that flows at repolarizing potentials when channels should reside in an inactivated / non-conducting state. The amplitude of this unique type of current, termed resurgent current, is increased upon artificial slowing of sodium channel inactivation using toxin application (Grieco and Raman, 2004). Therefore, inherited Na_v1.7 mutations implicated in PEPD would be predicted to increase resurgent sodium currents. We hypothesize that increased resurgent currents may be a novel reason for the difference between patients with PEPD, whose pain is associated with Na_v1.7 mutations that affect inactivation properties, compared to IEM, whose pain is associated with Na_v1.7 mutations that affect activation properties. Together, increases in resurgent sodium currents may help

explain the spectrum of severity of voltage-gated sodium channelopathies associated with mutations that alter channel inactivation and cellular excitability.

Our data show for the first time that (1) $\text{Na}_v1.4$, $\text{Na}_v1.5$ and $\text{Na}_v1.7$ channels have the capability to generate resurgent currents and (2) the relative amplitudes of resurgent sodium current observed with the disease mutations that impair inactivation are approximately of the same magnitude of the resurgent currents generated by $\text{Na}_v1.6$ under control conditions in cerebellar Purkinje neurons and DRG neurons (Raman et al., 1997; Cummins et al., 2005). An extensive series of studies on cerebellar Purkinje neurons indicates that resurgent currents have a major impact on excitability, contributing to spontaneous firing and accelerating the rate of repetitive firing of APs (Raman and Bean, 1997; Raman et al., 1997; Raman and Bean, 1999b, 2001; Khaliq et al., 2003). As a consequence, it is predicted that the resurgent currents associated with the inherited neuronal and muscle channelopathies could significantly impact AP firing in neurons and muscle and contribute to disease pathophysiology. Indeed, our computer models of a DRG neuron and cardiac myocyte indicate that resurgent currents could significantly exacerbate the effects of the disease mutations on cellular excitability (Jarecki et al., 2010).

Our data provide further evidence that the sodium channel isoforms differ in their proclivity to produce resurgent sodium currents. We show that, under normal conditions, $\text{Na}_v1.6$ is more inclined to generate resurgent currents than $\text{Na}_v1.4$, $\text{Na}_v1.5$ or $\text{Na}_v1.7$. Furthermore, the identical mutation produced a greater increase of resurgent currents in $\text{Na}_v1.6$ than in $\text{Na}_v1.7$. Although studies

of Na_v1.6 knock-out mice strongly indicate that Na_v1.6 is the predominant generator of resurgent currents in cerebellar Purkinje and DRG neurons (Raman et al., 1997; Cummins et al., 2005), resurgent currents have been detected in Purkinje and other CNS neurons from Na_v1.6 knock-out mice (Do and Bean, 2004). Na_v1.2 channels produce resurgent currents when expressed in DRG neurons, albeit in only two of 25 transfected cells (Rush et al., 2005). Although it is not known if Na_v1.1 and Na_v1.3 channels produce resurgent currents, mutations that slow the rate of inactivation have been identified in these isoforms in patients with epilepsy (Lossin et al., 2002; Holland et al., 2008). Therefore, it is conceivable that resurgent currents could also contribute to the pathophysiology of some inherited epilepsies.

In our study we show that a mutation that occurring in the voltage-sensing segment 4 of the fourth domain as well as mutations in the IFMT inactivation motif can induce enhanced resurgent currents, suggesting that any mutation that slows the rate of open channel fast inactivation might be able to induce resurgent currents.

To verify this hypothesis and expand this study, I further tested the ability of an additional Na_v1.7-PEPD mutation (V1299F) located in the D3 / S4-S5 linker to generate resurgent currents. This particular mutation was chosen for a few reasons. First, this Na_v1.7-PEPD mutation is located outside of the putative inactivation gate motif (IFMT) but within an intracellular linker region important for interactions critical for stabilizing transition to an inactivated state, as demonstrated within this dissertation. Second, based on the characterization

data shown in this dissertation, the V1299F PEPD mutation has differential effects on the kinetics of development of and recovery from inactivation compared to the inactivation gate mutation I1461T. As shown in Figure 38, transiently transfected rat DRG neurons, expressing the Na_v1.7r-V1299F PEPD mutant channels shift the inactivation profile rightward (Figure 38A) and can produce resurgent currents (Figure 38B) within a voltage-dependent window (Figure 38C) in a similar manner to the Na_v1.7r-I1461T inactivation gate mutation. However, my preliminary data suggests that the amplitude of resurgent currents is increased with the D3 / S4-S5 PEPD mutation (V1299F) compared to wild-type Na_v1.7r and inactivation gate mutant (I1461T) channels. These data may indicate that although the PEPD mutations, which all appear to disrupt inactivation, have the potential to generate resurgent currents, the location and the residue substitution may determine the relative amplitude of resurgent current.

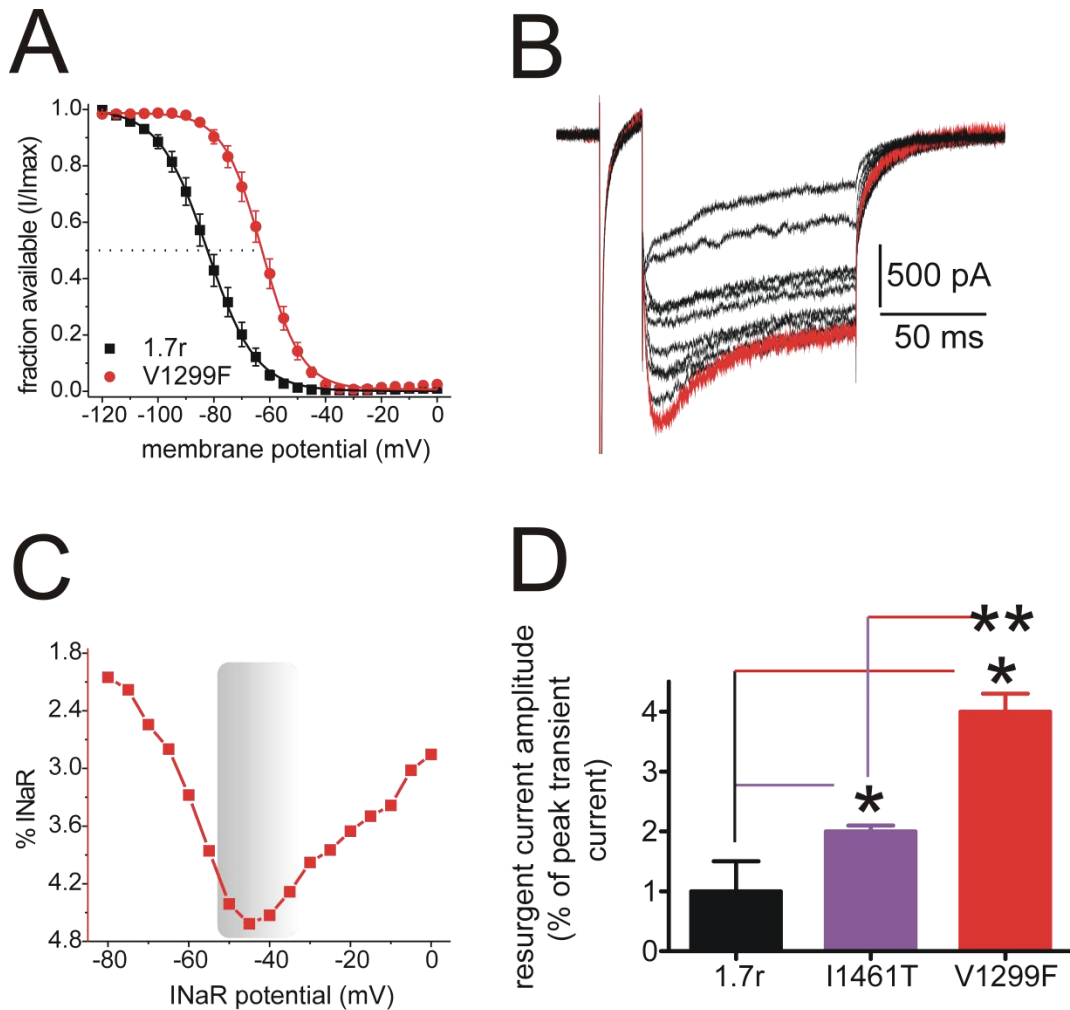


Figure 38. A D3 / S4-S5 PEPD mutation (V1299F) shifts steady-state inactivation and increases resurgent current amplitude compared to Na_v1.7r wild-type and I1461T channels in transfected DRG neurons. (A) Comparison of steady-state inactivation for wild-type Na_v1.7r and Na_v1.7r-V1299F channels. Representative trace (B) and voltage-dependence (C) of resurgent currents elicited for the Na_v1.7r-V1299F channel. The voltage-dependent plot shown was collected from the data in the representative trace illustrated in (B). The gray shading in (C) indicates the voltage window where peak resurgent current amplitude is typically observed. (D) Bar graph comparison of percentage of resurgent current amplitude for wild-type Na_v1.7r (5 of 21 cells), Na_v1.7r-I1461T (20 of 30 cells), and Na_v1.7r-V1299F (5 of 10 cells) PEPD mutant channels. The lines above each bar are color-coded to denote significance between the channels for generation of resurgent currents. Protocol used to generate the data for this graph is described in the *Methods* section of this dissertation.

important role in determining the amplitude of resurgent currents elicited. Collectively, these data may suggest a molecular / structural basis as to why some of the patients with PEPD respond to certain therapeutic agents better than others. One intriguing way to correlate amino acid substitutions (structure) to changes in resurgent current amplitude (function) could be via utilization of Cys substitutions. For example, if one was to compare the side chain volume and the effects on activation and inactivation properties, a relatively minor Cys substitution appears to be innocuous to steady-state channel properties compared to a more bulky Phe substitution, as seen in PEPD (Figure 39). Thus, using a series of MTS reagents that add charge (MTSET, MTSEA, MTSES), aromatic bulk (MTSBn), or photoactivatable moieties to an accessible engineered Cys residue may be a useful way of bridging changes in amino acid properties to voltage-dependent characteristics of resurgent currents to changes in an AP profile. Additionally, one may be able to “titrate” the effects using a series of site-directed mutagenesis techniques that involve substituting amino acids with varying side chain properties or inserting unnatural amino acids that are modified to test effects of chemical structure on current properties and correlate the replacements to changes in resurgent current characteristics and AP properties.

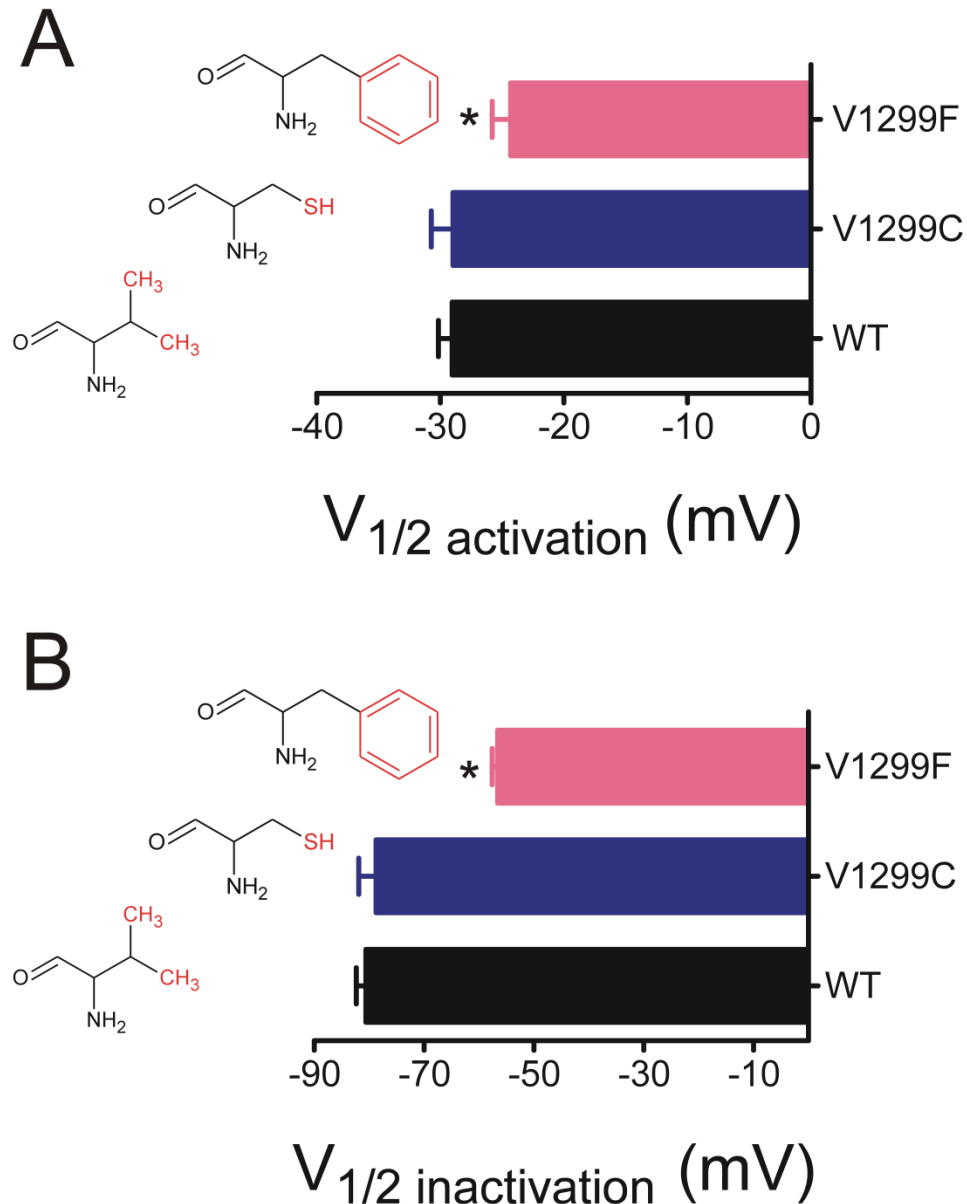


Figure 39. Side chain volume of amino acid substitutions made within the Na_v1.7 D3 / S4-S5 linker at a location critical for stabilizing inactivation which is mutated in PEPD. Comparison of amino acid side chain volume substitutions and resulting changes in V_{1/2} activation (**A**) and inactivation (**B**). The substitutions occur at the same location (1299 position) replacing a native Val to a Phe, as seen in PEPD, or Cys, which was used in this dissertation to probe interactions during transition to an inactivated state. The bulky Phe substitution had small, but significant effects on the activation profile, and more dramatic alterations to the voltage required to inactivate 50% of the channels, compared to WT Na_v1.7 and V1299C channels. These data were determined using transiently transfected hEK₂₉₃ cells with activation and inactivation protocols described in the Methods section. * denotes statistical significance.

However, it is important to note that the rate of inactivation cannot be the only determinant of resurgent current production. $\text{Na}_v1.8$ currents are slower to inactivate than $\text{Na}_v1.7r\text{-I1461T}$ channels. Despite this, in cultured rat DRG neurons treated with TTX that produced large endogenous $\text{Na}_v1.8$ currents (but no recombinant currents) resurgent currents were not observed (Jarecki et al., 2010). Thus, other factors must also contribute to the inclination of specific VGSC isoforms to generate resurgent currents.

The data presented in the resurgent currents *Results* section, in conjunction with a previous study (Cummins et al., 2005), clearly show that DRG neurons have the appropriate cellular environment for production of resurgent currents. By contrast, adult DRG sensory neurons do not express $\text{Na}_v1.4$ and $\text{Na}_v1.5$ and it is not known if cardiac and skeletal muscle cells have the appropriate cellular environment for the production of resurgent currents. Data from cerebellar Purkinje neurons indicate that the auxiliary sodium channel $\beta 4$ -subunit may be the putative blocking factor crucial to generation of resurgent currents with $\text{Na}_v1.6$ channels (Grieco et al., 2005). Previous work has demonstrated that DRG neurons, cardiac and skeletal muscle all express high levels of $\beta 4$ (Yu et al., 2003). However, while the $\beta 4$ -subunit may be necessary, it does not appear to be sufficient. Phosphorylation of the sodium channel, the $\beta 4$ -subunit, or possibly an unidentified protein also seems to be required (Grieco et al., 2002), at least in cerebellar Purkinje neurons. This indicates changes in kinase and phosphatase activity are likely to impact the generation of resurgent currents. Therefore, even if the conditions in normal cardiac and skeletal muscle

are not appropriate for generation of resurgent currents, under specific, possibly pathological, conditions these cells might express the appropriate accessory subunits and kinases. Since our optimized expression system utilized adult DRG neurons where $Na_v1.4$ and $Na_v1.5$ are not normally expressed, it would be of great interest to determine if $Na_v1.4$ and $Na_v1.5$ wild-type and mutant channels produce resurgent sodium currents in skeletal and cardiac muscle, respectively, under either normal or pathophysiological conditions.

It is important to note that not all of the DRG neurons expressing recombinant channels *capable* of generating resurgent currents *produced* detectable resurgent currents. This further indicates that the cellular environment is a crucial determinant of resurgent current production. Regional differences in the properties of sensory afferents that impact resurgent current generation might contribute to the phenotypical association of pain with particular body regions in PEPD. Over 40 cells with peak transient current amplitudes greater than 20 nA were recorded from that did not have detectable resurgent currents. Notably, the relative amplitude of resurgent currents is poorly correlated with peak transient current amplitude (Jarecki et al., 2010). At this time we do not know how DRG neurons that do and do not produce resurgent currents differ in terms of β -subunit expression and / or kinase activity. Our optimized DRG expression system could be very useful in identifying cellular factors that modulate resurgent currents.

Our data clearly show that resurgent sodium currents are likely to play a role in the functional consequences of inherited neuronal and muscle

channelopathies. In addition our data, in conjunction with the previous study indicating that beta-pompilidotoxin can artificially induce resurgent currents in cerebellar Purkinje neurons (Grieco et al., 2005), indicate that any manipulation which slows or destabilizes inactivation has the potential to induce resurgent currents. Many post-translational modifications have been reported to slow the rate of inactivation or increase the amplitude of persistent sodium currents, including hypoxia (Hammarstrom and Gage, 2002), phosphorylation (Numann et al., 1991), altered calcium signaling (Herzog et al., 2003a), G-protein activation (Ma et al., 1997) and oxidation (Kassmann et al., 2008). We propose that these alterations could also result in abnormal resurgent current generation. The induction of resurgent sodium currents likely contributes to the more extreme electrophysiological changes and disease sequelae that can be associated with both *inherited and acquired* disorders of neuronal and muscle excitability

E. Residues located within the D3 / S4-S5 of Na_v1.7 directly stabilize an inactivated configuration

A multitude of scanning mutagenesis studies localized to the S4-S5 segments of D3 and D4 in VGSCs suggest that these cytosolic linkers serve as putative “docking” sites for the mobile inactivation gate and that the biochemical properties of specific residues within the linkers can specifically stabilize an inactivated channel configuration (Lerche et al., 1997; Smith and Goldin, 1997; Filatov et al., 1998; McPhee et al., 1998; Popa et al., 2004). Additionally, inherited single point mutations in the D3 and D4 / S4-S5 that are implicated in several muscle and neuronal voltage-gated sodium channelopathies can alter transition to an inactivated state, which is postulated to contribute to the phenotype of the disease (Cannon, 2006; Koopmann et al., 2006; Catterall et al., 2008). However, the evidence for direct interactions with the VGSC inactivation gate motif and the means by which residues within the D3 and D4 / S4-S5 segments stabilize an inactivated configuration are unclear. The potential for interactions with the S4-S5 linkers, which lie outside of the pore and the inactivation gate, has proven to be a controversial issue as the VGSC inactivation gate has been proposed to interact and “dock” with residues inside the aqueous channel pore.

Interestingly, mutation of residues (V1298, V1299, and M1627) within the D3 and D4 / S4-S5 linker are implicated in a painful disorder termed PEPD (Fertleman et al., 2006). Results from this dissertation demonstrate that a

doublet of native Val residues within the D3 / S4-S5 linker of Na_v1.7 at the 1298 and 1299 positions and the native D4 / S4-S5 Met residue are critical for stabilizing an inactivated state and that upon mutation, can increase neuronal excitability (Dib-Hajj et al., 2008; Jarecki et al., 2008). Destabilized inactivation is predicted to be due to either direct alterations to a putative “docking” site for the inactivation gate outside of the aqueous channel pore, or alterations that indirectly decrease the stability of an inactivated configuration where the inactivation gate motif “docks” to sites within the channel pore. Therefore, I sought to determine if residues within the D3 / S4-S5 linker of Na_v1.7 can directly interact with the inactivation gate motif and serve as a putative “docking” site during transition to an inactivated state. Results from these studies reveal several layers of evidence that suggest the D3 / S4-S5 linker of Na_v1.7 can provide an accessible interface, dependent on membrane potential, to which the inactivation gate motif can “dock”.

First, the specific location and orientation as well as the biochemical properties of the side chain of the substituted amino acid within the D3 / S4-S5 linker of Na_v1.7 are important for stabilizing interactions required during inactivation. Substitution of the native V1298 and V1299 to Cys residues does not affect steady-state gating or kinetic properties, whereas the V1300C substitution reduced the voltage-sensitive response to depolarization, thus shifting the activation and inactivation potentials rightward. However, substitution to bulky (Phe) or charged (Asp) residues dramatically affects transition to an inactivated state at the 1298 and 1299 residue positions. These data suggest

that mild side chain substitutions (i.e. Val→Cys) do not significantly disrupt the van der Waals interactions that stabilize inactivation at the 1298 and 1299 positions, however, bulky groups that may add steric hindrance (i.e. Val→Phe), or charged groups (i.e. Val→Asp) that may alter neighboring electrostatic interactions can affect the stability of transition to an inactivated state. Furthermore, because substitution of bulky or charged residues at the 1298 and 1299 positions alter transition to an inactivated state, the native residues would be predicted to lie within an accessible region of the alpha helical D3 / S4-S5 linker (Filatov et al., 1998) that could interact with residues that stabilize inactivation. Indeed, upon homology model predictions performed by me, utilizing the K_v1.2 crystal structure, the native Val residues at the 1298 and 1299 positions appear to face away from the lipid membrane towards the cytosol on a single turn within the alpha helix suggesting they may be accessible for intramolecular interactions that stabilize inactivation.

Second, the Cys substitutions at the 1299 position, but not the 1300 position within the D3 / S4-S5 linker, were modifiable and disrupted transition to an inactivated state in the presence of MTSET similar to a Cys substitution at the 1461 position within the D3-D4 Na_v1.7 inactivation gate motif. It is important to note that modification was only seen at holding potentials (-120 mV) where a large fraction of the channels were captured in a closed state before test potentials were applied, and not at more depolarized potentials (-60 and -20 mV). These data indicate that before triggering the movement of the mobile components responsible for gating and altered channel configuration via

membrane depolarization, residues (C1299 and C1461) within regions of the VGSC critical for inactivation are accessible to MTSET modification. The MTSET modification of these residues disrupts transition to an inactivated state and increases the persistent component. However, upon depolarization, the same residues (C1299 and C1461) become inaccessible and are unable to be modified. This may suggest that the packing orientation of residues changes or that interacting residue pairs are now at distances that allow for formation of stabilizing intramolecular interactions that prevent cysteine modification. However, because the residues of both the D3 / S4-S5 (C1299) and D3-D4 inactivation gate (C1461) are located within cytosolic regions predicted to interact with one another during transition to an inactivated state, I hypothesized that these two residues could be covalently crosslinked, thus “locking” the channel in a specific conformation when the accessible Cys residues are in a predicted distance from one another in a similar manner to studies “locking” mobile components of hERG (Ferrer et al., 2006), HCN (Prole and Yellen, 2006; Bell et al., 2008), both of which trapped interactions between the S4-S5 linkers and the C-terminal portion of the S6, and the components responsible for the “ratcheting” S4 gating charge movement in a bacterial voltage-gated sodium channels (DeCaen et al., 2008). I postulated that this interaction may occur at intermediate potentials (i.e., -60 mV) that are more hyperpolarized than those required to transition the channel into a conducting (open) configuration. These intermediate potentials allow for the mobile S4 segments to “initiate” and translocate positive charges from a buried position to one that was more exposed

on the extracellular surface. At these intermediate potentials, inactivation can occur, and is termed closed-state inactivation. I hypothesized that, at the intermediate potentials, before channel opening, but during S4 activation, the mobile inactivation gate motif can “dock” and interact with residues outside of the mouth of the channel pore, such as the V1299 residue within the D3 / S4-S5 linker.

Third, upon intracellular application of a crosslinking reagent (MTS-1-MTS), substituted Cys residues at the 1299 position in the D3 / S4-S5 linker and the 1461 position in the D3-D4 inactivation gate motif of Na_v1.7 were covalently crosslinked at a holding potential of -60 mV, but not at -120 or -20 mV. This crosslinker covalently modifies nearby Cys residues within a predictable distance based on the alkyl spacer in between the bifunctional reactive moieties (~5 Å). The covalent modification with the MTS-1-MTS reagent thus, effectively “locked” a fraction of the channels in a non-conducting state mimicking inactivation. These results indicate that the D3 / S4-S5 can interact with the mobile inactivation gate within ~5 Å during transition to a closed-inactivated state. It is important to note that this interaction could suggest that the inactivation gate motif (IFMT) may not need to snugly bind within the aqueous mouth of the channel pore at these potentials to inactivate closed (or partially activated) channels.

An additional interpretation may be that the Cys substitution of the Ile within the inactivation gate motif may interact with residues outside of the mouth of the pore within a three-dimensional space. These data are intriguing because

the covalent “locking” interactions were not observed at -120 mV and -20 mV. Thus, it could be hypothesized that at -120 mV, when a large fraction of the channels are in a closed state, movement of the inactivation gate towards a “docking” site with which it has an affinity towards, has not been triggered, and therefore the distance is outside of the window of the 5 Å caliper used in this study. The limited range of the MTS crosslinker may also be a reason for why the channels were not “locked” at -20 mV. At a holding potential of -20 mV, a majority of the S4 segments have translocated their charges across the plasma membrane, which is electromechanically coupled to pore opening. The tethered interface for this coupling reaction is hypothesized to be the S4-S5 segments. Therefore, as the S4 segments move “outward” upon depolarization this is transmitted to the S4-S5 segments which would be predicted to move in the same three-dimensional direction as the S4 segments. This “outward” movement may put the substituted residues outside of the MTS-1-MTS 5 Å distance for crosslinking. Alternatively, the inactivation gate motif may interact with residues within the channel pore at this holding potential, which would not allow for direct interactions with residues in the S4-S5 segments at more depolarized potentials.

Together, these results could suggest two separate “docking” sites for the inactivation gate motif, one outside of the pore at the S4-S5 interface, and one within the mouth of the aqueous pore. However, the limitations of the reagents used in this study and the electrophysiological techniques render this hypothesis solely speculative at this point. With this in mind, there are alternative

approaches that I propose to answer these questions in more detail. First, to address the limited window of reactive crosslinking, one could use a variety of MTS crosslinking reagents with longer alkyl spacers that would probe for interactions up to ~ 20 Å. Similar experimental strategies taking advantage of the biochemical properties of site-engineered Cys residues and / or synthesized reagents that act like molecular “tape measures” have been used (Blaustein et al., 2000; Laine et al., 2003; Prole and Yellen, 2006; DeCaen et al., 2008; Bali et al., 2009). Additionally, experiments utilizing charged residue pairs with predictable electrostatic interaction limitations have shed light on intramolecular interactions of voltage-sensitive channels (Seoh et al., 1996; Smith and Goldin, 1997; Ferrer et al., 2006; Muroi et al., 2010). Furthermore, computer-based homology modeling (Sunami et al., 2004) have been resourcefully used to calculate approximate regional distances of different intramolecular components of ion channels. In the context of future experiments, the MTS crosslinkers would allow examination and calibration of the distance of interactions between residues in the S4-S5 segments and the inactivation gate motif at a range of potentials as the channel dynamically transits through gating states. In the absence of a fully solved crystal structure for the VGSC these types of studies, could provide insight into the approximate distance and potential interactions required to stabilize an inactivated configuration. Second, to address the issues related to a theoretical second “docking” site within the aqueous pore, a Cys residue within a region of the aqueous pore, focusing on the C-terminal portions of the S6 segments, where the inactivation gate motif may interact. Studies have

shown there are that residues lining the S6 segments are located in the aqueous portion of the channel pore (Lipkind and Fozzard, 2000). Interestingly, two studies in two different VGSC isoforms (Na_v1.4 and 1.7) have shown that there are two conserved Phe residues within the C-terminal portion of the D3 / S6 segment critical for gating (Lampert et al., 2008; Muroi et al., 2010). The importance of the Phe residue during channel opening suggests it may be useful when probing for interactions that stabilize an inactivated channel configuration. If the sidechain of the Phe residue is indeed confined to the aqueous pore, substituting this residue with a Cys and probing for covalent interactions with the inactivation gate motif would be useful. If the Phe sidechain is facing outside of the aqueous pore, but accessible for interactions with the D3 / S4-S5 linker, the side-chain accessibility could provide useful evidence of indirect interactions of the S4-S5 segments that stabilize a splayed open configuration of the channel pore, where within the pore lies a “docking” site for the inactivation gate motif. Therefore, engineering a Cys residue within the inactivation gate, the S6 segment and the S4-S5 linker could yield insight into interactions that stabilize particular transitions to an inactivated state. Taken together, these additional studies proposed could provide useful information of the channel configuration during inactivation and may yield information about potential regions of the VGSC that could be targeted by therapeutic agents to stabilize inactivation.

F. Summation and future directions

Results from this dissertation demonstrate that (1) PEPD mutations significantly shift the voltage-dependent properties of $\text{Na}_v1.7$ channels, destabilize an inactivated state in a residue specific manner, and render nociceptive neurons hyperexcitable; (2) alternative splicing can functionally impact PEPD; (3) channelopathies, resulting from slowed inactivation in neuronal and muscle VGSC isoforms, increase an unusual sodium conductance that flows during repolarization; and (4) specific residues located in distinct regions of $\text{Na}_v1.7$ serve as docking sites to stabilize inactivation at different membrane potentials. Overall, this dissertation addresses key questions regarding the molecular mechanics required during inactivation and the biophysical consequences of $\text{Na}_v1.7$ mutations implicated in painful disorders. The results of this dissertation are important for a more detailed understanding of pain perception and validate the applicability of studying $\text{Na}_v1.7$ for discovery of therapeutic targets for treatment of pain.

$\text{Na}_v1.7$ channels, highly expressed in peripheral and sympathetic nervous systems, are essential in nociception as evidenced by single point *missense* mutations causing a spectrum of pain syndromes (Drenth et al., 2001; Fertleman et al., 2006; Dib-Hajj et al., 2007), and *nonsense* mutations resulting in human insensitivity to pain (Cox et al., 2006). Therefore, further examination of the potential role these channels may have in diseases whose symptoms are associated with some type of pain, such as cancer, may become increasingly

important in the years to come. Because humans constantly evolve and adapt to their surroundings, the critical role of particular VGSCs isoforms in tuning the response to various stimuli will ultimately provide a wealth of information about how we understand the inner workings of human physiology and disease in the many years to come.

REFERENCES

- Adams PJ, Garcia E, David LS, Mulatz KJ, Spacey SD, Snutch TP (2009) Ca(V)₂.1 P/Q-type calcium channel alternative splicing affects the functional impact of familial hemiplegic migraine mutations: Implications for calcium channelopathies. *Channels* 3:110-121.
- Ahern CA, Kobertz WR (2009) Chemical tools for K(+) channel biology. *Biochemistry* 48:517-526.
- Akabas MH, Stauffer DA, Xu M, Karlin A (1992) Acetylcholine receptor channel structure probed in cysteine-substitution mutants. *Science* 258:307-310.
- Akopian AN, Sivilotti L, Wood JN (1996) A tetrodotoxin-resistant voltage-gated sodium channel expressed by sensory neurons. *Nature* 379:257-262.
- Akopian AN, Souslova V, England S, Okuse K, Ogata N, Ure J, Smith A, Kerr BJ, McMahon SB, Boyce S, Hill R, Stanfa LC, Dickenson AH, Wood JN (1999) The tetrodotoxin-resistant sodium channel SNS has a specialized function in pain pathways. *Nature neuroscience* 2:541-548.
- Alessandri-Haber N, Alcaraz G, Deleuze C, Jullien F, Manrique C, Couraud F, Crest M, Giraud P (2002) Molecular determinants of emerging excitability in rat embryonic motoneurons. *The Journal of physiology* 541:25-39.
- Altier C, Dale CS, Kisilevsky AE, Chapman K, Castiglioni AJ, Matthews EA, Evans RM, Dickenson AH, Lipscombe D, Vergnolle N, Zamponi GW (2007) Differential role of N-type calcium channel splice isoforms in pain. *J Neurosci* 27:6363-6373.
- Amaya F, Decosterd I, Samad TA, Plumpton C, Tate S, Mannion RJ, Costigan M, Woolf CJ (2000) Diversity of expression of the sensory neuron-specific TTX-resistant voltage-gated sodium ion channels SNS and SNS2. *Molecular and cellular neurosciences* 15:331-342.
- Amir R, Argoff CE, Bennett GJ, Cummins TR, Durieux ME, Gerner P, Gold MS, Porreca F, Strichartz GR (2006) The role of sodium channels in chronic inflammatory and neuropathic pain. *JPain* 7:S1-29.

Armstrong CM (1966) Time course of TEA(+)-induced anomalous rectification in squid giant axons. *The Journal of general physiology* 50:491-503.

Armstrong CM (1969) Inactivation of the potassium conductance and related phenomena caused by quaternary ammonium ion injection in squid axons. *The Journal of general physiology* 54:553-575.

Armstrong CM (1971) Interaction of tetraethylammonium ion derivatives with the potassium channels of giant axons. *The Journal of general physiology* 58:413-437.

Armstrong CM (1974) Ionic pores, gates, and gating currents. *Quarterly reviews of biophysics* 7:179-210.

Armstrong CM (1981) Sodium channels and gating currents. *Physiol Rev* 61:644-683.

Armstrong CM (2006) Na channel inactivation from open and closed states. *Proc Natl Acad Sci USA* 103:17991-17996.

Armstrong CM, Binstock L (1965) Anomalous Rectification in the Squid Giant Axon Injected with Tetraethylammonium Chloride. *The Journal of general physiology* 48:859-872.

Armstrong CM, Bezanilla F (1973) Currents related to movement of the gating particles of the sodium channels. *Nature* 242:459-461.

Armstrong CM, Bezanilla F (1974) Charge movement associated with the opening and closing of the activation gates of the Na channels. *The Journal of general physiology* 63:533-552.

Armstrong CM, Bezanilla F (1977) Inactivation of the sodium channel. II. Gating current experiments. *J Gen Physiol* 70:567-590.

Armstrong CM, Bezanilla F, Rojas E (1973) Destruction of sodium conductance inactivation in squid axons perfused with pronase. *J Gen Physiol* 62:375-391.

Arner S, Lindblom U, Meyerson BA, Molander C (1990) Prolonged relief of neuralgia after regional anesthetic blocks. A call for further experimental and systematic clinical studies. *Pain* 43:287-297.

Asamoah OK, Wuskell JP, Loew LM, Bezanilla F (2003) A fluorometric approach to local electric field measurements in a voltage-gated ion channel. *Neuron* 37:85-97.

Aydar E, Palmer C (2006) Expression and functional characterization of the human ether-a-go-go-related gene (HERG) K⁺ channel cardiac splice variant in *Xenopus laevis* oocytes. *The Journal of membrane biology* 211:115-126.

Baer M, Best PM, Reuter H (1976) Voltage-dependent action of tetrodotoxin in mammalian cardiac muscle. *Nature* 263:344-345.

Baker M, Bostock H, Grafe P, Martius P (1987) Function and distribution of three types of rectifying channel in rat spinal root myelinated axons. *The Journal of physiology* 383:45-67.

Bali M, Jansen M, Akabas MH (2009) GABA-induced intersubunit conformational movement in the GABA_A receptor alpha 1M1-beta 2M3 transmembrane subunit interface: experimental basis for homology modeling of an intravenous anesthetic binding site. *J Neurosci* 29:3083-3092.

Bassi MT, Balottin U, Panzeri C, Piccinelli P, Castaldo P, Barrese V, Soldovieri MV, Miceli F, Colombo M, Bresolin N, Borgatti R, Tagliatela M (2005) Functional analysis of novel KCNQ2 and KCNQ3 gene variants found in a large pedigree with benign familial neonatal convulsions (BFNC). *Neurogenetics* 6:185-193.

Bean BP (1981) Sodium channel inactivation in the crayfish giant axon. Must channels open before inactivating? *BiophysJ* 35:595-614.

Beckh S, Noda M, Lubbert H, Numa S (1989) Differential regulation of three sodium channel messenger RNAs in the rat central nervous system during development. *The EMBO journal* 8:3611-3616.

Bell DC, Turbendian HK, Valley MT, Zhou L, Riley JH, Siegelbaum SA, Tibbs GR (2008) Probing S4 and S5 segment proximity in mammalian hyperpolarization-

activated HCN channels by disulfide bridging and Cd(2+) coordination. *Pflugers Arch.*

Bendahhou S, Cummins TR, Kula RW, Fu YH, Ptacek LJ (2002) Impairment of slow inactivation as a common mechanism for periodic paralysis in DIIS4-S5. *Neurology* 58:1266-1272.

Beneski DA, Catterall WA (1980) Covalent labeling of protein components of the sodium channel with a photoactivable derivative of scorpion toxin. *Proceedings of the National Academy of Sciences of the United States of America* 77:639-643.

Benz I, Beck W, Kraas W, Stoll D, Jung G, Kohlhardt M (1997) Two types of modified cardiac Na⁺ channels after cytosolic interventions at the alpha-subunit capable of removing Na⁺ inactivation. *Eur Biophys J* 25:189-200.

Berkovic SF, Heron SE, Giordano L, Marini C, Guerrini R, Kaplan RE, Gambardella A, Steinlein OK, Grinton BE, Dean JT, Bordo L, Hodgson BL, Yamamoto T, Mulley JC, Zara F, Scheffer IE (2004) Benign familial neonatal-infantile seizures: characterization of a new sodium channelopathy. *AnnNeurol* 55:550-557.

Bezanilla F (2000) The voltage sensor in voltage-dependent ion channels. *Physiol Rev* 80:555-592.

Bezanilla F, Armstrong CM (1974) Gating currents of the sodium channels: three ways to block them. *Science* 183:753-754.

Bezanilla F, Armstrong CM (1977) Inactivation of the sodium channel. I. Sodium current experiments. *JGenPhysiol* 70:549-566.

Black JA, Liu S, Tanaka M, Cummins TR, Waxman SG (2004) Changes in the expression of tetrodotoxin-sensitive sodium channels within dorsal root ganglia neurons in inflammatory pain. *Pain* 108:237-247.

Black JA, Dib-Hajj S, McNabola K, Jeste S, Rizzo MA, Kocsis JD, Waxman SG (1996) Spinal sensory neurons express multiple sodium channel alpha-subunit mRNAs. *Brain research* 43:117-131.

Black JA, Cummins TR, Plumpton C, Chen YH, Hormuzdiar W, Clare JJ, Waxman SG (1999) Upregulation of a silent sodium channel after peripheral, but not central, nerve injury in DRG neurons. *Journal of neurophysiology* 82:2776-2785.

Blair NT, Bean BP (2002) Roles of tetrodotoxin (TTX)-sensitive Na⁺ current, TTX-resistant Na⁺ current, and Ca²⁺ current in the action potentials of nociceptive sensory neurons. *J Neurosci* 22:10277-10290.

Blaustein RO, Cole PA, Williams C, Miller C (2000) Tethered blockers as molecular 'tape measures' for a voltage-gated K⁺ channel. *Nat Struct Biol* 7:309-311.

Blunck R, Chanda B, Bezanilla F (2005) Nano to micro -- fluorescence measurements of electric fields in molecules and genetically specified neurons. *The Journal of membrane biology* 208:91-102.

Boucher TJ, Okuse K, Bennett DL, Munson JB, Wood JN, McMahon SB (2000) Potent analgesic effects of GDNF in neuropathic pain states. *Science* 290:124-127.

Bouhours M, Luce S, Sternberg D, Willer JC, Fontaine B, Tabti N (2005) A1152D mutation of the Na⁺ channel causes paramyotonia congenita and emphasizes the role of DIII/S4-S5 linker in fast inactivation. *JPhysiol* 565:415-427.

Bouhours M, Sternberg D, Davoine CS, Ferrer X, Willer JC, Fontaine B, Tabti N (2004) Functional characterization and cold sensitivity of T1313A, a new mutation of the skeletal muscle sodium channel causing paramyotonia congenita in humans. *The Journal of physiology* 554:635-647.

Butterworth JFt, Strichartz GR (1990) Molecular mechanisms of local anesthesia: a review. *Anesthesiology* 72:711-734.

Caffrey JM, Eng DL, Black JA, Waxman SG, Kocsis JD (1992) Three types of sodium channels in adult rat dorsal root ganglion neurons. *Brain Res* 592:283-297.

Campbell JN, Meyer RA (2006) Mechanisms of neuropathic pain. *Neuron* 52:77-92.

Cannon SC (2000) Spectrum of sodium channel disturbances in the nondystrophic myotonias and periodic paralyses. *Kidney Int* 57:772-779.

Cannon SC (2006) Pathomechanisms in channelopathies of skeletal muscle and brain. *Annual review of neuroscience* 29:387-415.

Casini S, Tan HL, Bhuiyan ZA, Bezzina CR, Barnett P, Cerbai E, Mugelli A, Wilde AA, Veldkamp MW (2007) Characterization of a novel SCN5A mutation associated with Brugada syndrome reveals involvement of DIIS4-S5 linker in slow inactivation. *CardiovascRes* 76:418-429.

Catterall WA (2000) From ionic currents to molecular mechanisms: the structure and function of voltage-gated sodium channels. *Neuron* 26:13-25.

Catterall WA, Goldin AL, Waxman SG (2005) International Union of Pharmacology. XLVII. Nomenclature and structure-function relationships of voltage-gated sodium channels. *PharmacolRev* 57:397-409.

Catterall WA, Dib-Hajj S, Meisler MH, Pietrobon D (2008) Inherited neuronal ion channelopathies: new windows on complex neurological diseases. *J Neurosci* 28:11768-11777.

Cha A, Bezanilla F (1998) Structural implications of fluorescence quenching in the Shaker K⁺ channel. *The Journal of general physiology* 112:391-408.

Cha A, Ruben PC, George AL, Jr., Fujimoto E, Bezanilla F (1999) Voltage sensors in domains III and IV, but not I and II, are immobilized by Na⁺ channel fast inactivation. *Neuron* 22:73-87.

Chahine M, Deschenes I, Trottier E, Chen LQ, Kallen RG (1997) Restoration of fast inactivation in an inactivation-defective human heart sodium channel by the cysteine modifying reagent benzyl-MTS: analysis of IFM-ICM mutation. *BiochemBiophysResCommun* 233:606-610.

Chahine M, Sirois J, Marcotte P, Chen L, Kallen RG (1998) Extrapore residues of the S5-S6 loop of domain 2 of the voltage-gated skeletal muscle sodium channel (rSkM1) contribute to the mu-conotoxin GIIIA binding site. *Biophysical journal* 75:236-246.

Chahine M, George AL, Jr., Zhou M, Ji S, Sun W, Barchi RL, Horn R (1994) Sodium channel mutations in paramyotonia congenita uncouple inactivation from activation. *Neuron* 12:281-294.

Chalfie M, Tu Y, Euskirchen G, Ward WW, Prasher DC (1994) Green fluorescent protein as a marker for gene expression. *Science* 263:802-805.

Chanda B, Bezanilla F (2002) Tracking voltage-dependent conformational changes in skeletal muscle sodium channel during activation. *The Journal of general physiology* 120:629-645.

Chanda B, Asamoah OK, Bezanilla F (2004) Coupling interactions between voltage sensors of the sodium channel as revealed by site-specific measurements. *The Journal of general physiology* 123:217-230.

Chatelier A, Dahllund L, Eriksson A, Krupp J, Chahine M (2008) Biophysical properties of human nav1.7 splice variants and their regulation by protein kinase a. *JNeurophysiol* 99:2241-2250.

Chen J, Mitcheson JS, Tristani-Firouzi M, Lin M, Sanguinetti MC (2001) The S4-S5 linker couples voltage sensing and activation of pacemaker channels. *Proceedings of the National Academy of Sciences of the United States of America* 98:11277-11282.

Chen LQ, Santarelli V, Horn R, Kallen RG (1996) A unique role for the S4 segment of domain 4 in the inactivation of sodium channels. *The Journal of general physiology* 108:549-556.

Chen Y, Yu FH, Sharp EM, Beacham D, Scheuer T, Catterall WA (2008) Functional properties and differential neuromodulation of Na(v)1.6 channels. *Molecular and cellular neurosciences* 38:607-615.

Chen YH, Dale TJ, Romanos MA, Whitaker WR, Xie XM, Clare JJ (2000) Cloning, distribution and functional analysis of the type III sodium channel from human brain. *EurJNeurosci* 12:4281-4289.

Cheng X, Dib-Hajj SD, Tyrrell L, Waxman SG (2008) Mutation I136V alters electrophysiological properties of the Na(v)1.7 channel in a family with onset of erythromelalgia in the second decade. *Molecular pain* 4:1.

Chi XX, Nicol GD (2007) Manipulation of the potassium channel Kv1.1 and its effect on neuronal excitability in rat sensory neurons. *Journal of neurophysiology* 98:2683-2692.

Choi JS, Zhang L, Dib-Hajj SD, Han C, Tyrrell L, Lin Z, Wang X, Yang Y, Waxman SG (2009) Mexiletine-responsive erythromelalgia due to a new Na(v)1.7 mutation showing use-dependent current fall-off. *Experimental neurology* 216:383-389.

Clark JD, Tempel BL (1998) Hyperalgesia in mice lacking the Kv1.1 potassium channel gene. *Neurosci Lett* 251:121-124.

Coetzee WA, Amarillo Y, Chiu J, Chow A, Lau D, McCormack T, Moreno H, Nadal MS, Ozaita A, Pountney D, Saganich M, Vega-Saenz de Miera E, Rudy B (1999) Molecular diversity of K⁺ channels. *Annals of the New York Academy of Sciences* 868:233-285.

Cole KS (1949a) Some physical aspects of bioelectric phenomena. *Proceedings of the National Academy of Sciences of the United States of America* 35:558-566.

Cole KS (1949b) Dynamic electrical characteristics of the squid axon membrane. *Arch Sci Physiol* 3:253-258.

Copley RR (2004) Evolutionary convergence of alternative splicing in ion channels. *Trends Genet* 20:171-176.

Costigan M, Scholz J, Woolf CJ (2009) Neuropathic pain: a maladaptive response of the nervous system to damage. *Annual review of neuroscience* 32:1-32.

Courtemanche M, Ramirez RJ, Nattel S (1998) Ionic mechanisms underlying human atrial action potential properties: insights from a mathematical model. *The American journal of physiology* 275:H301-321.

Cox JJ, Reimann F, Nicholas AK, Thornton G, Roberts E, Springell K, Karbani G, Jafri H, Mannan J, Raashid Y, Al-Gazali L, Hamamy H, Valente EM, Gorman S, Williams R, McHale DP, Wood JN, Gribble FM, Woods CG (2006) An SCN9A channelopathy causes congenital inability to experience pain. *Nature* 444:894-898.

Craner MJ, Klein JP, Renganathan M, Black JA, Waxman SG (2002) Changes of sodium channel expression in experimental painful diabetic neuropathy. *Annals of neurology* 52:786-792.

Crill WE (1996) Persistent sodium current in mammalian central neurons. *AnnuRevPhysiol* 58:349-362.

Cummins TR, Sigworth FJ (1996) Impaired slow inactivation in mutant sodium channels. *BiophysJ* 71:227-236.

Cummins TR, Waxman SG (1997) Downregulation of tetrodotoxin-resistant sodium currents and upregulation of a rapidly repriming tetrodotoxin-sensitive sodium current in small spinal sensory neurons after nerve injury. *J Neurosci* 17:3503-3514.

Cummins TR, Howe JR, Waxman SG (1998) Slow closed-state inactivation: a novel mechanism underlying ramp currents in cells expressing the hNE/PN1 sodium channel. *JNeurosci* 18:9607-9619.

Cummins TR, Aglieco F, Dib-Hajj SD (2002) Critical molecular determinants of voltage-gated sodium channel sensitivity to mu-conotoxins GIIIA/B. *Molecular pharmacology* 61:1192-1201.

Cummins TR, Dib-Hajj SD, Waxman SG (2004) Electrophysiological properties of mutant Nav1.7 sodium channels in a painful inherited neuropathy. *JNeurosci* 24:8232-8236.

Cummins TR, Sheets PL, Waxman SG (2007) The roles of sodium channels in nociception: Implications for mechanisms of pain. *Pain* 131:243-257.

Cummins TR, Dib-Hajj SD, Herzog RI, Waxman SG (2005) Nav1.6 channels generate resurgent sodium currents in spinal sensory neurons. *FEBS Lett* 579:2166-2170.

Cummins TR, Dib-Hajj SD, Black JA, Akopian AN, Wood JN, Waxman SG (1999) A novel persistent tetrodotoxin-resistant sodium current in SNS-null and wild-type small primary sensory neurons. *J Neurosci* 19:RC43.

Davis MD, Sandroni P (2002) Lidocaine patch for pain of erythromelalgia. *Archives of dermatology* 138:17-19.

DeCaen PG, Yarov-Yarovoy V, Zhao Y, Scheuer T, Catterall WA (2008) Disulfide locking a sodium channel voltage sensor reveals ion pair formation during activation. *Proceedings of the National Academy of Sciences of the United States of America* 105:15142-15147.

Deschenes I, Trottier E, Chahine M (1999) Cysteine scanning analysis of the IFM cluster in the inactivation gate of a human heart sodium channel. *Cardiovascular research* 42:521-529.

Devor M (2006) Sodium channels and mechanisms of neuropathic pain. *J Pain* 7:S3-S12.

Dib-Hajj SD, Tyrrell L, Black JA, Waxman SG (1998) Na_vN, a novel voltage-gated Na channel, is expressed preferentially in peripheral sensory neurons and down-regulated after axotomy. *Proceedings of the National Academy of Sciences of the United States of America* 95:8963-8968.

Dib-Hajj SD, Cummins TR, Black JA, Waxman SG (2007) From genes to pain: Na_v1.7 and human pain disorders. *Trends Neurosci* 30:555-563.

Dib-Hajj SD, Choi JS, Macala LJ, Tyrrell L, Black JA, Cummins TR, Waxman SG (2009) Transfection of rat or mouse neurons by biolistics or electroporation. *Nature protocols* 4:1118-1126.

Dib-Hajj SD, Fjell J, Cummins TR, Zheng Z, Fried K, LaMotte R, Black JA, Waxman SG (1999) Plasticity of sodium channel expression in DRG neurons in the chronic constriction injury model of neuropathic pain. *Pain* 83:591-600.

Dib-Hajj SD, Rush AM, Cummins TR, Hisama FM, Novella S, Tyrrell L, Marshall L, Waxman SG (2005) Gain-of-function mutation in Nav1.7 in familial erythromelalgia induces bursting of sensory neurons. *Brain* 128:1847-1854.

Dib-Hajj SD, Estacion M, Jarecki BW, Tyrrell L, Fischer TZ, Lawden M, Cummins TR, Waxman SG (2008) Paroxysmal extreme pain disorder M1627K mutation in human Nav1.7 renders DRG neurons hyperexcitable. *MolPain* 4:37.

Dietrich PS, McGivern JG, Delgado SG, Koch BD, Eglén RM, Hunter JC, Sangameswaran L (1998) Functional analysis of a voltage-gated sodium channel and its splice variant from rat dorsal root ganglia. *JNeurochem* 70:2262-2272.

Djoughri L, Newton R, Levinson SR, Berry CM, Carruthers B, Lawson SN (2003) Sensory and electrophysiological properties of guinea-pig sensory neurones expressing Nav 1.7 (PN1) Na⁺ channel alpha subunit protein. *The Journal of physiology* 546:565-576.

Do MT, Bean BP (2004) Sodium currents in subthalamic nucleus neurons from Nav1.6-null mice. *Journal of neurophysiology* 92:726-733.

Doyle DA, Morais CJ, Pfuetschner RA, Kuo A, Gulbis JM, Cohen SL, Chait BT, Mackinnon R (1998) The structure of the potassium channel: molecular basis of K⁺ conduction and selectivity. *Science* 280:69-77.

Drenth JP, Michiels JJ (1992) Clinical characteristics and pathophysiology of erythromelalgia and erythermalgia. *AmJMed* 93:111-114.

Drenth JP, te Morsche RH, Guillet G, Taieb A, Kirby RL, Jansen JB (2005) SCN9A mutations define primary erythermalgia as a neuropathic disorder of voltage gated sodium channels. *JInvest Dermatol* 124:1333-1338.

Drenth JP, Finley WH, Breedveld GJ, Testers L, Michiels JJ, Guillet G, Taieb A, Kirby RL, Heutink P (2001) The primary erythermalgia-susceptibility gene is located on chromosome 2q31-32. *AmJHumGenet* 68:1277-1282.

Durell SR, Guy HR (1992) Atomic scale structure and functional models of voltage-gated potassium channels. *Biophysical journal* 62:238-247; discussion 247-250.

Eaholtz G, Scheuer T, Catterall WA (1994) Restoration of inactivation and block of open sodium channels by an inactivation gate peptide. *Neuron* 12:1041-1048.

Eaholtz G, Zagotta WN, Catterall WA (1998) Kinetic analysis of block of open sodium channels by a peptide containing the isoleucine, phenylalanine, and methionine (IFM) motif from the inactivation gate. *The Journal of general physiology* 111:75-82.

Eaholtz G, Colvin A, Leonard D, Taylor C, Catterall WA (1999) Block of brain sodium channels by peptide mimetics of the isoleucine, phenylalanine, and methionine (IFM) motif from the inactivation gate. *The Journal of general physiology* 113:279-294.

Eaton DC, Brodwick MS, Oxford GS, Rudy B (1978) Arginine-specific reagents remove sodium channel inactivation. *Nature* 271:473-476.

Elliott AA, Elliott JR (1993) Characterization of TTX-sensitive and TTX-resistant sodium currents in small cells from adult rat dorsal root ganglia. *The Journal of physiology* 463:39-56.

Estacion M, Dib-Hajj SD, Benke PJ, Te Morsche RH, Eastman EM, Macala LJ, Drenth JP, Waxman SG (2008) NaV1.7 gain-of-function mutations as a continuum: A1632E displays physiological changes associated with erythromelalgia and paroxysmal extreme pain disorder mutations and produces symptoms of both disorders. *J Neurosci* 28:11079-11088.

Featherstone DE, Richmond JE, Ruben PC (1996) Interaction between fast and slow inactivation in Skm1 sodium channels. *BiophysJ* 71:3098-3109.

Featherstone DE, Fujimoto E, Ruben PC (1998) A defect in skeletal muscle sodium channel deactivation exacerbates hyperexcitability in human paramyotonia congenita. *JPhysiol* 506 (Pt 3):627-638.

Ferrante FM, Paggioli J, Cherukuri S, Arthur GR (1996) The analgesic response to intravenous lidocaine in the treatment of neuropathic pain. *Anesthesia and analgesia* 82:91-97.

Ferrer T, Rupp J, Piper DR, Tristani-Firouzi M (2006) The S4-S5 linker directly couples voltage sensor movement to the activation gate in the human ether-a'-go-go-related gene (hERG) K⁺ channel. *JBiolChem* 281:12858-12864.

Fertleman CR, Baker MD, Parker KA, Moffatt S, Elmslie FV, Abrahamsen B, Ostman J, Klugbauer N, Wood JN, Gardiner RM, Rees M (2006) SCN9A mutations in paroxysmal extreme pain disorder: allelic variants underlie distinct channel defects and phenotypes. *Neuron* 52:767-774.

Fertleman CR, Ferrie CD, Aicardi J, Bednarek NA, Eeg-Olofsson O, Elmslie FV, Griesemer DA, Goutieres F, Kirkpatrick M, Malmros IN, Pollitzer M, Rossiter M,

Roulet-Perez E, Schubert R, Smith VV, Testard H, Wong V, Stephenson JB (2007) Paroxysmal extreme pain disorder (previously familial rectal pain syndrome). *Neurology* 69:586-595.

Filatov GN, Nguyen TP, Kraner SD, Barchi RL (1998) Inactivation and secondary structure in the D4/S4-5 region of the SkM1 sodium channel. *JGenPhysiol* 111:703-715.

Fischer TZ, Gilmore ES, Estacion M, Eastman E, Taylor S, Melanson M, Dib-Hajj SD, Waxman SG (2009) A novel Nav1.7 mutation producing carbamazepine-responsive erythromelalgia. *Annals of neurology* 65:733-741.

Fjell J, Cummins TR, Dib-Hajj SD, Fried K, Black JA, Waxman SG (1999) Differential role of GDNF and NGF in the maintenance of two TTX-resistant sodium channels in adult DRG neurons. *Brain research* 67:267-282.

Foulkes T, Wood JN (2007) Mechanisms of cold pain. *Channels (Austin, Tex)* 1:154-160.

Fozzard HA, Hanck DA (1996) Structure and function of voltage-dependent sodium channels: comparison of brain II and cardiac isoforms. *Physiological reviews* 76:887-926.

Fozzard HA, Lee PJ, Lipkind GM (2005) Mechanism of local anesthetic drug action on voltage-gated sodium channels. *CurrPharmDes* 11:2671-2686.

Fraser SP et al. (2005) Voltage-gated sodium channel expression and potentiation of human breast cancer metastasis. *ClinCancer Res* 11:5381-5389.

Gellens ME, George AL, Jr., Chen LQ, Chahine M, Horn R, Barchi RL, Kallen RG (1992) Primary structure and functional expression of the human cardiac tetrodotoxin-insensitive voltage-dependent sodium channel. *Proceedings of the National Academy of Sciences of the United States of America* 89:554-558.

George AL, Jr. (2005) Inherited disorders of voltage-gated sodium channels. *JClinInvest* 115:1990-1999.

George AL, Jr., Komisarof J, Kallen RG, Barchi RL (1992) Primary structure of the adult human skeletal muscle voltage-dependent sodium channel. *Annals of neurology* 31:131-137.

Goldberg YP et al. (2007) Loss-of-function mutations in the Nav1.7 gene underlie congenital indifference to pain in multiple human populations. *Clinical genetics* 71:311-319.

Goldman L, Schauf CL (1972) Inactivation of the sodium current in *Myxicola* giant axons. Evidence for coupling to the activation process. *JGenPhysiol* 59:659-675.

Gorostiza P, Isacoff EY (2008) Nanoengineering ion channels for optical control. *Physiology (Bethesda)* 23:238-247.

Gould HJ, 3rd, Gould TN, England JD, Paul D, Liu ZP, Levinson SR (2000) A possible role for nerve growth factor in the augmentation of sodium channels in models of chronic pain. *Brain Res* 854:19-29.

Green NS, Reisler E, Houk KN (2001) Quantitative evaluation of the lengths of homobifunctional protein cross-linking reagents used as molecular rulers. *Protein Sci* 10:1293-1304.

Grieco TM, Raman IM (2004) Production of resurgent current in Nav1.6-null Purkinje neurons by slowing sodium channel inactivation with beta-pompilidotoxin. *JNeurosci* 24:35-42.

Grieco TM, Afshari FS, Raman IM (2002) A role for phosphorylation in the maintenance of resurgent sodium current in cerebellar purkinje neurons. *J Neurosci* 22:3100-3107.

Grieco TM, Malhotra JD, Chen C, Isom LL, Raman IM (2005) Open-channel block by the cytoplasmic tail of sodium channel beta4 as a mechanism for resurgent sodium current. *Neuron* 45:233-244.

Groome JR, Fujimoto E, George AL, Ruben PC (1999) Differential effects of homologous S4 mutations in human skeletal muscle sodium channels on deactivation gating from open and inactivated states. *The Journal of physiology* 516 (Pt 3):687-698.

Guy HR, Seetharamulu P (1986) Molecular model of the action potential sodium channel. *Proceedings of the National Academy of Sciences of the United States of America* 83:508-512.

Guy HR, Conti F (1990) Pursuing the structure and function of voltage-gated channels. *Trends Neurosci* 13:201-206.

Hamill OP, Marty A, Neher E, Sakmann B, Sigworth FJ (1981) Improved patch-clamp techniques for high-resolution current recording from cells and cell-free membrane patches. *Pflugers Arch* 391:85-100.

Hammarstrom AK, Gage PW (2002) Hypoxia and persistent sodium current. *Eur Biophys J* 31:323-330.

Han C, Lampert A, Rush AM, Dib-Hajj SD, Wang X, Yang Y, Waxman SG (2007) Temperature dependence of erythromelalgia mutation L858F in sodium channel Nav1.7. *Molecular pain* 3:3.

Han C, Dib-Hajj SD, Lin Z, Li Y, Eastman EM, Tyrrell L, Cao X, Yang Y, Waxman SG (2009) Early- and late-onset inherited erythromelalgia: genotype-phenotype correlation. *Brain*.

Han C, Rush AM, Dib-Hajj SD, Li S, Xu Z, Wang Y, Tyrrell L, Wang X, Yang Y, Waxman SG (2006) Sporadic onset of erythromelalgia: a gain-of-function mutation in Nav1.7. *Annals of neurology* 59:553-558.

Hartshorne RP, Catterall WA (1981) Purification of the saxitoxin receptor of the sodium channel from rat brain. *ProcNatlAcadSciUSA* 78:4620-4624.

Harty TP, Dib-Hajj SD, Tyrrell L, Blackman R, Hisama FM, Rose JB, Waxman SG (2006) Na(V)1.7 mutant A863P in erythromelalgia: effects of altered activation and steady-state inactivation on excitability of nociceptive dorsal root ganglion neurons. *J Neurosci* 26:12566-12575.

Haufe V, Camacho JA, Dumaine R, Gunther B, Bollensdorff C, von Banchet GS, Benndorf K, Zimmer T (2005) Expression pattern of neuronal and skeletal muscle voltage-gated Na⁺ channels in the developing mouse heart. *The Journal of physiology* 564:683-696.

Hayden R, Grossman M (1959) Rectal, ocular, and submaxillary pain; a familial autonomic disorder related to proctalgia fugax: report of a family. *AMAJDisChild* 97:479-482.

Heatwole CR, Moxley RT, 3rd (2007) The nondystrophic myotonias. *Neurotherapeutics* 4:238-251.

Heron SE, Crossland KM, Andermann E, Phillips HA, Hall AJ, Bleasel A, Shevell M, Mercho S, Seni MH, Guiot MC, Mulley JC, Berkovic SF, Scheffer IE (2002) Sodium-channel defects in benign familial neonatal-infantile seizures. *Lancet* 360:851-852.

Herzog RI, Cummins TR, Waxman SG (2001) Persistent TTX-resistant Na⁺ current affects resting potential and response to depolarization in simulated spinal sensory neurons. *Journal of neurophysiology* 86:1351-1364.

Herzog RI, Liu C, Waxman SG, Cummins TR (2003a) Calmodulin binds to the C terminus of sodium channels Nav1.4 and Nav1.6 and differentially modulates their functional properties. *J Neurosci* 23:8261-8270.

Herzog RI, Cummins TR, Ghassemi F, Dib-Hajj SD, Waxman SG (2003b) Distinct repriming and closed-state inactivation kinetics of Nav1.6 and Nav1.7 sodium channels in mouse spinal sensory neurons. *JPhysiol* 551:741-750.

Hilber K, Sandtner W, Kudlacek O, Schreiner B, Glaaser I, Schutz W, Fozzard HA, Dudley SC, Todt H (2002) Interaction between fast and ultra-slow inactivation in the voltage-gated sodium channel. Does the inactivation gate stabilize the channel structure? *The Journal of biological chemistry* 277:37105-37115.

Hille B (1968) Pharmacological modifications of the sodium channels of frog nerve. *The Journal of general physiology* 51:199-219.

Hille B (1977) Local anesthetics: hydrophilic and hydrophobic pathways for the drug-receptor reaction. *JGenPhysiol* 69:497-515.

Hille B (2001) *Ion channels of excitable membranes*. Sunderland, Mass: Sinauer.

Hines ML, Carnevale NT (1997) The NEURON simulation environment. *Neural Comput* 9:1179-1209.

Hirschberg B, Rovner A, Lieberman M, Patlak J (1995) Transfer of twelve charges is needed to open skeletal muscle Na⁺ channels. *The Journal of general physiology* 106:1053-1068.

Hodgkin AL (1937a) Evidence for electrical transmission in nerve: Part I. *The Journal of physiology* 90:183-210.

Hodgkin AL (1937b) Evidence for electrical transmission in nerve: Part II. *The Journal of physiology* 90:211-232.

Hodgkin AL, Katz B (1949) The effect of sodium ions on the electrical activity of the giant axon of the squid. *The Journal of physiology* 108:37-77.

Hodgkin AL, Huxley AF (1952) A quantitative description of membrane current and its application to conduction and excitation in nerve. 1952. *BullMathBiol* 52:25-71.

Hodgkin AL, Keynes RD (1955) The potassium permeability of a giant nerve fibre. *The Journal of physiology* 128:61-88.

Hodgkin AL, Huxley AF, Katz B (1952) Measurement of current-voltage relations in the membrane of the giant axon of Loligo. *The Journal of physiology* 116:424-448.

Holland KD, Kearney JA, Glauser TA, Buck G, Keddache M, Blankston JR, Glaaser IW, Kass RS, Meisler MH (2008) Mutation of sodium channel SCN3A in a patient with cryptogenic pediatric partial epilepsy. *Neurosci Lett* 433:65-70.

Hong S, Morrow TJ, Paulson PE, Isom LL, Wiley JW (2004) Early painful diabetic neuropathy is associated with differential changes in tetrodotoxin-sensitive and -resistant sodium channels in dorsal root ganglion neurons in the rat. *The Journal of biological chemistry* 279:29341-29350.

Horn R, Patlak J, Stevens CF (1981) Sodium channels need not open before they inactivate. *Nature* 291:426-427.

Horn R, Ding S, Gruber HJ (2000) Immobilizing the moving parts of voltage-gated ion channels. *The Journal of general physiology* 116:461-476.

Hoyt RC (1963) The Squid Giant Axon. *Mathematical Models. Biophysical journal* 3:399-431.

Hoyt RC (1968) Sodium inactivation in nerve fibers. *Biophysical journal* 8:1074-1097.

Hoyt RC (1971) Independence of the sodium and potassium conductance channels. A kinetic argument. *BiophysJ* 11:110-122.

Hu HJ, Carrasquillo Y, Karim F, Jung WE, Nerbonne JM, Schwarz TL, Gereau RWt (2006) The kv4.2 potassium channel subunit is required for pain plasticity. *Neuron* 50:89-100.

Isacoff EY, Jan YN, Jan LY (1991) Putative receptor for the cytoplasmic inactivation gate in the Shaker K⁺ channel. *Nature* 353:86-90.

Isom LL, Scheuer T, Brownstein AB, Ragsdale DS, Murphy BJ, Catterall WA (1995a) Functional co-expression of the beta 1 and type IIA alpha subunits of sodium channels in a mammalian cell line. *JBiolChem* 270:3306-3312.

Isom LL, Ragsdale DS, De Jongh KS, Westenbroek RE, Reber BF, Scheuer T, Catterall WA (1995b) Structure and function of the beta 2 subunit of brain sodium channels, a transmembrane glycoprotein with a CAM motif. *Cell* 83:433-442.

Isom LL, De Jongh KS, Patton DE, Reber BF, Offord J, Charbonneau H, Walsh K, Goldin AL, Catterall WA (1992) Primary structure and functional expression of the beta 1 subunit of the rat brain sodium channel. *Science* 256:839-842.

Jarecki BW, Sheets PL, Jackson li JO, Cummins TR (2008) Paroxysmal Extreme Pain Disorder mutations within the D3/S4-S5 Linker of Nav1.7 cause moderate destabilization of fast-inactivation. *JPhysiol*.

Jarecki BW, Piekarz AD, Jackson JO, 2nd, Cummins TR (2010) Human voltage-gated sodium channel mutations that cause inherited neuronal and muscle channelopathies increase resurgent sodium currents. *The Journal of clinical investigation* 120:369-378.

Jarecki BW, Sheets PL, Xiao Y, Jackson JO, 2nd, Cummins TR (2009) Alternative splicing of Na(V)1.7 exon 5 increases the impact of the painful PEPD mutant channel I1461T. *Channels (Austin, Tex)* 3:259-267.

Jiang Y, Lee A, Chen J, Cadene M, Chait BT, Mackinnon R (2002) Crystal structure and mechanism of a calcium-gated potassium channel. *Nature* 417:515-522.

Jiang Y, Lee A, Chen J, Ruta V, Cadene M, Chait BT, Mackinnon R (2003) X-ray structure of a voltage-dependent K⁺ channel. *Nature* 423:33-41.

Karlin A, Akabas MH (1998) Substituted-cysteine accessibility method. *Methods in enzymology* 293:123-145.

Kassmann M, Hansel A, Leipold E, Birkenbeil J, Lu SQ, Hoshi T, Heinemann SH (2008) Oxidation of multiple methionine residues impairs rapid sodium channel inactivation. *Pflugers Arch* 456:1085-1095.

Kastrup J, Petersen P, Dejgard A, Angelo HR, Hilsted J (1987) Intravenous lidocaine infusion--a new treatment of chronic painful diabetic neuropathy? *Pain* 28:69-75.

Kellenberger S, Scheuer T, Catterall WA (1996) Movement of the Na⁺ channel inactivation gate during inactivation. *JBiolChem* 271:30971-30979.

Kellenberger S, West JW, Scheuer T, Catterall WA (1997) Molecular analysis of the putative inactivation particle in the inactivation gate of brain type IIA Na⁺ channels. *JGenPhysiol* 109:589-605.

Keynes RD, Rojas E (1973) Characteristics of the sodium gating current in the squid giant axon. *The Journal of physiology* 233:28P-30P.

Keynes RD, Rojas E (1974) Kinetics and steady-state properties of the charged system controlling sodium conductance in the squid giant axon. *The Journal of physiology* 239:393-434.

Khaliq ZM, Gouwens NW, Raman IM (2003) The contribution of resurgent sodium current to high-frequency firing in Purkinje neurons: an experimental and modeling study. *J Neurosci* 23:4899-4912.

Kim CH, Oh Y, Chung JM, Chung K (2001) The changes in expression of three subtypes of TTX sensitive sodium channels in sensory neurons after spinal nerve ligation. *Brain research* 95:153-161.

Kim SH, Chung JM (1992) An experimental model for peripheral neuropathy produced by segmental spinal nerve ligation in the rat. *Pain* 50:355-363.

Klugbauer N, Lacinova L, Flockerzi V, Hofmann F (1995) Structure and functional expression of a new member of the tetrodotoxin-sensitive voltage-activated sodium channel family from human neuroendocrine cells. *EMBO J* 14:1084-1090.

Kohrman DC, Smith MR, Goldin AL, Harris J, Meisler MH (1996) A missense mutation in the sodium channel *Scn8a* is responsible for cerebellar ataxia in the mouse mutant jolting. *JNeurosci* 16:5993-5999.

Kontis KJ, Goldin AL (1997) Sodium channel inactivation is altered by substitution of voltage sensor positive charges. *The Journal of general physiology* 110:403-413.

Kontis KJ, Rounaghi A, Goldin AL (1997) Sodium channel activation gating is affected by substitutions of voltage sensor positive charges in all four domains. *The Journal of general physiology* 110:391-401.

Koopmann TT, Bezzina CR, Wilde AA (2006) Voltage-gated sodium channels: action players with many faces. *Annals of medicine* 38:472-482.

Kostyuk PG, Veselovsky NS, Tsyndrenko AY (1981) Ionic currents in the somatic membrane of rat dorsal root ganglion neurons-I. Sodium currents. *Neuroscience* 6:2423-2430.

Kuhnert SM, Phillips WJ, Davis MD (1999) Lidocaine and mexiletine therapy for erythromelalgia. *Archives of dermatology* 135:1447-1449.

Kuo CC, Bean BP (1994) Na⁺ channels must deactivate to recover from inactivation. *Neuron* 12:819-829.

Labro AJ, Raes AL, Grottesi A, Van HD, Sansom MS, Snyders DJ (2008) Kv channel gating requires a compatible S4-S5 linker and bottom part of S6, constrained by non-interacting residues. *JGenPhysiol* 132:667-680.

Laine M, Lin MC, Bannister JP, Silverman WR, Mock AF, Roux B, Papazian DM (2003) Atomic proximity between S4 segment and pore domain in Shaker potassium channels. *Neuron* 39:467-481.

Lampert A, O'Reilly AO, Dib-Hajj SD, Tyrrell L, Wallace BA, Waxman SG (2008) A pore-blocking hydrophobic motif at the cytoplasmic aperture of the closed-state Nav1.7 channel is disrupted by the erythromelalgia-associated F1449V mutation. *The Journal of biological chemistry* 283:24118-24127.

Larsson HP, Baker OS, Dhillon DS, Isacoff EY (1996) Transmembrane movement of the shaker K⁺ channel S4. *Neuron* 16:387-397.

Leffler A, Herzog RI, Dib-Hajj SD, Waxman SG, Cummins TR (2005) Pharmacological properties of neuronal TTX-resistant sodium channels and the role of a critical serine pore residue. *Pflugers Arch* 451:454-463.

Leffler A, Cummins TR, Dib-Hajj SD, Hormuzdiar WN, Black JA, Waxman SG (2002) GDNF and NGF reverse changes in repriming of TTX-sensitive Na⁽⁺⁾ currents following axotomy of dorsal root ganglion neurons. *Journal of neurophysiology* 88:650-658.

Legroux-Crespel E, Sassolas B, Guillet G, Kupfer I, Dupre D, Misery L (2003) [Treatment of familial erythromelalgia with the association of lidocaine and mexiletine]. *Annales de dermatologie et de venerologie* 130:429-433.

Lerche H, Peter W, Fleischhauer R, Pika-Hartlaub U, Malina T, Mitrovic N, Lehmann-Horn F (1997) Role in fast inactivation of the IV/S4-S5 loop of the human muscle Na⁺ channel probed by cysteine mutagenesis. *JPhysiol* 505 (Pt 2):345-352.

Levinson SR, Ellory JC (1973) Molecular size of the tetrodotoxin binding site estimated by irradiation inactivation. *Nature: New biology* 245:122-123.

Liao P, Yu D, Li G, Yong TF, Soon JL, Chua YL, Soong TW (2007) A smooth muscle Cav1.2 calcium channel splice variant underlies hyperpolarized window

current and enhanced state-dependent inhibition by nifedipine. *The Journal of biological chemistry* 282:35133-35142.

Liao P, Yu D, Lu S, Tang Z, Liang MC, Zeng S, Lin W, Soong TW (2004) Smooth muscle-selective alternatively spliced exon generates functional variation in Cav1.2 calcium channels. *The Journal of biological chemistry* 279:50329-50335.

Lipkind GM, Fozzard HA (2000) KcsA crystal structure as framework for a molecular model of the Na(+) channel pore. *Biochemistry* 39:8161-8170.

Liu H, Wu MM, Zakon HH (2008) A novel Na⁺ channel splice form contributes to the regulation of an androgen-dependent social signal. *J Neurosci* 28:9173-9182.

Long SB, Campbell EB, Mackinnon R (2005a) Voltage sensor of Kv1.2: structural basis of electromechanical coupling. *Science* 309:903-908.

Long SB, Campbell EB, Mackinnon R (2005b) Crystal structure of a mammalian voltage-dependent Shaker family K⁺ channel. *Science* 309:897-903.

Long SB, Tao X, Campbell EB, Mackinnon R (2007) Atomic structure of a voltage-dependent K⁺ channel in a lipid membrane-like environment. *Nature* 450:376-382.

Loo TW, Clarke DM (2001) Determining the dimensions of the drug-binding domain of human P-glycoprotein using thiol cross-linking compounds as molecular rulers. *The Journal of biological chemistry* 276:36877-36880.

Lossin C (2009) A catalog of SCN1A variants. *Brain & development* 31:114-130.

Lossin C, Wang DW, Rhodes TH, Vanoye CG, George AL, Jr. (2002) Molecular basis of an inherited epilepsy. *Neuron* 34:877-884.

Lossin C, Rhodes TH, Desai RR, Vanoye CG, Wang D, Carniciu S, Devinsky O, George AL, Jr. (2003) Epilepsy-associated dysfunction in the voltage-gated neuronal sodium channel SCN1A. *J Neurosci* 23:11289-11295.

Lu Z, Klem AM, Ramu Y (2001) Ion conduction pore is conserved among potassium channels. *Nature* 413:809-813.

Lu Z, Klem AM, Ramu Y (2002) Coupling between voltage sensors and activation gate in voltage-gated K⁺ channels. *JGenPhysiol* 120:663-676.

Luo CH, Rudy Y (1994) A dynamic model of the cardiac ventricular action potential. I. Simulations of ionic currents and concentration changes. *Circ Res* 74:1071-1096.

Ma JY, Catterall WA, Scheuer T (1997) Persistent sodium currents through brain sodium channels induced by G protein betagamma subunits. *Neuron* 19:443-452.

Marban E, Yamagishi T, Tomaselli GF (1998) Structure and function of voltage-gated sodium channels. *JPhysiol* 508 (Pt 3):647-657.

Marmont G (1949) Studies on the axon membrane; a new method. *Journal of cellular physiology* 34:351-382.

Matzner O, Devor M (1994) Hyperexcitability at sites of nerve injury depends on voltage-sensitive Na⁺ channels. *Journal of neurophysiology* 72:349-359.

McPhee JC, Ragsdale DS, Scheuer T, Catterall WA (1994) A mutation in segment IVS6 disrupts fast inactivation of sodium channels. *ProcNatlAcadSciUSA* 91:12346-12350.

McPhee JC, Ragsdale DS, Scheuer T, Catterall WA (1995) A critical role for transmembrane segment IVS6 of the sodium channel alpha subunit in fast inactivation. *JBiolChem* 270:12025-12034.

McPhee JC, Ragsdale DS, Scheuer T, Catterall WA (1998) A critical role for the S4-S5 intracellular loop in domain IV of the sodium channel alpha-subunit in fast inactivation. *JBiolChem* 273:1121-1129.

Meadows LS, Chen YH, Powell AJ, Clare JJ, Ragsdale DS (2002) Functional modulation of human brain Nav1.3 sodium channels, expressed in mammalian cells, by auxiliary beta 1, beta 2 and beta 3 subunits. *Neuroscience* 114:745-753.

Meisler MH, Kearney JA (2005) Sodium channel mutations in epilepsy and other neurological disorders. *JClinInvest* 115:2010-2017.

Meves H (1974) The effect of holding potential on the asymmetry currents in squid giant axons. *The Journal of physiology* 243:847-867.

Mikami M, Yang J (2005) Short hairpin RNA-mediated selective knockdown of NaV1.8 tetrodotoxin-resistant voltage-gated sodium channel in dorsal root ganglion neurons. *Anesthesiology* 103:828-836.

Morin TJ, Kobertz WR (2008) Tethering chemistry and K⁺ channels. *The Journal of biological chemistry* 283:25105-25109.

Muroi Y, Arcisio-Miranda M, Chowdhury S, Chanda B (2010) Molecular determinants of coupling between the domain III voltage sensor and pore of a sodium channel. *Nat Struct Biol*.

Nakamura Y, Nakajima S, Grundfest H (1965) The action of tetrodotoxin on electrogenic components of squid giant axons. *The Journal of general physiology* 48:975-996.

Narahashi T, Moore JW, Scott WR (1964) Tetrodotoxin Blockage of Sodium Conductance Increase in Lobster Giant Axons. *The Journal of general physiology* 47:965-974.

Narahashi T, Haas HG, Therrien EF (1967) Saxitoxin and tetrodotoxin: comparison of nerve blocking mechanism. *Science* 157:1441-1442.

Nassar MA, Levato A, Stirling LC, Wood JN (2005) Neuropathic pain develops normally in mice lacking both Na(v)1.7 and Na(v)1.8. *Molecular pain* 1:24.

Nassar MA, Stirling LC, Forlani G, Baker MD, Matthews EA, Dickenson AH, Wood JN (2004) Nociceptor-specific gene deletion reveals a major role for Nav1.7 (PN1) in acute and inflammatory pain. *Proceedings of the National Academy of Sciences of the United States of America* 101:12706-12711.

Nathan A, Rose JB, Guite JW, Hehir D, Milovcich K (2005) Primary erythromelalgia in a child responding to intravenous lidocaine and oral mexiletine treatment. *Pediatrics* 115:e504-507.

Noda M, Shimizu S, Tanabe T, Takai T, Kayano T, Ikeda T, Takahashi H, Nakayama H, Kanaoka Y, Minamino N, et al. (1984) Primary structure of

Electrophorus electricus sodium channel deduced from cDNA sequence. *Nature* 312:121-127.

Nonner W (1980) Relations between the inactivation of sodium channels and the immobilization of gating charge in frog myelinated nerve. *The Journal of physiology* 299:573-603.

Novella SP, Hisama FM, Dib-Hajj SD, Waxman SG (2007) A case of inherited erythromelalgia. *NatClinPractNeurol* 3:229-234.

Numann R, Catterall WA, Scheuer T (1991) Functional modulation of brain sodium channels by protein kinase C phosphorylation. *Science* 254:115-118.

Nuss HB, Balsler JR, Orias DW, Lawrence JH, Tomaselli GF, Marban E (1996) Coupling between fast and slow inactivation revealed by analysis of a point mutation (F1304Q) in mu 1 rat skeletal muscle sodium channels. *The Journal of physiology* 494 (Pt 2):411-429.

O'Reilly AO, Charalambous K, Nurani G, Powl AM, Wallace BA (2008) G219S mutagenesis as a means of stabilizing conformational flexibility in the bacterial sodium channel NaChBac. *Molecular membrane biology* 25:670-676.

Ogata N, Tatebayashi H (1993) Kinetic analysis of two types of Na⁺ channels in rat dorsal root ganglia. *The Journal of physiology* 466:9-37.

Okuse K, Malik-Hall M, Baker MD, Poon WY, Kong H, Chao MV, Wood JN (2002) Annexin II light chain regulates sensory neuron-specific sodium channel expression. *Nature* 417:653-656.

Onkal R, Mattis JH, Fraser SP, Diss JK, Shao D, Okuse K, Djamgoz MB (2008) Alternative splicing of Nav1.5: an electrophysiological comparison of 'neonatal' and 'adult' isoforms and critical involvement of a lysine residue. *Journal of cellular physiology* 216:716-726.

Orstavik K, Mork C, Kvernebo K, Jorum E (2004) Pain in primary erythromelalgia--a neuropathic component? *Pain* 110:531-538.

Oxford GS (1981) Some kinetic and steady-state properties of sodium channels after removal of inactivation. *JGenPhysiol* 77:1-22.

Oxford GS, Pooler JP (1975) Selective modification of sodium channel gating in lobster axons by 2, 4, 6-trinitrophenol: Evidence for two inactivation mechanisms. *JGenPhysiol* 66:765-779.

Oxford GS, Wu CH, Narahashi T (1978) Removal of sodium channel inactivation in squid giant axons by n-bromoacetamide. *The Journal of general physiology* 71:227-247.

Papazian DM, Timpe LC, Jan YN, Jan LY (1991) Alteration of voltage-dependence of Shaker potassium channel by mutations in the S4 sequence. *Nature* 349:305-310.

Patton DE, West JW, Catterall WA, Goldin AL (1992) Amino acid residues required for fast Na(+)-channel inactivation: charge neutralizations and deletions in the III-IV linker. *ProcNatlAcadSciUSA* 89:10905-10909.

Patton DE, West JW, Catterall WA, Goldin AL (1993) A peptide segment critical for sodium channel inactivation functions as an inactivation gate in a potassium channel. *Neuron* 11:967-974.

Popa MO, Alekov AK, Bail S, Lehmann-Horn F, Lerche H (2004) Cooperative effect of S4-S5 loops in domains D3 and D4 on fast inactivation of the Na⁺ channel. *JPhysiol* 561:39-51.

Prasher DC, Eckenrode VK, Ward WW, Prendergast FG, Cormier MJ (1992) Primary structure of the *Aequorea victoria* green-fluorescent protein. *Gene* 111:229-233.

Prole DL, Yellen G (2006) Reversal of HCN channel voltage dependence via bridging of the S4-S5 linker and Post-S6. *JGenPhysiol* 128:273-282.

Quandt FN (1987) Burst kinetics of sodium channels which lack fast inactivation in mouse neuroblastoma cells. *The Journal of physiology* 392:563-585.

Raman IM, Bean BP (1997) Resurgent sodium current and action potential formation in dissociated cerebellar Purkinje neurons. *JNeurosci* 17:4517-4526.

Raman IM, Bean BP (1999a) Properties of sodium currents and action potential firing in isolated cerebellar Purkinje neurons. *Annals of the New York Academy of Sciences* 868:93-96.

Raman IM, Bean BP (1999b) Ionic currents underlying spontaneous action potentials in isolated cerebellar Purkinje neurons. *J Neurosci* 19:1663-1674.

Raman IM, Bean BP (2001) Inactivation and recovery of sodium currents in cerebellar Purkinje neurons: evidence for two mechanisms. *Biophysical journal* 80:729-737.

Raman IM, Sprunger LK, Meisler MH, Bean BP (1997) Altered subthreshold sodium currents and disrupted firing patterns in Purkinje neurons of *Scn8a* mutant mice. *Neuron* 19:881-891.

Raymond CK, Castle J, Garrett-Engle P, Armour CD, Kan Z, Tsinoremas N, Johnson JM (2004) Expression of alternatively spliced sodium channel alpha-subunit genes. Unique splicing patterns are observed in dorsal root ganglia. *JBiolChem* 279:46234-46241.

Renganathan M, Cummins TR, Waxman SG (2001) Contribution of Na(v)1.8 sodium channels to action potential electrogenesis in DRG neurons. *Journal of neurophysiology* 86:629-640.

Renganathan M, Dib-Hajj S, Waxman SG (2002) Na(v)1.5 underlies the 'third TTX-R sodium current' in rat small DRG neurons. *Brain research* 106:70-82.

Richmond JE, VanDeCarr D, Featherstone DE, George AL, Jr., Ruben PC (1997) Defective fast inactivation recovery and deactivation account for sodium channel myotonia in the I1160V mutant. *BiophysJ* 73:1896-1903.

Ritchie JM, Rogart RB (1977) The binding of saxitoxin and tetrodotoxin to excitable tissue. *Reviews of physiology, biochemistry and pharmacology* 79:1-50.

Rizzo MA, Kocsis JD, Waxman SG (1994) Slow sodium conductances of dorsal root ganglion neurons: intraneuronal homogeneity and interneuronal heterogeneity. *Journal of neurophysiology* 72:2796-2815.

Rogart RB, Cribbs LL, Muglia LK, Kephart DD, Kaiser MW (1989) Molecular cloning of a putative tetrodotoxin-resistant rat heart Na⁺ channel isoform. *Proceedings of the National Academy of Sciences of the United States of America* 86:8170-8174.

Rogawski MA (1985) The A-current: How ubiquitous a feature of excitable cells is it? *Trends Neurosci* 8:214-219.

Rohl CA, Boeckman FA, Baker C, Scheuer T, Catterall WA, Klevit RE (1999) Solution structure of the sodium channel inactivation gate. *Biochemistry* 38:855-861.

Rojas E, Atwater I (1967) Blocking of potassium currents by pronase in perfused giant axons. *Nature* 215:850-852.

Rojas E, Armstrong C (1971) Sodium conductance activation without inactivation in pronase-perfused axons. *Nature: New biology* 229:177-178.

Rojas E, Rudy B (1976) Destruction of the sodium conductance inactivation by a specific protease in perfused nerve fibres from *Loligo*. *The Journal of physiology* 262:501-531.

Roy ML, Narahashi T (1992) Differential properties of tetrodotoxin-sensitive and tetrodotoxin-resistant sodium channels in rat dorsal root ganglion neurons. *J Neurosci* 12:2104-2111.

Ruben PC, Starkus JG, Rayner MD (1992) Steady-state availability of sodium channels. Interactions between activation and slow inactivation. *Biophysical journal* 61:941-955.

Rudy B (1978) Slow inactivation of the sodium conductance in squid giant axons. Pronase resistance. *The Journal of physiology* 283:1-21.

Rush AM, Dib-Hajj SD, Waxman SG (2005) Electrophysiological properties of two axonal sodium channels, Nav1.2 and Nav1.6, expressed in mouse spinal sensory neurones. *The Journal of physiology* 564:803-815.

Rush AM, Cummins TR, Waxman SG (2007) Multiple sodium channels and their roles in electrogenesis within dorsal root ganglion neurons. *JPhysiol* 579:1-14.

Rush AM, Brau ME, Elliott AA, Elliott JR (1998) Electrophysiological properties of sodium current subtypes in small cells from adult rat dorsal root ganglia. *The Journal of physiology* 511 (Pt 3):771-789.

Rush AM, Dib-Hajj SD, Liu S, Cummins TR, Black JA, Waxman SG (2006) A single sodium channel mutation produces hyper- or hypoexcitability in different types of neurons. *ProcNatlAcadSciUSA* 103:8245-8250.

Ruta V, Chen J, MacKinnon R (2005) Calibrated measurement of gating-charge arginine displacement in the KvAP voltage-dependent K⁺ channel. *Cell* 123:463-475.

Sakmann B, Neher E (1984) Patch clamp techniques for studying ionic channels in excitable membranes. *Annual review of physiology* 46:455-472.

Sangameswaran L, Fish LM, Koch BD, Rabert DK, Delgado SG, Ilnicka M, Jakeman LB, Novakovic S, Wong K, Sze P, Tzoumaka E, Stewart GR, Herman RC, Chan H, Eglon RM, Hunter JC (1997) A novel tetrodotoxin-sensitive, voltage-gated sodium channel expressed in rat and human dorsal root ganglia. *The Journal of biological chemistry* 272:14805-14809.

Sarao R, Gupta SK, Auld VJ, Dunn RJ (1991) Developmentally regulated alternative RNA splicing of rat brain sodium channel mRNAs. *Nucleic Acids Res* 19:5673-5679.

Scholz J, Woolf CJ (2002) Can we conquer pain? *Nature neuroscience* 5 Suppl:1062-1067.

Scholz J, Woolf CJ (2007) The neuropathic pain triad: neurons, immune cells and glia. *Nature neuroscience* 10:1361-1368.

Seoh SA, Sigg D, Papazian DM, Bezanilla F (1996) Voltage-sensing residues in the S2 and S4 segments of the Shaker K⁺ channel. *Neuron* 16:1159-1167.

Shcheglovitov A, Vitko I, Bidaud I, Baumgart JP, Navarro-Gonzalez MF, Grayson TH, Lory P, Hill CE, Perez-Reyes E (2008) Alternative splicing within the I-II loop controls surface expression of T-type Ca(v)3.1 calcium channels. *FEBS letters* 582:3765-3770.

Sheets MF, Hanck DA (2005) Charge immobilization of the voltage sensor in domain IV is independent of sodium current inactivation. *JPhysiol* 563:83-93.

Sheets PL, Jackson JO, Waxman SG, Dib-Hajj SD, Cummins TR (2007) A Nav1.7 channel mutation associated with hereditary erythromelalgia contributes to neuronal hyperexcitability and displays reduced lidocaine sensitivity. *JPhysiol* 581:1019-1031.

Shen Y, Yu D, Hiel H, Liao P, Yue DT, Fuchs PA, Soong TW (2006) Alternative splicing of the Ca(v)1.3 channel IQ domain, a molecular switch for Ca²⁺-dependent inactivation within auditory hair cells. *J Neurosci* 26:10690-10699.

Shrager PG, Strickholm A, Macey RI (1969) Chemical modification of crayfish axons by protein crosslinking aldehydes. *Journal of cellular physiology* 74:91-100.

Sigg D, Bezanilla F (2003) A physical model of potassium channel activation: from energy landscape to gating kinetics. *Biophysical journal* 84:3703-3716.

Sindrup SH, Jensen TS (1999) Efficacy of pharmacological treatments of neuropathic pain: an update and effect related to mechanism of drug action. *Pain* 83:389-400.

Singer SJ, Nicolson GL (1972) The fluid mosaic model of the structure of cell membranes. *Science* 175:720-731.

Smith MR, Goldin AL (1997) Interaction between the sodium channel inactivation linker and domain III S4-S5. *BiophysJ* 73:1885-1895.

Smith MR, Smith RD, Plummer NW, Meisler MH, Goldin AL (1998) Functional analysis of the mouse Scn8a sodium channel. *J Neurosci* 18:6093-6102.

Smith RD, Goldin AL (1998) Functional analysis of the rat I sodium channel in xenopus oocytes. *J Neurosci* 18:811-820.

Smits JP, Veldkamp MW, Bezzina CR, Bhuiyan ZA, Wedekind H, Schulze-Bahr E, Wilde AA (2005) Substitution of a conserved alanine in the domain III S4-S5 linker of the cardiac sodium channel causes long QT syndrome. *CardiovascRes* 67:459-466.

Soler-Llavina GJ, Chang TH, Swartz KJ (2006) Functional interactions at the interface between voltage-sensing and pore domains in the Shaker K(v) channel. *Neuron* 52:623-634.

Sorensen JB, Cha A, Latorre R, Rosenman E, Bezanilla F (2000) Deletion of the S3-S4 linker in the Shaker potassium channel reveals two quenching groups near the outside of S4. *The Journal of general physiology* 115:209-222.

Starace DM, Bezanilla F (2001) Histidine scanning mutagenesis of basic residues of the S4 segment of the shaker k⁺ channel. *The Journal of general physiology* 117:469-490.

Starace DM, Stefani E, Bezanilla F (1997) Voltage-dependent proton transport by the voltage sensor of the Shaker K⁺ channel. *Neuron* 19:1319-1327.

Starkus JG, Shrager P (1978) Modification of slow sodium inactivation in nerve after internal perfusion with trypsin. *The American journal of physiology* 235:C238-244.

Stewart T, Beyak MJ, Vanner S (2003) Iletis modulates potassium and sodium currents in guinea pig dorsal root ganglia sensory neurons. *The Journal of physiology* 552:797-807.

Strichartz GR (1973) The inhibition of sodium currents in myelinated nerve by quaternary derivatives of lidocaine. *The Journal of general physiology* 62:37-57.

Stuhmer W, Conti F, Suzuki H, Wang XD, Noda M, Yahagi N, Kubo H, Numa S (1989) Structural parts involved in activation and inactivation of the sodium channel. *Nature* 339:597-603.

Sugiura Y, Makita N, Li L, Noble PJ, Kimura J, Kumagai Y, Soeda T, Yamamoto T (2003) Cold induces shifts of voltage dependence in mutant SCN4A, causing hypokalemic periodic paralysis. *Neurology* 61:914-918.

Sunami A, Tracey A, Glaaser IW, Lipkind GM, Hanck DA, Fozzard HA (2004) Accessibility of mid-segment domain IV S6 residues of the voltage-gated Na⁺ channel to methanethiosulfonate reagents. *JPhysiol* 561:403-413.

Takenaka T, Yamagishi S (1969) Morphology and electrophysiological properties of squid giant axons perfused intracellularly with protease solution. *The Journal of general physiology* 53:81-96.

Tan J, Liu Z, Nomura Y, Goldin AL, Dong K (2002) Alternative splicing of an insect sodium channel gene generates pharmacologically distinct sodium channels. *JNeurosci* 22:5300-5309.

Tang L, Kallen RG, Horn R (1996) Role of an S4-S5 linker in sodium channel inactivation probed by mutagenesis and a peptide blocker. *The Journal of general physiology* 108:89-104.

Tang L, Chehab N, Wieland SJ, Kallen RG (1998) Glutamine substitution at alanine1649 in the S4-S5 cytoplasmic loop of domain 4 removes the voltage sensitivity of fast inactivation in the human heart sodium channel. *The Journal of general physiology* 111:639-652.

Tang ZZ, Liao P, Li G, Jiang FL, Yu D, Hong X, Yong TF, Tan G, Lu S, Wang J, Soong TW (2008) Differential splicing patterns of L-type calcium channel Cav1.2 subunit in hearts of Spontaneously Hypertensive Rats and Wistar Kyoto Rats. *Biochimica et biophysica acta* 1783:118-130.

Tasaki I, Hagiwar AS (1957) Demonstration of two stable potential states in the squid giant axon under tetraethylammonium chloride. *The Journal of general physiology* 40:859-885.

Tasaki I, Takenaka T (1964) Effects of Various Potassium Salts and Proteases Upon Excitability of Intracellularly Perfused Squid Giant Axons. *Proceedings of the National Academy of Sciences of the United States of America* 52:804-810.

Toledo-Aral JJ, Brehm P, Haleboua S, Mandel G (1995) A single pulse of nerve growth factor triggers long-term neuronal excitability through sodium channel gene induction. *Neuron* 14:607-611.

Toledo-Aral JJ, Moss BL, He ZJ, Koszowski AG, Whisenand T, Levinson SR, Wolf JJ, Silos-Santiago I, Haleboua S, Mandel G (1997) Identification of PN1, a predominant voltage-dependent sodium channel expressed principally in peripheral neurons. *Proceedings of the National Academy of Sciences of the United States of America* 94:1527-1532.

Tombola F, Pathak MM, Isacoff EY (2006) How does voltage open an ion channel? *AnnuRevCell DevBiol* 22:23-52.

Trimmer JS, Rhodes KJ (2004) Localization of voltage-gated ion channels in mammalian brain. *Annual review of physiology* 66:477-519.

Trimmer JS, Cooperman SS, Tomiko SA, Zhou JY, Crean SM, Boyle MB, Kallen RG, Sheng ZH, Barchi RL, Sigworth FJ, et al. (1989) Primary structure and functional expression of a mammalian skeletal muscle sodium channel. *Neuron* 3:33-49.

Ukomadu C, Zhou J, Sigworth FJ, Agnew WS (1992) μ l Na⁺ channels expressed transiently in human embryonic kidney cells: biochemical and biophysical properties. *Neuron* 8:663-676.

Ulbricht W (2005) Sodium channel inactivation: molecular determinants and modulation. *Physiological reviews* 85:1271-1301.

Vandenberg CA, Bezanilla F (1991) A sodium channel gating model based on single channel, macroscopic ionic, and gating currents in the squid giant axon. *BiophysJ* 60:1511-1533.

Vassilev P, Scheuer T, Catterall WA (1989) Inhibition of inactivation of single sodium channels by a site-directed antibody. *ProcNatlAcadSciUSA* 86:8147-8151.

Vassilev PM, Scheuer T, Catterall WA (1988) Identification of an intracellular peptide segment involved in sodium channel inactivation. *Science* 241:1658-1661.

Vedantham V, Cannon SC (1998) Slow inactivation does not affect movement of the fast inactivation gate in voltage-gated Na⁺ channels. *JGenPhysiol* 111:83-93.

Vedantham V, Cannon SC (1999) The position of the fast-inactivation gate during lidocaine block of voltage-gated Na⁺ channels. *JGenPhysiol* 113:7-16.

Vilin YY, Ruben PC (2001) Slow inactivation in voltage-gated sodium channels: molecular substrates and contributions to channelopathies. *Cell BiochemBiophys* 35:171-190.

Voet D, Voet JG (1990) *Biochemistry*. New York: Wiley.

Wang DW, Yazawa K, George AL, Jr., Bennett PB (1996) Characterization of human cardiac Na⁺ channel mutations in the congenital long QT syndrome. *ProcNatlAcadSciUSA* 93:13200-13205.

Wang DW, Desai RR, Crotti L, Arnestad M, Insolia R, Pedrazzini M, Ferrandi C, Vege A, Rognum T, Schwartz PJ, George AL, Jr. (2007) Cardiac sodium channel dysfunction in sudden infant death syndrome. *Circulation* 115:368-376.

Waxman SG, Kocsis JD, Black JA (1994) Type III sodium channel mRNA is expressed in embryonic but not adult spinal sensory neurons, and is reexpressed following axotomy. *Journal of neurophysiology* 72:466-470.

West JW, Patton DE, Scheuer T, Wang Y, Goldin AL, Catterall WA (1992) A cluster of hydrophobic amino acid residues required for fast Na⁽⁺⁾-channel inactivation. *ProcNatlAcadSciUSA* 89:10910-10914.

Wood JN, Boorman JP, Okuse K, Baker MD (2004) Voltage-gated sodium channels and pain pathways. *JNeurobiol* 61:55-71.

Woolf CJ, Salter MW (2000) Neuronal plasticity: increasing the gain in pain. *Science* 288:1765-1769.

Woolf CJ, Ma Q (2007) Nociceptors--noxious stimulus detectors. *Neuron* 55:353-364.

Xu T, Nie L, Zhang Y, Mo J, Feng W, Wei D, Petrov E, Calisto LE, Kachar B, Beisel KW, Vazquez AE, Yamoah EN (2007) Roles of alternative splicing in the functional properties of inner ear-specific KCNQ4 channels. *The Journal of biological chemistry* 282:23899-23909.

Yang N, Horn R (1995) Evidence for voltage-dependent S4 movement in sodium channels. *Neuron* 15:213-218.

Yang N, Ji S, Zhou M, Ptacek LJ, Barchi RL, Horn R, George AL, Jr. (1994) Sodium channel mutations in paramyotonia congenita exhibit similar biophysical phenotypes in vitro. *ProcNatlAcadSciUSA* 91:12785-12789.

Yang Y, Wang Y, Li S, Xu Z, Li H, Ma L, Fan J, Bu D, Liu B, Fan Z, Wu G, Jin J, Ding B, Zhu X, Shen Y (2004) Mutations in SCN9A, encoding a sodium channel alpha subunit, in patients with primary erythralgia. *Journal of medical genetics* 41:171-174.

Yellen G (1998) The moving parts of voltage-gated ion channels. *Quarterly reviews of biophysics* 31:239-295.

Yiangou Y, Facer P, Chessell IP, Bountra C, Chan C, Fertleman C, Smith V, Anand P (2007) Voltage-gated ion channel Nav1.7 innervation in patients with idiopathic rectal hypersensitivity and paroxysmal extreme pain disorder (familial rectal pain). *Neurosci Lett* 427:77-82.

Yu FH, Westenbroek RE, Silos-Santiago I, McCormick KA, Lawson D, Ge P, Ferriera H, Lilly J, DiStefano PS, Catterall WA, Scheuer T, Curtis R (2003) Sodium channel beta4, a new disulfide-linked auxiliary subunit with similarity to beta2. *J Neurosci* 23:7577-7585.

Zhao Y, Yarov-Yarovoy V, Scheuer T, Catterall WA (2004) A gating hinge in Na⁺ channels; a molecular switch for electrical signaling. *Neuron* 41:859-865.

Zimmer T, Bollensdorff C, Haufe V, Birch-Hirschfeld E, Benndorf K (2002) Mouse heart Na⁺ channels: primary structure and function of two isoforms and alternatively spliced variants. *American journal of physiology* 282:H1007-1017.

Zimmermann K, Leffler A, Babes A, Cendan CM, Carr RW, Kobayashi J, Nau C, Wood JN, Reeh PW (2007) Sensory neuron sodium channel Nav1.8 is essential for pain at low temperatures. *Nature* 447:855-858.

CIRRICULUM VITAE

Brian W. Jarecki

EDUCATION

- August 2005 – February 2010
Indiana University, Indianapolis, IN
Department of Pharmacology and Toxicology
Doctor of Philosophy (Ph.D.)
- August 1999 – May 2003
Butler University, Indianapolis, IN
School of Pharmacy and Health Sciences / Liberal Arts and Sciences
Dual Bachelor of Science (B.S. / B.S.) in Pharmaceutical Sciences and Chemistry

PUBLICATIONS

1. **Jarecki, B.W.**, Jackson II, J.O., Cummins, T.R., Stabilizing interactions of D3 / S4-S5 residues during Na_v1.7 inactivation. (*in preparation*).
2. Sheets, P.L., **Jarecki, B.W.**, Jackson II, J.O., Cummins, T.R., Lidocaine stabilizes Na_v1.7 in a configuration that decreases transition to the slow-inactivated state of the channel. (*in preparation*).
3. **Jarecki, B.W.**, Piekarz, A.D., Jackson II, J.O., Cummins, T.R., Human voltage-gated sodium channel mutations that cause inherited neuronal and muscle channelopathies increase resurgent sodium currents. *J. Clin. Invest.* Jan; 120(1):369-78, 2010.
4. **Jarecki, B.W.**, Sheets, P.L., Jackson II, J.O., Cummins, T.R., Alternative splicing of Na_v1.7 exon 5 increases the impact of the painful PEPD mutant channel I1461T. *Channels.* 3(4): 259-67, 2009.
5. Dib-Hajj, S.D., Estacion, M., **Jarecki, B.W.**, Tyrrell, L., Fischer, T.Z., Lawden, M., Cummins, T.R., Waxman, S.G., M1627K PEPD mutation impairs inactivation, accelerates repriming, enhances ramp responses and renders DRG neurons hyperexcitable. *Mol. Pain.* 4:37, 2008.
6. **Jarecki, B.W.**, Sheets, P.L., Jackson II, J.O., Cummins, T.R., Paroxysmal Extreme Pain Disorder mutations within the D3 / S4-S5 Linker of Na_v1.7 cause moderate destabilization of fast-inactivation. *J. Physiol.* 586 (Pt 17): 4137-53, 2008.

SELECTED PRESENTATIONS

1. **Jarecki, B.W.**, Piekarz, A.D., Jackson II, J.O., Cummins, T.R., Resurgent Sodium Currents in Inherited Neuronal and Cardiac Channelopathies. National Society for Neuroscience, Chicago, IL, October 2009. Poster Presentation.
2. **Jarecki, B.W.**, Piekarz, A.D., Jackson II, J.O., Cummins, T.R., Impact of Na_v1.7-PEPD Missense Mutations that Slow the Rate of Inactivation on Sensory Neuronal Resurgent Sodium Currents. National Biophysical Society Meeting, Boston, MA, February 2009. Poster Presentation.
3. **Jarecki, B.W.**, Sheets, P.L., Jackson II, J.O., Cummins, T.R., Na_v1.7 Exon 5A Splice Variant Moderately Increases Ramp Current Elicited for PEPD Mutant Channel (I1461T) Compared to the 5N Form. Society for Neuroscience, Washington, D.C., November 2008. Poster Presentation.
4. **Jarecki, B.W.**, Sheets, P.L., Jackson II, J.O., Cummins, T.R., PEPD Mutations within the D3 / S4-S5 Linker of Na_v1.7 Alter Fast and Slow Inactivation and Increase Ramp Current from a Slow Depolarizing Stimulus. Midwest Pain Interest Group (PIG), Kansas City, KS, May 2008. Poster Presentation.
5. **Jarecki, B.W.**, Structural and Functional Role of the Na_v1.7 D3 and D4 / S4-S5 Linkers in Paroxysmal Extreme Pain Disorder. Indiana University School of Medicine Sigma Xi Chapter, Indianapolis, IN, May 2008. Seminar Presentation.
6. **Jarecki, B.W.**, Sheets, P.L., Jackson II, J.O., Cummins, T.R., PEPD Mutations within the D3 / S4-S5 Linker of Na_v1.7 Alter Fast and Slow Inactivation and Increase Ramp Current from a Slow Depolarizing Stimulus. Society for Neuroscience, San Diego, CA, November 2007. Poster Presentation.
7. **Jarecki, B.W.**, Esteb J.J., Synthesis of Propylene-Bridged Bis-Indanones and Bis-Indenes. Indiana Local American Chemical Society, Indianapolis, IN, October 2002. Poster Presentation.
8. **Jarecki, B.W.**, Esteb J.J., Synthesis of Propylene-Bridged Bis-Indanones and Bis-Indenes. Indiana Academy of Science, Indianapolis, IN, October 2002. Poster Presentation.

SCHOLARSHIPS AND AWARDS

1. Pharmacology and Toxicology Departmental K.K. Chen Award Recipient, Fall 2009.
2. Graduate Student Organization Education Enhancement Grant (EEG) Award Recipient, Spring 2009.
3. Best Graduate Student Poster, Society for Neuroscience (SFN), Indianapolis Chapter, October 2009.
4. Indiana Clinical and Translational Sciences Institute (CTSI) Fellowship, (*12 month funding period*), August 2009.
5. Graduate Student Organization Education Enhancement Grant (EEG) Award Recipient, Spring and Fall 2008.
6. National Society for Neuroscience (SFN) Ph.D. Graduate Student Travel Grant Award Recipient, November 2008.
7. Best Graduate Student Poster, Society for Neuroscience (SFN), Indianapolis Chapter, November 2008.
8. Best Graduate Student Poster, *First Place Award*, Society for Neuroscience (SFN), Indianapolis Chapter, November 2007.
9. Andrew S. Cebula Scholarship Recipient, (*12 month scholarship*), August 2005.
10. Butler University "Top 100 Students" Nominee, August 2002.
11. Butler University Heritage Award and Academic Scholarship, (*4 year scholarship*), August 1999.

RESEARCH EXPERIENCE

1. Indiana University School of Medicine, Indianapolis, IN, April 2006 – February 2010.
 - a) Department of Pharmacology and Toxicology – Ph.D. Thesis Project.
 - b) Gating of the Sensory Neuronal Voltage-gated Sodium Channel Na_v1.7: Analysis of the role of D3 and D4 / S4-S5 Linkers in Transition to an Inactivated State.
 - c) Mentor: Theodore R. Cummins, Ph.D.

2. Indiana University School of Medicine, Indianapolis, IN, December 2005 – April 2006.
 - a) Department of Pharmacology and Toxicology – Research Rotation.
 - b) Determine the cellular mechanisms mediating the release of neurotransmitters from pain-sensing (nociceptive) sensory neurons.
 - c) Mentor: Michael R. Vasko, Ph.D.

3. Indiana University School of Medicine, Indianapolis, IN, August 2005 – December 2005.
 - a) Department of Pharmacology and Toxicology – Research Rotation.
 - b) Investigated mechanisms by which environmental agents and therapeutic drugs elicit liver cancer.
 - c) Mentor: Lisa M. Kamendulis, Ph.D.

4. Indiana University School of Medicine, Indianapolis, IN, May 2005 – December 2005.
 - a) Department of Pharmacology and Toxicology – Work Study.
 - b) Focused on subcloning a voltage-gated sodium channel (VGSC) isoforms into an eGFP vector and evaluating the differential pharmacological sensitivity of two VGSC isoforms to local anesthetics using electrophysiological techniques of two VGSC isoforms.
 - c) Advisor: Theodore R. Cummins, Ph.D.

5. Purdue University, West Lafayette, IN, May 2003 – June 2005.
 - a) Organic Chemistry Department – Research Chemist.
 - b) Utilized various synthetic steps to extract, separate, isolate, and purify compounds to develop general procedures for undergraduate organic chemistry students.
 - c) Advisor: Kurt Keyes

6. Butler University, Indianapolis, IN, June 2002 – June 2003.
 - a) Liberal Arts and Sciences, Department of Chemistry – Research Student.
 - b) Synthetic methods and aspects in organic, organometallic, and polymer chemistry. Primary research focused on the synthetic design of novel C2-bridged indenyl metallocenes.
 - c) Mentor: John J. Esteb, Ph.D.

PROFESSIONAL ACTIVITIES

1. National Biophysical Society (BPS) Member, 2008 – present.
2. National Society for Neuroscience (SFN) Member, 2007 – present.

3. Local Society for Neuroscience (SFN) Student Member, Indianapolis Chapter, 2007 – 2010.
4. Chemistry Mentor and Tutor, Butler University, Indianapolis, IN, 2002 – 2003.
5. Member of ACS Chemistry Club, Butler University, Indianapolis, IN, 2001 – 2003.
6. Licensed Pharmacy Intern, Butler University, Indianapolis, IN, 2001.
7. Pharmacy Mentor, Butler University, Indianapolis, IN, 2000 – 2001.